ELECTRON SPECTROSCOPIC MEASUREMENTS ON THE SURFACES OF SOME III - V SEMICONDUCTORS

David Norman, M.A.

A Thesis submitted for the degree of

Doctor of Philosophy

in the

FACULTY OF SCIENCE

UNIVERSITY OF LEICESTER

September 1977

This Thesis is dedicated to the memory of

Mr. H. T. Lovett.

His enthusiastic and lucid teaching of Physics inspired many who were fortunate enough to experience it .

Abstract

Ultra-violet photoelectron spectroscopy (UPS) and other surface-sensitive electron spectroscopies (Auger electron spectroscopy, low energy electron diffraction, electron energy loss spectroscopy and X-ray photoelectron spectroscopy) have been used to study the electronic properties of the cleavage (110) faces of GaP, InP and GaAs, both in their clean state and during oxygen adsorption.

UPS shows that filled surface states are absent from the bulk bandgap in all three compounds, and only the tail of the empty surface state distribution extends into the bandgap on InP (110) and GaAs (110). The Fermi level of GaP(110) is pinned 1.50eV above the valence band maximum by a band of empty surface states which is also seen in synchrotron radiation-excited photoemission partial-yield measurements. The sticking coefficient for oxygen is very small on all three compounds studied here, exposures around 10^7 Langmuirs (10 Torr. sec) being necessary for monolayer coverage on the (110) faces. The Fermi level on GaP remains pinned after adsorption of 10^8 Langmuirs of oxygen, and for InP and GaAs pinning within the gap is induced by extrinsic states at coverages of less than one-thousandth of a monolayer.

The energies of some symmetry points in the bulk bandstructures of GaP and InP are determined unambiguously for the first time from a direct-transition analysis of the low-energy UPS data. The assignment of Auger peaks in clean GaP and the nature of the P-O interatomic Auger transitions and interface plasmons found during oxygen adsorption are discussed in detail. Electron beam-enhanced oxidation was observed, and a new mechanism proposed for this, involving adsorption of oxygen into the ceramic parts of the electron gun, followed by the projection of oxygen ions towards the sample.

Acknowledgements

I wish to record my gratitude to Dr.C.Norris for introducing me to photoemission and for his unfailing and helpful supervision of this work.
I also wish to thank the Science Research Council for the award of a maintenance grant and the Plessey Co.Ltd. for so generously fulfilling their part of the CAPS Research Studentship by provision of semiconductor crystals and facilities to perform experiments in their Allen Clark Research Centre. I am grateful for the gift of InP crystals by Dr.R.F.C. Farrow, R.R.E.,Malvern.

At Leicester, I have been greatly helped by the expert technical support of Mr.J.S.G.Taylor, Mr.C.Clark, Mr.A.R.Wardle and Dr.J.P.D.Hennessey

At the Allen Clark Research Centre, Dr.M.Pepper guided my attempts to learn about semiconductor surfaces and Mr.D.K.Skinner and Mr.P.D.Augustus provided invaluable assistance in performing and interpreting LEED/Auger experiments.

Some of the experiments at Daresbury Laboratory were performed in collaboration with Dr.I.T.McGovern and Dr.G.P.Williams. I am most grateful to them for their help.

Discussions with fellow physicists, at Conferences and elsewhere, have proved very useful in formulating and clarifying some of the ideas presented in this Thesis. I wish especially to thank my colleagues, and friends, at the University of Leicester, the University of Warwick and the New University of Ulster.

It is impossible to express sufficient thanks to my parents for their unstinting support throughout my education and to my wife for her encouragement and for enduring many long, lonely days and nights during the course of this work.

Finally, I am grateful to Mrs.A.Shaw for her careful and neat typing of this Thesis.

Errors, like straws, upon the surface flow;

He who would search for pearls must dive below.

John Dryden.

CONTENTS

CHAPTER 1

INTRODUCTION

1.0. Introduction

For many years semiconductor technologists have recognised that the properties of so-called "bulk" devices are often in fact dominated by surface effects (Grove 1967). The relatively recent emergence of the MOS transistor as a serious competitor to traditional bipolar devices shows that the technologies involved in production of thin oxide layers are now well understood, but the actual physics of electron states at and near surfaces and interfaces is still only poorly comprehended.

The operation of all semiconductor devices depends on the detailed electronic band structure of the material used, both within the bulk of the crystal and at or near the surface. The present work has been undertaken in an attempt to determine some of these fundamental electronic properties for Gallium Phosphide, Indium Phosphide and Gallium Arsenide, and the ways in which they may be modified during the initial stages of oxidation of these compounds.

Gallium Arsenide is the material in which the Gunn effect was first demonstrated and is now used commercially for production of microwave emitters based on this principle. InP also exhibits the Gunn effect, but has been observed to produce sinusoidal oscillations rather than the pulsed oscillations of GaAs: this is believed to be due to transitions of electrons between higher conduction bands without relaxation to their ground state, and potentially InP should be a more efficient microwave emitter than GaAs. Considerable effort is currently being expended on development of these Indium Phosphide three-level oscillators. Gallium Phosphide finds its main application in the production of electroluminescent light-emitting diodes. Reddish-orange light is given out by forward-biased diodes with efficiencies of around 10% (in terms of photons out per electron input). GaAs and InP are also very efficient photon-emitters, but they both emit in the near infra-red. Alloys of these compounds can be made to reduce the wavelength of the emitted light or anti-Stokes phosphors applied to convert the infra-red to green. In addition almost all of the III-V compounds are under investigation for use

as photocathode materials in image intensifiers and photomultipliers: they then have to be covered with very thin layers of the oxide of an alkali metal (usually caesium).

The electronic states which exist at a surface or interface purely because the infinite periodic lattice is disrupted (first predicted theoretically in 1932 (Tamm))give rise to narrow regions of very high charge density, known as the surface space-charge layer. Until a few years ago, the properties of the interface electronic states could be measured only indirectly, usually by experiments on the effect of varying some external parameter such as the electric or magnetic field close to the surface (Many et al. 1965). This phenomenological approach has proved remarkably successful for deducing properties of interface states, but has revealed a further problem, the existence of so-called "slow" and "fast" states. These are classified according to the relative speeds with which these states interact with the space-charge region of the crystal: the fast states are the true surface states, situated actually at the surface of the crystal, whereas the slow states are associated with the layer of oxide and chemisorbed impurity atoms which inevitably forms on any surface exposed to the atmosphere.

With the development, within the last ten years, of techniques for reproducibly obtaining vacua of the order of 10^{-10} torr, or better, it has become possible to create perfectly clean surfaces, by cleavage, heat treatment, evaporation, ion-bombardment, or other means, and maintain these surfaces in their pristine condition for long enough for experiments to be carried out upon them. Thus the problem of slow states and other effects of chemisorbed impurity atoms can be avoided, and the intrinsic properties of clean crystal surfaces can be studied.

Many different types of experiment which can be performed in u.h.v. on clean surfaces have been devised, the majority of which involve the movement of low energy electrons through a solid-vacuum interface. Such electrons have short mean free paths for inelastic scattering, typically of the order of a few atomic layers, and thus are highly sensitive to the properties of the surface.

Low energy-electron-diffraction (LEED) is the most widely used means of determining the spatial arrangement of the atoms in the surface layer. It is usually combined with Auger electron spectroscopy (AES) in order to monitor the impurity species present on the surface. Electron energy loss spectroscopy (ELS), until recently an under-utilised technique, can also easily be performed with the same experimental apparatus as for AES and LEED, and gives information which is particularly useful in studying the electronic states of adsorbed layers.

Photoelectron emission spectroscopy (PES), in which photons incident on a sample excite electrons from filled states within the crystal, has traditionally been divided, according to the wavelength of the light source used, into X-ray photoemission spectroscopy (XPS), normally with photons with $h\nu > 1000$ eV, and ultraviolet photoemission spectroscopy (UPS), with sources available with $h\nu < 40$eV. UPS has proved of increasing importance after the pioneering work of Spicer and others (reviewed by Spicer (1966)), and the majority of the work reported in this Thesis has been carried out using this technique. A wide range of photon energies has been used in the present study. Conventional laboratory sources are available with the hydrogen discharge continuum up to 11.8eV, neon discharge lines at 16.9 and 26.8eV and helium discharge lines at 21.2eV and 40.8eV. Several experiments were performed at the Synchrotron Radiation Facility at Daresbury Laboratory, Cheshire, using a normal incidence monochromator which makes available any photon energy from 15 to 40eV. Experiments have also been performed using LEED, AES and ELS at the Allen Clark Research Centre of the Plessey Co.Ltd.

Although some emphasis has been placed in the foregoing on the fact that crystal surfaces can, and often do, have completely different properties from the bulk and the techniques used are relatively surface-sensitive, in practice it is extremely difficult to distinguish between the surface and bulk electronic states. Many of the results obtained are thus characteristic of the bulk band structure. Although GaAs has been extensively studied by a variety of techniques, the bulk band structures of GaP and InP have not

in fact previously been examined by UPS.

The following Chapter of this Thesis outlines the theory of the surface and the bulk, and Chapter 3 describes in greater detail the process of photoemission, with the present state of the theory of the subject, and also outlines the other electron spectroscopies used in this work. The experimental apparatus and techniques, including the advances and improvements made during this work, are described in Chapter 4. The next three chapters deal with the results obtained on the three materials studied, Chapter 5 being concerned with GaP, Chapter 6 with InP and Chapter 7 with GaAs. The conclusions of the work described in this Thesis are presented in Chapter 8.

CHAPTER 2 : THE SURFACE AND THE BULK

2.1. Crystal Structure

2.2. Bulk electronic band structure

2.3. Surface structure

2.4. Surface electronic band structure

2.5. Review of numerical calculations of surface states

2.1. Crystal Structure

Almost all of the stable III -V compounds crystallize in the structure known as the zincblende, or, more properly, the sphalerite structure (Figure 2.1). This can be regarded as consisting of two intersecting face-centred-cubic sublattices, one composed entirely of atoms of group III in the periodic table, and the other of group V atoms. The origins of the unit cells are shifted in the [111]direction from each other by a translation vector [a/4,a/4,a/4] , a being the lattice constant. It is readily seen from Figure 2.1 that each group III atom is tetrahedrally-bonded to its four nearest-neighbour group V atoms, and vice versa.

Translation of this lattice into reciprocal space yields a Brillouin Zone (BZ) of the form shown in Figure 2.2. Standard notations have been adopted for some of the points of high symmetry in the BZ, and the lines joining them, these being shown in the Figure. Γ denotes the origin (0, 0, 0) and X the points $2\pi/a$ (1, 0, 0), with Δ the line [100] joining them. L is the point at the centre of the hexagon on the BZ face, $2\pi/a(\frac{1}{2}, \frac{1}{2}, \frac{1}{2})$ and Λ joins Γ and L. K is the point $2\pi/a(\frac{3}{4}, \frac{3}{4}, 0)$, joined by Σ to Γ . The corner points W have coordinates $2\pi/a(1, \frac{1}{2}, 0)$, joined to X points by lines Z.

It is implicit in the depiction only of the reduced Brillouin Zone that any point in $\underline{k}$ - space can be linearly translated into a point of identical symmetry on the reduced BZ, by addition or subtraction of an integral number of reciprocal lattice vectors, and also that the axes k_x , k_y and k_z can be treated as equivalent, in the sense that, for example, three X-points are visible on the surface, at k= $2\pi/a(1,0,0)$, $2\pi/a(0,1,0)$ and $2\pi/a(0,0,1)$.

2.2. Bulk electronic band structure

In this section we shall outline the methods used to calculate E-$\underline{k}$ diagrams, with particular reference to those techniques which have been successful for the III-V semiconductors. An understanding of the methods of calculation is fundamental both for the consideration of differences between the bulk and the surface, which follows in this Chapter, and for the analysis of the electron spectroscopic results to be presented in Chapters 5 to 7.

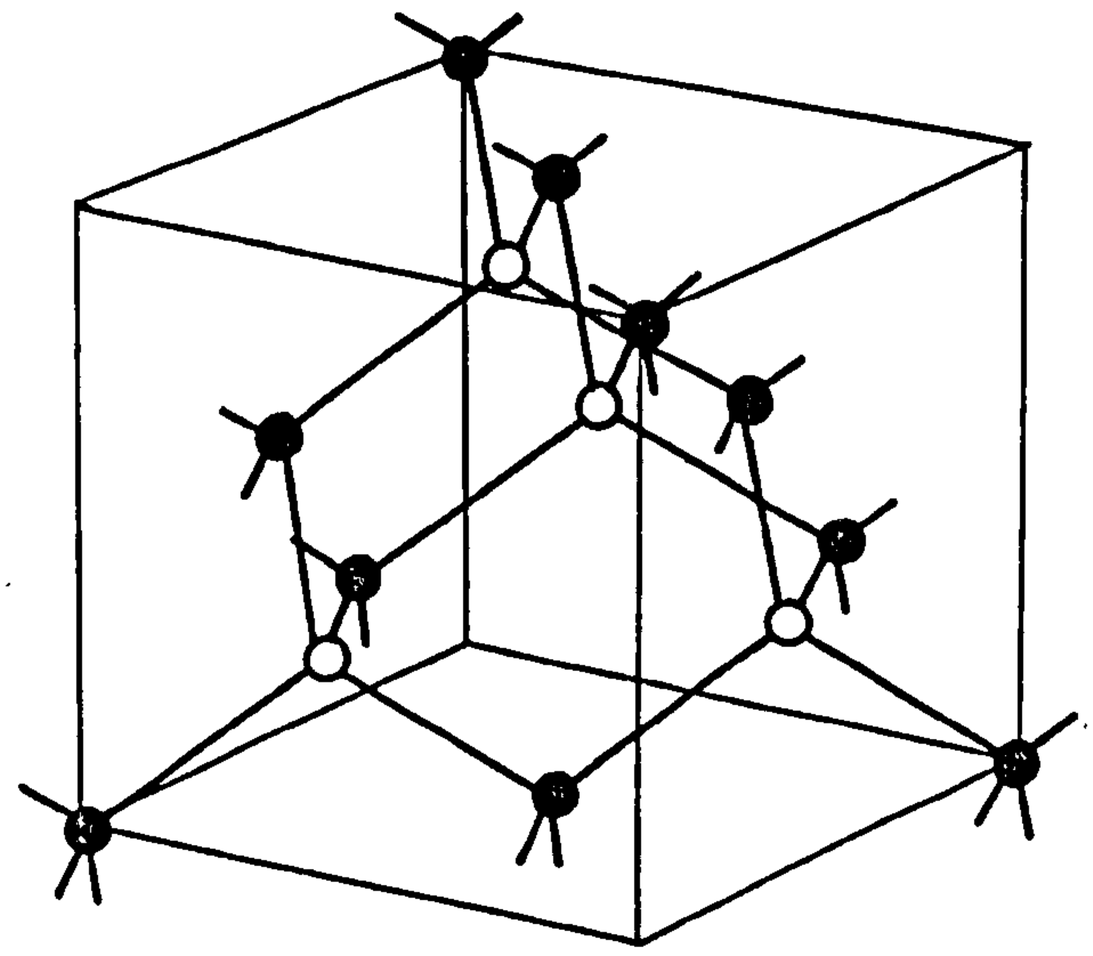

Figure 2.1. Unit cell of the zincblende (sphalerite) lattice. Atoms of one type are depicted by open circles and the others by full circles.

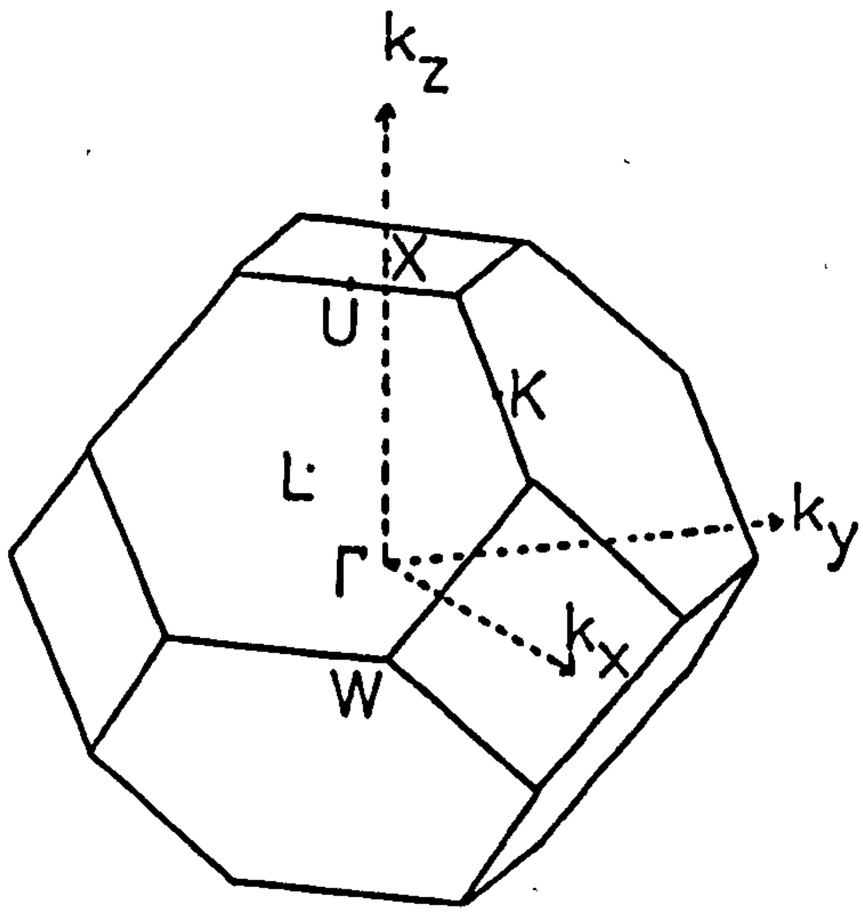

Figure 2.2. Brillouin Zone of the zincblende lattice

It is well known that free electrons have energies given by $E=\hbar^2k^2/2m$. For a real crystal the lattice potential $V(\underline{r})$ splits the bands at the BZ boundaries. A semiconductor has a gap extending throughout the BZ at normal temperatures, although some electrons can acquire sufficient thermal energy to raise them from the valence into the conduction bands and so contribute to conduction processes.

Schrödinger's equation

$$\left[\frac{-\hbar^2}{2m}\nabla^2 + V(\underline{r})\right] \psi_{n\underline{k}}(\underline{r}) = E_{n\underline{k}}\,\psi_{n\underline{k}}(\underline{r})$$

has to be solved for electron energies $E_{n\underline{k}}$ and wavefunctions $\psi_{n\underline{k}}$.

The wavefunctions have the Floquet form (Floquet 1883)

$$\psi_{nk}(\underline{r}+\underline{R}_n) = \exp(i\underline{k}.\underline{R}_n)\,\psi_{nk}(\underline{r})$$

where $\underline{R}_n$ is a vector sum of an integral number of the lattice constants of the crystal in three dimensions. With an infinite crystal and a periodic potential $V(\underline{r})$ this reduces to the usual Bloch form (Bloch 1928), the difference being that $\underline{k}$ is real.

The central problem is the construction of a suitable potential $V(\underline{r})$. The Born-Oppenheimer approximation is always invoked : the ion cores are assumed to be stationary, defining a field in which the valence electrons move. It is usual also to apply the Hartree approximation and consider just one electron which feels an average potential due to all the other electrons and ions. The effect of these electrons is incorporated in two additional terms, known as the "exchange" and "correlation" corrections. These are both derived from electronic spin. By the Pauli exclusion principle, two electrons with the same spin cannot occupy the same state: this leads to an exchange potential of the form

$$V_{exchange}(\underline{r}) = -\frac{3}{2}\alpha e^2 \left(\frac{3n(\underline{r})}{\pi}\right)^{\frac{1}{3}}$$

where α is a parameter which has been given any value from 1 (Slater 1951) to $\frac{2}{3}$ (Gaspar 1954, Kohn & Sham 1965), with varying degrees of theoretical justification. Also, electrons of opposite spins will tend to stay apart to minimize the potential energy. The motion of the electrons is thus correlated, and a correlation correction to $V(\underline{r})$ is introduced. Unfortunately, it happens that energy band structures are extremely sensitive to the form chosen for these potential correction terms.

Various methods have been employed to calculate energy band structures. Conceptually the most simple technique is the orthogonalized plane wave (OPW) method (Herring 1940). Suppose that $\Phi_a (\underline{r} - \underline{\ell})$ is an atomic orbital for a free atom centred at $\underline{\ell}$: then a function can be constructed, to satisfy the Bloch condition

$$\Phi_{ck} (\underline{r}) = \sum_{\ell} \exp (i\underline{k}.\ell) \; \Phi_a (\underline{r} - \underline{\ell}) .$$

This function has the form we would expect within the ion core, with highly localized atomic-like orbitals, multiplied by an exponential phase factor. The higher states, for the less tightly-bound electrons outside the core, having eigenfunctions $\psi_{\underline{k}}$, are still solutions of the same Schrödinger equation and so must be orthogonal to the core wavefunctions :

$$\langle \psi_{\underline{k}} , \Phi_{c\underline{k}} \rangle = 0$$

We also require $\psi_{\underline{k}}$ to be free-electron-like in the regions between the atoms and so use

$$\psi_{\underline{k}} = \exp (i\underline{k} . \underline{r}) - \sum_{c} \langle \Phi_{c\underline{k}} , \exp (i\underline{k}.\underline{r}) \rangle \; \Phi_{c\underline{k}}$$

This is known as an orthogonalized plane wave. It is readily seen that this is a reasonable guess at a higher state because it looks like $\exp(i\underline{k}.\underline{r})$ in the interstitial region, where each $\Phi_{c\underline{k}}$ is small (because the core states are highly localized), and yet within the core itself it will be orthgonal to all the core

states and thus a likely eigenfunction for a higher atomic orbital.

A linear combination of OPW's, with suitable coefficients, usually gives a good picture of the E-$\underline{k}$ diagram for all materials except transition metals and highly ionic compounds. The first application of the OPW method to III-V compounds (Bassani and Yoshimine 1963) used just a spatial superposition of overlapping atomic potentials, ignoring charge redistribution from the group III to the group V element, and results were obtained for GaAs which coincided to within 2 eV at every symmetry point of the BZ with the most recently accepted results. Herman et al (1964, 1966) discovered that their first-principles OPW calculations for the group IV semiconductors could be made to yield values for interband splitting which were in excellent agreement with experimental optical spectra by the addition of a small, empirically-determined adjustment to the crystal potential. They then used this technique for many II-VI and III-V semiconductors, including GaAs and GaP (Herman et al. 1968) and InP (Herman et al. 1969). These calculations also included relativistic corrections and spin-orbit splitting. Collins et al. (1970), using a non-relativistic OPW calculation for GaAs, obtained results agreeing with those of Herman et al to within 1 eV at all the major symmetry points. This calculation was performed with a self-consistent crystal potential : the energies of the core states, which are shifted slightly from their free-atomic values, are calculated from $V(\underline{r})$, and then used to adjust the crystal potential. This procedure is continued until self-consistency is obtained. In the calculations of Collins et al this took about ten iterations.

A more rigorous, but very difficult, method of obtaining self-consistency would be to calculate exact wavefunctions and hence charge densities, then alter $V(\underline{r})$ accordingly and repeat this procedure until no change in $V(\underline{r})$ is needed. This is obviously not possible with any procedure which approximates real wavefunctions by sums of plane waves.

The pseudopotential method (Cohen and Heine 1970), which follows from the OPW method, relies on the fact that terms originating from orthogonalization to core functions cancel the high-frequency components of the crystal potential in the Schrödinger equation. The remaining terms are expressed as a local

potential, the so-called pseudopotential. This method is not necessarily appropriate for all crystals, since the resulting "potential" term may not always be well-approximated by a local potential. In applying the empirical pseudopotential method (EPM) to obtain electronic band structures, we use a pseudopotential Hamiltonian

$$H = \frac{-\hbar^2}{2m} \nabla^2 + V_{pp}(\underline{r})$$

where $V_{pp}(\underline{r})$ is a weak pseudopotential which is taken to be a superposition of spherical atomic pseudopotentials. The potential $V_{pp}(\underline{r})$ is then expanded in reciprocal lattice vectors, and for convenience expressed in terms of a symmetric and antisymmetric part :

$$V_{pp}(\underline{r}) = \sum_{\underline{G}} \exp(-i\,\underline{G}.\underline{r}) \left[V^S(G) \cos \underline{G}.\underline{\tau} + i\, V^A(G) \sin \underline{G}.\underline{\tau} \right]$$

where $\underline{\tau} = \frac{1}{8} a\,(1,1,1)$. This series usually converges so rapidly that only three values of V^S and V^A are needed for each atom. Of course here we have dropped all pretence that the potential actually used bears any relation to the physics of the solid concerned[++].

The lowest three form factors of the pseudopotential are generally adjusted to reproduce certain experimentally-determined band splittings. The band structures of a large number of semiconductors have been derived by this method, following Cohen and Bergstresser (1966). Pseudopotentials for III - V compounds were formed from pseudopotentials for valence-IV elements by the addition of a small antisymmetric potential.

The EPM has certainly been the most popular, and probably the most successful method for determining band structures of III-V compounds. Several small refinements to the results of Cohen and Bergstresser have been proposed, notably the inclusion of spin-orbit interaction (Zucca et al. 1970) and the inclusion of a non-local, directional, term in the pseudopotential to account for the ionicity of the compounds (Chelikowsky and Cohen 1974). A simpler way to remove the discrepancies found between theory and experiment is to

++ "With five parameters I will fit the shape of an elephant; with a sixth I will wag its tail." Attributed to A.L.Cauchy.

allow the electron mass in the Hamiltonian to be replaced by an effective mass m * . Chelikowsky et al. (1973) found that this gave results very similar to those they obtained by use of a full non-local pseudopotential operator. It must be remembered that all these EPM calculations concentrate on fitting data, usually obtained from reflectivity measurements, in the region within a few electron Volts of the principal band-gap, and are not normally fitted to data at considerably greater energies than the principal band-gap. It may thus be somewhat surprising that the EPM works well for most compounds and most ranges of energy. EPM results for GaAs and InP are given in Figures 5.5 and 6.5.

We shall now discuss two methods which have been used occasionally for computation of the energy bands of semiconductors. As has been mentioned earlier, within the ionic cores the wavefunctions look very much like atomic orbitals, so we can try to construct the total crystal wavefunctions from a linear combination of atomic orbitals (LCAO). In fact, although this works well for ionic crystals and solid raregases, the LCAO method has not proved very successful for covalent materials, where there is large overlap between the AO centred on different lattice sites, and electrons tend to be localized mid-way between such sites. Another drawback of tight-binding (TB) methods is that they are essentially designed to give the form of occupied states, that is, the valence bands, and many excited states of the initial AO have to be included to obtain a reasonable picture of conduction bands. To some extent charge localization can be dealt with by the inclusion of directional states (e.g. p states).

Despite these problems the TB approach is intuitively attractive, as it gives a picture, in real space, of the electronic interactions which give rise to the particular features of the energy band structure and density of states. This is extremely useful in studies of how these features change when the electronic configuration is altered, for instance at a surface. Chadi and Cohen (1975b) have recently presented TB calculations of valence band structures and densities of states for several diamond and zincblende structure crystals, and compared their result for GaAs with that obtained

using the EPM (Chelikowsky and Cohen 1974). It was found that, as well as all possible interactions of orbitals on nearest-neighbour atoms, it was necessary to include one second-nearest-neighbour interaction between the Ga p-states in order to broaden the p-like bands along all symmetry directions sufficiently to give good agreement with the non-local EPM work. From the band structure diagram comparing these two results, which is presented in Figure 2.3., it can be seen that there remains a discrepancy of up to one electron Volt along the Σ direction. A particularly useful feature of TB calculations is that the orbital character of each valence band can be determined : Chadi and Cohen (1975b) give the lowest band of GaAs as s-like around As, the second band as mainly s-like around Ga and p-like around As, while the top two bands are totally p-like.

The last technique we shall consider is the Bond-Orbital Method (BOM), which has been recently applied to tetrahedrally-coordinated semiconductors by Harrison (1973) and Pantelides and Harrison (1975). The basis of this model is the well-known sp^3 hybrid orbital. On each ion is constructed a tight-binding combination of s- and p-atomic states of the form

$$|h> = \frac{1}{2}\left(|s> + \sqrt{3}\ |p> \right)$$

where $|h>$ is the hybrid wavefunction. The "bond orbitals" of Harrison consist of the bonding combination of sp^3 hybrids located on the nearest atoms on either side of the bonding site, together with the anti-bonding combination of the same sp^3 hybrids and, in some cases, additional localized orbitals to supplement the basis set. The eigenvalues at seven points of high symmetry in the BZ are given by Pantelides and Harrison for a large number of covalent and partially ionic zincblende-structure semiconductors (including GaAs, GaP and InP), and agree fairly well with values obtained by other methods. The BOM is essentially limited to calculation only of valence bands, and cannot deal with conduction bands, but it does go some way towards elucidating the important relationship between bonds and bands in crystals.

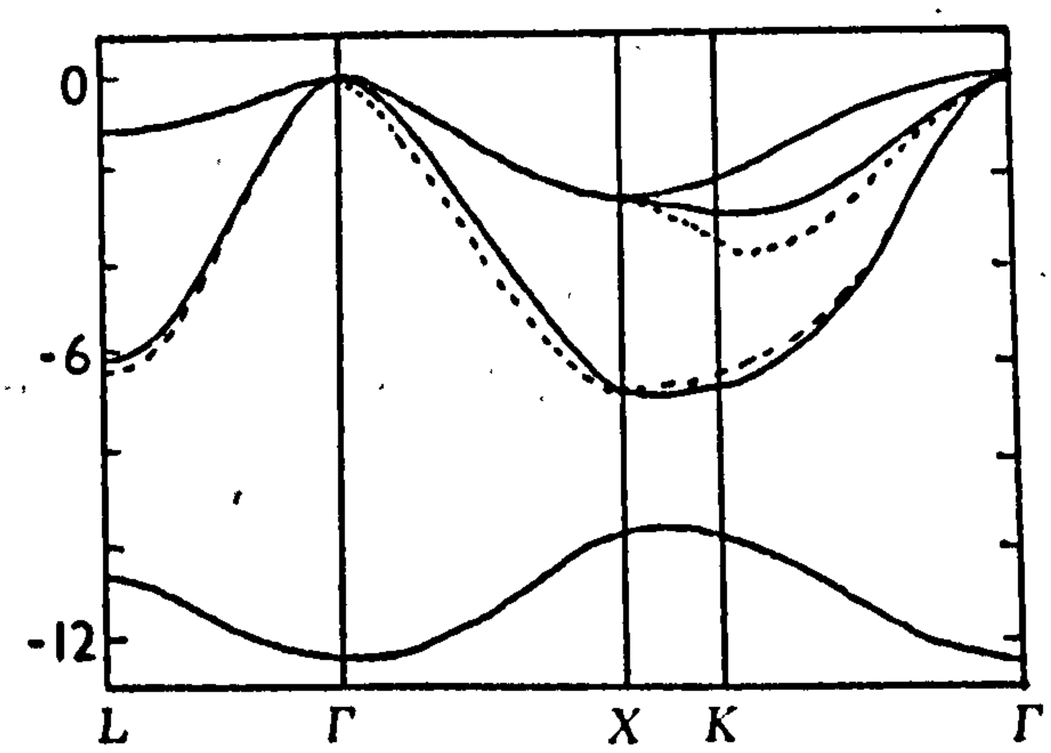

Figure 2.3. E - $\underline{k}$ diagram for the valence bands of GaAs.

——— tight-binding (Chadi and Cohen 1975b);----empirical pseudopotential (Chelikowsky et al (1973)

2.3. Surface Structure

Diamond, silicon and germanium, which have the same crystal structure as the III-V compounds but with all the atoms of one type, cleave along $\{111\}$ planes , because these planes have a lower bond density than any other. The III-V compounds differ because their bonding is not perfectly covalent but has some ionic character. The $\{111\}$ planes consist alternately of group III-atoms and group V-atoms, and thus are polar. This slight ionicity causes III -V compounds to cleave along $\{110\}$ planes, which are electrically neutral. The $\{110\}$ surface of a sphalerite compound is shown in Figure 2.4.

Many semiconductor surfaces exhibit a periodicity different from that of a parallel plane within the bulk. This is the process termed reconstruction, wherein the surface atoms rearrange themselves to minimize the free energy due to the unfilled bonds left by the creation of the surface. However, none of the cleavage planes of GaAs , GaP and InP is reconstructed: this important difference from the elemental semiconductors is also attributable to the electrostatic stabilization provided by the partially ionic bonding.

2.4. Surface electronic band structure

The translational symmetry of the lattice potential does not hold over all space for a finite crystal. Floquet's theorem is still obeyed, but the propagation vector $\underline{k}$ is complex , $\underline{k} = \underline{\lambda} + i\underline{\kappa}$. Obviously for ψ to be physically real, it must be bounded, and so for an infinite lattice $\underline{\kappa} = \underline{0}$ and the usual Bloch form is produced. However, for a finite lattice it is possible to have a wavefunction divergent in the outward direction normal to the surface, provided it is matched properly to a decaying wavefunction outside the surface. Now considering the one-dimensional case, with the surface in the (xy) plane (Figure 2.5) the probability density becomes

$$\left|\psi\left(z + na_z\right)\right|^2 = \exp\left(-2n\kappa_z a_z\right) \left|\psi\left(z\right)\right|^2$$

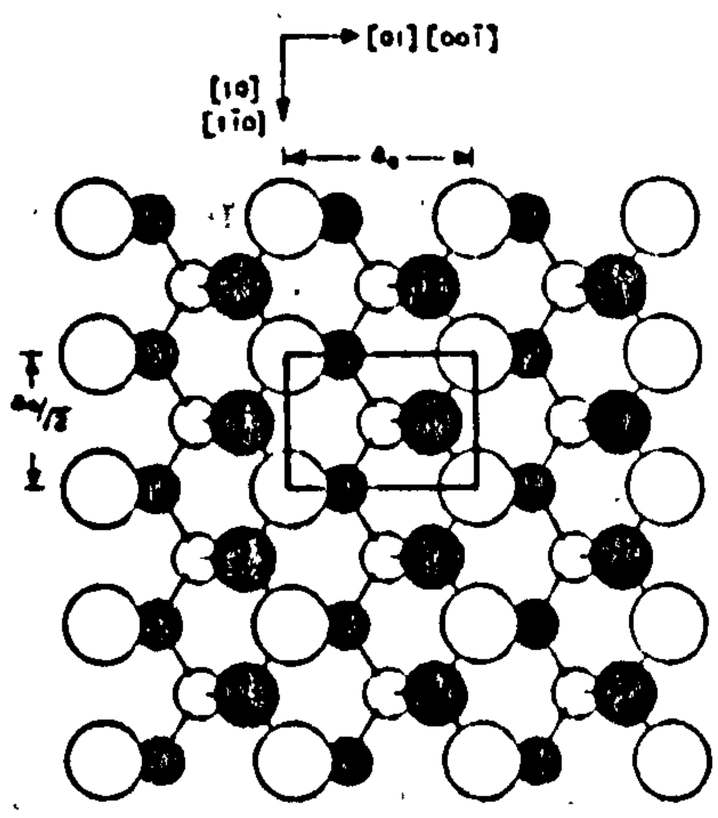

Figure 2.4. {110} plane of zincblende structure

The open circles represent atoms of one type and the full circles atoms of the other type. Relative sizes of circles are an indication of depth into the crystal, the smaller circles being situated in deeper layers. The substrate unit mesh and its dimensions are marked.

which shows that the imaginary part of $\underline{k}$ is an attenuation coefficient. Assuming the nearly-free-electron approximation, near the band edges the curve of energy against wavevector is parabolic, and so

$$E = \frac{\hbar^2}{2m^*} |\underline{k}|^2$$

$$= \frac{\hbar^2}{2m^*} \left[|\underline{\lambda}|^2 - |\underline{\kappa}|^2 + 2i\, \underline{\lambda} . \underline{\kappa} \right]$$

But E is the eigenvalue of a Hermitian operator and so must be real. Hence $\underline{\lambda} . \underline{\kappa} = 0$: this can be satisfied by $\underline{\kappa} = \underline{0}$ which is the infinite lattice solution, or by $\underline{\lambda} \perp \underline{\kappa}$ with $\underline{\kappa} \neq \underline{0}$. Since we have taken $\underline{\kappa}$ in the z direction, when $\kappa_z \neq 0$, $\lambda_z = 0$, which shows that the attenuated wavefunctions do not represent propagation. Then $E = \hbar^2/2m^* \left[|\underline{\lambda}|^2 - |\underline{\kappa}|^2 \right]$, which is shown graphically in Figure 2.6. Bands of "surface states" have become split off from the bulk energy bands, with their energies lying within the forbidden gap of the bulk states, and their wavefunctions highly localized in a narrow region around the surface. Thus violation of local charge neutrality is possible and space-charge-layers are created in the surface region.

As with bulk band structures, the procedures used for theoretical treatment of surface states fall into two main groups : nearly-free-electron-like methods, and tight-binding models. Several comprehensive reviews have been published recently (Davison and Levine 1970, Jones 1976, García-Moliner and Flores 1976). We shall consider initially one-dimensional models since these give one a reasonable insight into the spectrum of surface states.

Soon after Kronig and Penney (1931) published their classic paper on the representation of the crystal potential by a linear array of δ-function attractive potential wells, Tamm (1932, 1933) considered the effect of termination of this model at a potential minimum. By matching the wavefunction and its derivative across the discontinuity for a semi-infinite crystal, he found that one discrete level occurred in each band-gap, corresponding to a wavefunction localized at the surface, provided that the surface perturbation was large enough. Later work with the same model showed that the levels should occur in pairs in a finite lattice, because of the effect of the two surfaces.

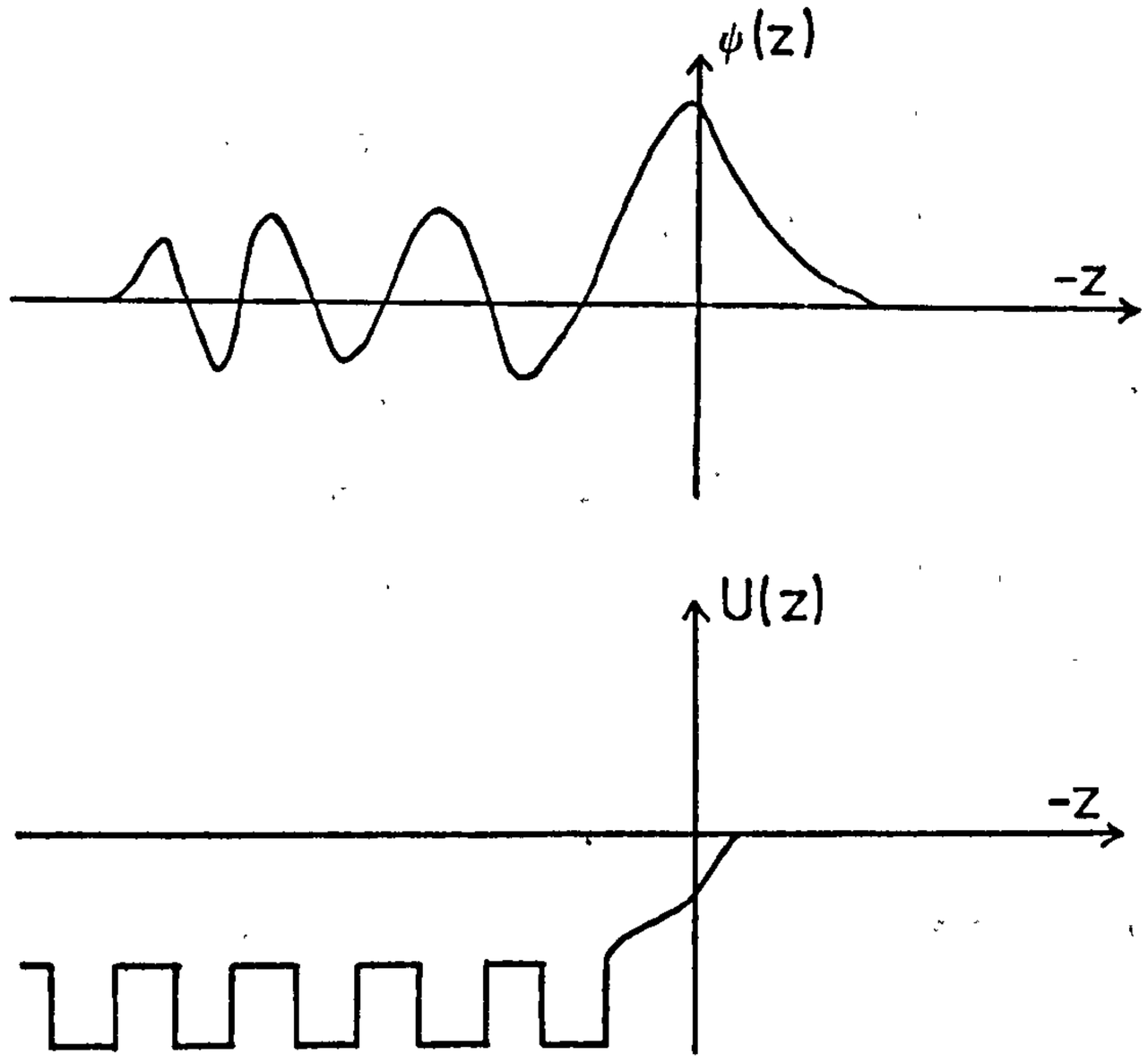

Figure 2.5. Schematic one-dimensional representation of the variation of wavefunction $\Psi(z)$ and lattice potential $U(z)$ near a surface.

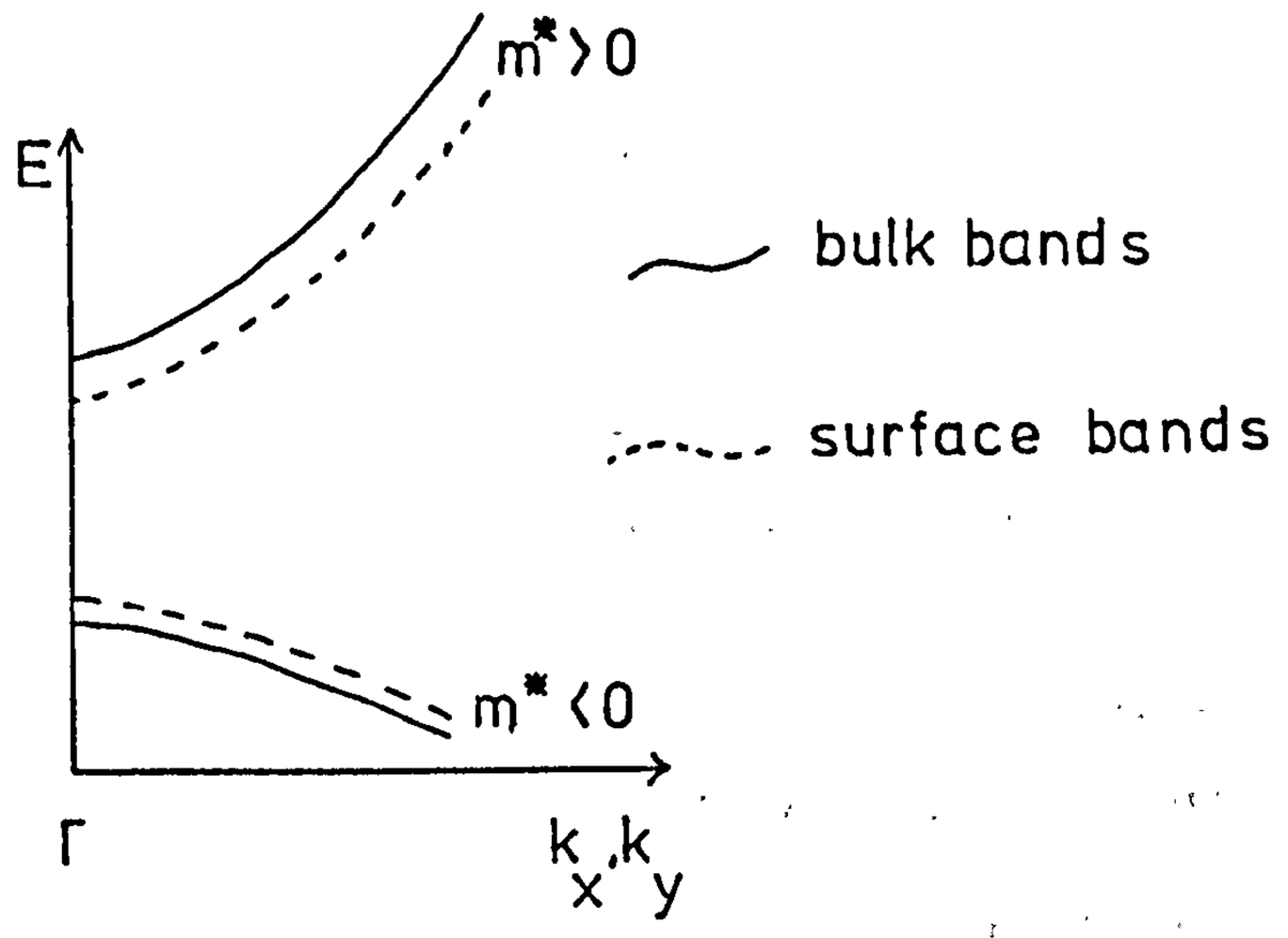

Figure 2.6. $E - \underline{k}$ diagram for bulk and surface bands in the nearly-free-electron approximations.

Shockley (1939) considered the same model terminated at a potential maximum, treated from the point of view of breaking bonds and found that surface states appeared when the surface perturbation was sufficiently small: this was in contrast to Tamm's result and has led to states being called "Tamm states" and "Shockley states." In fact this is an academic distinction since, if the co-ordinate origin is translated by half a lattice constant, the one-dimensional theory of Shockley levels becomes equivalent to the Tamm theory with an added surface perturbation. In other words, depending on where the origin of the unit cell is taken, surface states may be seen as arising from the breaking of a bond (Shockley) or from the perturbation of the crystal potential at the surface (Tamm).

One particular one-dimensional nearly-free-electron model which seems to be particularly useful is that of Levine (1968), who used a Mathieu potential $V(z) = -V_0 + V_1 \cos \frac{2\pi z}{a}$, with a the lattice constant. This has several factors to recommend it; the technique has been applied to the infinite-lattice problem and the problem is exactly soluble. Also, the various principal bonding types can be simulated by different choices of lattice constant and lattice termination (by shifting the potential termination to a suitable point z_0), and so can all be handled in one analysis. For metallic bonding, the ion cores are located at the potential minima and the lattice terminated midway between lattice sites (i.e. at a potential maximum), with a step discontinuity to the vacuum level. But for covalent bonding, the saturated electron pair bonds strongly localize electrons midway between lattice sites, and so these sites are situated at the potential maxima and the covalent lattice is terminated at a minimum of $V(z)$. A binary ionic lattice is represented by an alternating sequence of cations (M) and anions (X). The anions have the greater electron affinity and are situated at the potential minima, because the valence electrons tend to localize there.

For a binary solid with mixed bonding, like the III-V semiconductors, the Mathieu potential represents the antisymmetric part of the total potential.

The ionic lattice may terminate in either an M-like or an X-like constituent, and so the potential is broken at points of maximum positive or negative slope respectively.

Solution of the Schrödinger equation

$$\left[-\frac{\hbar^2}{2m} \frac{d^2}{dz^2} + V_0 - V_1 \cos \frac{2\pi}{a} z + E \right] \psi(z) = 0$$

and some mathematical manipulation yields results which can be expressed diagrammatically in Figure 2.7. Surface states are allowed in the gaps where the unbroken curve intersects the lines $z_0 = \frac{na}{4}$; covalent bonding is represented by m = odd and m = 2 models the ionic case. Figure 2.7 shows, for instance, ionic states (open circles) in the lower and upper half of the m = 2 gap at $z_0 = \frac{a}{4}$ and $\frac{3a}{4}$ corresponding to termination of the lattice with an anion or cation outermost. Thus the upper and lower surface states of an ionic lattice become associated with the M-like and X-like constituents.

However, the crystal potential methods are not very satisfactory, for two main reasons. Real crystals require potentials with a greater variety of harmonics than can be accommodated by δ-wells, square wells or sinusoidal wells. Secondly, the continuity condition becomes unwieldy for three-dimensions, because matching at an infinite number of points in the surface plane is necessary. One would expect matching difficulties to be more significant for localized than for extended states. A crude approach to three-dimensional problems has been obtained by matching the wavefunctions only at a few symmetry points in the unit cell of the surface plane. Irrespective of the particular crystal potential employed , the most questionable aspect of most surface state calculations is the abrupt termination of the lattice by a planar potential discontinuity.

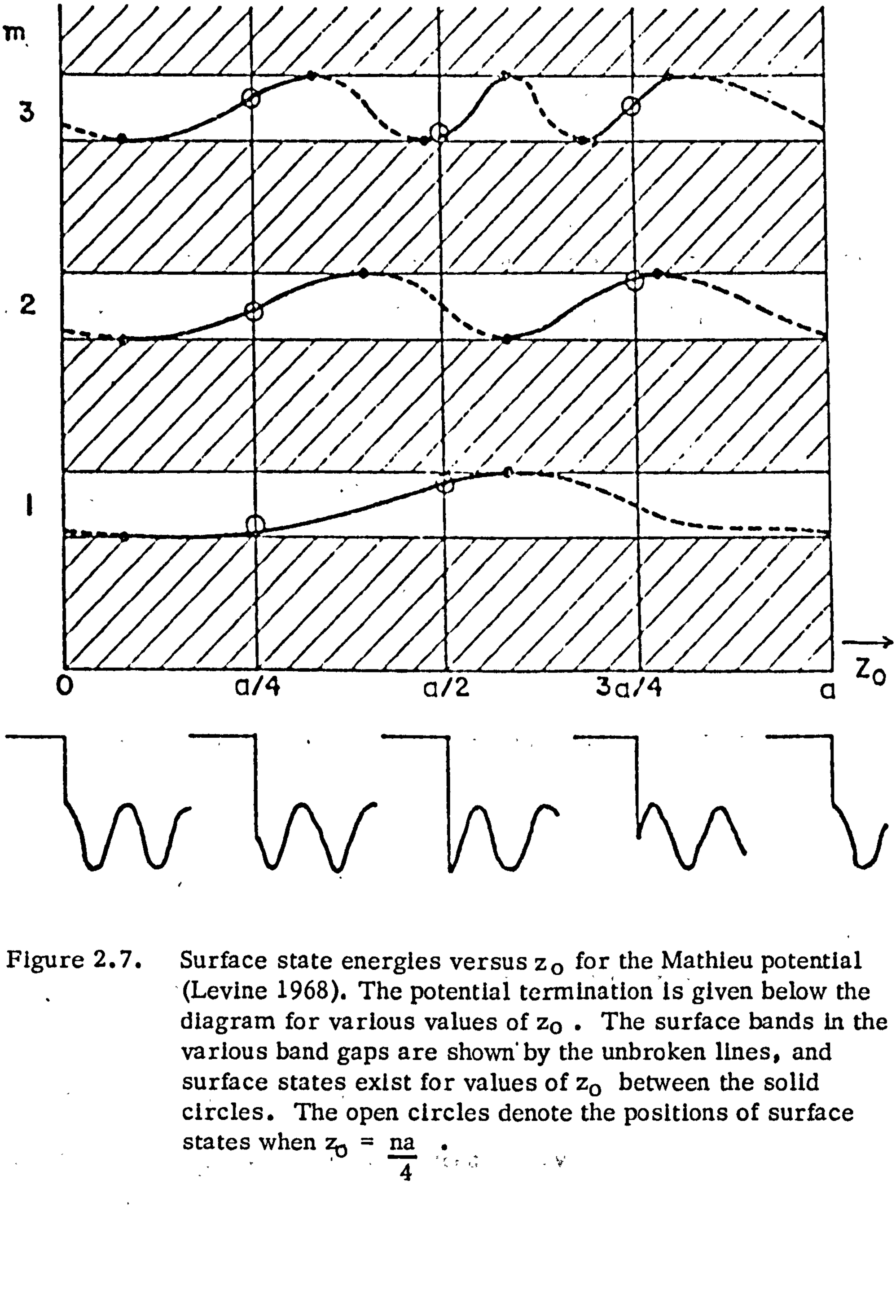

Figure 2.7. Surface state energies versus z_0 for the Mathieu potential (Levine 1968). The potential termination is given below the diagram for various values of z_0 . The surface bands in the various band gaps are shown by the unbroken lines, and surface states exist for values of z_0 between the solid circles. The open circles denote the positions of surface states when $z_0 = \frac{na}{4}$.

Flores et al (1972) have shown, by considering a potential termination in the form of a linear barrier of finite width sloping upwards to join to the vacuum level, that even a different number of surface states is obtained for quite realistic values of their potential barrier. Two methods avoid this particular difficulty : crystal orbital (tight-binding) methods and Green's function methods.

We can follow the normal LCAO type of calculation and solve the Schrödinger equation (in Dirac notation)

$$(H - E)\,|\Psi\rangle = 0$$

with $|\Psi\rangle = \sum_n C_n\,|\Phi_n\rangle$ where $|\Phi_n\rangle$ represents the motion of an electron in the field of the n^{th} atom only, and hence obtain $\sum_n (H_{mn} - E\,S_{mn})\,C_n = 0$

with $H_{mn} = \langle \Phi_m | H | \Phi_n \rangle$

and $S_{mn} = \langle \Phi_m | \Phi_n \rangle$

As usual, the AO are taken to form an orthonormal set so

$$S_{mn} = \delta_{mn}$$

and, ignoring next-nearest-neighbour interactions for the time being,

$$H_{mn} = \alpha \quad m = n$$

$$= \beta \quad m = n \pm 1$$

$$= 0 \quad \text{otherwise.}$$

where α is the Coulomb integral, around one atom, and β is the resonance integral, between atoms. Then we find

$$2X\,C_n = C_{n+1} + C_{n-1}$$

where $X = \dfrac{E - \alpha}{2\beta}$, the reduced energy.

Thus Schrödinger's differential equation is transformed into a second-order difference equation with constant coefficients.

Now it is easy to characterize the surface, by assigning to surface atoms different Coulomb and resonance integrals from the bulk atoms. The surface Coulomb integral α' is usually different from α, due to surface perturbation, and deformation can make β' differ from β. This shows the chief conceptual advantage of the LCAO method : rather than an arbitrary potential discontinuity the surface is characterized by α' and β' .

The surface states of a binary crystal have been found by Levine and Davison (1968). They took a semi-infinite linear array of equally-spaced lattice sites, with an s-orbital associated with each A atom and a p-orbital with each B atom. Again two states, one anion-like and one cation-like are found in each band-gap, provided the surface perturbation is large enough.

However, inclusion of next-nearest-neighbour interactions and the extension to three dimensions considerably complicate this method and there are fundamental reasons for objection to the molecular orbital methods, given by Heine (1964) and Jones (1972). Almost all the methods used for calculation of the bulk electronic band structure of non-transition metals and semiconductors are of the form of plane waves being scattered by some weak pseudopotential of the atoms (as described in Chapter 2.2) : in the LCAO method localized functions are needed but it is not possible to form a realistic LCAO which is localized to better than about five atomic spacings, so the overlap matrices have very high order. Finally, and most fundamentally, the tight-binding scheme cannot easily describe the sharp curvature of the bands near their maxima and minima, which is just where the evanescent waves in the band structure also lie.

The Green's function methods obviate two of the major problems associated with the traditional crystal potential calculations. Computation of the band structure for complex wavenumber is avoided because the Green's function for the perfect bulk crystal implicitly contains the behaviour for complex $\underline{k}$ and forbidden values of energy. The main conceptual difficulty is also bypassed as no assumption of the abrupt

potential termination is necessary.

The most important result seems to be that of García-Moliner and Rubio (1969) : the relationship between the surface Green's function G_S and the Green's functions outside (G_o) and inside (G_i) the crystal is simply :

$$G_s^{-1} = \tfrac{1}{2}(G_o^{-1} + G_i^{-1}) = \tfrac{1}{2} G_o^{-1}(G_o + G_i) G_i^{-1} \quad .$$

Thus the singularities of G_s consist of the singularities of G_o (plane waves outside) the singularities of G_i (Bloch waves inside) and the singularities of $(G_o + G_i)^{-1}$. These are the new eigenvalues due to the boundary condition imposed by the surface. Hence the secular equation for the surface states is

$$\det \quad (G_o + G_i) = 0$$

However, it seems that the mathematical elegance of the surface Green's function method does not lead to ease of computation in any cases of practical importance.

Perhaps the most interesting, and certainly the most realistic of all the surface state calculations so far reported, is that of Levine and Freeman (1970), who included information on surface structure in their computation of surface state energies for the (110) surface of zincblende crystals. They calculated the surface bands by a tight-binding model, with an s orbital placed on the cation site and three directed p orbitals on the anion site, and solved for a variety of surface strcutures consistent with the observed LEED patterns on several zincblende III - V and II - VI compounds. These allow for different ways in which it is possible that the surface may be changed without modifying the periodicity of the lattice parallel to the surface plane.

The computed form of the bands near the energy gap is shown in Figure 2.8. It is known that the valence bands are inaccurately represented in this approximation, and too much attention should not be paid to the lower bands of surface states, which are derived from the X ion. The most

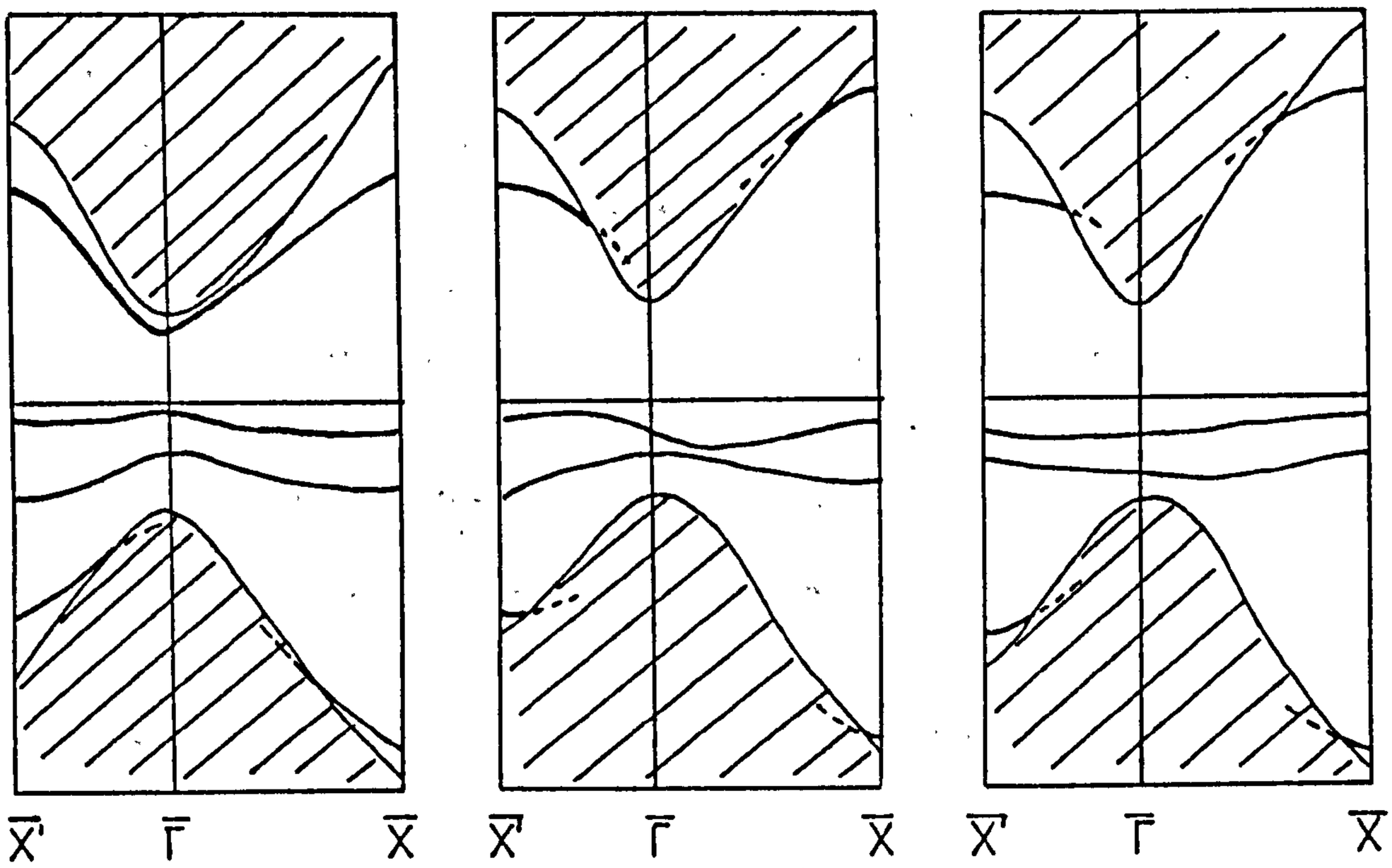

Figure 2.8. Bulk and surface energy bands for a zincblende (110) surface (Levine and Freeman 1970). (a) cations rotated out of surface by 34.9° . (b) undistorted surface. (c) anions rotated out of surface by 34.9°. The notation for symmetry points in the two-dimensional Brillouin Zone follows Jones (1969) : see Figure 2.9.

significant result of this work is that an upper surface state does not appear on an undistorted surface at the point Γ of the surface Brillouin zone, but is found only when the cations (M) are rotated upwards - out of the surface - and the anions (X) are rotated downwards. The bond lengths are kept constant, and the angle of rotation for this calculation was 34.9^{o}, which corresponds to the anion's being closest to the sp^2 planar coordination : this may make that particular configuration more stable. The effect of varying the bandgap was also investigated : increasing the gap lowers the empty, cation-derived, surface states towards mid-gap.

While there are admittedly inaccuracies in the fine details of this calculation, it does contain two important concepts which have been developed in more recent work. There are two bands of surface states, with the lower (acceptor) states derived from the anion and the upper from the cation; and the upper states do not appear unless surface atoms are rotated out of the surface plane.

2.5. Review of numerical calculations of surface states

In view of all the attention that the theory of surface states has attracted over the past 45 years it is perhaps surprising how few actual calculations for realistic crystals have in fact been performed. Until very recently few results for III - V semiconductor surfaces had been published, but the profusion of experimental results in recent years has prompted more calculations, and the relevant papers are summarized here. Unlike the bulk case, there is no universally accepted nomenclature for the two-dimensional Brillouin zone, but the usual notation for the symmetry points of the (110) face of the zincblende structure is illustrated in Figure 2.9.

Jones (1969) found surface bands for the (110) faces of GaAs and InP, extending through most of the bulk band gap, by using a pseudopotential complex band-structure calculation with an abrupt potential termination. Vyatkin et al (1970) with a similar approach, found several bands of surface states, some of which lie far below the Fermi level. This seems to be a feature of recent work;

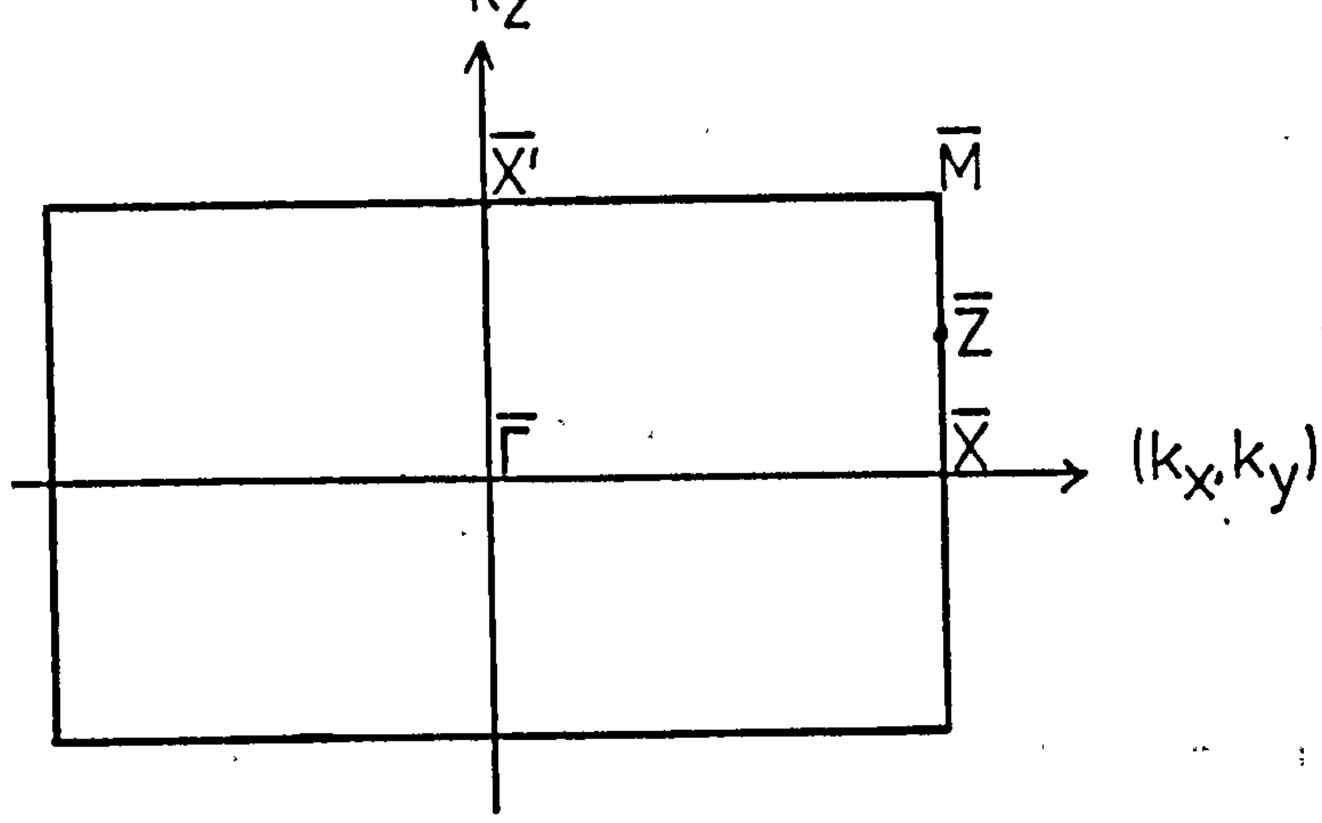

Figure 2.9. Notation for symmetry points in the two-dimensional Brillouin Zone of the (110) surface of the zincblende structure.

it has been realized that surface states may exist at any energy values, but of course they are less likely to be observed if they are not within the bulk gap. Ball and Morgan (1972), again using the EPM and matching wavefunctions, showed that the results obtained depend critically on the position of the matching plane between the atomic layers. They produced results only for the symmetry points $\bar{\Gamma}$ and $\bar{X}$ in the surface BZ of GaAs (110) and InP (110) and, although their results do not agree with Jones (1969), he is now inclined to believe their calculation to be better than his own (R.O.Jones, personal communication). García (1975) has used a similar method and finds two or three states at each point of high symmetry in the surface BZ , with one band completely within the bulk valence band.

Considering the remarks made in Chapter 2.4 on the applicability of tight-binding calculations to the bulk band structure of covalent crystals and the inability to construct well-localized linear combinations of atomic orbitals, it may be felt surprising that tight-binding models are now providing very good results. The validity of this approach in dealing with surface states in semiconductors has been confirmed by work on Si (Pandey and Phillips 1974), which has shown that it leads to essentially the same results as a very accurate self-consistent pseudopotential calculation (Appelbaum and Hamann 1974). In the vicinity of the bandgap, surface states are found on GaAs (110) ~ 0.4 eV below and ~ 1.2 eV above the valence band maximum (Calandra and Santoro 1975), both bands extending throughout the surface BZ with little dispersion . Inclusion of next-nearest-neighbour interactions (Calandra and Santoro 1976) brings both bands nearer to the valence band maximum and increases their dispersion. The results of this calculation for GaAs and GaP are given in Figure 2.10 : this is the only recent calculation which considers any III- V compound other than GaAs. The method of computation of the tight-binding models summarized here, in which planes parallel to the surface are added together until the bulk is well-approximated (which can take as few as five atomic layers), makes possible the calculation of the density of states within any particular layer. The localization of the GaAs surface states within the outermost layer has been strikingly demonstrated in this way (Joannopoulos

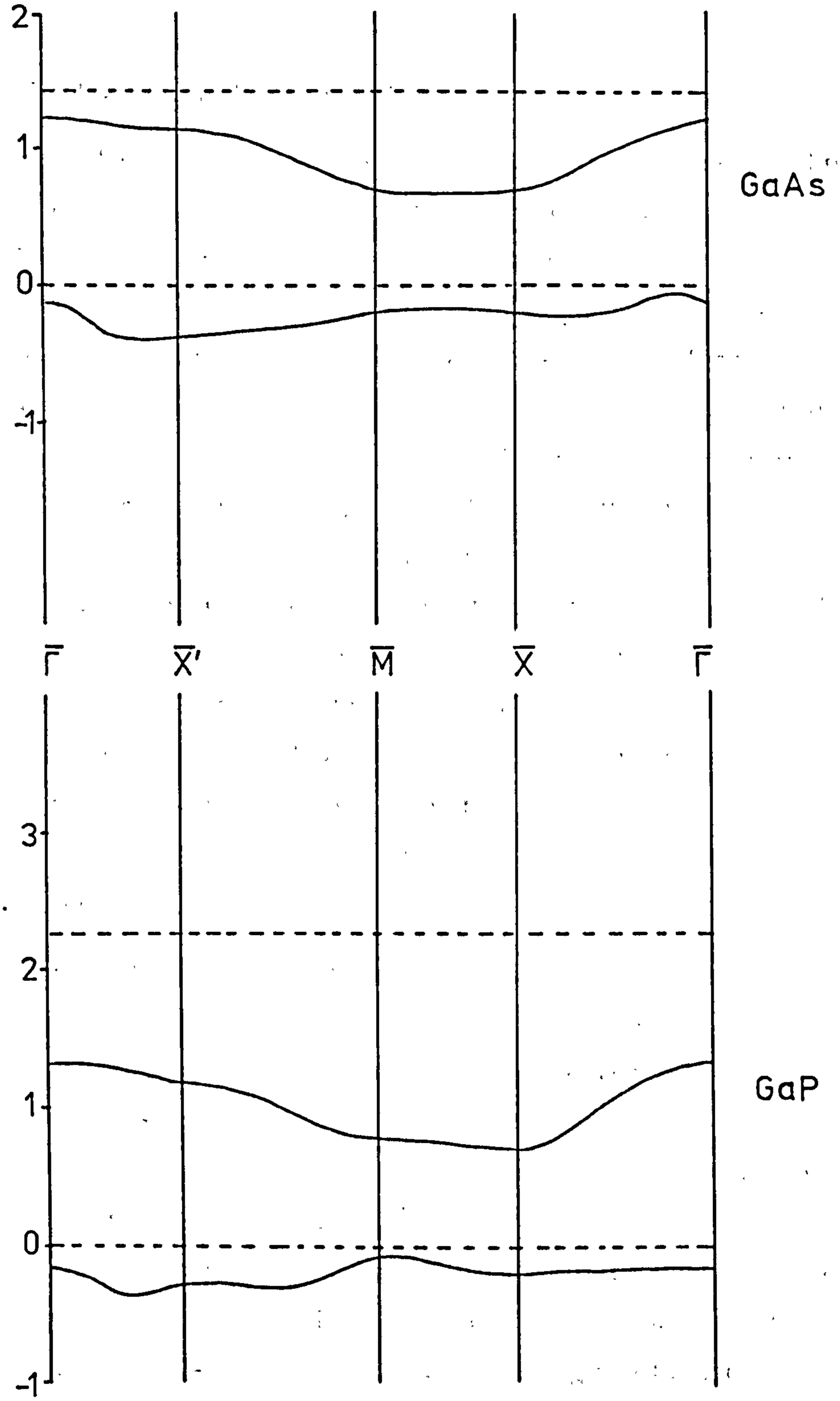

Figure 2.10. Surface energy bands near the bulk bandgap (dotted lines) for GaAs (110) and GaP (110) (Calandra and Santoro 1976)

and Cohen 1974a, 1974b, Chadi and Cohen 1975a).

The self-consistent pseudopotential method (recently reviewed by Appelbaum and Hamann 1976) has also been applied to GaAs (110) (Chelikowsky and Cohen 1976a). Several surface features are found near the bulk bandgap : three states or resonances associated with the As atom at 2.0, 0.5 and 0.25 eV below the valence band maximum are ascribed respectively to "back bonds," with the charge localized between the first and second layers along the bonding direction, "parallel bonds" with charge localized along the bonding direction between neighbouring surface atoms, and the familiar dangling bonds broken by the formation of the surface. Dangling bonds associated with the Ga atom occur at+1.0 eV, in the bulk bandgap. The charge densities of the Ga and the As dangling bond surface states found in this calculation are given in Figure 2.11, which emphasizes their dangling nature, with charge localized outside the surface atomic layer. It is readily seen that the As (occupied) state has predominantly p character, whereas the Ga state is mainly s-like, with some admixture of p-symmetry as indicated by the small lobe opposite to the charge density maximum.

The effect of relaxation of the surface layer has very recently been investigated with this same method (Chelikowsky et al 1976). The surface Ga atoms are allowed to relax inward to the sp^2 planar configuration and the anions shift outwards to maintain bond lengths. This is exactly the model considered by Levine and Freeman (1970). The empty cation dangling bond states are moved to higher energies, the peak in the density of states now lying above the bulk conduction band minimum, but the tail of the distribution still extending into the bandgap. The filled, As-derived, states are lowered in energy by $\sim$ 1eV, as shown in Figure 2.12, which gives the local density of states of the surface layer for the relaxed and un-relaxed geometries. The effect on the charge densities of the dangling bond surface states is profound: Figure 2.13 shows that the cation states no longer protrude into the vacuum (Figure 2.11 (a)) but the charge is now weakened and localized between the first and second layers. In a sense, they are not now dangling bond states.

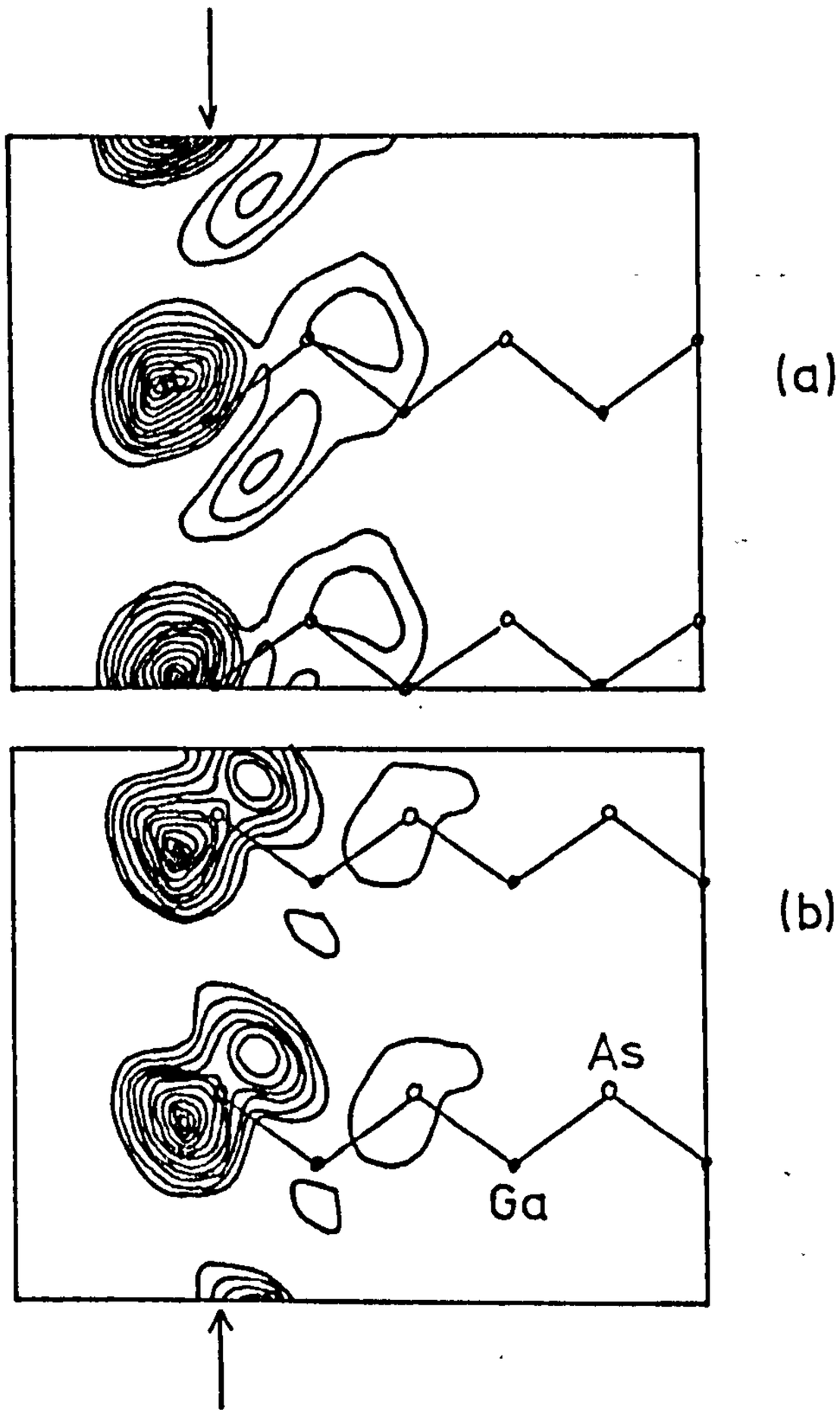

Figure 2.11. Charge density plot of the GaAs (110) surface for the (a) Ga dangling bond and (b) As dangling bond surface states. The arrows indicate the plane of the surface atomic layer. The contours are in units of two electrons per unit cell volume (812 $Å^3$). From Chelikowsky and Cohen (1976a).

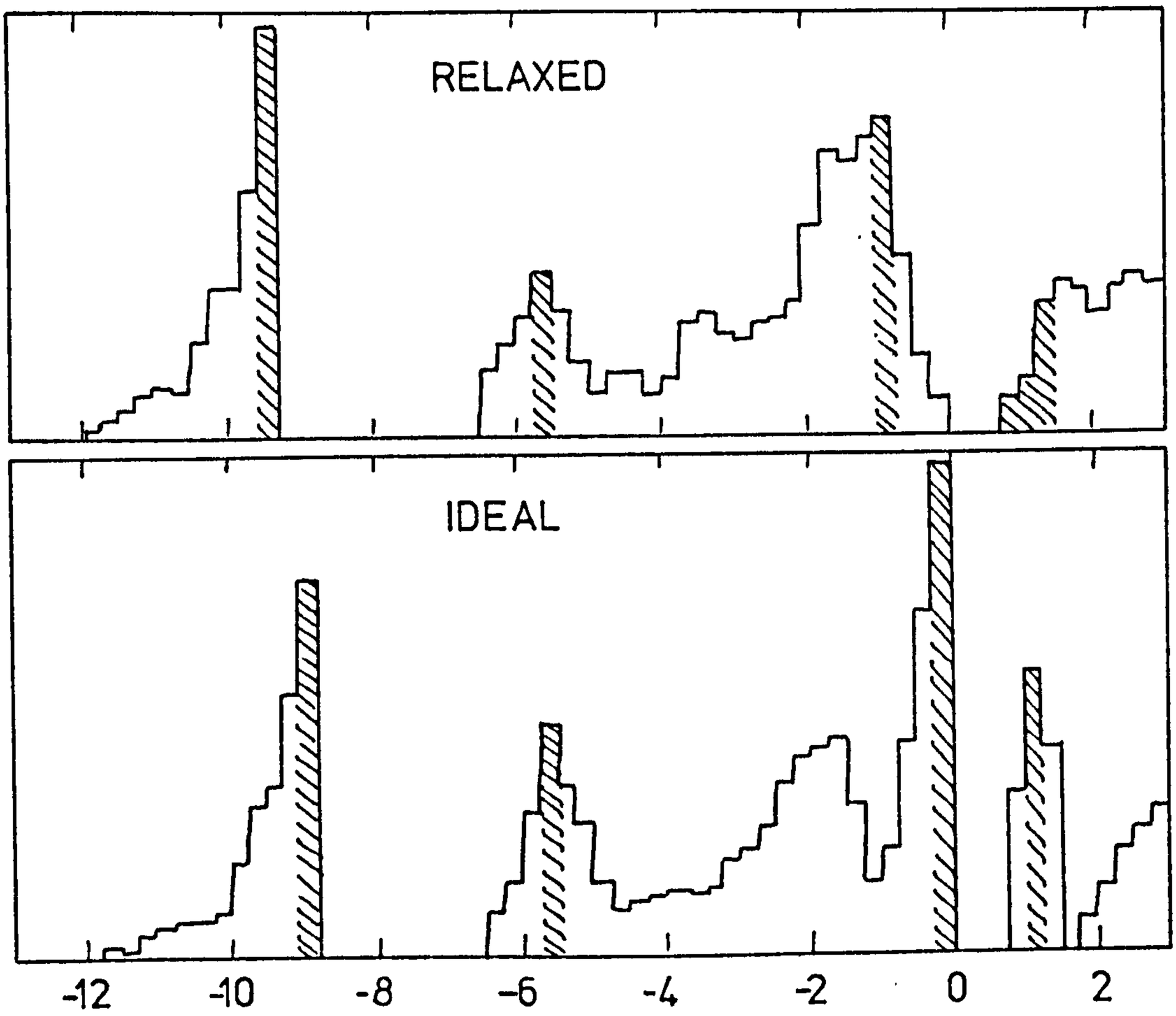

Figure 2.12. Local density of states of the outermost atomic layers of GaAs (110) for the ideal surface (Chelikowsky and Cohen 1976a) and relaxed surface (Chelikowsky et al 1976). Prominent surface states are indicated by the shaded areas.

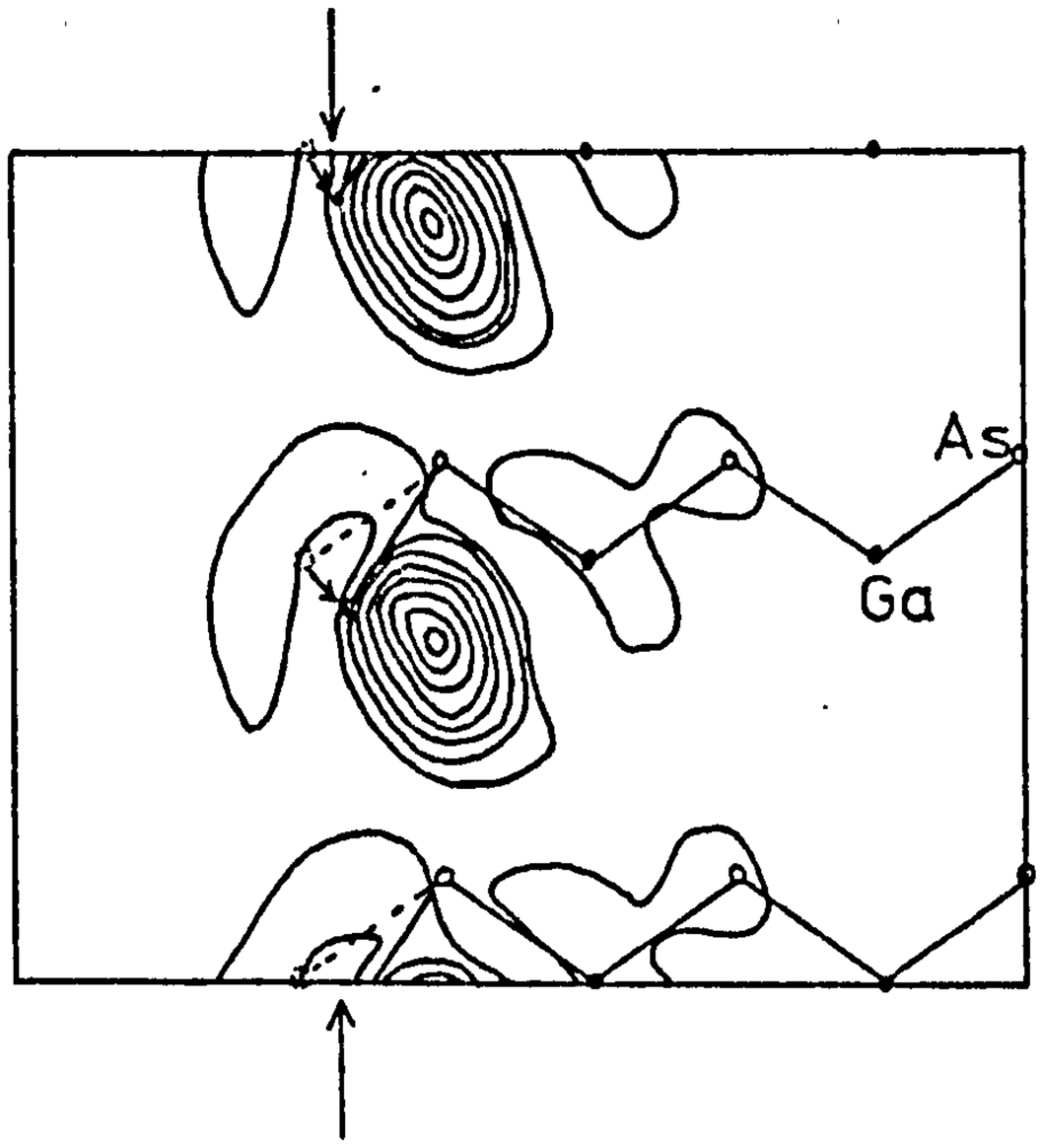

Figure 2.13. Charge density plot of the Ga dangling bond surface state on the GaAs (110) relaxed surface (Chelikowsky et al 1976). The surface plane is marked by the arrows and the relaxation of the surface Ga atoms is indicated. The contours are in units of two electrons per unit cell volume.

The Bond Orbital Method has been used (Gregory et al 1974) for GaAs, giving results which are shown in Figure 2.14.This model has many deficiencies : it is not specific to any particular surface plane, cannot be used to calculate charge densities, is unable to give more than a schematic view of the general distribution of the surface density of states, and is particularly poor for describing the empty surface states. Indeed the position of the empty surface band has been moved out of the bulk bandgap in recent publications of this model (Spicer et al 1976b, 1976c, Lindau et al 1977). This result is included here merely because its qualitative features have been extensively used by its authors -who refer to it as the GSCH model (Gregory-Spicer-Çiraci-Harrison) - to justify the derivation of a filled surface state band from the cation and an empty state from the anion. This particular association seems to have been well-established in earlier work by many authors, in particular Levine and co-workers (Levine and Mark, 1966, Levine and Davison 1968, Levine and Freeman 1970).

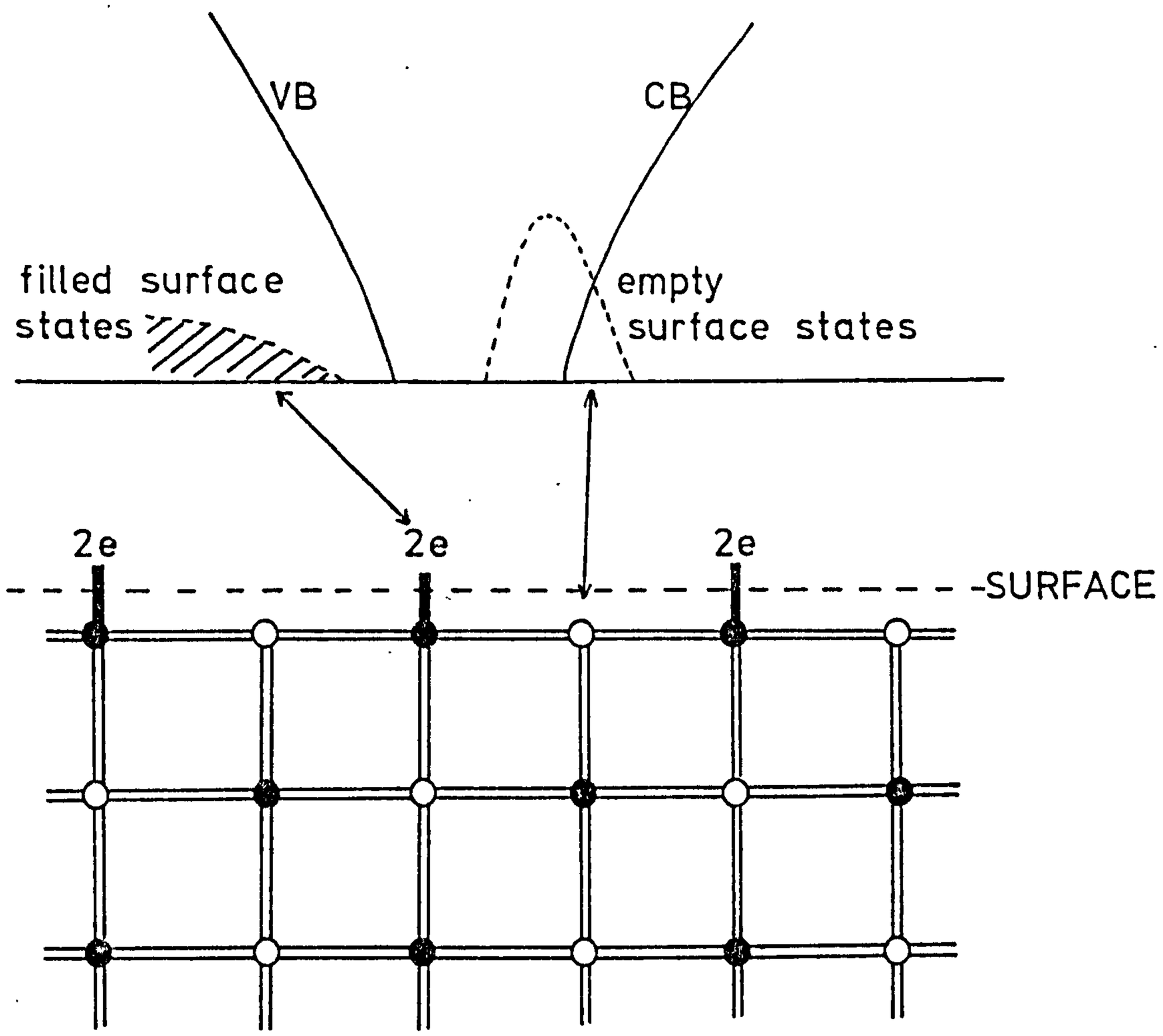

Figure 2.14. Model for the GaAs (110) surface indicating the association of the filled and empty intrinsic surface states with the surface As and Ga atoms respectively. The distribution and position of the surface bands is only schematic. From Spicer and Gregory (1975).

CHAPTER 3

ELECTRON SPECTROSCOPY

3.1. Ultra-violet photoemission spectroscopy (UPS)

Since its discovery in 1887 (Hertz 1887), the photoeffect has played an important part in advancing physical knowledge. It led Einstein (1906) to postulate his quantum theory of light. It was not until 1948, however, (Apker et al. 1948) that the relation between photoemission and the electronic structure of solids was recognized, and only in the last decade have reliable experimental data been produced and the fundamental processes become reasonably well understood. There are now a large number of reviews of UPS in the literature (e.g. Spicer and Eden 1968; Smith 1971; Eastman 1972; Spicer 1974; Abbati and Braicovich 1974; Feuerbacher and Willis 1976).

The basic process is simple (Figure 3.1). Light of energy $h\nu$ is incident on the sample; some proportion R (the reflectivity) is reflected from the surface but the remainder (1-R) is absorbed within the specimen. A photon gives up its energy to an electron with initial energy E_i, referred to the Fermi level. This electron is elevated into the conduction band; eventually, provided its energy is great enough, it may escape into vacuum and be detected.

For the III - V semiconductors considered here, the optical absorption coefficient α (for light of photon energy above the fundamental bandgap) is about $0.01\ \text{Å}^{-1}$ so the light penetrates approximately 100 Å. Values of electron mean free path against electron energy tend to lie close to a "universal curve" for all materials; two recent papers (Brundle 1974; Lindau and Spicer 1974) give extensive compilations and Figure 3.2 is derived from these references.

It can be seen from this figure that the hot-electron scattering length is very much less than the optical absorption length and so we can safely assume that all photons are absorbed and many of the electrons are scattered before being emitted. Thus UPS is a technique which is very sensitive to the surface, most of the electrons having been ejected from within the first few atomic layers.

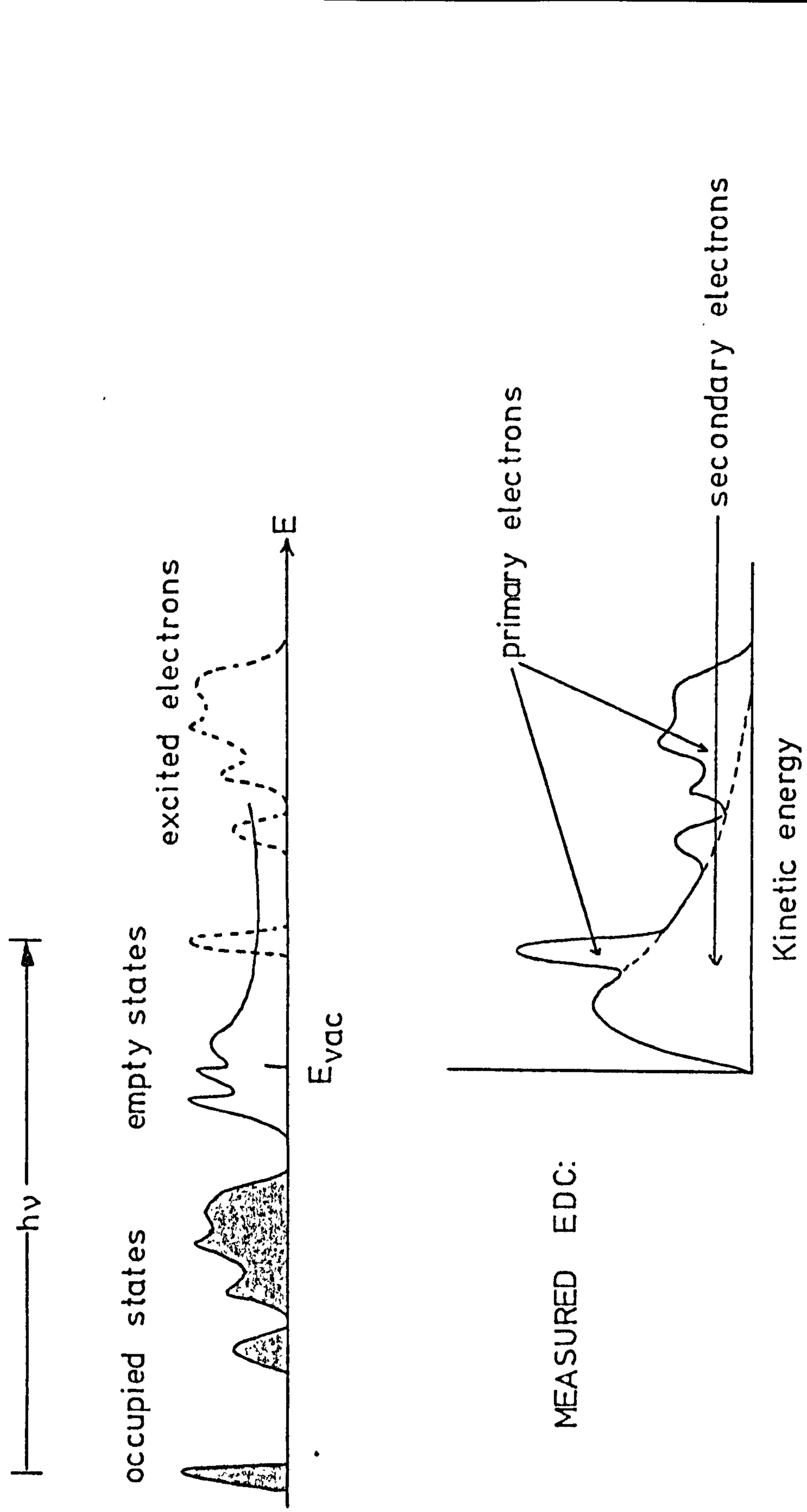

Figure 3.1. The photoemission process

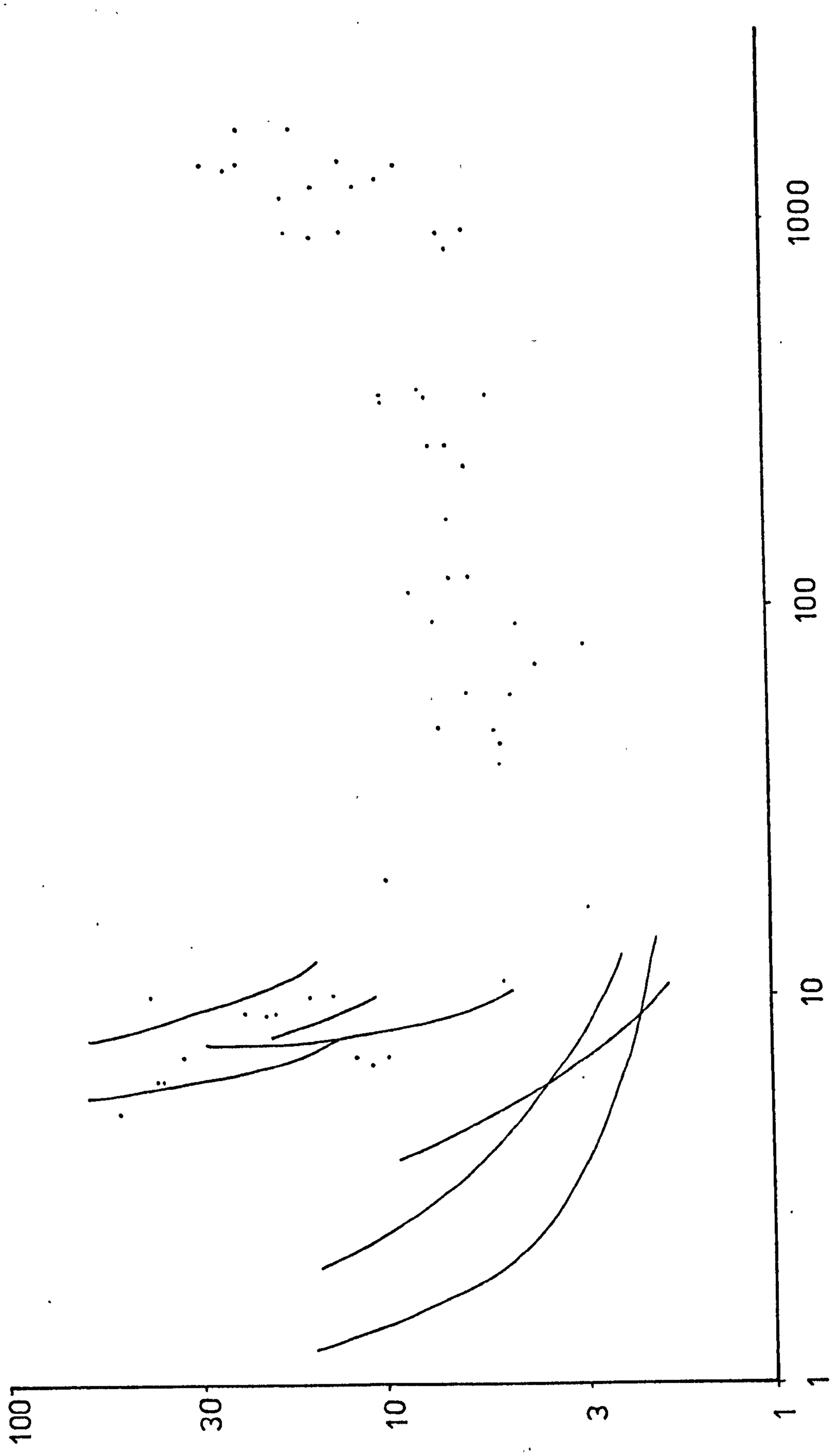

Figure 3.2. Compilation of values of electron mean-free-path versus energy for many materials.

It seems that almost all of the early workers on photoemission were obsessed with measurement of the photoelectric yield Y and the form of the curve of Y against hν near the photoelectric threshold (e.g. Gobeli and Allen 1966). It was thought from the theory of Kane (1962) and others, that the mechanism of emission could be determined from such a plot. Although some useful information can be gained from a curve of yield against photon energy, more informative is the electron energy distribution curve (edc), the spectrum of the number of electrons emitted versus their kinetic energies, E_{kin}, for a fixed hν. Thus an edc scans a range of initial energy levels E_i, and the edc gives some sort of reproduction of the initial density of states within the solid. Obviously the number of electrons emitted at a particular energy will be a complicated convolution of the probability of occupation of the initial energy level, the probability of finding a vacant energy level hν above E_i, and the matrix element for this transition :electron-electron and other forms of scattering will also affect the edc obtained. These, and other factors in the theory of UPS, will be considered in greater detail in Chapter 3.6.

It is now customary for solid state physicists to plot edc's in the form of n(E) vs E_i, which means that the zero of energy will be the Fermi energy, E_F, and initial energies are negative, referred to E_F. Of course, in a non-degenerate semiconductor, apart from electrons in the space-charge layer near the surface, the highest-energy electrons which can be emitted come from the top of the valence band, which is in general different from the Fermi level. A typical edc, for an evaporated film of gold, obtained in the course of this work, is given in Figure 3.3. Families of edc's, taken at different photon energies, are given in Chapter 5 to 7.

Two other ways of using photoemission have been developed recently, both prompted by the availability of synchrotron radiation. Lapeyre et al. (1974) have taken constant-initial-state (CIS) spectra to emphasize features in the normally unoccupied conduction band density of states. The CIS technique, in essence the same as was used by Brodén et al. (1973),

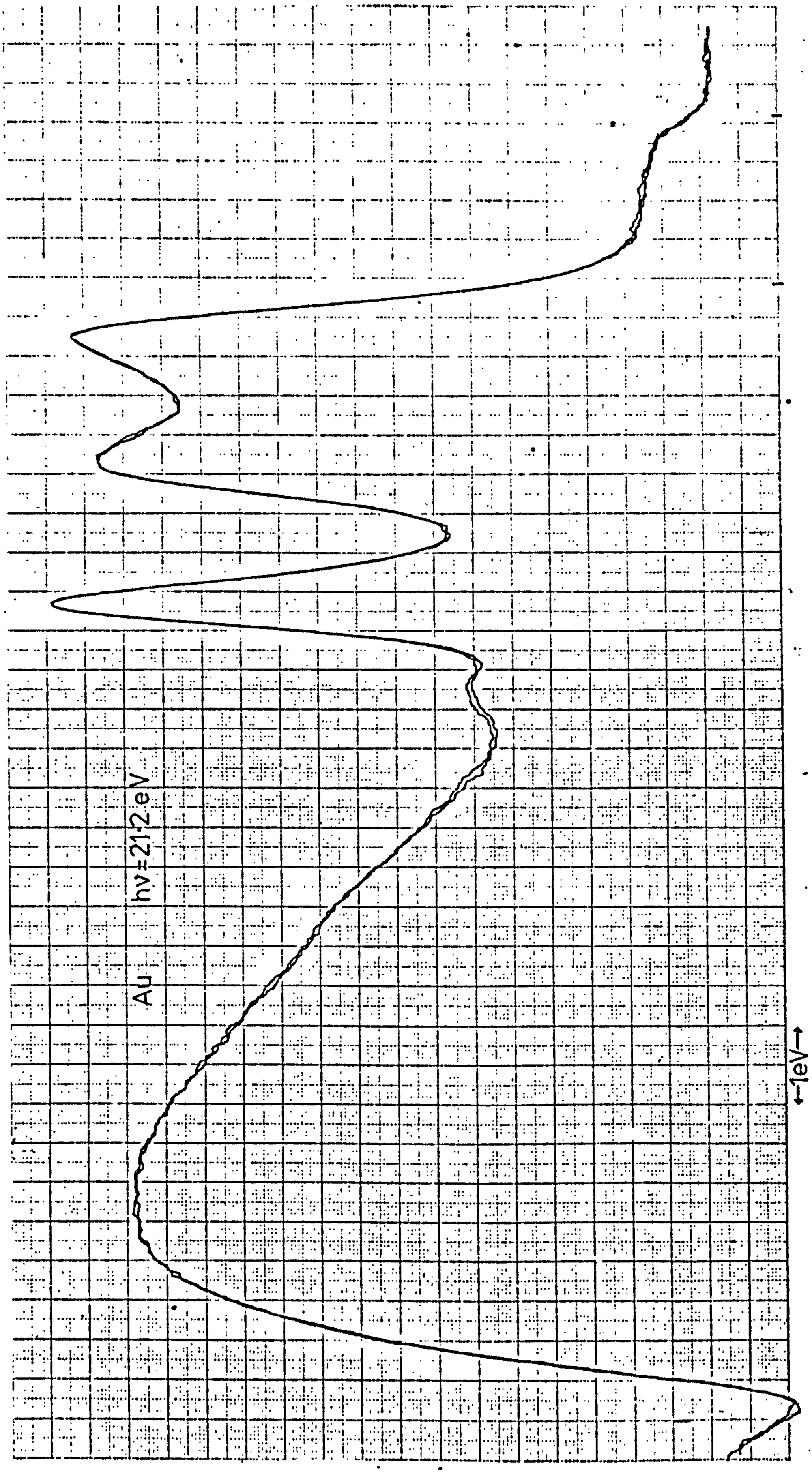

Figure 3.3. Energy distribution curve (edc) for an evaporated film of gold.

works by scanning photon energy hν and electron analyser energy E_f simultaneously so that $E_f - h\nu = E_i$ is held constant. A family of CIS's is obtained by scanning hν and E_f for different values of initial energy and E_i becomes the parameter which identifies a given CIS, as hν characterized an edc.

Partial yield distributions (PYD's) are measured similarly, by varying hν , but now E_f is fixed at a small value (a few eV) and the yield of secondary electrons is recorded as a function of hν (Figure 3.4). Eastman and Freeouf (1974) used PYD's to probe unoccupied states by exciting electrons from a core level to surface states or conduction bands, and observing the yield of Auger electrons produced in filling the core hole.

3.2. X-ray photoemission spectroscopy (XPS)

Traditionally the distinction between UPS and XPS has been that UPS has been confined to photon energies of the order of tens of eV, whereas XPS uses incident radiation with energies in the soft X-ray range -around 1keV. Apart from the obvious difference that many core levels can be revealed and the technique is not as surface-sensitive as UPS (from Fig.3.2), it has recently been realized that XPS can be utilized for valence band studies, and the data so obtained are usually more directly representative of the single electron bulk density of states than the UPS results. The reason for this is that at energies considerably above the Fermi level, the conduction bands become free-electron-like, and so, in a reduced-zone picture, the number of available final states increases as $\sqrt{E}$, and also the initial hole is strongly localized, i.e. momentum-broadened, and hence the probability of exciting electrons into final states from all initial states is greatly increased. This "X-ray limit," which will be discussed somewhat further in Section 3.6 , has been found to occur at a photon energy around 30eV in gold, from one much-published experiment (Freeouf et al. 1973; Feibelman and Eastman 1974; Eastman 1974) , and a similar value has been found for a large number of metals (Cu, Ag, Ni, Pd, Pt and Ti) (G.P.Williams and C.Norris, personal communication). With the increasing use of synchrotron radiation as a

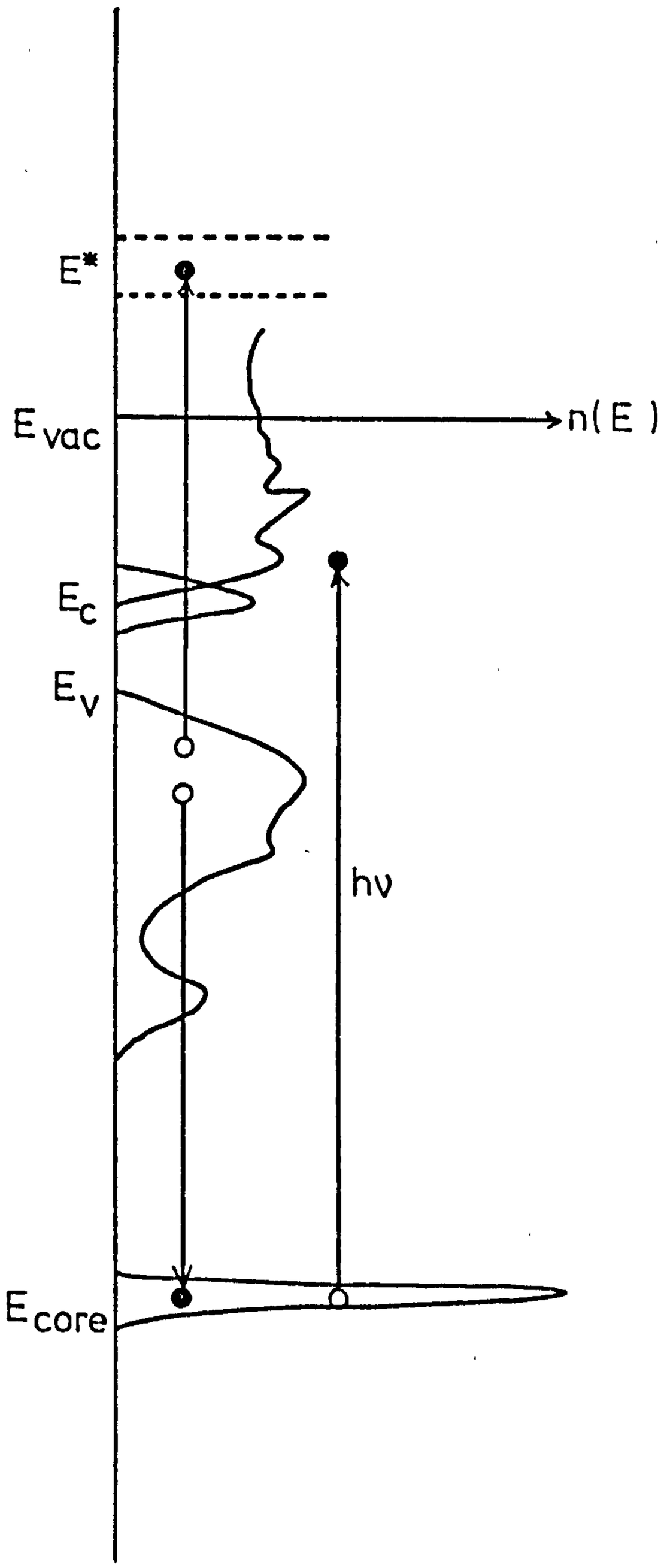

Figure 3.4. Mechanism of the photoemission partial-yield process . An electron is excited from the core level to an empty state below the vacuum level. The core hole is filled by an electron from the valence band and an Auger electron emitted. The emitted yield (in a selected energy range) is recorded as a function of photon energy.

photon source, and the consequent invalidity of the traditional distinction between UPS and XPS, (their discrete and very different exciting sources), this X-ray limit will probably be adopted as the dividing-line between UPS, sampling band structure and matrix elements, and XPS, sampling valence band and core density of states.

Emission from core levels, which are characteristic of particular elements, is useful for identification of contaminant or adsorbate species, and also the "chemical shift" is indicative of changes in bonding of compounds and adsorbates (Park and Houston 1973; Langer 1973; Shirley 1975; Pierce 1975). Siegbahn et al (1967) and many subsequent workers, have observed small differences - up to a few eV - between the binding energy of a particular core level in the elemental form, and in compounds of the element. This chemical shift, which led to Siegbahn's acronym ESCA (Electron Spectroscopy for Chemical Analysis), reflects changes in the coulombic interaction between valence and core electrons and it is therefore sensitive to the spatial distribution of the outer electronic wavefunctions.

3.3. Auger Electron Spectroscopy (AES)

Although Auger electrons were first observed half-a-century ago (Auger 1925), and their possible use as a tool for surface analysis pointed out in 1953 (Lander), only recently has AES been developed for routine use. It is now probably the most widely used electron spectroscopic technique for surface analysis, and review articles proliferate (e.g. Chang 1971; Palmberg 1971; Gallon and Matthew 1972; Rivière 1973).

The Auger process is not particularly simple; a hole is formed in one of the inner (core) levels of the material, and an electron drops down to fill this hole, from some level higher in energy, either a less-tightly bound core level or the valence bands; the energy released by this electron is transferred to another electron, which may then be energetic enough to be ejected from the solid. (Of course this process can occur just as readily in

gases or liquids and the problem of theoretical interpretation is obviously more tractable for atoms). The initial hole may be created by any particle of sufficient energy (ion, electron, or photon), but AES is now almost invariably performed with an incident beam of high-energy (typically 2.5 keV) electrons.

The only process competing with the Auger effect in the de-excitation of core holes is the emission of X-ray photons; but the X-ray yield is considerably less than one-tenth of the Auger electron yield for all elements of the first two rows of the periodic table (up to Argon). This includes almost all the common surface contaminants, and so the Auger effect is useful for identification of surface elements.

The notation adopted by practitioners of this spectroscopy must be explained. An Auger electron is denoted by the expression $W_p X_q Y_r$, where W is the level of the initial hole, in X-ray notation (K, L, M, N...), X is the level from which the electron dropped into the initial hole, and Y the level of the electron which is emitted. The suffices p, q and r represent the quantum numbers in the usual way, e.g. $L_1 \equiv 2s$, $L_2 \equiv 2p_{\frac{1}{2}}$, $L_3 \equiv 2p_{\frac{3}{2}}$ etc.. X and Y, or Y only, may be levels in the valence band, in which case the transition is denoted by, for instance, $W_p VV$ or $W_p X_q V$, the suffix on V usually being dropped. Obviously the Auger peak for a WXV transition will be as wide as the valence band (typically 12eV for a III-V compound); we should expect the structure of the peak to be similar to the valence band density of states. Likewise the width of a WVV Auger peak will be twice the width of the valence bands, and it may be expected to have a shape corresponding to some complicated self-convolution of the valence band density of states. However, there is another important factor contributing to the width of all Auger peaks, not just those involving the valence bands: "lifetime broadening." All Auger transitions occur very quickly, 10^{-16} s being a normal time. Hence, since $\Delta E \, \Delta t = \hbar$ we obtain a peak with ΔE of the order of 6eV. Transitions of the form $W_p W_q Y_r$, known as Coster-Kronig transitions, where the initial hole is filled by an electron with the same total momentum,

but greater angular momentum , occur even more quickly than standard Auger transitions, and thus the peaks have a greater width: several tens of eV is typical.

It is, in principle, easy to calculate the expected values of energy of Auger electrons. Using the well-known atomic energy levels (Bearden and Burr 1967; Sevier 1972), for an atom of atomic number Z

$$E_{WXY}(Z) = E_W(Z) - E_X(Z) - E_Y(Z) \qquad (3.1.)$$

The work function must be subtracted from this energy for emission from a solid, but a more fundamental correction also has to be applied. Once the hole has been created, re-distribution of the Coulomb field in which the electrons move takes place. The consequent shift in the energy levels means that binding energies for excited atoms must be used. Several approximations have been suggested, but a simple expression due to Chung and Jenkins (1971) has been found to give sufficiently accurate values for the energies of Auger electrons in most cases. The binding energies of levels X and Y are replaced by the mean of E(Z) and E(Z + 1) to give

$$E_{WXY}(Z) = E_W(Z) - \tfrac{1}{2}(E_X(Z) + E_X(Z+1)) - \tfrac{1}{2}(E_Y(Z) + E_Y(Z+1)) \qquad (3.2.)$$

3.4. Electron Energy Loss Spectroscopy (ELS)

When a beam of mono-energetic electrons is incident on a surface, the curve of the number of backscattered electrons versus their energy has the form shown in Figure 3.5. This spectrum, with electrons of energy $E_p = 100$ eV , was obtained on a GaP (110) surface, as detailed in Chapter 5.6. The peak at low energy is due to secondary electrons created as a result of inelastic collisions between the primary (incident) electrons and the electrons bound within the solid. In each collision only a small amount of energy is transferred, so a single primary electron can create several secondary electrons.

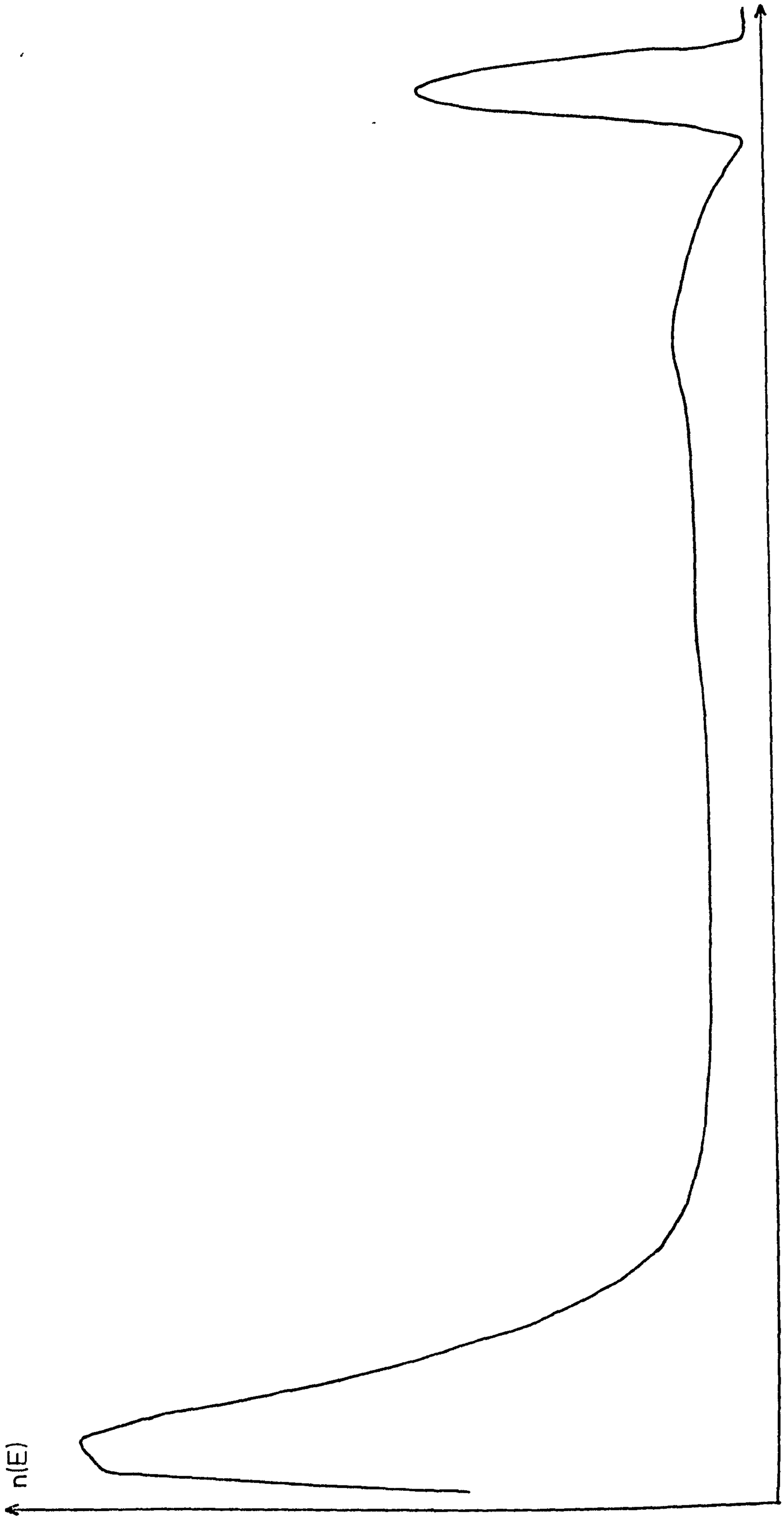

Figure 3.5. Spectrum of backscattered electrons from GaP at an initial electron energy of 100 eV

A small fraction of the primary electrons, typically a few per cent, is backscattered from the surface elastically, without suffering any noticeable energy loss. This is shown in the high-energy sharp peak in Fig.3.5. These electrons are used in LEED, to be described in Chapter 3.5.

The central portion of the energy distribution consists of a smooth background on which small peaks are superposed. Some of these peaks are due to emission of Auger electrons: these appear at fixed emission energies irrespective of the primary electron energy. The remainder of these small peaks is due to characteristic energy losses of the primary electrons due to single and collective excitation of the electrons within the solid: these peaks appear at fixed loss energies, and thus move synchronously with E_p as the primary energy is varied.

The different types of loss process which can occur may be divided into four categories.

(i) Excitation of core electrons. The primary electrons may interact with a core electron of a surface atom and transfer to it an amount of energy which is sufficient to ionize the atom by exciting the core electron to an unfilled state above the Fermi level. The magnitudes of the energy losses are determined by the binding energies of the core level electrons and thus are in the same range as the energies of Auger electrons.

(ii) Excitation of surface vibrations. The primary electrons may lose a small amount of energy (fractions of an eV) by phonon-assisted inelastic scattering. These electrons cannot normally be resolved from the true elastic peak.

(iii) One-electron excitations of valence electrons. An electron in the valence band of a solid may be excited to a higher (empty) level of the same band- an intraband transition- or into another energy band- an interband transition. More complicated transitions can occur if chemisorbed atoms are present, since additional electronic states at the surface, or levels within the absorbate itself, may be involved. The energy losses of the primary

electrons associated with these processes are typically of the order of 2 to 20e V. The excited electrons themselves have a small probability of escaping from the solid to appear in the broad secondary electron peak.

(iv) Collective excitations of valence electrons. This process, the excitation of plasmons, is the most important of the possible energy loss mechanisms. Plasmons are oscillations of the free-electron-like gas within the solid; that is, the conduction electrons.

The frequency ω_p of the undamped plasma oscillation of a free electron is given by

$$\omega_p = \left(\frac{4\pi ne^2}{m^*}\right)^{\frac{1}{2}}$$

where n is the density of the electrons, m* their effective mass and e is the electronic charge. For solids which are not well-approximated by the free-electron theory, ω_p is shifted from the value given by the above formula. It is also possible for surface plasmons to be excited. The theory of surface plasmons was established by Ritchie (1957) who demonstrated that the frequency of a surface plasmon (ω_s) depends on the dielectric constant ϵ of the medium outside the solid and is related to the bulk plasmon frequency by the formula

$$\omega_s = \frac{\omega_p}{\sqrt{1+\epsilon}}$$

For a solid-vacuum interface, $\omega_s = \omega_p/\sqrt{2}$ but if an adsorbed layer is on the surface, with $\epsilon > 1$, then ω_s will be decreased. Energies for plasmon oscillations are usually in the range 5 to 50 eV, with ω_p for many solids being between 10 and 20 eV. Provided there are not too many other competing mechanisms, multiple plasmons, at frequencies $2\omega_p$, $\omega_s + \omega_p$, etc. may be excited.

It is evident that plasmon losses, and indeed any of the other characteristic energy losses, may be undergone not only by primary electrons with energy E_p, but also by any other electron with sufficient energy. For instance, plasmon losses are frequently observed as satellites of Auger peaks, and have also been seen in UPS.

3.5. Low Energy Electron Diffraction (LEED)

The classic experiment by Davisson and Germer (1927) showed that electrons are associated with waves, in accordance with the hypothesis of de Broglie. The wavelength is related to the electron energy (in eV) by the expression

$$\lambda = \sqrt{\frac{150}{E}} \quad \text{Å}$$

so that electrons with an energy around 100eV have a wavelength of about 1.2Å , of the order of the lattice spacing in a solid surface. Thus those incident electrons which are elastically scattered may be diffracted by the periodic arrangement of the surface atoms into discrete beams. This is the basis of LEED.

Because the electron-electron scattering length is so small (Figure 3.2.) LEED is particularly sensitive to the atomic layers at, and very near to, the surface: LEED is thus the two-dimensional analogue of X-ray crystallography. A comprehensive notation has been developed of the many types of surface structure which may be encountered. Most of these structures are well described in the review articles by MacRae and Gobeli (1966), Prutton (1971), Mitchell (1973) and Duke (1973). However, the complications of nomenclature need not concern us here, since the cleavage planes of III-V semiconductors are not reconstructed, and the surface is known as a (1x1) structure. This means simply that the unit mesh of the surface atoms has the same dimensions as the projection of the bulk unit cell onto that plane.

Although the (110) surfaces of the III-V semiconductors are not reconstructed, it has been recognized from the earliest experiments(Macrae and Gobeli 1964, 1966) that the periodicity perpendicular to the surface is not maintained. It is not normally possible to infer this just from one LEED pattern but in this case two factors suggest this perturbation : the extreme asymmetry in the intensity of the hk and $h\bar{k}$ beams and the strong intensity of the 10 and $\bar{1}0$ beams from both GaAs and InSb. If there were no displacement of the positions of the atoms in these materials and if their scattering factors

were similar -which might be expected for atoms of comparable atomic number - the 10 and $\bar{1}0$ spots would be very weak, since the scattering from the rows of surface atoms defined by the A and B atoms would be out of phase (see Figure 2.4). The asymmetric intensities of the hk and $h\bar{k}$ beams also indicate that the group III and group V atoms in the surface layer are displaced with respect to each other in a horizontal or vertical direction. However, since no LEED spots are seen corresponding to a superstructure of some integral multiple of the { 110 } unit mesh, the dimensions within a bulk plane must be preserved. The relative incompressibility of the mainly covalent bond in these compounds suggests that bond angles may be altered but bond lengths remain the same.

It is possible to obtain information on the surface structure by studying the dependence of the intensity of various LEED beams on the voltage of the incident electrons, but the analysis is complex and often controversial. Such an analysis has recently been performed for GaAs (110) (Lubinsky et al 1976, Duke et al 1976). The agreement between experiment and theory is not good, even by the standards of LEED intensity calculations, but the best fit to the experimental data was found with the As atoms rotated outward by 34.9^{o} and the Ga atoms similarly rotated inwards to achieve the closest possible approach to the planar sp^2 coordinated position, as suggested earlier (Levine and Freeman 1970, Rowe et al 1975). The most interesting feature of this calculation from the point of view of surface electronic structure is that the separation between the bands of surface states derived from the anion and cation is greatly increased, and both filled and empty states are removed from the vicinity of the bulk bandgap. (A.R. Lubinsky, personal communication). Since the LEED patterns (although not the intensity-voltage plots) of the (110) faces of all III-V semiconductors are similar, we may expect this model to apply to GaP and InP as well.

3.6. Theories of UPS

There have been many different approaches to the theory of UPS, but review articles (Gadzuk 1975; Feuerbacher and Willis 1976) have shown

that all recent single-electron theories give equivalent expressions for the energy- and angle-resolved photocurrent, namely

$$\frac{d^2j}{dEd\Omega} \quad \alpha \quad \sum_i \left| < E_f \mid H \mid E_i > \right|^2 \quad \delta \, (E - E_i - h\nu) \qquad (3.3.)$$

Here H is the Hamiltonian coupling initial states, with energy E_i, to final states with energy E_f, the sum is taken over all occupied states, and the δ-function establishes the energy selection rule. All contemporary theoretical work is aimed at finding how eq.(3.3) can best be expressed to facilitate calculation of theoretical predictions and aid comparison with experimentally-determined results, including in particular scattering and surface effects (e.g. Caroli et al. 1973; Feibelman and Eastman 1974; Pendry 1976).

Before examining some of these recent methods in detail it is instructive to consider the "three-step" model of photoemission which has enjoyed a virtual monopoly in the interpretation of UPS results over the past ten years. This model, developed by Berglund and Spicer (1964) following earlier work by Mayer and Thomas (1957) and Fan (1945), views the photoemission process in three parts: (1) optical excitation of an electron within the material; (2) transport of the electron to the surface; and (3) escape into vacuum. Each of these stages is dealt with below.

(1) Optical Excitation

The absorption of photons in a material proceeds according to the formula

$$P\,(x, h\nu) = \alpha\,(h\nu)\, \exp\,(-\alpha x).$$

Here P is the probability that a photon will have been absorbed within a depth x of the solid, and α is the absorption coefficient. The photons are absorbed by exciting electrons to higher energies, and we may define an internal energy distribution of photoexcited electrons $N_{int}(E, h\nu)$, where E is the final energy of the excited electron. The form of $N_{int}(E, h\nu)$ is intimately related to the band structure of the solid. Two alternative approaches have been proposed: direct transitions and "non-direct" transitions.

In simple band theory, optical interband (direct) transitions occur only between states with the same reduced $\underline{k}$ vector. If $E_f(\underline{k})$ and $E_i(\underline{k})$ denote the energies in a final band f and an initial band i, the condition $E_f(\underline{k}) - E_i(\underline{k}) = h\nu$ must also be satisfied. The internal energy distribution is then given by

$$N_{int}(E, h\nu) \alpha \sum_{f,i} \int d^3k \left| P_{fi} \right|^2 \delta(E_f(\underline{k}) - E_i(\underline{k}) - h\nu) \times \delta(E - E_f(\underline{k}))$$

where $\left| P_{fi} \right|^2$ is the square of the momentum matrix element between the states $|f>$ and $|i>$ and is a measure of the strength of the optical transition. The first δ-function imposes the energy- and $\underline{k}$-conservation restrictions, and the second δ-function selects the transitions with final energies equal to the specified E.

However, a phenomenological relation, which has worked surprisingly well in some cases, completely ignores the $\underline{k}$-conservation selection rule and considers just the energy conservation. In this non-direct case, the internal distribution is given by a product of initial and final density of states,

$$N_{int}(E, h\nu) \alpha \rho(E-h\nu) \rho(E)$$

The $\rho(E)$ involved here may not be the same as the electronic density of states, since this function should be weighted by some function which expresses the varying probability of optical excitation. The success of this type of non-direct explanation led to speculation, notably by Spicer (1967), on possible mechanisms beyond one-electron theory which could bring about the violation of $\underline{k}$ - conservation. Localization of the hole left behind by the excited electron has been investigated in this context (Doniach 1970).

The non-direct model predicts that structure in an edc will move linearly in energy with a change in photon energy; $\Delta E = \Delta h\nu$. But the conventional direct-transition theory gives no such simple prediction. Because changing $h\nu$ involves moving through $\underline{k}$-space, and since bands are not generally flat, $\Delta E \neq \Delta h\nu$. Also, we should expect peaks in the edc to appear or disappear

rather sharply as hν is changed, as the corresponding transitions become permitted or forbidden. For several years, there was much controversy over which model was correct, and many of the papers on UPS in the late 1960's are devoted to discussion of this important point.

This question seems to have been resolved satisfactorily in favour of the direct optical transition model. Although the early work on noble metals, copper, silver and gold, gave results which apparently could be interpreted well in terms of non-direct transitions, the edc's were taken only over a narrow range of photon energy where the curves were dominated by the prominent d-bands of these metals, which are relatively flat in $\underline{k}$-space. Further work over an extended range of energies gave results which could be satisfactorily explained only by invoking direct transitions.

This is not meant to imply that direct transitions account for all the observed photoelectrons . There may be a contribution due to electrons excited by the mechanisms (Spicer 1967) which violate the $\Delta\underline{k} = \underline{0}$ rule. And it is certain that a large fraction of the photoemitted electrons is excited from the surface layer. Obviously $\underline{k}$ is not a good quantum number for such a process.

(2) Transport to the surface

Before the photoexcited electron can reach the surface and escape, it suffers a high probability of being scattered. The dominant scattering mechanism is the electron-electron interaction, whose strength may be represented by an energy-dependent lifetime τ . To a first approximation the scattering frequency τ^{-1} is proportional to $(E-E_F)^2$ and the hot electron mean free path is given by $\ell(E) = \tau v_g$ where v_g is the group velocity of the final state. The subject of the electron's transport to the surface was treated in detail by Berglund and Spicer (1964) in the manner of the classical kinetic theory of gases.

The final result is an expression for the "transport function," the probability that an electron will travel from the position in which it was

photoexcited to the surface without scattering, of the form

$$T(\alpha, \ell) = A \frac{\alpha\ell}{1+\alpha\ell}$$

Here A is a geometrical factor which is slowly varying and takes values between $\frac{1}{2}$ and 1. Clearly the dominant term containing the scattering effects is $\alpha\ell/(1+\alpha\ell)$. The basic physics behind this expression is readily seen by considering the two extremes: when $\alpha\ell \gg 1$, the mean free path ℓ is much greater than the photoabsorption depth, so $\alpha\ell/(1+\alpha\ell) \rightarrow 1$ and all electrons propagating towards the surface will reach the surface without scattering. When $\alpha\ell \ll 1$, $\alpha\ell/(1+\alpha\ell) \rightarrow \alpha\ell$, which is the fraction of the total photoexcited electrons lying within ℓ of the surface. This is the fraction which can escape without scattering.

This treatment is greatly over-simplified, however. The mean free path ℓ has been assumed to be a function only of E. Clearly for real band structures ℓ will also be dependent on $\underline{k}$ via the group velocity v_g. Also, it has been assumed that the only form of scattering is inelastic electron-electron scattering, wherein the energy of the photoexcited electron is reduced below the vacuum level, and thus it will not be able to escape. Elastic scattering will have the effect only of altering the direction of propagation, without any loss of energy, but it is possible for an electron which has lost some energy through inelastic scattering still to have sufficient energy to reach the surface. Furthermore, other scattering events, such as electron-phonon, and electron-ion have not been included.

(3) Escape into Vacuum

. We shall here ignore scattering on the way to the surface and show that only electrons which have a component of kinetic energy normal to the surface which is greater than the potential barrier can actually escape. This condition was introduced, without any accompanying justification, by Fowler(1931), but it is easily explained by considering free electrons in a potential well (Smith 1971). If $\underline{k}$ is the wavevector of a plane wave electron excited within the solid, and $\underline{k}'$ is its wavevector outside the solid, then the kinetic energies

inside and outside the solid are related by

$$\frac{\hbar^2}{2m} \left|\underline{k}'\right|^2 = \frac{\hbar^2}{2m} \left|\underline{k}\right|^2 - W$$

where W is the depth of the potential well. With the z-direction perpendicular to the surface, conservation of k parallel to the surface gives

$$\frac{\hbar^2}{2m} k_z'^2 = \frac{\hbar^2}{2m} k_z^2 - W .$$

Thus, for the electron to escape,

$$\frac{\hbar^2}{2m} k_z^2 \geq W \qquad (3.4.)$$

If θ is the angle between $\underline{k}$ and the surface normal then eq. (3.4.) becomes

$$\cos\theta = \frac{k_z}{k} \geq \left(\frac{W}{E}\right)^{\frac{1}{2}} \qquad (3.5)$$

where $E = \hbar^2 k^2/2m$, the kinetic energy inside the solid.

Eq. (3.5) defines a cone, the escape cone, of solid angle $2\pi \left[1 - \left(\frac{W}{E}\right)^{\frac{1}{2}}\right]$.

It is normal to lump together several of the terms in the "three-step" model, and it is easy to produce an expression for the probability, T (E, $h\nu$), that a photon excites an electron which is initially heading for the surface with enough energy to escape and does not scatter on its way there :

$$T(E, h\nu) = \frac{\alpha\ell}{1+\alpha\ell} \cdot \frac{1}{2} \cdot \left[1 - \left(\frac{W}{E}\right)^{\frac{1}{2}}\right] .$$

An expression of this type has been derived by, for example, Janak et al. (1970) and Alward and Fong (1975). A formula for edc's may be similarly obtained from the "three-step" model :

$$n(E\ ,\ h\nu\ )\ \alpha \sum_{f,i} \int \delta\ (E_f - E_i - h\nu)\ \left| P_{fi} \right|^2 \delta\ (E_f - E)\ T(E_f, h\nu)\ d^3k.$$

The "three-step" model has been extensively used, and many good results have been obtained, of which perhaps the most striking are those of Janak et al (1975) for edc's from polycrystalline copper at nineteen photon energies from 8eV to 26eV. But Grobman and co-workers have found that it gives poor agreement for the cleaved faces of semiconductors (Grobman et al (1974), Grobman and Eastman (1974), Grobman (1975), Grobman et al (1975)). The factor which appears to be most at fault is the assumption of isotropic propagation of photoexcited electrons within the solid. In fact the different final states in step (1) of the photoemission model have very different directions of propagation. For example, a final state with group velocity nearly perpendicular to the surface will have a short path to the surface and thus a much smaller chance of scattering than one travelling at a greater angle to the surface normal. Also, the wavefunction of the final state may have plane wave components which contain momentum normal to the surface sufficient to surmount the surface potential step, an effect which can be incorporated in step (3) of the model. Such an optical transition would then lead to a strong photoemission peak, while one whose final state did not possess these properties would be much attenuated in the experiment, and might not even be observed if it happened to overlap the tail of another large peak.

Grobman and co-workers have used their anisotropic-emission, direct transition theory on the cleaved (111) surface of Ge, and obtained a spectacular improvement on the predictions of the standard isotropic theory. However, they state that experimental results on emission from different faces of single-crystal silver and copper (Nilsson and Eastman (1973), Rowe and Smith (1974)) were not well described by simplified anisotropic models. They speculate that this is probably due to "the different specular/diffuse nature of a metal surface compared with a cleaved semiconductor" : this is difficult to understand. It is true that the great majority of the

experiments performed on perfect single-crystal surfaces have been on cleaved semiconductors. Single-crystal metal surfaces are notoriously difficult to clean perfectly in such a way as to maintain perfect stoichiometry, and it may be that surface scattering destroys some of the anisotropy of emission which should be observed.

It is of interest to note that the differences between the isotropic and anisotropic models should be greatly emphasized by angularly-resolved photoemission experiments. The recent prolliferation of such experiments should lead to a refinement of this model.

We now return to the various attempts to produce a full quantum-mechanical theory of photoemission, as opposed to the semi-classical "three-step" model. Such theories seem to have been prompted by the work of Schaich and Ashcroft (1970, 1971 and Ashcroft and Schaich 1969), and Mahan (1970). Schaich and Ashcroft noted that the photocurrent emitted has been observed to be linearly proportional to the intensity (I) of the radiation illuminating the sample, over at least eight decades of intensity, and thus constructed a linear coupling term between the vector potential ($\underline{A}$), representing the electromagnetic radiation, and the electron current within the sample. They then sought a response of the system which was quadratic in this vector potential (since $I \propto |\underline{A}|^2$) and showed that the photocurrent can be expressed exactly in terms of a correlation function between three electronic current-density operators. Hermeking (1973) produced a decoupling scheme for this three-current correlation function. Mahan (1970) gave a microscopic formulation of the photoemission process for an electron gas in the presence of a one-electron lattice potential and obtained the first results for the angular dependence of photoemission from free-electron-like metals. Neither of these approaches included scattering, except indirectly as a mean free path in the excited state in the final result for the current. Such a scattering term is inevitably elastic but inelastic scattering has been thoroughly discussed by Caroli et al. (1973). Ashcroft (1974) points out that scattering effects are clearly very important in volume photoemission and their proper inclusion into the theory remains the central difficulty.

A very interesting method, adopted by several authors, follows from LEED theory. Whereas LEED theory is concerned with the amplitude of reflected beams of electrons, photoemission in effect samples the transmitted components. The photoemission process may be regarded, therefore, as a time-reversed LEED process, in which the transmitted beams represent those internal Bloch waves which contribute to emission in the direction of the incoming beam in LEED. This method looks particularly promising because the large computer programmes necessary for calculation of wavefunctions already exist, having been developed for, and tested in, the multiple scattering theory of LEED (Pendry 1974). However, it must be noted that these wavefunctions have been calculated for electrons with energies in the approximate range 30 to 300 eV. The present theory should apply to higher energies than this, although the number of phase shifts required in the calculation is prohibitive, but it appears doubtful whether the approximation of LEED multiple-scattering theory will permit the calculation of continuum wavefunctions for $0 < E \leq 30eV$. The main problem is the extent to which the surface potential barrier must be described self-consistently in this lower energy range.

Using this formalism, Feibelman and Eastman (1974) derived an expression of the form of Eq.(3.3), for the angle- and energy- resolved photocurrent density $j(\hat{R}, E, h\nu)$ from an independent-particle solid

$$R^2 j(\hat{R}, E, h\nu) = 2ev \left(\frac{e}{2mc}\right)\left(\frac{m}{h}\right)^2 \sum_{\substack{\text{occupied} \\ j}} \delta(E - E_j - h\nu) \left| \int d^3r \; \Phi^*_{>}(\underline{r}, \hat{R}, E) \hat{O}(\underline{r}) \psi_j(\underline{r}) \right|^2 \qquad (3.6.)$$

Here $\hat{R}$ is a unit vector in the direction of the detector at a distance R from the surface, v is the outgoing electron velocity ($\equiv \sqrt{2E/m}$), $\psi_j(\underline{r})$ are the occupied eigenstates with energies E_j for the semi-infinite solid, $\hat{O}(\underline{r})$ is the usual dipole operator and $\Phi_{>}(\underline{r}, \hat{R}, E)$ is the wavefunction of the final state electron of energy E emitted in the direction R. $\Phi_{>}$ is in fact identical to the incoming, time-reversed, LEED wavefunction; that is, to the wavefunction suitable for a LEED experiment in which electrons of energy E impinge on the surface along the direction -R. All aspects of the photoemission

process, optical excitation, transport, and escape, are included in the matrix element $\left| < \Phi_> | \hat{O} | \psi_j > \right|^2$ of equation (3.6.). This equation resembles the familiar Fermi's Golden Rule formula of quantum mechanics. A similar expression was derived by Adawi (1964) for photoexcitation at a surface.

It is of interest to consider the effect of the dipole operator $\hat{O}$ ($\underline{r}$). We have

$$O(\underline{r}) = \tfrac{1}{2} \{ \underline{A}(\underline{r}) \cdot \underline{p}(\underline{r}) + \underline{p}(\underline{r}) \cdot \underline{A}(\underline{r}) \} \qquad (3.7.)$$

where $\underline{A}$ is the total vector potential corresponding to the incident electromagnetic radiation (the photon field) and $\underline{p}$ is the electron momentum operator. Calculations of photoemission from gases retain only the first term of Eq. (3.7.), in the matrix element, since $\nabla \cdot \underline{A} = 0$ everywhere in a medium with constant dielectric properties. This is true for a solid at high enough frequencies, where the refractive index is unity, and the photon field may be represented by a transverse plane wave, appropriately polarized, which is undisturbed by its crossing of the solid surface. However, for a wide variety of solids, especially at low frequencies ($\lesssim 30$ eV) the index of refraction is far from 1, and the amplitude and phase of an electromagnetic wave will change rapidly within a few Angstrom units of the surface. Thus the commutator $\left[\underline{p} , \underline{A} \right] \neq 0$ and we expect the $\underline{p} \cdot \underline{A}$ term to contain surface-specific information. The calculation by Feibelman (1975) shows the violent oscillations undergone by $\underline{A}$ near the surface, for a free-electron-like metal. It should be noted, however, that although refraction effects will play an important role in determining the intensities of surface-related peaks in edc's , the positions of peaks are fixed by energy conservation. The way that the refractive index changes with frequency will also affect the manner in which the peak intensities vary with ω.

Another important point raised by Feibelman and Eastman (1974) is that the value of the final-state wave vector $\underline{k}$ determines the sort of information which can be obtained from the photoemission experiment.

Since the imaginary part of $\underline{k}$ perpendicular to the surface, denoted by $k_\perp^{(2)}$, is related to the inelastic scattering length $\ell(E, \underline{k})$ by $\ell^{-1}(E, \underline{k}) = k_\perp^{(2)} \cos\theta$ it is obvious that sampling depths are different for different ranges of values of $\underline{k}$. But, more fundamentally, the dissimilar edc's obtained in UPS and XPS can be theoretically justified. To show the trend to the "X-ray limit," we consider a nearly-free-electron model. The density of final states per unit volume varies as $\rho(E) = \frac{3}{2} \frac{E^{\frac{1}{2}}}{E_{BZ}^{\frac{3}{2}}}$ and

the average band width of each band (in the reduced-zone scheme) is $W \approx \left(\frac{2\hbar^2 E}{m}\right)^{\frac{1}{2}} k_{BZ}$. Here k_{BZ} is the Brillouin-zone momentum and $\rho(E)$ has been normalized to one state for $E = E_{BZ} = \frac{\hbar^2}{2m} k_{BZ}^2$. Thus the number of bands $N_B(E)$ at energy E is $N_B(E) \approx \rho(E) W = \frac{3E}{E_{BZ}}$.

Since each band passes through one $k_\perp$ point for each $k_\parallel$, the average separation $\delta k_\perp$ of available $k_\perp$ states at an energy E is $\delta k_\perp \approx k_{BZ} / N_B = E_{BZ} k_{BZ} / 3E$. As discussed in Chapter 3.2, the criterion for the XPS limit is the existence of a "quasi-continuum" of final states so that all initial states can be excited : thus if the average separation $\delta k_\perp$ of available $k_\perp$ states at energy $E_f = E_i + h\nu$ is less than the broadening $k_\perp^{(2)}$, then all initial states at energy E_i are excited with equal probability. This trend is illustrated in Figure 3.6. Here the "universal curve" of Fig.3.2. (ℓ against E) is converted to $k_\perp^{(2)}$ versus E. Also shown is the line $\delta k_\perp = E_{BZ} k_{BZ} / 3(E + V_o)$ as derived above. This shows that the X-ray limit is typically reached for $h\nu \gtrsim$ 20 to 40 eV. It should be noted that "X-ray limit" in this context means merely that structures in edc's taken with photon energies above this value tend to have invariant binding energies, but relative peak heights and peak shapes are often energy-dependent due to frequency-dependence in the dipole matrix elements for various s, p, d and f states. It is of interest that changes in the relative heights of the two main peaks within the d-bands of gold have been observed over the energy range 60eV to 200eV (Lindau et al.1976a) :

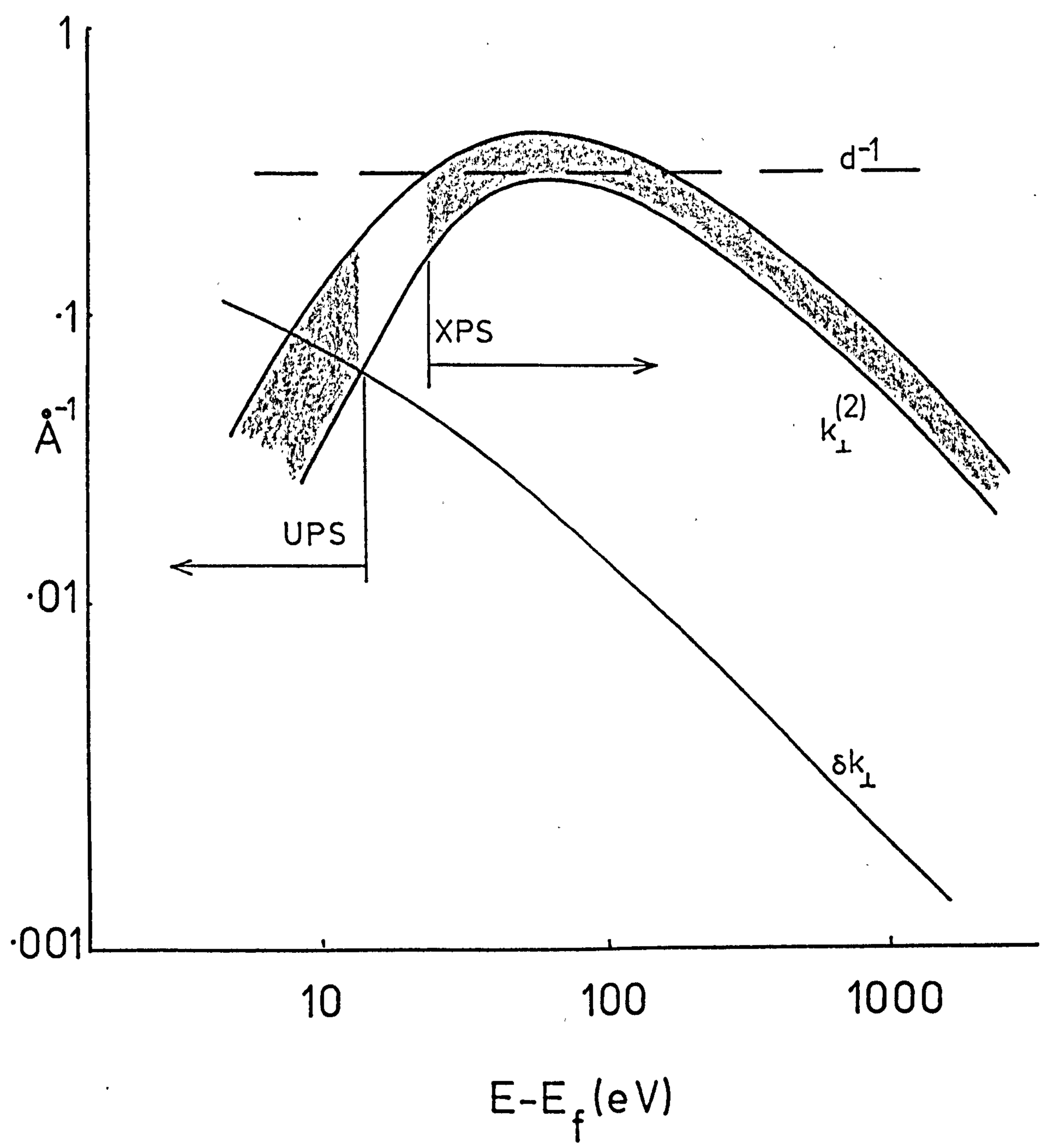

Figure 3.6. Variation with final state energy of the imaginary part of the final state wavevector ($k_\perp^{(2)}$) and a lower bound on the spacing between final state bands in momentum space ($\delta k_\perp$) .After Grobman et al (1975) .

this surprising result has yet to be explained.

All of this discussion has been based on the formula obtained by Feibelman and Eastman for the angle-resolved photocurrent. However, they show simply that the Golden Rule expression (Eq. 3.6) can be approximately reduced to the "three-step model" for angle-integrated photoemission , provided that the inelastic electron mean free path ℓ is much greater than the lattice translation vector (d) perpendicular to the surface. Included in Figure 3.6 is a typical value of the wave-vector d^{-1} associated with the interlayer spacing (this is taken for the $<111>$ direction of a diamond lattice (Grobman et al 1975)): this shows that, for a small range of energies, $k_\perp^{(2)} > d^{-1}$ and thus $\ell(E) < d^{-1}$. This regime will therefore be dominated by surface effects. We have just seen that the momentum broadening $k_\perp^{(2)}$ is sufficiently small (in the UPS regime) for conservation of crystal momentum still to be an important selection rule, and since the region with $\ell(E) < d^{-1}$ does not overlap the UPS region, one is justified in trying to obtain bulk band structures with low-energy photoemission - as is implicit in the "direct-transition three-step model" - as well as some surface information.

Finally we note that, despite the considerable progress in understanding of the photoemission process that has occurred in the past few years, none of the rigorous quantum-mechanical models has yet been tested in any comparison of experiment and theory. The recent model of Pendry (1976), which uses the time-reversed multiple scattering formalism of LEED to treat layers of muffin-tin potentials, seems to be an efficient method which may yet yield a true test of photoemission theory.

CHAPTER 4

EXPERIMENTAL TECHNIQUES

4.1. UPS at Leicester

Any experiment which is sensitive to the surface of materials should be conducted in ultra-high vacuum (u.h.v.). The reason for this may be readily seen. It follows directly from the kinetic theory of gases that the average number $\bar{n}$ of gas molecules striking a surface is given by

$$\bar{n} \approx 3.5 \times 10^{22} \frac{p}{\sqrt{MT}} \quad \text{cm}^{-2}\,\text{s}^{-1}$$

where p is the gas pressure in Torr, T is the absolute temperature and M is the molecular weight. A monolayer of a surface contains about 3×10^{14} atoms. cm^{-2}, so at room temperature, with an average molecular weight of 28,

$$\bar{n} \approx 10^{6}\, sp \quad \text{monolayers}\ \text{s}^{-1}$$

where s is the sticking coefficient, the probability that an impinging molecule is adsorbed. Hence p must be reduced to increase the length of time available for performing an experiment with a clean surface; for example, if s = 1, a pressure of 10^{-10} Torr gives $3\frac{1}{2}$ hours before a monolayer of gas is adsorbed .

The techniques for obtaining u.h.v. are now standard (Redhead et al. 1968) and will not be discussed in detail here. The chamber used for the UPS experiments at Leicester (visible in Plates III and V) is manufactured from stainless steel grade EN58B, which is nominally non-magnetic, and all tubes and flanges are argon-arc welded (Rosebury 1965). Flanges are sealed by copper gaskets. The chamber is rough-pumped by a separate rotary and diffusion pump system which can be detached from the u.h.v. chamber. The main pumping is performed by a 140 $\ell.\text{s}^{-1}$ ion pump and a titanium sublimation pump. Within approximately 60 hours of installing a sample, including a bake of up to 24 hours at 200°C, pressures of 5×10^{-11} Torr were routinely obtained. Total pressures were measured with a nude Bayard-Alpert ionization gauge: analysis of the residual gas was not usually performed, but a mass spectrometer which was fitted on two occasions revealed the main constituents of the residual gas to be methane, water, carbon monoxide and carbon dioxide.

The semiconductor crystals were about 30mm x 10mm x 3mm , oriented with the [110] axis parallel to the longest side. They were mounted in a stainless steel block, lined with lead sheet, and cleaved by placing an anvil, also covered with lead sheet, against the side whilst a steadily increasing force was applied to a cleaver which was moved against the other side of the crystal. The cleaver is shown in Plate I, and is made, apart from the tungsten carbide blades, entirely from stainless steel. The design shown gave an easy way of obtaining two cleaves from the same sample without breaking vacuum. Other workers on III-V semiconductors have used annealed copper as the soft material for anvils or sample holders (James and Moll 1969, Galbraith and Fischer 1972), but I felt that this was unwise in view of the very high diffusion coefficient of Cu in III-V compounds and its known deleterious effect on their electrical properties (Hall and Racette 1964).

Almost all of the surfaces revealed by cleaving had a mirror finish as viewed by eye (see Plate II). No attempt was made to measure the perfection of cleavage by any other means, but it is believed that very few surface steps existed.

Occasionally difficulty was experienced in making contact to the crystals, owing to their high resistivity. The first GaP crystal had a silver/tin ohmic contact evaporated onto one face but the problem was solved more easily with other samples, within the u.h.v. chamber. The cleaver was pushed into contact with the side of the crystal, thus earthing it rather effectively, and a 15V , 30 μF capacitor was discharged between the sample and earth. This proved to be sufficient to break down any surface barrier which was preventing ohmic contact.

For experiments at low photon energies, the many-lined quasi-continuum from a Hinteregger-type hydrogen discharge lamp was used with a 1-metre McPherson monochromator. The lamp was modified slightly by replacing the aluminium air-cooled cathode with a stainless steel water-cooled one. The cooling was provided by a closed system of deionised water, which had a high enough resistivity to enable the normal cathode voltage of about 600V to be

Plate I. The cleaver.

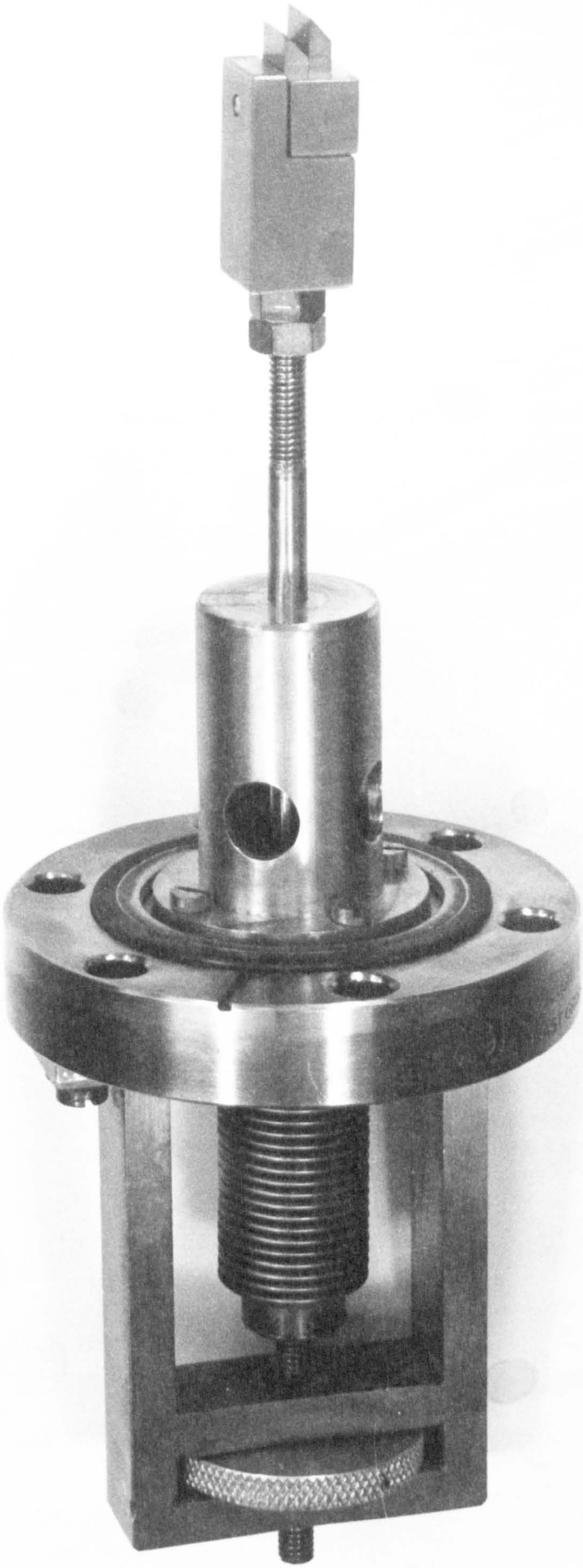

Plate II. A typical cleave of GaP (110)

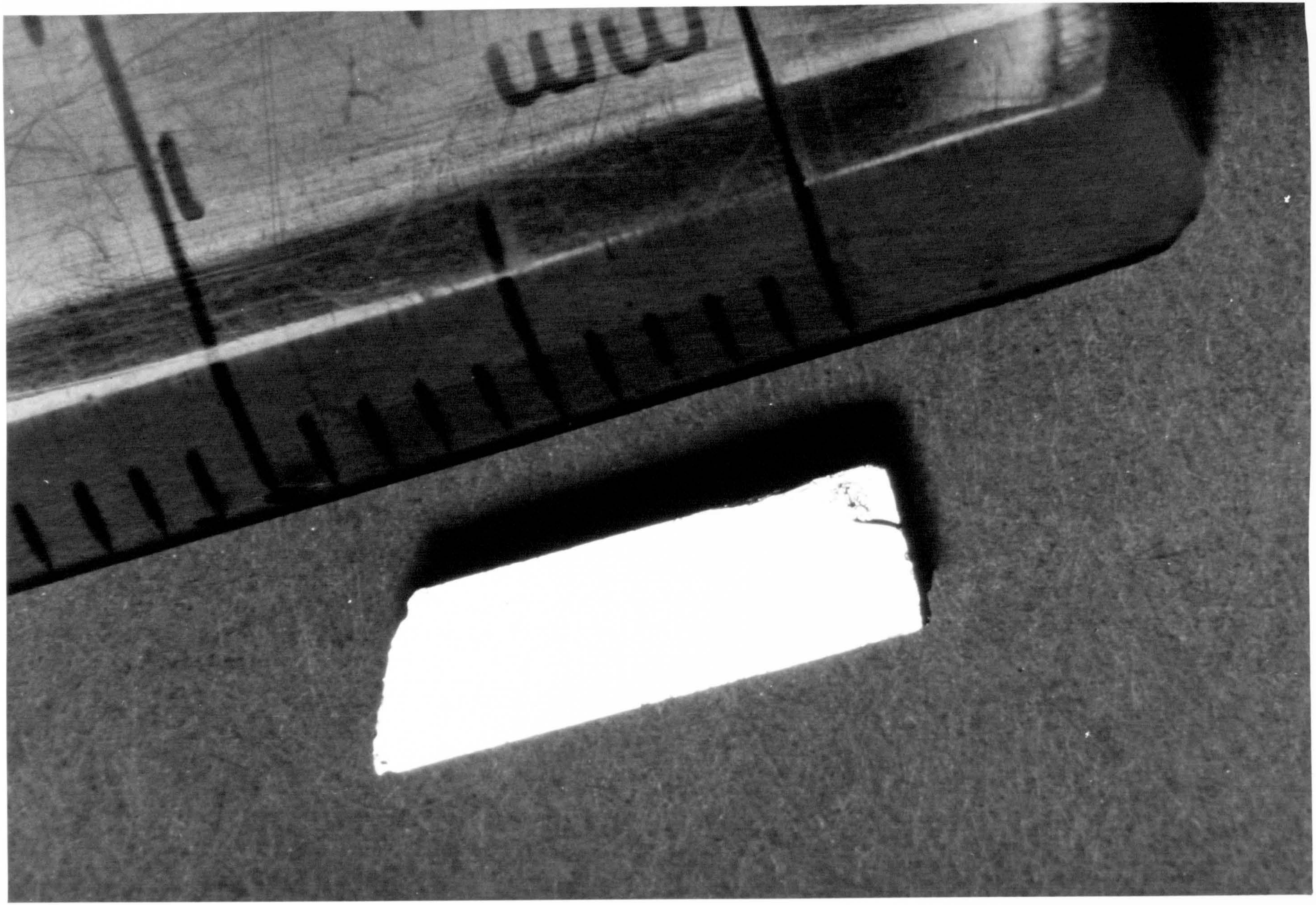

maintained safely. A typical spectrum of the hydrogen lamp output is given in Figure 4.1. This was measured by placing a film of sodium salicylate, coated on glass, after the exit slit of the monochromator. This phosphor is known to convert u.v. light to visible light with an almost constant efficiency over the wavelength range 1000 to 1800 Å (Samson 1967). The visible light is detected by a photomultiplier.

An attempt was made to convert the H_2-lamp to run with a hot filament (Eastman and Donelon 1970). It proved possible to increase greatly the proportion of higher-energy light emitted (see Figure 4.2., which has an identical vertical scale to Figure 4.1), but the discharge tended to extinguish often, and large amounts of cathode and filament material were sputtered onto the quartz capillary. It was feared that some of this sputtered metal might reach the grating, and so this experiment was not continued. It was later discovered that the modified light source had not proved particularly useful, and had indeed damaged gratings (D.E.Eastman, personal communication). With care, however, it appears that a hot-filament hydrogen discharge can be made to work satisfactorily (Gregory and Spicer 1975).

The discharge was constrained with its axis pointing towards the grating, a Bausch and Lomb three-section replica grating, ruled at 600 lines/mm, blazed at 1500Å and coated with magnesium fluoride. This gave a dispersion of 16Å/mm at the exit slit, one metre away: with the usual slit width of 1.25mm, a resolution of 0.08eV ($h\nu$ = 7.4eV) to 0.2eV ($h\nu$ = 11eV) is obtained. The light, after dispersion by the monochromator, was deflected vertically downwards and focussed by a concave and a plane mirror to a line 3mm x 1 mm on the sample. It entered the u.h.v. chamber through a window of lithium fluoride. The transmission of a typical LiF window as a function of wavelength is given in Figure 4.3. This curve was plotted from the performance of one of our windows, and agrees well with data given by Samson (1967). It can be seen that LiF transmits light of energy up to 11.8eV, but, after exposure to high-energy photons for some time, defect centres are produced which form electronic traps within the band-gap of the insulator, considerably impairing its transmission

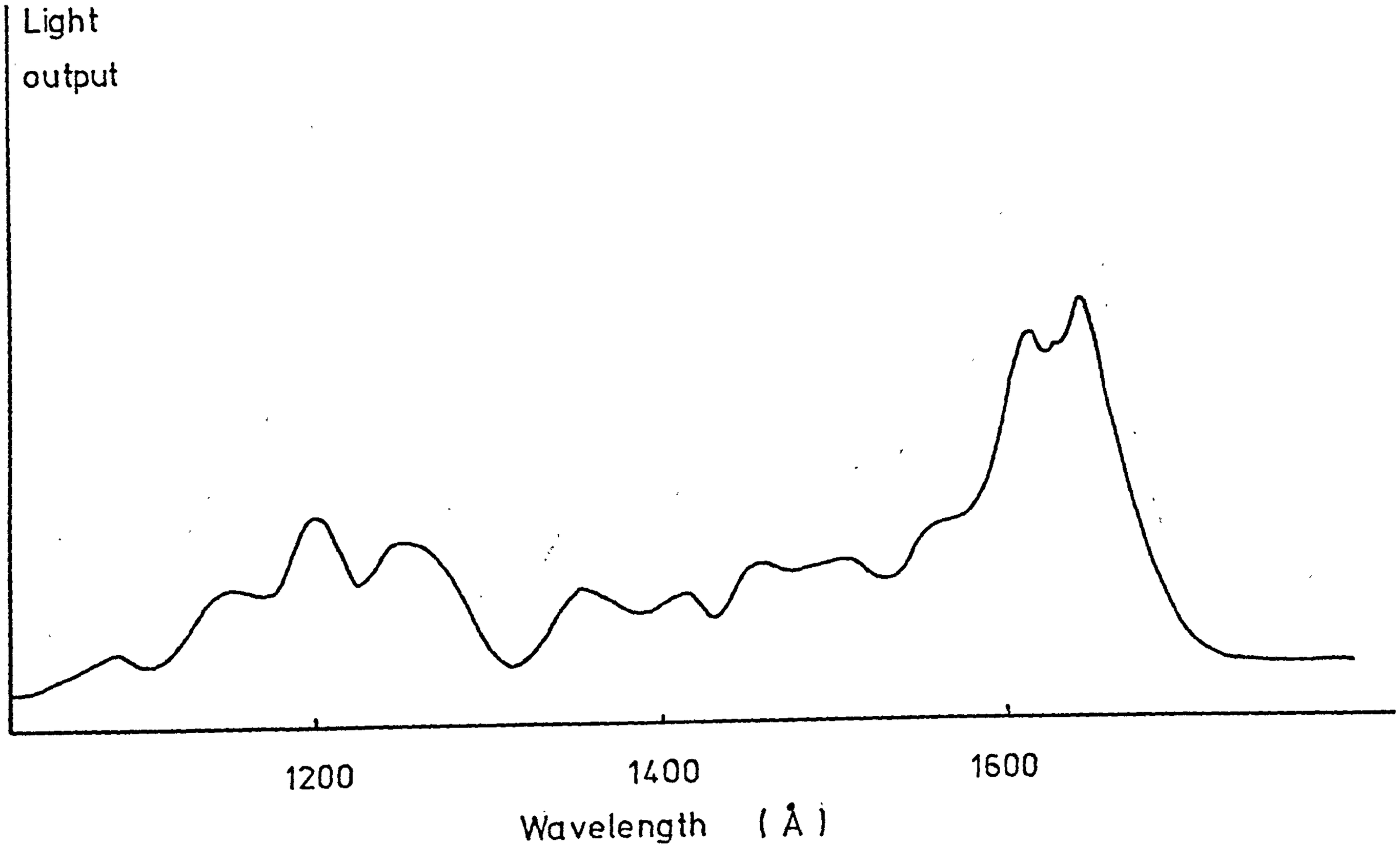

Figure 4.1. Spectrum of hydrogen-lamp output.

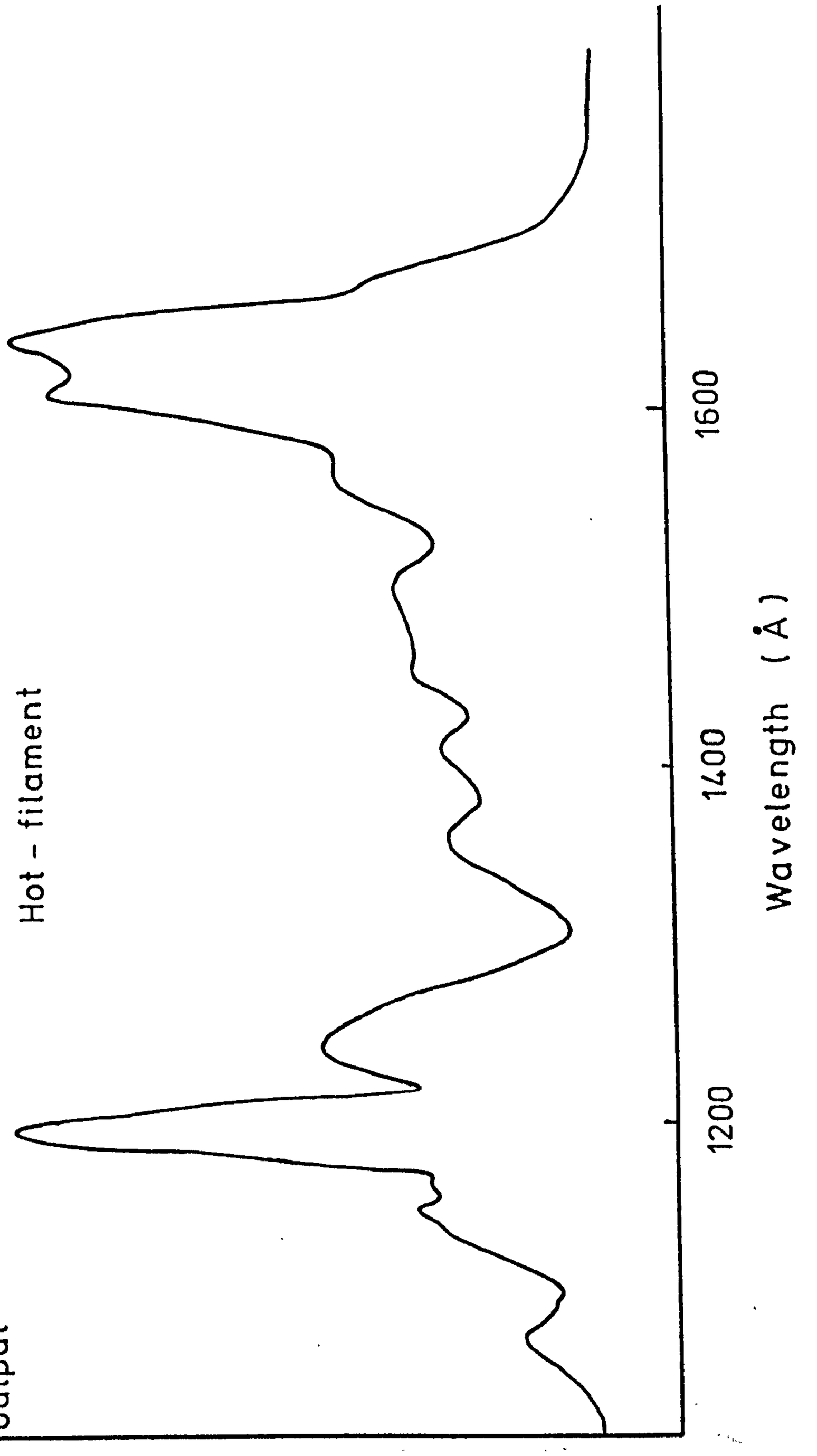

Figure 4.2. Spectrum of hydrogen-lamp output when modified by inclusion of a hot filament. Vertical scale is identical to Figure 4.1.

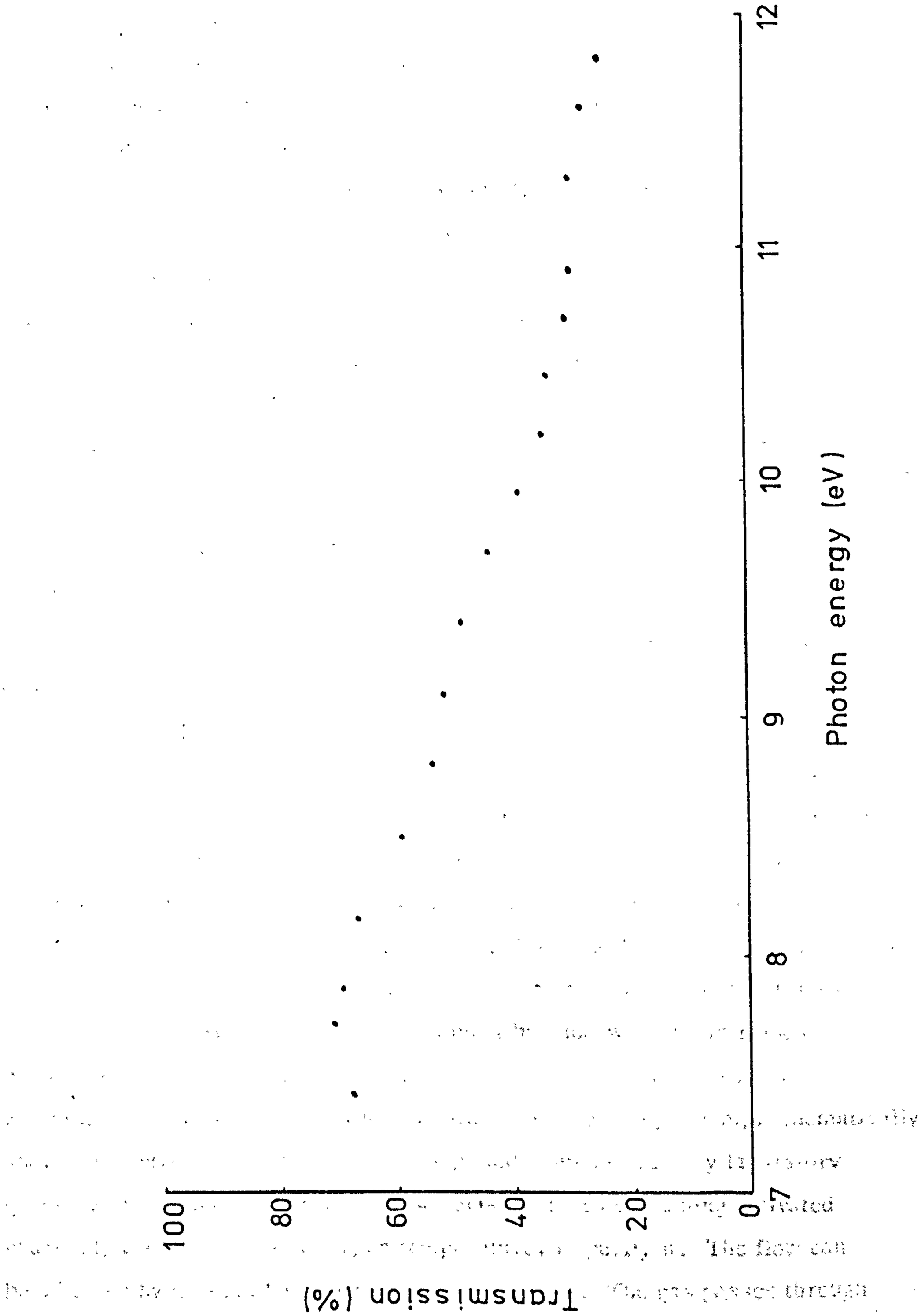

Figure 4.3. Transmission of a LIF window as a function of photon energy.

at energies >10eV.

The lamp was normally operated with about 0.7 Torr of hydrogen, and the monochromator pressure around 8×10^{-5} Torr. It was found to be essential to keep the oil-filled diffusion pump on the monochromator extremely well trapped, as any oil in the monochromator system seriously degraded the light output. On occasions when oil accidentally entered the system, it was found to be concentrated on the optical surfaces, and was worst where the light was focussed on the LiF window. The same phenomenon has been observed in the oil-pumped beam-lines of the Daresbury Laboratory S.R.F. (see Chapter 4.2.). It is probable that the electrostatic charging effect of the high energy photons tends to agglomerate the oil; a particularly unfortunate occurrence since the contaminants are concentrated just where they are most harmful.

The chamber is shown connected to the hydrogen lamp monochromator in Plate III.

Another light source used for UPS experiments at Leicester is a rare-gas discharge lamp. The transition from singlet 2P to singlet 2S in a helium atom gives an intense line at 584Å (21.22eV) with a width of <0.01Å. Under certain conditions a second series of lines can be excited, known as HeII lines, the Roman numeral indicating that emission is from singly ionized He^+, rather than the neutral atom. From this series, only the line at 304 Å (40.81eV) can normally be excited with sufficient intensity to be used. Similar excitations in neon give NeI (a doublet at 16.67 and 16.85eV) and NeII (26.85eV). There is no window material which can be used to transmit photons of these energies, so rare-gas discharge lamps must be windowless: this raises problems for u.h.v. work, since a pressure of 0.1 to 10 Torr is needed within the discharge. The solution is a differentially-pumped lamp, schematically shown in Figure 4.4. The helium is supplied from an ordinary laboratory grade cylinder, and passed through two glass U-tubes containing activated charcoal, cooled to liquid nitrogen temperature, to purify it. The flow can be adjusted by means of a fine-control needle valve. The gas passes through

Plate III The u.h.v.chamber attached to the hydrogen-lamp monochromator

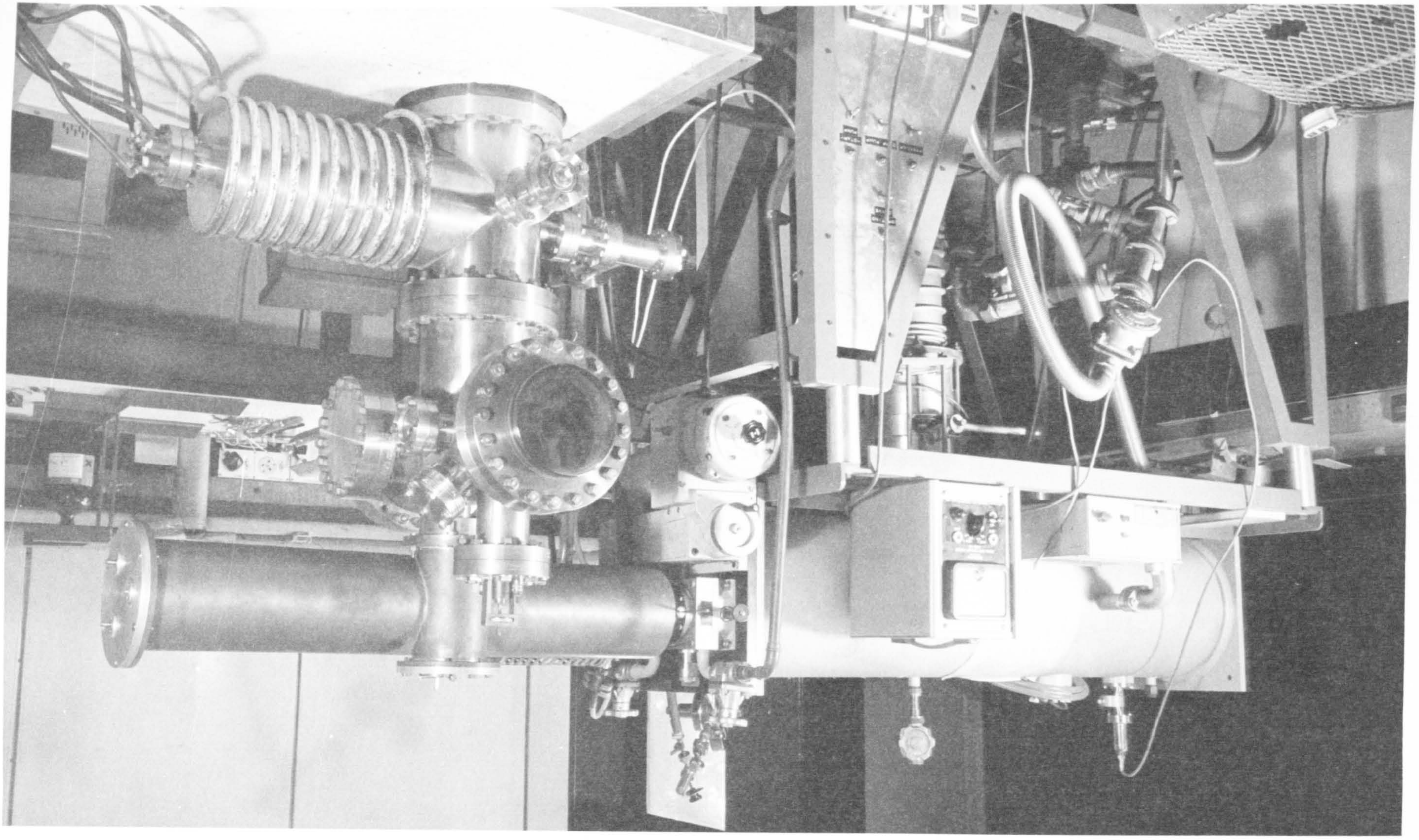

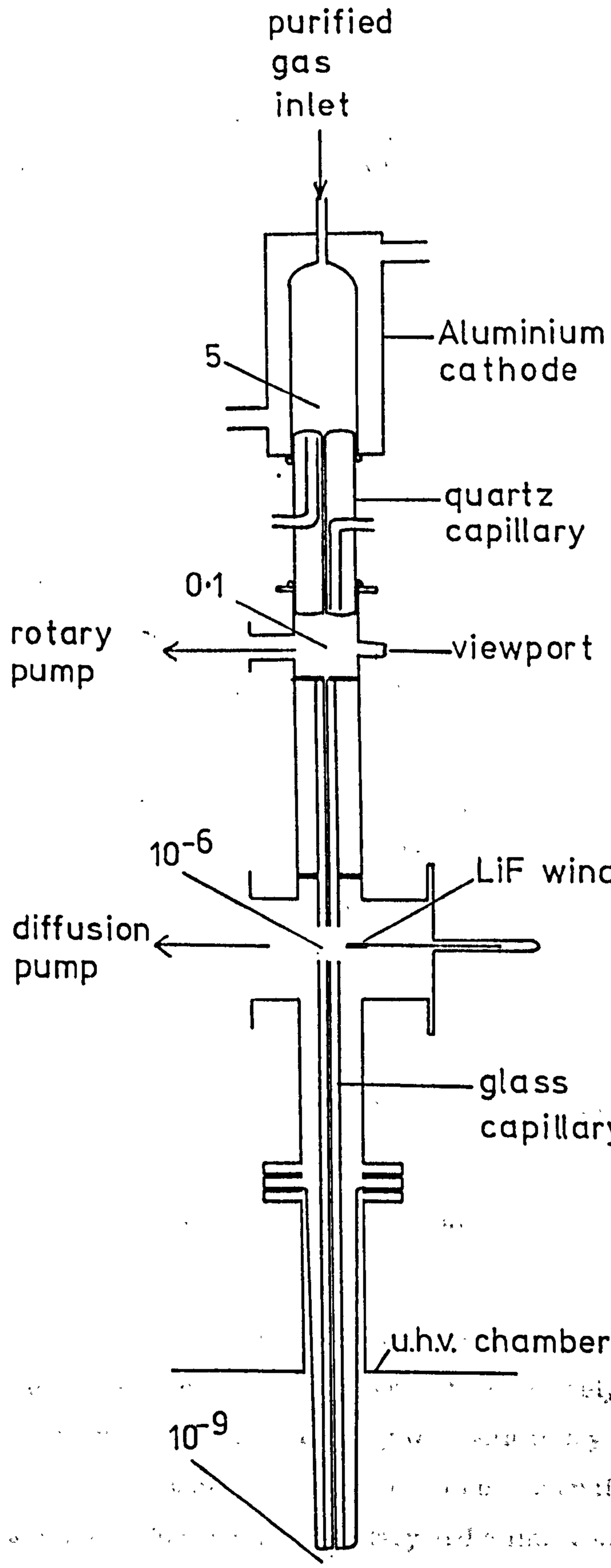

Figure 4.4. Schematic diagram of differentially-pumped discharge lamp. Approximate operating pressures (in Torr) are indicated.

an aluminium cathode, and along a water-cooled quartz capillary, 1.8 mm diameter and 15 cm in length. At the end of this capillary is a small chamber, with a side-tube leading to a rotary pump, and a glass window for viewing the discharge.

The discharge is struck along this quartz capillary by applying a negative voltage to the aluminium cathode. The rest of the lamp body is connected to the vacuum chamber, which is earthed. The voltage is supplied from a power supply which can give up to 5kV at 250mA. The power actually needed depends on the hellum pressure, but the discharge strikes at about 3.1kV and the resistance then drops so that the lamp runs at about 600V at 100mA. The power supply is connected in series with a 25kΩ resistor chain to drop the extra voltage: this resistor chain has to dissipate 250W, and is cooled by a fan.

The light passes along a glass capillary tube, 1.25mm in diameter and about 15 cm long and through another chamber which has a side-tube leading to a diffusion pump. Another attachment to this chamber is a rod holding a cleaved piece of lithium fluoride: because LiF cuts out all radiation of $h\nu > 11.8eV$,insertion of this filter can check whether longer wavelength light is being generated. The light finally passes along a continuation of this capillary, about 50 cm long, into the vacuum chamber and onto the specimen.

Typical operating pressures, with a fully baked u.h.v.chamber, are indicated in Figure 4.4.

It is not easy to obtain the HeII and NeII lines: the main requirements are a stable low pressure of gas - typically 0.1 Torr - and extremely pure gas (D.W.Turner, personal communication). This lamp was built to my design incorporating several features to enable a low pressure to be maintained; a large cathode volume, a narrow, long quartz capillary and a fine-control needle valve all helped to keep the pressure uniformly low. This opportunity was taken to change from the previous air-cooled cathode to a water-cooled

aluminium one, using the same circulation of deionised water as the hydrogen lamp described above. The assembled lamp is shown in Plate IV. The procedure for obtaining the higher-energy lines is to strike the discharge at a gas pressure around 5 Torr and then gradually to reduce the pressure, whilst observing the colour of the discharge. HeI gives out white light with a pinkish tinge to it. As the pressure is reduced to ~ 2 Torr, there is a definite difference in colour between the top and the bottom of the discharge, the top being more pink and the bottom more mauve. At <0.5 Torr the whole column becomes bluish-green with a gradation of colour along the tube. It is believed that this colour accompanies the emission of a larger proportion of HeII radiation.

The greatest intensity ratio of HeII :HeI achieved with this lamp was approximately 1 : 8. This was not large enough to do any useful work with HeII or NeII. It is felt that the main reason that a higher intensity was not reached was the presence of impurities in the gas and within the lamp itself: impurities within the discharge will readily quench the emission of the higher-energy lines. The lamp gave its best performance when it had been running for several hours, and thus was reasonably well outgassed. A bakeable lamp could be expected to be more efficient at production of HeII, and indeed such a lamp now commercially available gives a best ratio of HeII:HeI of 1:3 (Brundle et al. 1974).

However, this discharge lamp, as modified, produced a more stable and more intense emission of HeI and NeI than the previous design, with considerably decreased sputtering of the cathode. The lamp is shown connected to the u.h.v. chamber in Plate V.

A further possible complication with a windowless discharge lamp is the production of electrons, ions and metastable atoms. It is conceivable that these excited species could drift down the glass capillary and impinge on the sample. A simple test showed that there was no change in the current emitted from the crystal (to better than 1%) when a small magnet was placed at the side of the lower part of the lamp: there is thus a

Plate IV The differentially-pumped discharge lamp

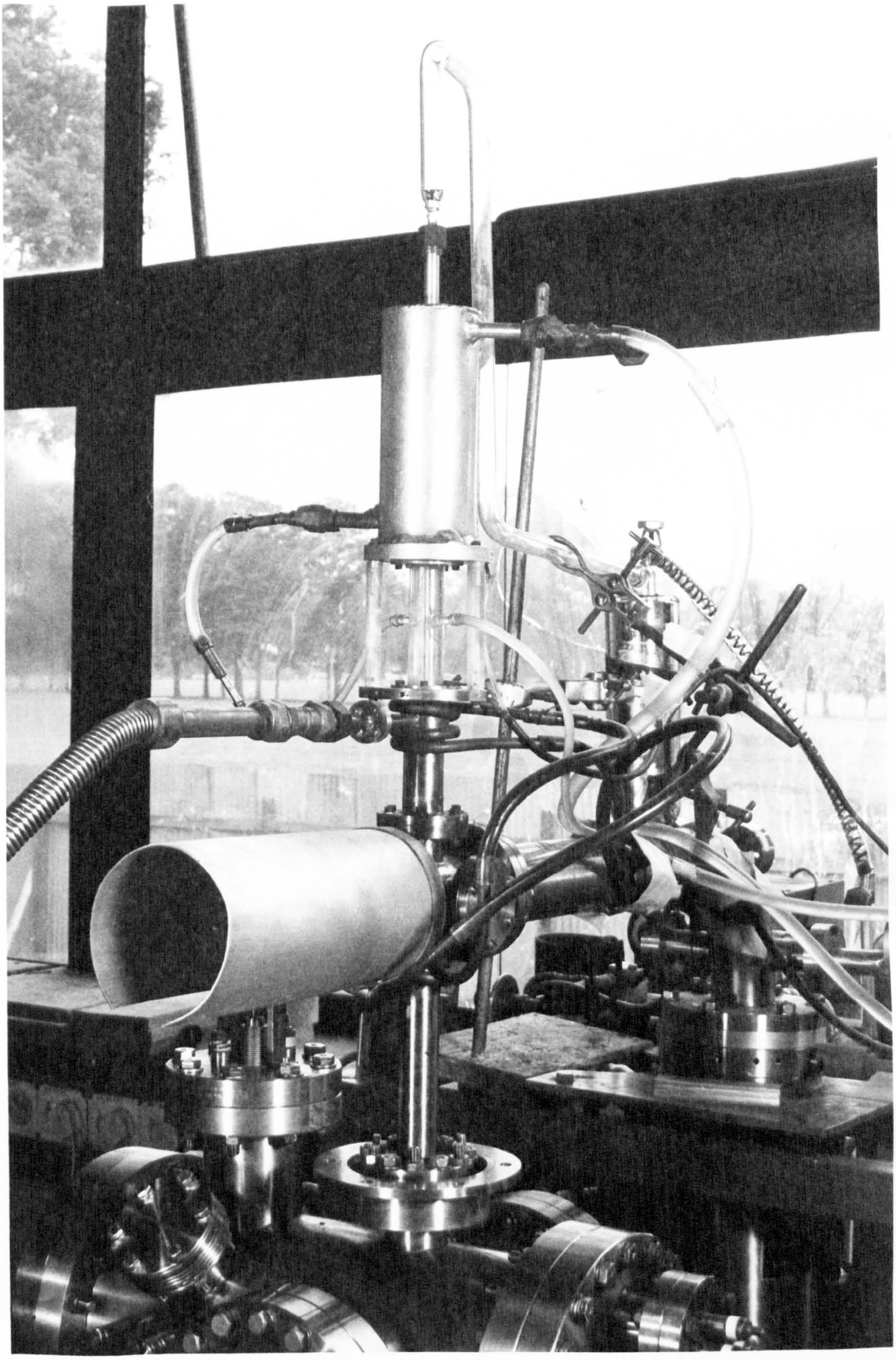

Plate V The u.h.v. chamber attached to the discharge lamp.

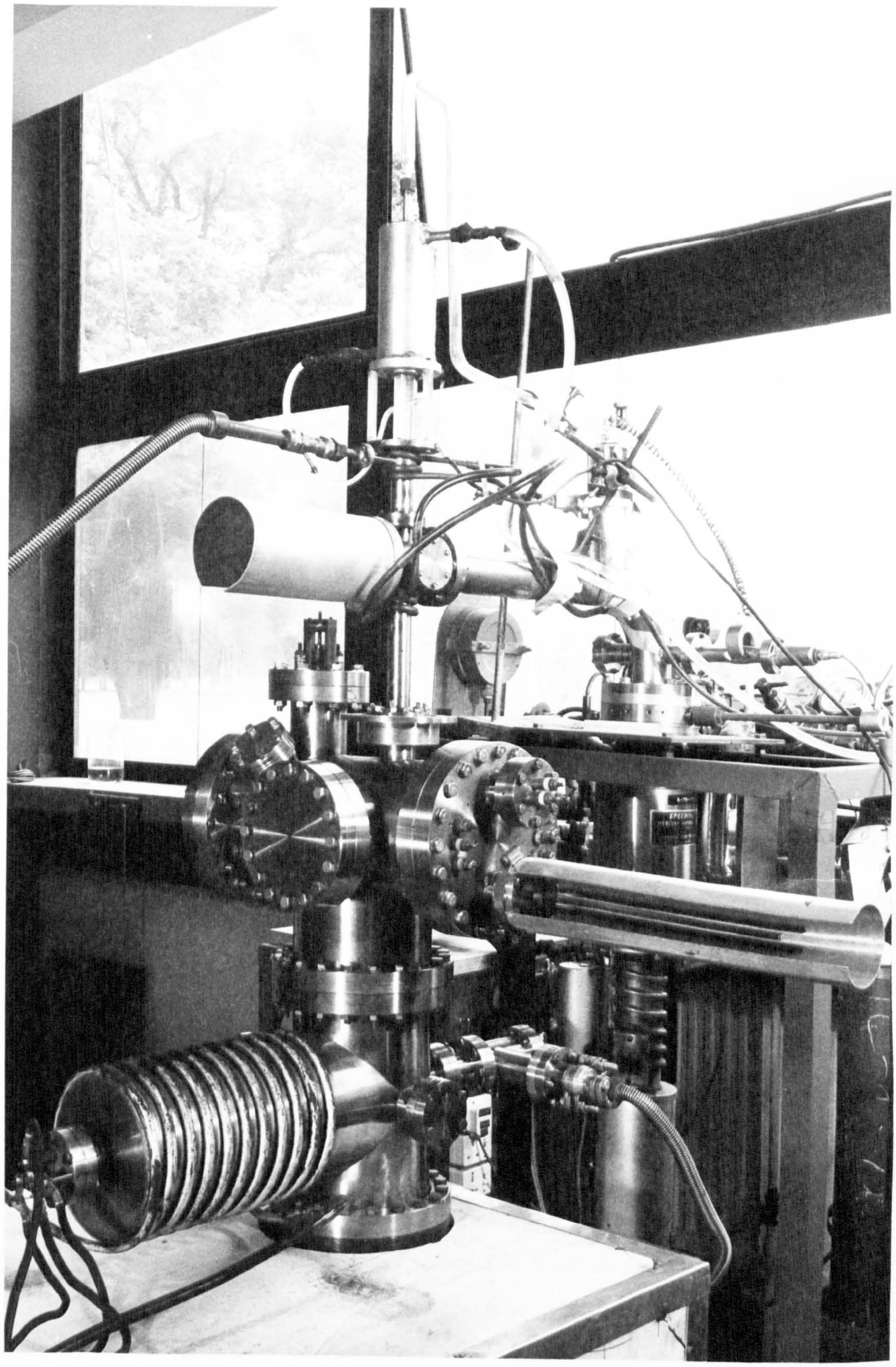

negligible contribution from electrons and ions. The neutral metastable atoms should be deflected in a strong magnetic field because of their spin, and it was not felt that, in normal circumstances, any metastable atoms which might be excited could travel the length of the capillary without de-excitation.

Energy distribution curves (edc's) were measured using an adaptation of a method described by Eden (1970). A schematic diagram of the signal detection circuit is included in Figure 4.5. The emitted electrons are collected by a hemispherical retarding field analyser (RFA) with one grid. The sample is fitted with shielding such that the electrostatic fields due to ion pumps, pick-up, etc. are effectively screened. A ripple frequency of 18-19 Hz was found to be best for minimizing pick-up and interference with harmonics from mains frequency.

In the RFA, the potential of the sample-and the grid- is linearly ramped so that only electrons whose component of kinetic energy perpendicular to the grid is sufficient to overcome the potential barrier can reach the collector. The collected current I (V) is thus proportional to $\int_{V_R}^{\infty} n\,(E)\,dE$. With the small sinusoidal variation $k\sin\omega t$ applied to the collector, a Taylor series expansion of I $(V + k\sin\omega t)$ gives the amplitudes of the fundamental signal A (with frequency ω) to be

$$A = k\frac{dI}{dV} + \frac{k^3}{8}\frac{d^3I}{dV^3} + \ldots$$

Thus the proportionality between A and $dI/_{dV}$, which is n (E), depends on k being sufficiently small. Taylor (1969) has shown that, for a Gaussian peak, the peak-to-peak modulating amplitude may be as large as the full width at half-maximum of the peak and still introduce an error of less than 13% in intensity. One must also ensure that V_R is swept slowly enough compared to the other time constants in the system. The lock-in amplifier was usually operated with a time constant of 100 or 330 ms, so the normal ramp speeds of 16 to 22 mV/s are seen to give adequate resolution. The total energy resolution of the RFA and its associated detection circuit was around 2%.

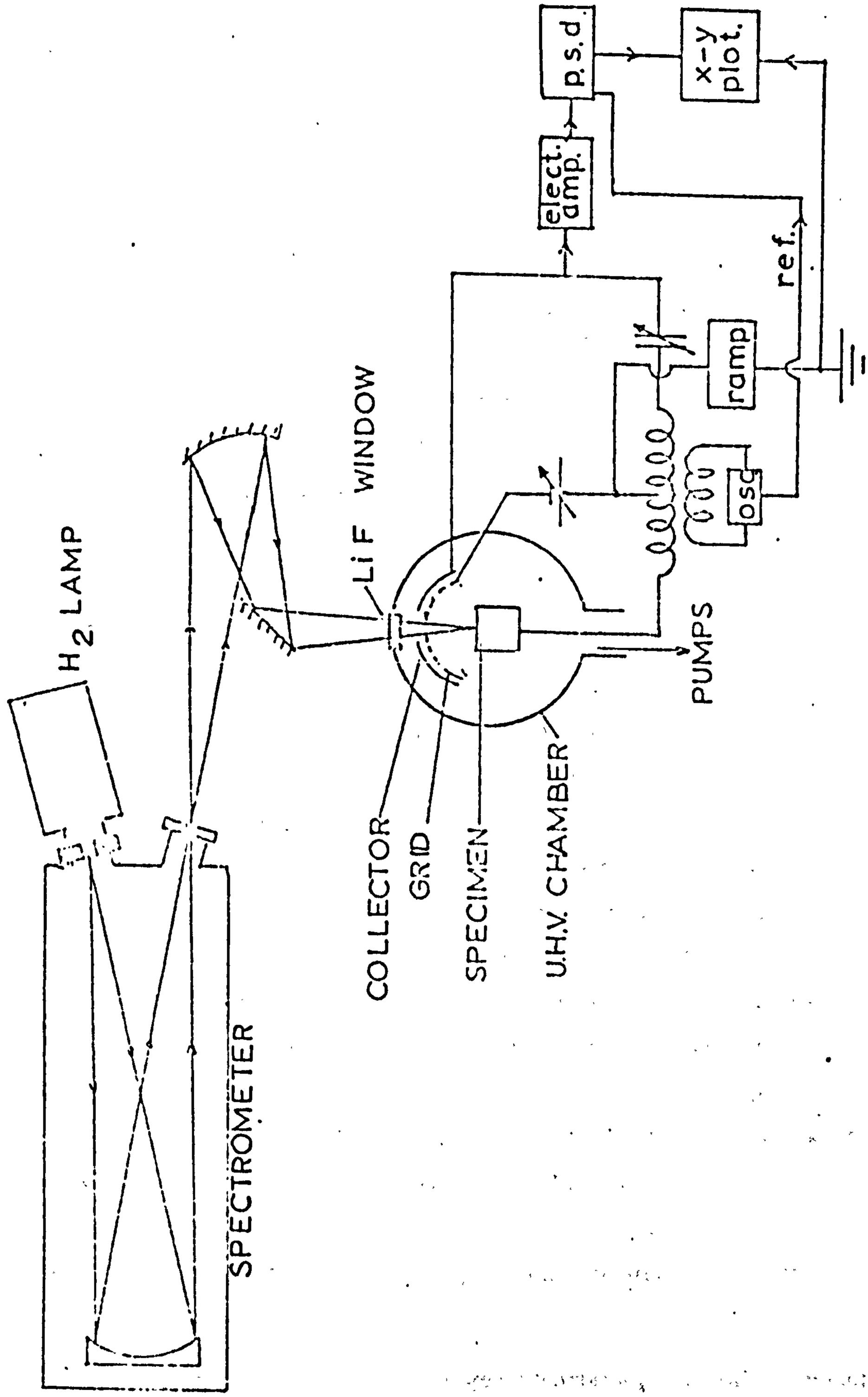

Figure 4.5. Schematic diagram of vacuum chamber attached to hydrogen-lamp monochromator, with the electronic detection circuitry.

4.2. LEED/AES/ELS/UPS at Caswell

LEED patterns were observed, and Auger electron energy spectra and electron energy loss spectra recorded, using a standard four-grid RFA in a 12" diameter vacuum chamber. The chamber was rough-pumped by two sorption pumps, and u.h.v. obtained with a 140 $\ell.s^{-1}$ ion pump and a titanium sublimation pump. A gas-handling line, pumped by a separate small ion pump, allowed admission of controlled amounts of pure gases from one-litre glass bottles via fine-control leak-valves. The semiconductor crystal was mounted in a tantalum holder, in contact with a resistive heater, at the end of a universal manipulator which entered the chamber from the top: this allowed movement in both horizontal and vertical directions and rotation about the vertical axis.

Samples were cleaned by argon-ion bombardment and annealing. Argon was admitted via a leak valve and the ion pump throttled so that a dynamic equilibrium was established with a pressure of 8×10^{-5} Torr of argon in the chamber. The crystal was earthed and rotated to face the ion gun, with an accelerating voltage of about 400 V applied to the gun, giving an ion current density of 0.5 $\mu A\ cm^{-2}$. The system was left in this condition for about 16 hours, then the argon was pumped out and the pressure allowed to restore to less than 10^{-9} Torr. The crystal was then heated to $550^{o}C$ and this temperature maintained for an hour, after which the sample cooled naturally to room temperature in about half-an-hour. During this annealing process the pressure was kept below 5×10^{-7} Torr. LEED and AES showed that clean stoichiometric surfaces were obtained with this procedure. The cleaning sequence was repeated every time an Auger electron spectrum indicated significant contamination.

For the experiments on oxygen adsorption, controlled amounts of oxygen of 99.99% purity were admitted. A dynamic equilibrium was established, as with argon, in order to retain the purity of the gas: with the ion pump valved-off, large quantities of carbon monoxide were desorbed from the walls of the chamber. An ionisation gauge was used to determine the total

pressure in the chamber; checks with the Q7 quadrupole mass spectrometer showed that the partial pressures of contaminant gases were always less than 1% of that of oxygen. The ionisation gauge had no direct line-of-sight to the specimen, and the Q7 was not operated during oxygen adsorption. Oxygen pressures in the range 10^{-6} Torr to 10^{-4} Torr were used.

Diffraction patterns were obtained with the low-current electron gun mounted in the centre of the optics. The voltages on the grids and collector were as shown in Figure 4.6.

Auger electron and electron energy-loss spectra were obtained using both the LEED gun and a high-current electron gun mounted at an angle of 12^{o} to the sample. A standard incident electron current of 10μA, measured with an attractive voltage of 9V, from a small battery, connected to the sample, was used for taking Auger spectra. The battery was removed before spectra were recorded, to avoid shifting the energy scale . To extract the Auger signal the second derivative of the collected current was recorded: a small a.c. voltage was applied to the analysing grids and the component of the collected current having a frequency of twice this ripple voltage was detected. The energy-loss spectra were treated in a similar way to reveal better the small changes in the curves, which otherwise showed up merely as points of inflection. The electrical configuration of the optics for these modes is shown in Figure 4.7.

A scanning device was attached to the x- and y-deflection plates of the glancing-incidence electron gun. With the specimen connected to an oscilloscope it was possible to raster the deflection voltages and hence display a picture of the sample on the 'scope. Different parts of the specimen and its holder have different secondary electron emission coefficients and thus show up as light and dark areas in the oscilloscope pattern. This facility made it possible to focus the gun on different parts of the sample as desired.

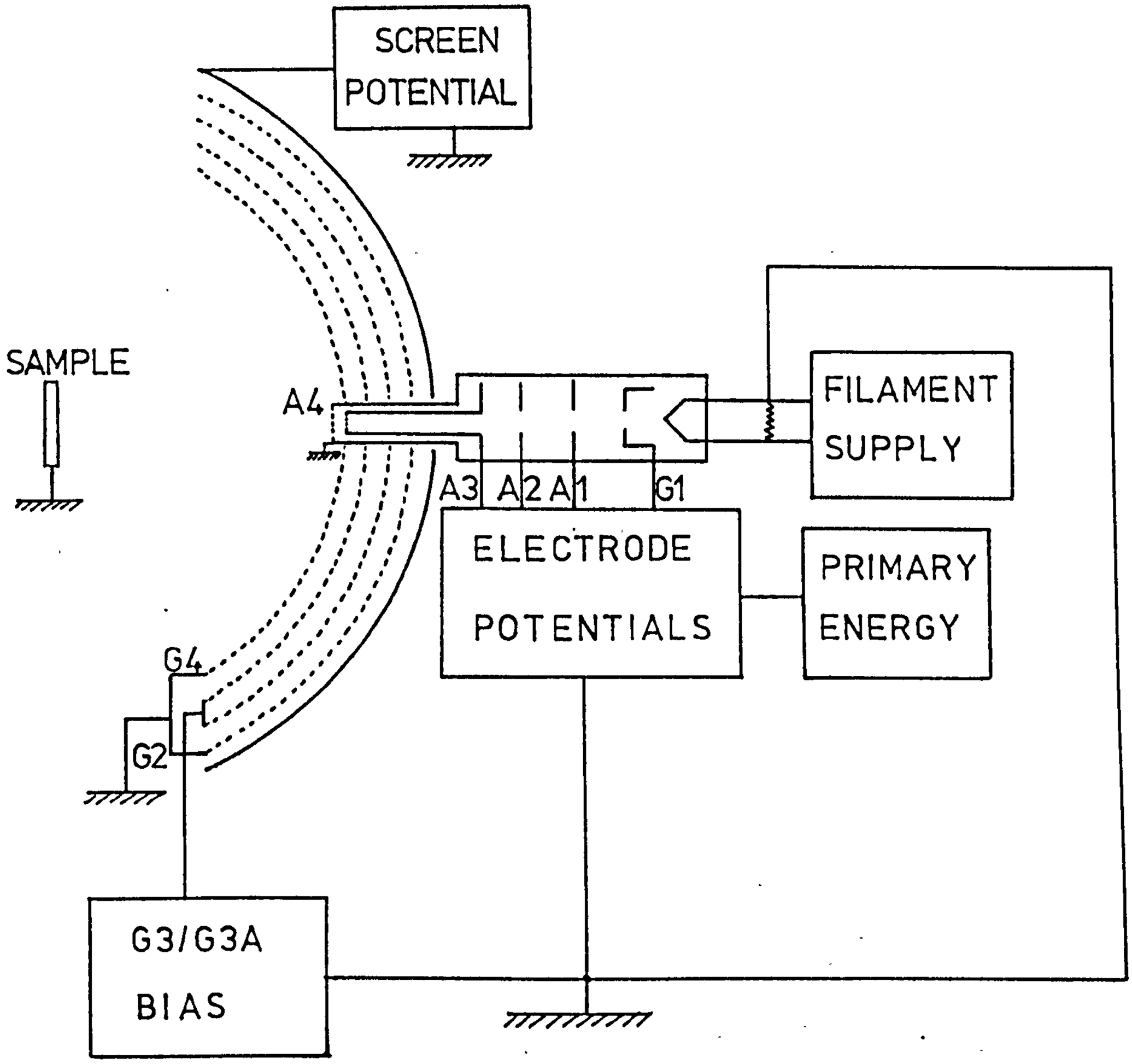

Figure 4.6. Configuration of 4-grid RFA and electronics for LEED

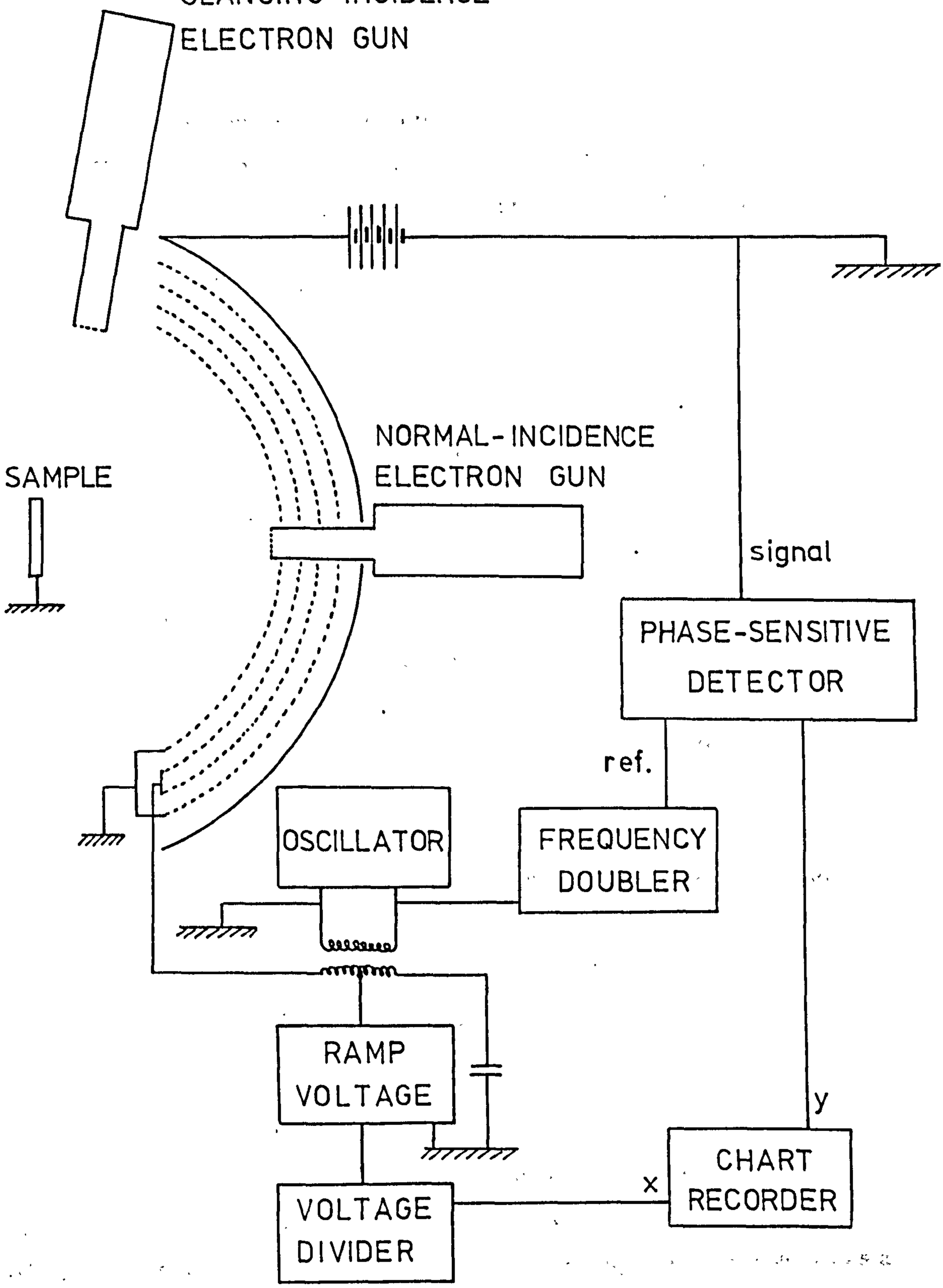

Figure 4.7. Configuration of 4-grid RFA and electronics for AES/ELS. The power supplies for the electron guns, shown in detail in Figure 4.6, are omitted here. The glancing-incidence electron gun includes two pairs of mutually perpendicular deflection plates.

An attempt was made to perform UPS experiments in this system. The helium lamp, already described in Chapter 4.1., was fitted to one of the 8" diameter flanges so as to point at the sample. The distance from the specimen meant that the light spot was about 5mm in diameter, but this still remained solely on the sample. A thin piece of polycrystalline silver was used as a test sample. It proved possible to obtain a surface with less than a few percent of contamination, as judged by an Auger spectrum, merely by heating the silver to a temperature of about 650^{o}C.

Analysis of photoemitted electrons was performed with the four-grid RFA. Several problems were encountered. The phosphor coating on the screen, essential for viewing LEED patterns, charged-up, and made collection of low currents impossible. After trying many different combinations of voltages on the grids and sample, it was found that the best possible spectra were obtained with a circuit similar to that normally used at Leicester, and described in Chapter 4.1 : the back three grids were connected together and used as a collector, with the front grid and screen earthed. The sample was ramped. The best spectrum obtained had the d-bands of Ag clearly visible, but the noise level was such that any meaningful experiment was impossible with this apparatus.

A new type of analyser, designed to avoid the problems encountered here, is described in Chapter 4.4.

4.3. UPS at Daresbury

The main form of energy loss in a synchrotron is the emission of radiation. This synchrotron radiation is just a by-product of the machines of high-energy physics , but has been used increasingly in recent years as a unique light source for spectroscopy (Hayes 1972, Codling 1973). The emitted radiation has a smooth spectral distribution extending from hard X-rays through the vacuum ultraviolet and into the infra-red. The 5GeV synchrotron NINA at Daresbury Laboratory is used as a source of vuv light for experiments on photoemission from solids.

This experiment is equipped with a monochromator which covers the range 15 to 40eV. It is a Wadsworth-type, with a Bausch and Lomb replica grating ruled at 1200 lines/mm and blazed at an angle of $1^{o}47'$, corresponding to a peak wavelength of 520Å (Howells et al. 1977). The instrument has a dispersion of 8.3 Å/mm, and a fixed exit slit giving a constant bandpass of 6 Å. Thus the energy resolution of the monochromator varies from about 0.08eV to 0.8eV across its useful range, being about 0.2eV at its peak energy of 20eV. The monochromated light is focussed to a spot about 2 mm in diameter on the sample 1 m away.

The electron spectrometer is a Vacuum Generators ESCAIII, modified to accept the monochromated synchrotron light. This apparatus has two chambers separated by a gate-valve, with the sample on a probe which has a linear travel of 6" between the two chambers. The preparation chamber is equipped with several sample cleaning and preparation techniques. My cleaver and an anvil were modified to facilitate the cleavage of crystals, and a focussed ion gun made possible argon ion bombardment. The sample could be heated to about $600^{o}C$ for annealing.

Analysis of the photoemitted electrons is performed in the other chamber. The analyser is a modified concentric hemispherical analyser with a slit in front which defines an acceptance angle of approximately $18^{o} \times 90^{o}$. The sample is ramped so the analyser operates at a constant pass energy of 10eV. The analysed electrons are amplified by a channeltron and counted using standard pulse-counting techniques.

The preparation chamber is pumped by a liquid nitrogen-trapped 2" oil-filled diffusion pump and the analyser chamber by a similarly-trapped 4" diffusion pump, also filled with a polyphenyl ether oil, and a small ion pump with a titanium sublimation pump. The normal beam-line pressure is around 10^{-6} Torr but differential pumping with a 6" oil-filled diffusion pump after the monochromator enables pressures of about 8×10^{-11} Torr to be routinely maintained in the analyser chamber. The normal preparation chamber pressure during cleavage was around 2×10^{-10} Torr.

The apparatus is shown connected to the synchrotron beam-line in Plate VI, and a schematic diagram is given in Figure 4.8.

Because of the possible radiation hazard from a high-energy beam of electrons, all work whilst a synchrotron beam is in the beam-line has to be performed by remote control. This adds considerably to the complexity of the experiment. A PDP8 mini-computer was used to control the voltages on the sample and analyser and the pulse-counting of the analysed electrons. The monochromator grating is driven by stepping-motors controlled remotely. All the cleaning and sample preparation was carried out manually during short periods of access negotiated with other users of the same beam-line.

Before the ESCAIII was installed on the synchrotron, a series of experiments was performed, using conventional sources of a rare-gas discharge lamp and a twin-anode X-ray source. The Kα lines of aluminium and magnesium could be excited, giving X-rays with energies 1486.6eV (Al) and 1253.6eV (Mg). Plate VII shows the apparatus in the laboratory equipped with these sources.

4.4. Cylindrical Mirror Analyser

The problems encountered in the UPS experiment at Caswell made evident the need for a more suitable type of electron energy analyser. The very high background noise level necessitated an analyser incorporating an electron multiplier, which acts as a pre-amplification stage actually within the chamber. Any noise picked up outside the chamber is thus not amplified, and no great demands are placed on the electronic detection circuits.

Early electron spectrometers, for the analysis of high-energy electrons, used magnetic fields to disperse the electron beam and so select the energy of interest, but this technique is not suitable for analysing low-energy electrons which are very sensitive to stray magnetic fields. Shielded electrostatic spectrometers are suitable, and several different types have been

Plate VI

The ESCA III electron spectrometer attached to the normal-incidence monochromator. This view is taken looking away from NINA, with the beam-line on the right and the monochromator hidden behind the electron analyser chamber in the centre. The various pumps are prominent towards the left of the picture.

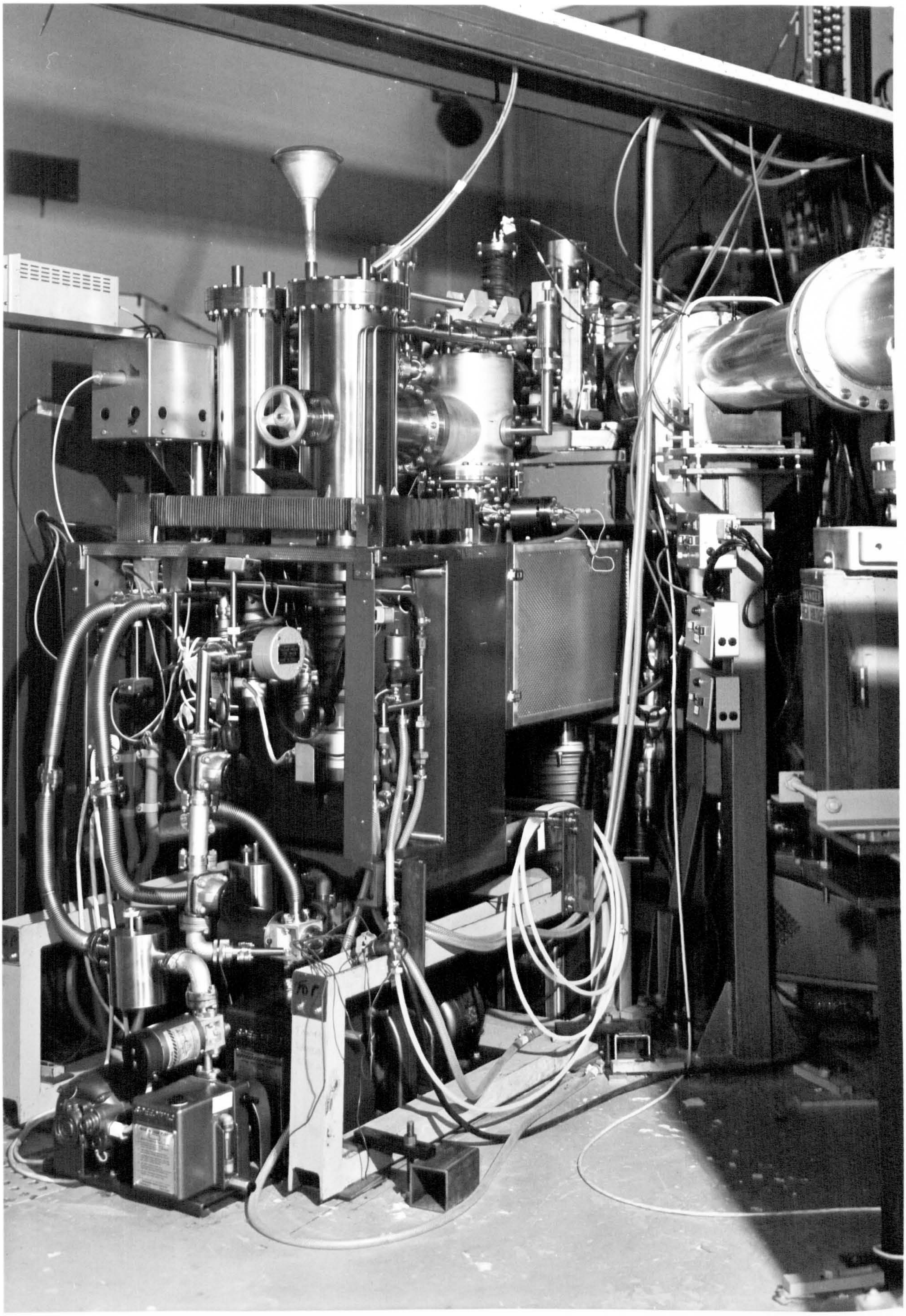

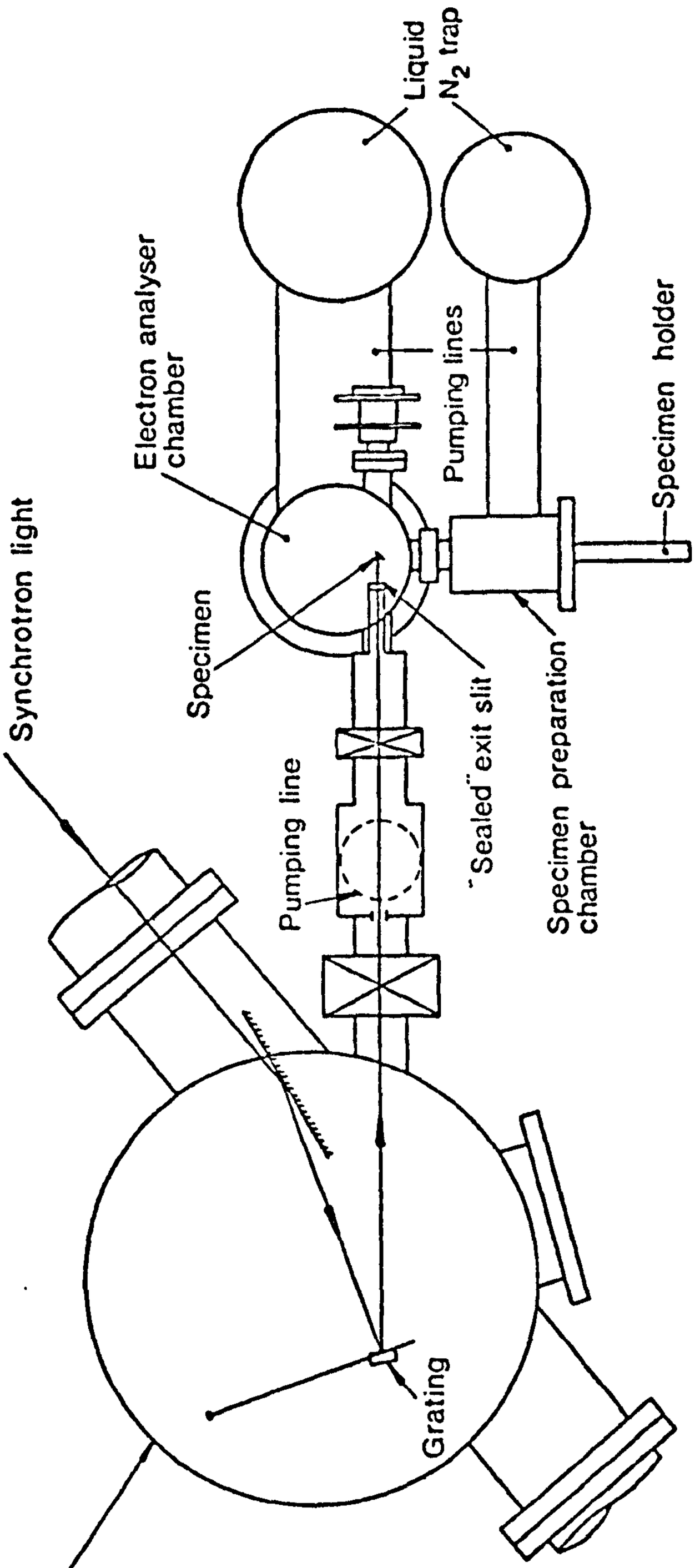

Figure 4.8. Schematic diagram of normal-incidence monochromator and electron spectrometer.

Plate VII The ESCA III electron spectrometer complete with its computer-controlled data acquisition system

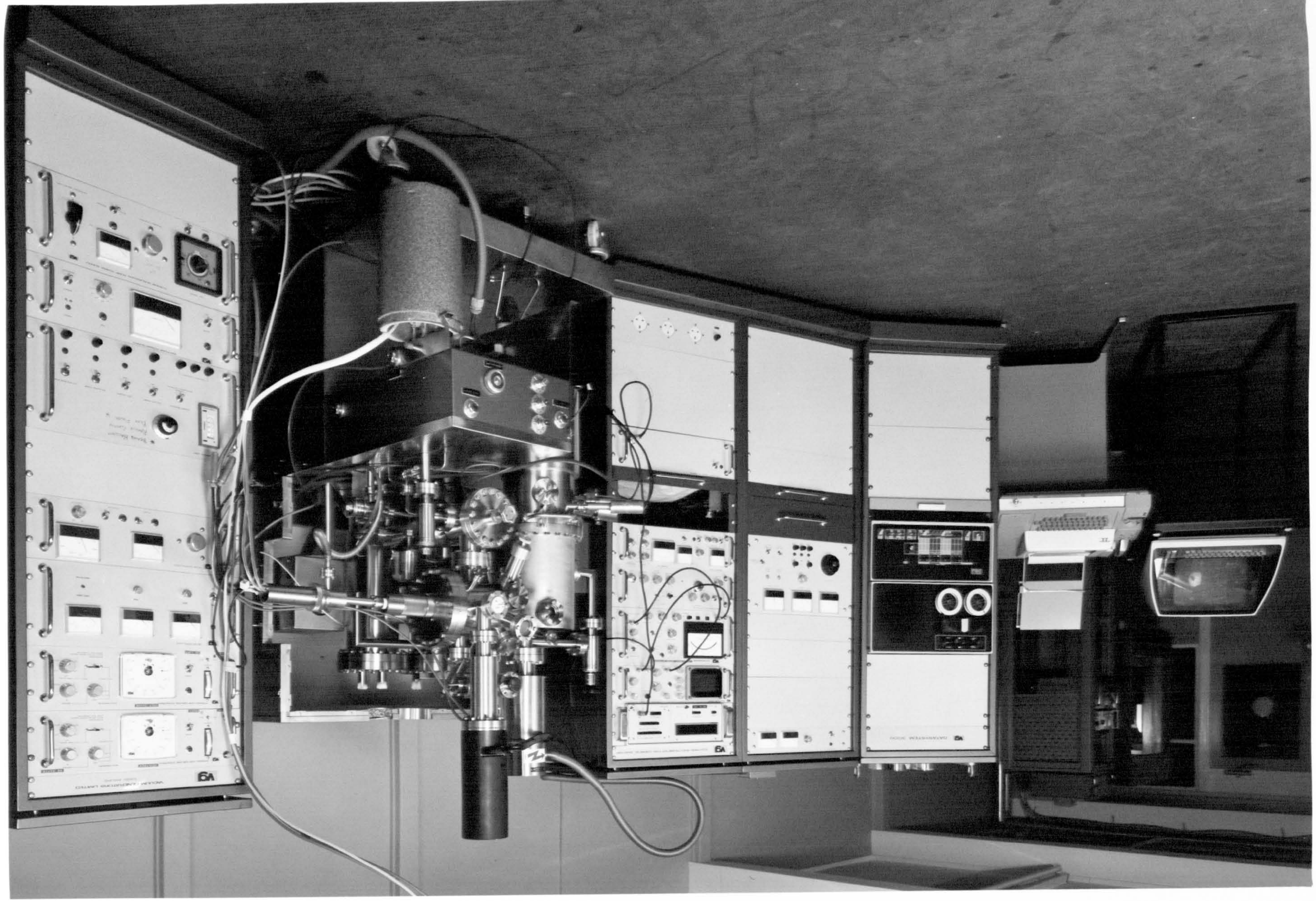

used for electrons with energies less than 100eV.

Dispersive analysers, such as the three types mentioned below, enjoy several significant advantages over non-dispersive types such as the RFA, the most important being their greatly improved signal-to-noise ratios. Since only those electrons within the selected bandpass reach the detector, the noise is proportional to this current, and not to the total integrated current, as is the case with non-dispersive analysers.

A cylindrical energy selector with an angle of $127^{\circ}17'$ ($\pi/\sqrt{2}$ radians) has been used by Feuerbacher and Fitton (1972). This is small and could be very useful for studies of the variation of emission with angle but it appears to be difficult to remove distortions due to the termination of the field, and, more importantly, the angle subtended, and thus the signal accepted must be greatly reduced to obtain good resolution.

Hemispherical deflectors have been extensively used, often with a lens system to retard the incident electrons. Lindau and Hagstrom (1971) describe a hemispherical analyser which achieved a resolution of 30meV, for 10eV incident energy, but they found a large background of low energy electrons (0-4eV) caused by secondary electron emission from the walls of the analyser. Such a spectrometer is also available commercially (Brundle et al. 1974), as used in the ESCAIII described in Chapter 4.3 above.

Some of the most successful low-energy electron spectroscopy of the last few years has been achieved using a cylindrical mirror analyser (e.g. Eastman and Grobman 1972, Rowe and Ibach 1974). This has the particular advantage that it can be made to accept a large variation in the angles of incidence of the electrons without greatly affecting the resolution, and so a balance between the transmission and the resolution of the analyser can more easily be obtained. It is also possible to position hemispherical grids in front of the analyser for pre-retardation or acceleration of the incident electrons so that the analyser itself can be operated at a constant pass energy. This overcomes the problem, inherent in all three types of electrostatic analyser described here, that the resolution is proportional to

the energy of the electrons within the analyser and so the resolution varies across an edc.

It was therefore decided to attempt the design and construction of a cylindrical mirror analyser (CMA).

Design principles of a CMA

Several theoretical analyses of the CMA have been published (e.g. Zashkvara et al. 1966, Sar-El 1967, Risley 1972), and so only the relevant equations will be summarized here. With the notation of Figure 4.9, it is found that electrons which leave the axis with an energy eV_o at an angle $\alpha=42.3^o$, are focussed again on the axis at a distance $L = 6.12r_1$ from the source, if the potential applied to the outer cylinder is $V=0.769V_o \ell n(r_2/r_1)$. Electrons with a slightly different energy $e(V_o+\Delta V_o)$, leaving the axis at an angle $(\alpha + \Delta\alpha)$, cross the axis again at a distance ΔL from the focus, where

$$\Delta L = 5.6\, r_1 \left(\frac{\Delta V_o}{V_o}\right) - 15.4\, r_1 (\Delta\alpha)^3 + 10.3\, r_1 \left(\frac{\Delta V_o}{V_o}\right) \Delta\alpha \qquad (4.1.)$$

Since the focus-point is shifted only by a term of order $(\Delta\alpha)^3$ the angular acceptance $2(\Delta\alpha)$ can be increased greatly while the electron beam is still focussed near the focal-point. It can be shown that

$$\frac{\partial L}{\partial \alpha} = \frac{\partial^2 L}{\partial \alpha^2} = 0$$

and thus the focussing is of second order; the mean angle $\alpha = 42.3^o$ is crucial to this argument.

Several factors will degrade the performance of the CMA from the ideal theoretical values. Because of the wide angular aperture of the analyser, the size of the electron source can limit the resolution obtained. A disc source of electrons of radius ρ ($\ll r_1$) is equivalent to a line source on the axis of length $\rho \cot \alpha$ and thus the trace width, the length of the image

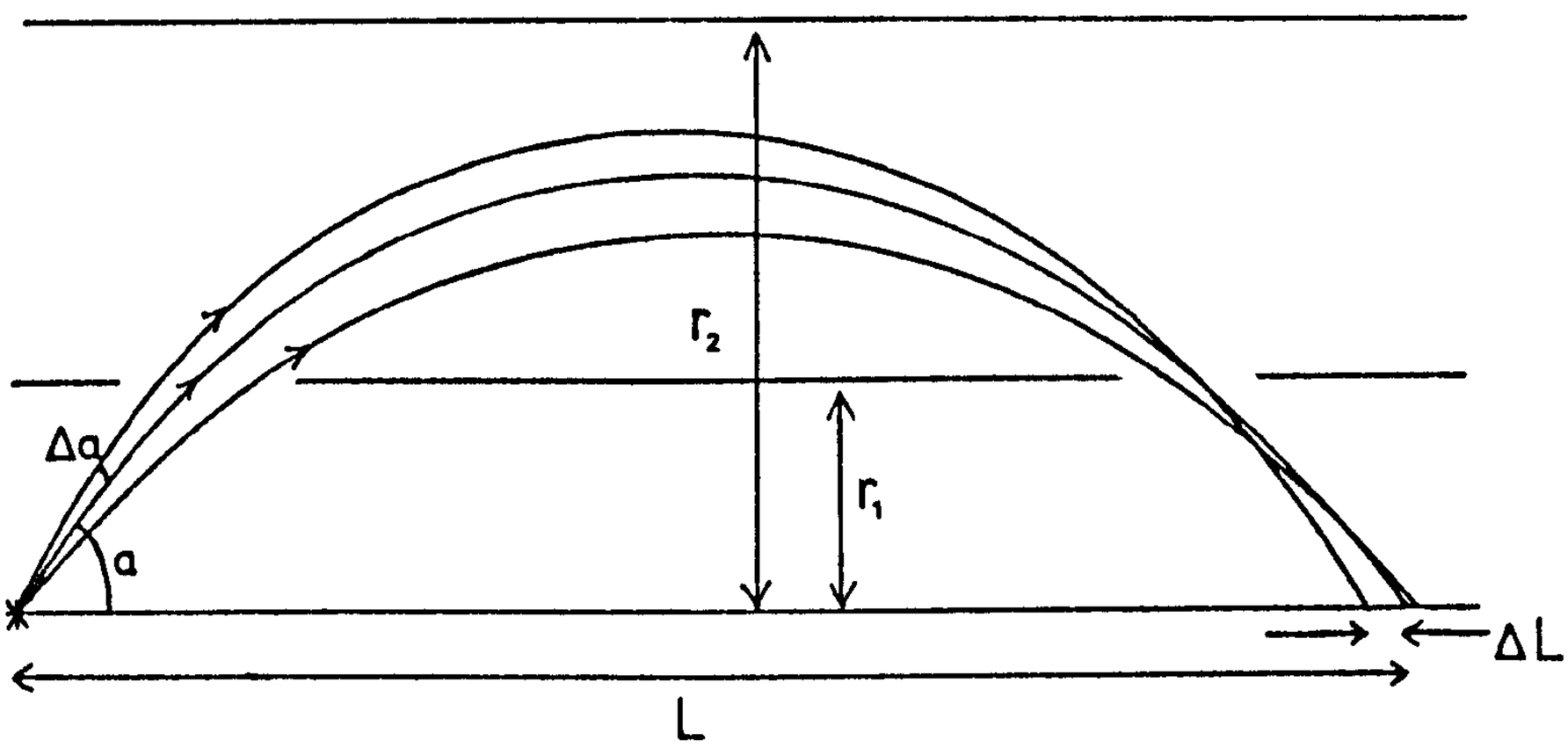

Figure 4.9. Notation for CMA.

r_2 = outer cylinder radius

r_1 = inner cylinder radius

α = angle to axis of perfectly-focussed electron beam

$\Delta\alpha$ = divergence of beam

L = distance along axis to focus

ΔL = shift in focal position

of a point source of monoenergetic electrons, is increased by $\rho \cot \alpha$.

Magnetic fields will very seriously degrade the performance of the analyser. The effects of a weak uniform field along the axis of the analyser will tend to cancel out over the whole electron trajectory, but a transverse field will displace the focal-point by a distance δ, where $\delta = 9.55\, BL^2/\sqrt{V}$, with δ in mm, B in Gauss, L in inches and V in eV. Thus a magnetic field will be particularly harmful for low-energy electrons.

Misalignment of the cylinders can appreciably worsen the resolution, and, of course, the transmission. If one cylinder is displaced a distance x from the axis of the other cylinder, this introduces an energy spread of

$$\frac{\delta V_o}{V_o} = \frac{-2x}{r_2 \ln (r_2 / r_1)} .$$

The analyser built for this work is a development of the simple CMA and is similar to one recently made available commercially (Physical Electronics Industries, Inc., model PHI 15-250). This consists of two cylindrical mirror analysers in series, preceded by a pair of hemispherical grids (Figure 4.10). The resolution should now be determined only by the second section of the CMA and this double-pass CMA should be insensitive to the precise position of the sample with respect to the focal point of the analyser.

Construction of a CMA

The dimensions of the vacuum chamber form the main constraints to be considered in the design of our analyser. Most chambers are of 12" diameter with 6" diameter main ports. The electron multiplier and supporting structure for the analyser occupies a few inches behind the cylinders, and so the total length of the cylinders is limited to about 6". In fact we chose $r_1 = 0.5"$, which gives 2L=6.12". The outer cylinder has $r_2 = 1.5"$, so $V = 0.838 V_o$.

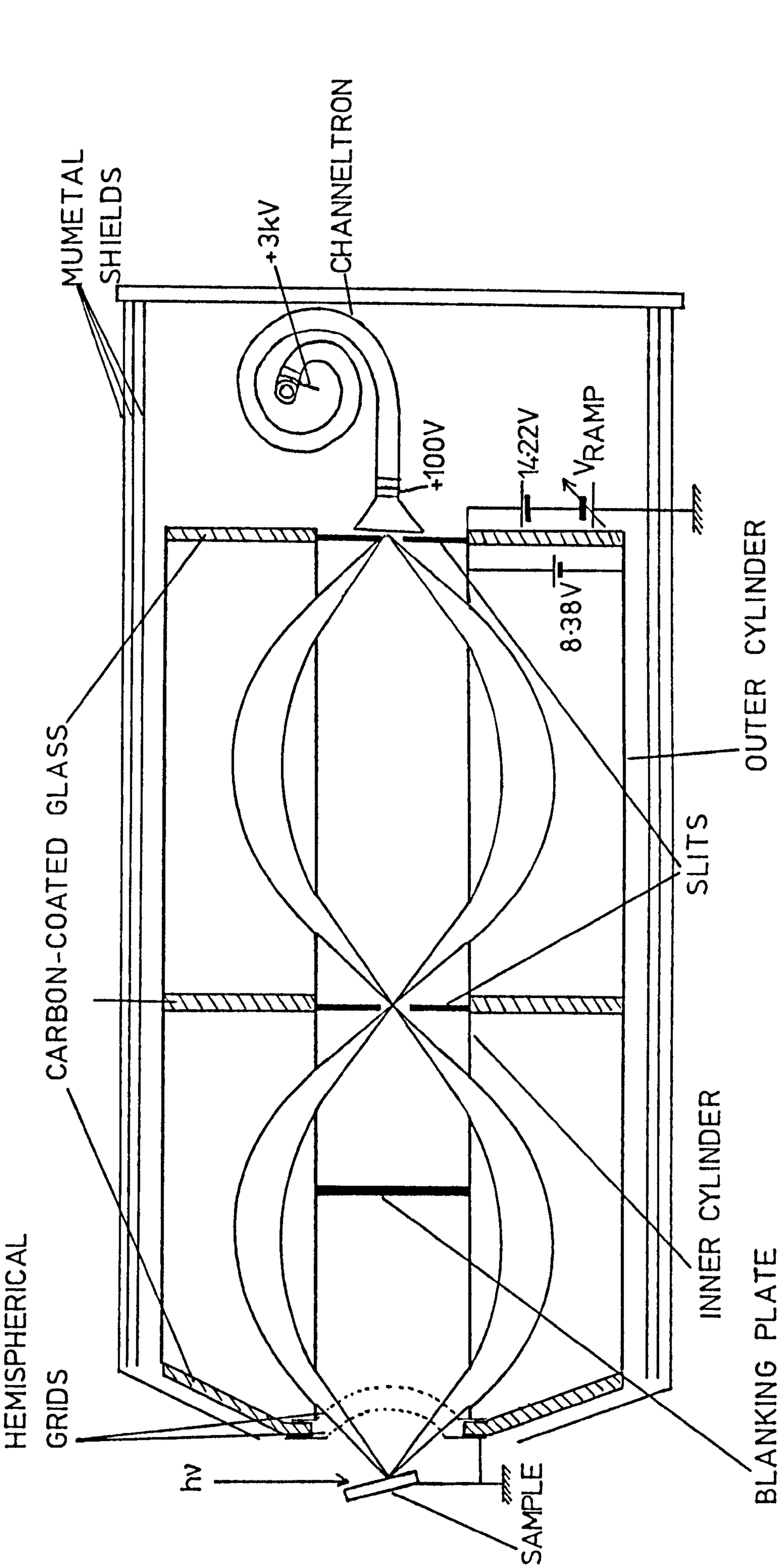

Figure 4.10. Double-pass CMA with pre-retarding grids. The extreme electron trajectories are shown. The cylinder voltages are appropriate to analysis at a constant pass energy of 10eV. Drawn approximately full-size.

The windows in the inner cylinders limit $\Delta\alpha$ to $^{+1.5^o}_{-6.7^o}$, so the solid angle accepted is 0.69 sr, i.e. 11% of 2π .

The cylinders and slit-holders were machined from a bar of oxygen-free, high-conductivity copper, which is one of the few materials which are non-magnetic and compatible with u.h.v.. The hemispherical grids in front of the CMA were manufactured fromstainless-steel mesh, 0.001" wire on 0.010" spacing, which gives a transparency of 81%. These grids were mounted on stainless-steel shim, and a similar arrangement used for grids to cover the four sets of windows in the inner cylinders. The slits themselves were made from 0.010" thick stainless-steel, five pairs being made with slit diameters 0.020", 0.028" , 0.033", 0.040" and 0.048" to enable the effect of slit size on resolution to be measured. Although stainless-steel cannot normally be guaranteed to be free from residual magnetic fields, the whole analyser was tested both before and after bake-out and it appeared not to be magnetised. The cylinders and other parts were held together by 10BA stainless steel screws, and again this caused no apparent problems, although in a similar hemispherical analyser all stainless-steel screws had to be replaced by ones made from tantalum (M.Prutton, personal communication). All stainless-steel parts were covered with a film of copper, evaporated from a tantalum boat, so that all surfaces with which electrons might come into contact should have the same work function. A blanking plate made from o.f.h.c. copper was fitted inside the inner cylinder to stop any electrons passing straight through the centre of the analyser, through the pair of slits and into the channeltron.

An extremely important requirement, which we solved in a novel way, is to ensure that the electrostatic field between the cylinders is uniform, and remains so up to the end of the cylinders. One way of approximating to a uniform field is to position several narrow rings, concentric with the cylinders, each maintained at the voltage appropriate to its distance from the inner cylinder (Bishop et al 1972). However, we need to stop stray electrons from the first stage of the analyser from reaching the second stage, since

it is just conceivable that electrons could have trajectories which would take them through the fourth set of windows without their having undergone proper analysis by the first stage, and so a plate is needed between the two cylinders, level with the first slit. The basic principle of our solution is to use a thin film of carbon, with copper evaporated in a ring at the centre and at the edge, where contact was to be made to the cylinders. It was found that such a coating of carbon, produced by spark evaporation of a rod of carbon against a rod of carbon and clay, had a resistance of about 20KΩ between the inner and outer contacts: this is sufficient to enable a potential of several tens of volts to be held across it, with the potentials in between being automatically maintained. My first attempt was to make these plates, and the cone at the front end of the CMA, from aluminium machined with flanges which interlocked with the cylinders and slits, thus ensuring perfect concentricity and location of the important parts. The aluminium was anodized to give an insulating layer, and then coated with carbon. Unfortunately the anodic oxide on one of the three plates broke down after a short time, and it proved impossible to create a satisfactory plate for this position. The plates and cone were then made from glass, manufactured to the required shape by ultrasonic milling, and treated in a shot-blaster to obtain a suitably rough surface to which the carbon film would adhere readily. This then gave no further trouble.

An awkward characteristic of the CMA is the small distance from the focal point to the front of the analyser. This means that there is very little room for the light beam and that therefore the positioning of the sample is critical. By careful design and very tight tolerances in the twin-grid system at the front of the CMA, the distance from the focal point to the front of the analyser was made 0.25". Calculation reveals that the sample could be moved up to 0.15" linearly closer to or further away from the CMA with some electrons still able to pass through the 0.033" slits, but the total intensity drops off very rapidly as the sample leaves the ideal position. The whole analyser could be moved on a bellows supported by a three-point mounting system.

In an attempt to reduce the penetration of stray magnetic fields into the CMA, it was surrounded by three closely-fitting layers of mumetal, an alloy of nickel, iron, copper and chromium with high magnetic permeability. To form the conical shape over the end of the analyser, pieces of mumetal sheet were spot-welded together. It appeared that this process did not introduce magnetic inhomogeneities.

The analyser had to be assembled very carefully, using a dial gauge bore comparator to ensure coaxiality of the cylinders to within 0.0005". It was realized, after manufacture, that the flange supporting the inner cylinders had been made on the outside of these cylinders and so penetrated into the region between the inner and outer cylinders where the voltages determine the trajectories of the electrons. A scale drawing of the configuration was made on conducting paper, with the cylinders represented by silver dag paint, and the equipotentials plotted. This test, as shown in Figure 4.11, revealed that the voltages in the areas around the windows through which the electrons pass did not differ significantly from their ideal values, despite the undesirable intrusion of the inner cylinder flanges.

The collection of the analysed electrons was achieved by a Mullard 419BL/01 channeltron. An open- ended channeltron was used, with the current leaving the device impinging on a small stainless-steel plate, so that it would be possible to employ analogue current detection, but in fact standard pulse-counting techniques were used.

The assembled CMA is shown in Plate VIII.

Testing of the CMA

The electron energy analyser was tested with electrons produced in three different ways : thermal emission from a tungsten filament, photoemission from an evaporated film of gold, and photoemission from a jet of argon gas. The electrical connections to the CMA, for operation at a constant analysis energy of 10eV, are included in Figure 4.10. It was usually found advantageous to apply a small negative voltage, up to 10V, to the sample to aid analysis of

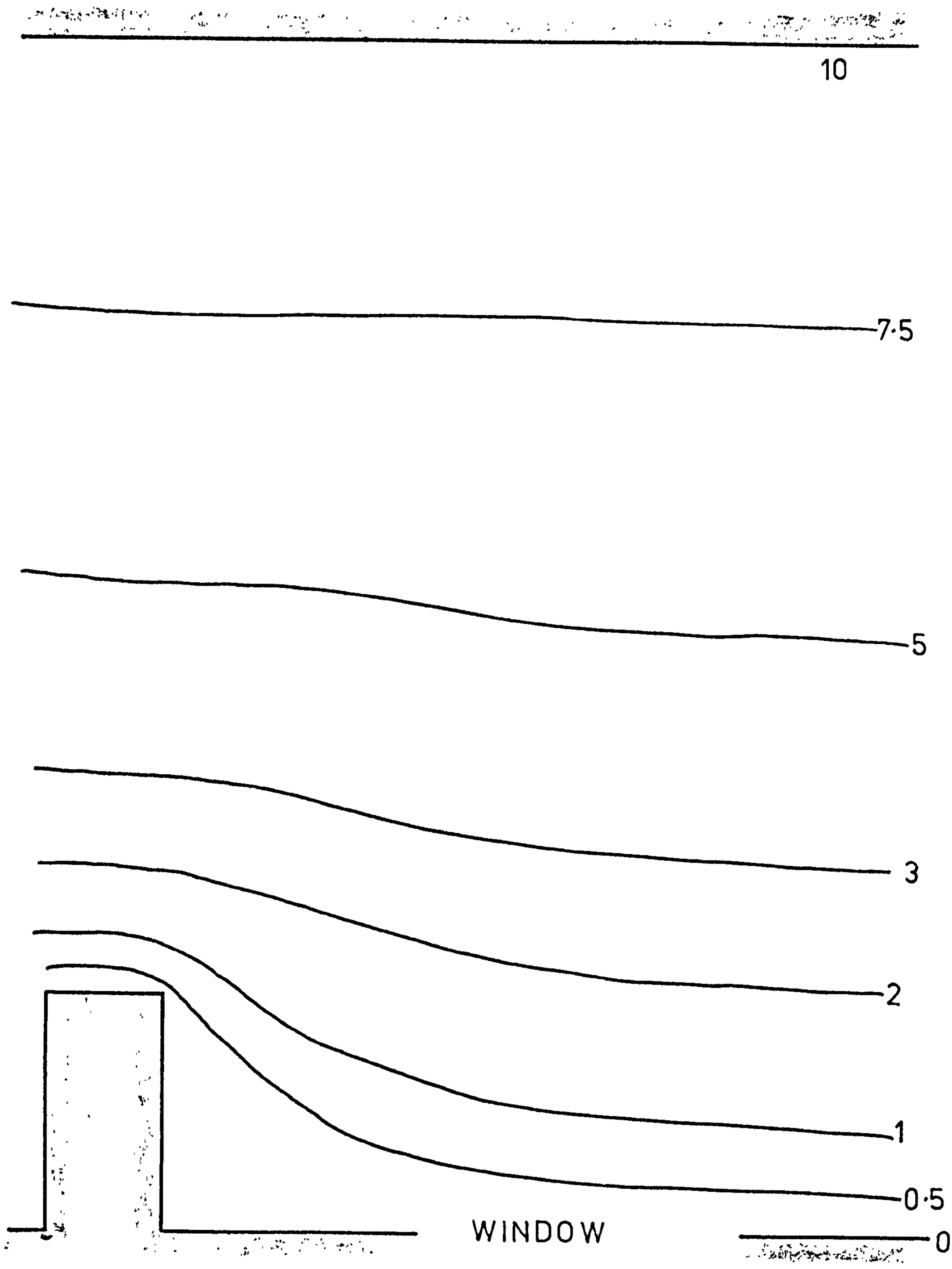

Figure 4.11. Result of simulation, with conducting paper, of voltages between cylinders in CMA.

Plate VIII The assembled CMA. The outer mumetal shields have been removed to reveal the outer copper cylinders and the channeltron.

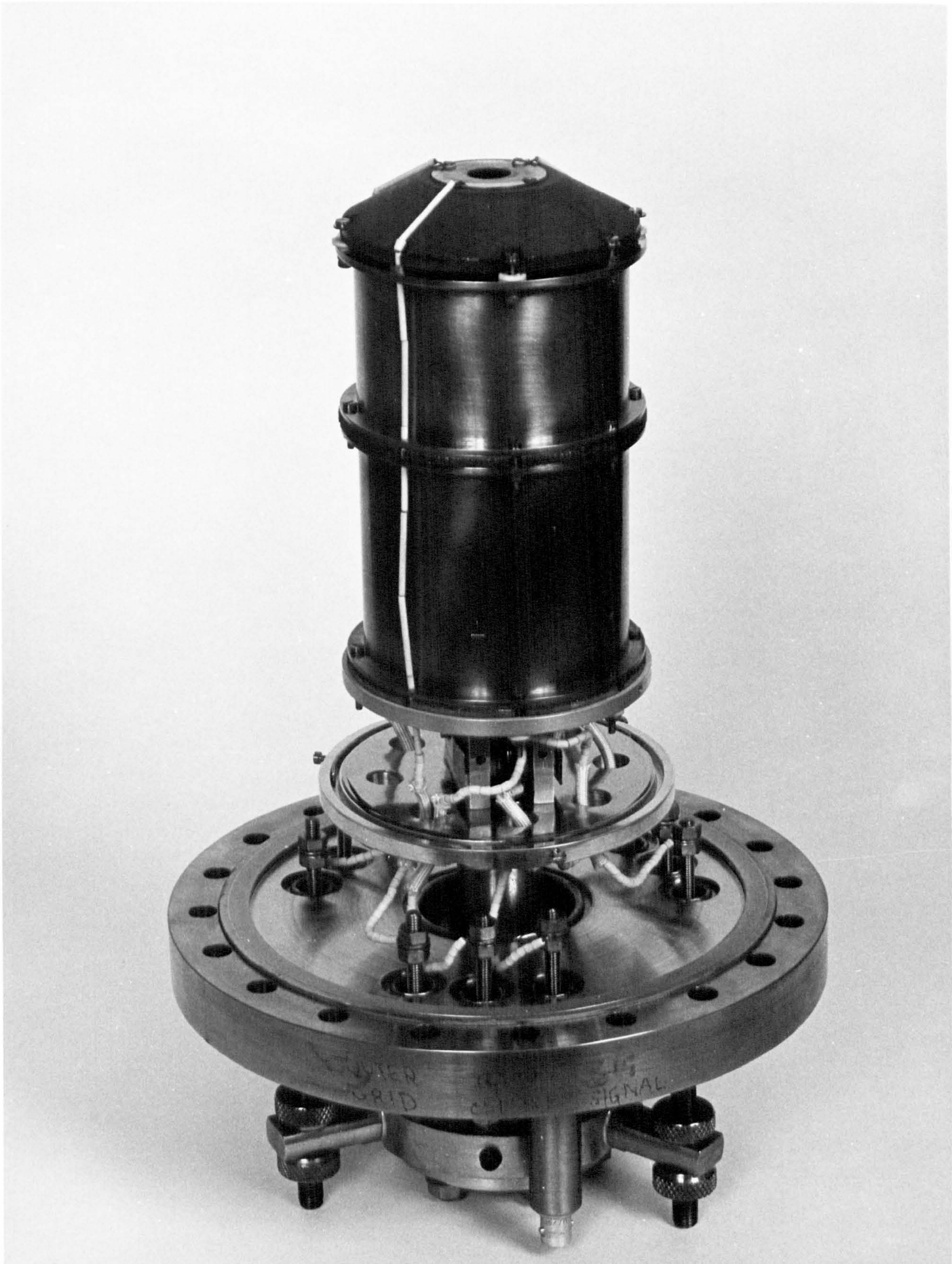
GRID
SIGNAL

the very low energy electrons emitted.

Figure 4.12 shows the analysis of electrons emitted from resistively-heated coiled tungsten filaments. These show a curious feature in that a separate peak is obtained from each coil of the filament. This is explicable by the voltage drop across the filament, which results in electrons from the three (or two) coils having slightly different potential energies.

Photoemission from argon was attempted in order to measure the resolution of the instrument, but this proved an unsatisfactory method. Although a system of moveable capillaries was arranged to produce a fine jet of gas concentrated immediately under the helium discharge lamp, in front of the analyser, such large pressures of argon were needed that it turned out to be impossible to perform this experiment in the ion-pumped chamber. When the apparatus was transferred to a large diffusion-pumped chamber, a broad peak of electrons photoemitted from argon was seen, centred at ~15.8eV. With some imagination, it could be said that a doublet was observed , but the expected sharp structure of two peaks at 15.76 and 15.94eV (Samson 1967) was not well-resolved.

Photoemission from gold, at hydrogen-lamp, NeI and HeI energies, produced encouraging results (Figures 4.13 and 4.14). The lower energy curves appear identical to those obtained with a hemispherical retarding-field analyser, but the higher-energy edc's of Figure 4.14 show considerable evidence that the CMA enhances emission at high kinetic energy and suppresses the low kinetic energy side. Moreover, it was always extremely difficult to obtain reproducible results: a very small shift in the position of the analyser was sometimes sufficient to reduce the signal almost to nothing. It was found also that a small bar magnet, placed next to the vacuum chamber, would totally destroy the signal. It seemed that the large spot size of both lamps made it particularly difficult to focus the analyser satisfactorily.

A series of experiments, to test the resolution of the CMA, was performed on the gold films, the width of the Fermi edge being measured under different operating conditions. The theoretical width of the Fermi edge,

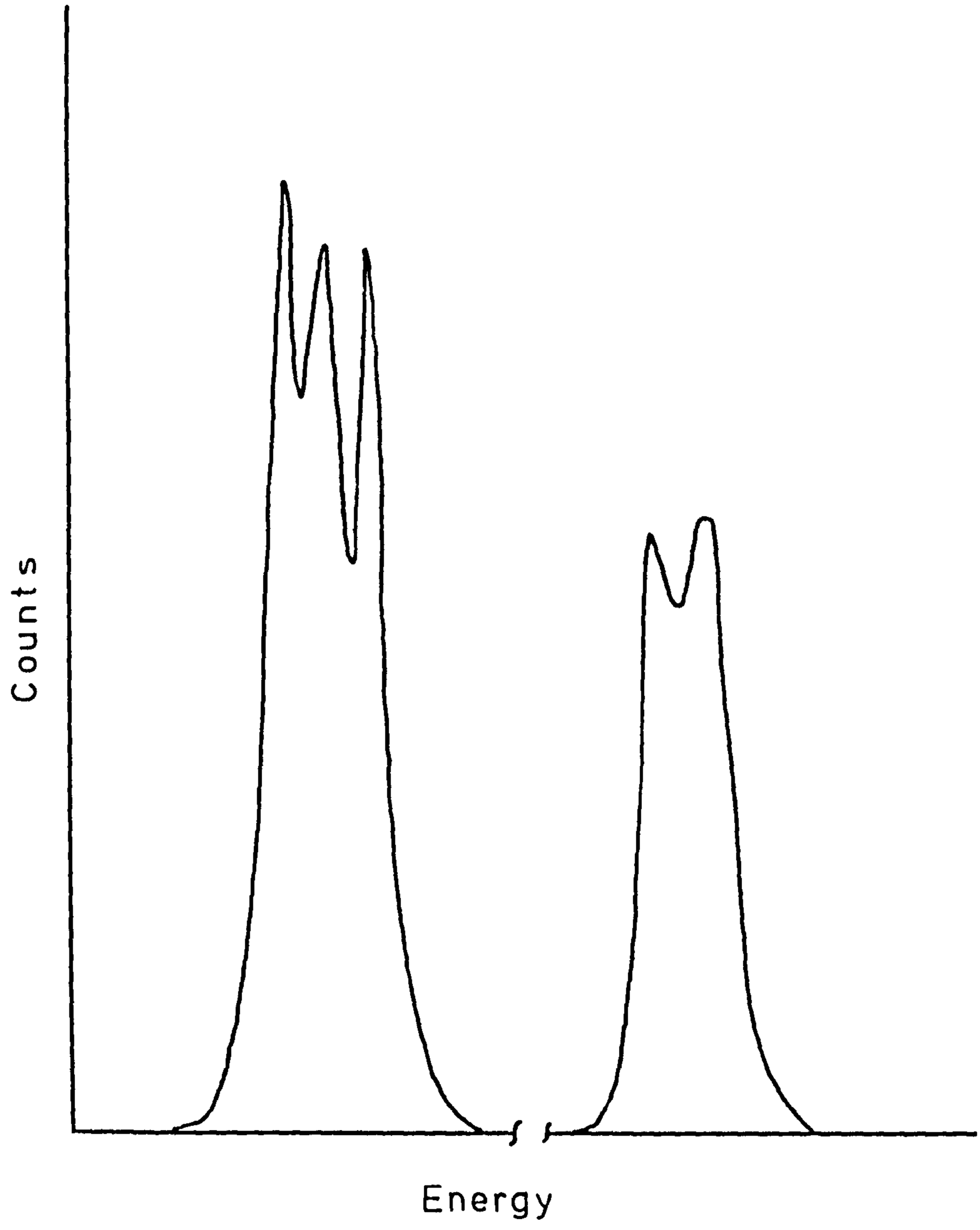

Figure 4.12. Analysis of electrons emitted from heated filaments.

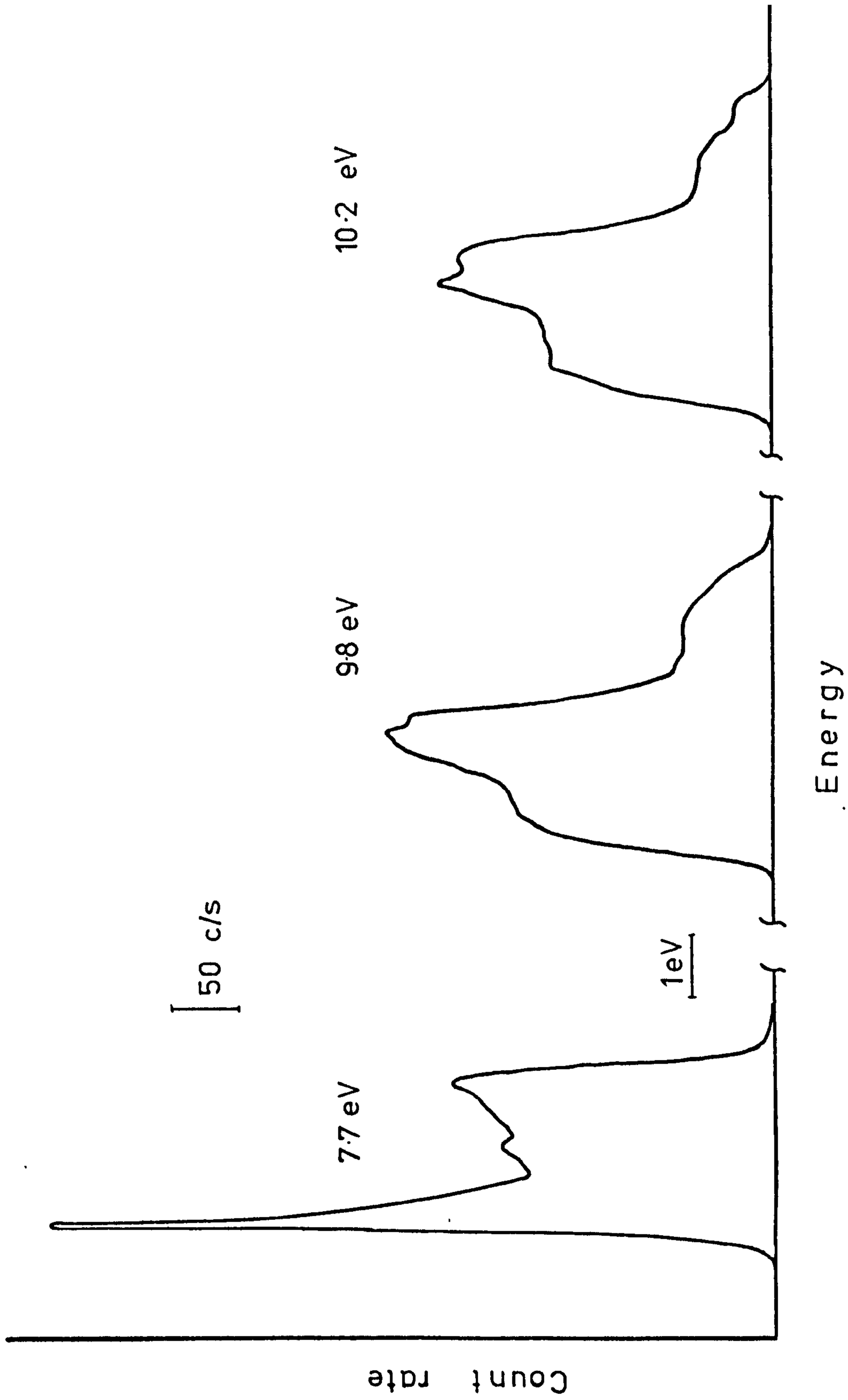

Figure 4.13. Photoemission from gold, at several photon energies, detected by the CMA.

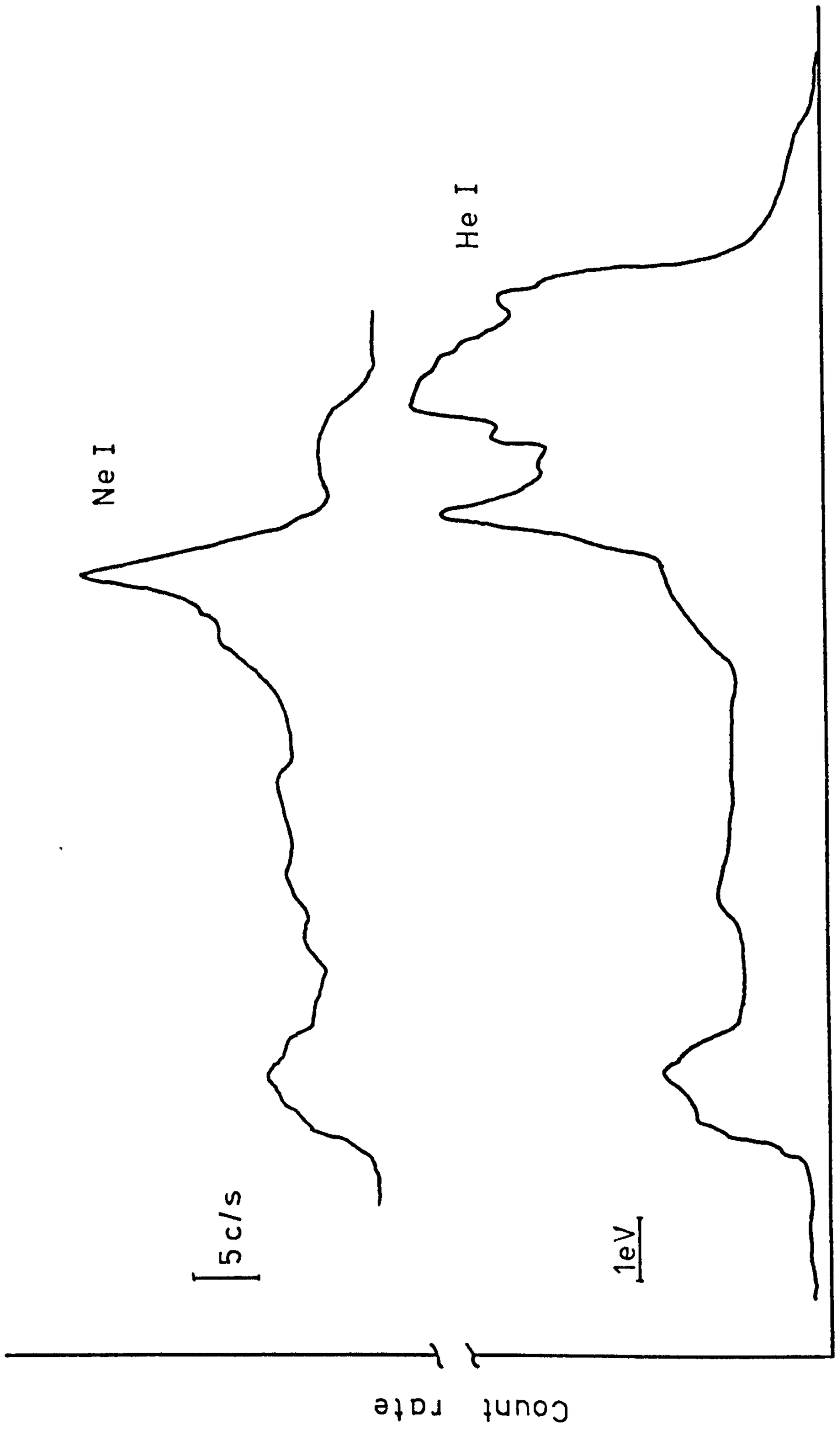

Figure 4.14. Photoemission from gold, excited by NeI and HeI radiation, detected by the CMA.

at room temperature, is readily calculated to be 0.110eV from 10% to 90% of the peak height, and 0.069eV from 20% to 80%. The results, obtained with the H_2- lamp at 10.2eV, are tabulated in Table 4.1. None of the conclusions is surprising : increased analysis energy gives poorer resolution, although a better percentage resolution : narrow monochromator slits marginally improve the resolution, and a slower ramp speed gives better resolution. A further experiment, with 0.033" slits in the analyser in place of the 0.048" slits used in the above tests, yielded the result of 0.199 eV (10% - 90%) and 0.137 eV (20% - 80%) for an analysis energy of 10eV, ramp speed of 60 s/V and 0.25mm monochromator slits. Thus, if we merely subtract from the measured widths the calculated intrinsic widths of the Fermi edge, which is a reasonable procedure if the intrinsic width is narrower than the instrumental broadening function, we obtain values for the broadening introduced by the analyser of 0.175eV (10%-90%) and 0.127eV (20%-80%) for the 0.048" analyser slits, and 0.089eV (10%-90%) and 0.066eV (20%-80%) for the 0.033" slits. Thus, when the area of the slit is doubled, so is the resolution of the analyser. This is, of course, not an unexpected finding, assuming that the analysed electron beam overfills the final slit, and so the resolution is determined largely by the size of the final slit. In fact the theoretical resolution is given by $\Delta V/V = d/5.6r_1$, where d is the trace width . If we assume that d is defined by the final slit, we obtain values for ΔV (at V=10eV) of 0.172eV with 0.048" analyser slits and 0.118eV with 0.033" slits, very close to the values which were actually measured.

Finally, we consider the count rate which theoretically would be expected. The CMA accepts 0.069 sr , which, assuming isotropic emission, means that 11% of the emitted electrons can enter the analyser. Support posts for the windows take up one-quarter of the circumference, and so this figure is reduced to 8.25%. Electrons have to pass through six grids, each of 81% transparency, with four of them at an average angle of 42.3^{o} to the trajectory, so the total transmission $= (0.81)^6 \times \sin^4(42.3^{o}) = 0.06$. From Eq. 4.1 with $\Delta L \sim 0.5$ mm and $\Delta\alpha = 4.1^{o}$, $\Delta V_o/V_o = 0.0071$: at

Table 4.1. Effect of operating parameters on CMA resolution

Analysis energy	10% - 90%	20% - 80%
10eV	0.285	0.195
15eV	0.380	0.227
20eV	0.405	0.255

Ramp 60 s/V Monochromator slit 0.250mm

Monochromator slit	10% -90%	20% - 80%
0.25mm	0.285	0.195
0.125mm	0.260	0.185
0.05 mm	0.241	0.154

Analysis energy 10eV; Ramp 60s/V

Ramp speed	10% - 90%	20% - 80%
16 s/V	0.626	0.430
60 s/V	0.285	0.195
160 s/V	0.247	0.182

Analysis energy 10eV; Monochromator slits 0.250 mm

10eV analyser energy, $\Delta V = 0.07$. Thus, for a spectrum 16eV wide, $0.0825 \times 0.06 \times 0.07/16 = 2 \times 10^{-5}$ of the total emitted signal can reach the channeltron. For an emitted current of 10^{-10} A this gives 30,000 counts/s. So the actual signal is lower than the theoretical signal by a factor of between 100 and 1000.

Although this CMA, as has been shown, did work, and produced some results of high quality, it was extremely sensitive to the exact alignment with respect to the sample and reproducible results were very difficult to obtain. The low count rates obtained and the susceptibility to changes in magnetic fields were defects which had to be remedied. It was only after I had taken the decision to modify the CMA that it came to light that other workers with double-pass CMA's had often tolerated a resolution around 0.5eV in order to obtain enough current (Ibach and Rowe 1974, Eastman and Freeouf 1974).

The main modifications carried out were the manufacture of new inner cylinders, with flanges on the inside, and provision for larger, more precisely located slits. The problem of magnetic fields was not tackled because no solution was apparent. It seems that the mumetal shielding may have done more harm than good, since it necessarily finished near the sample and perhaps concentrated magnetic field lines there, just where the electrons were emitted. The most satisfactory solution would be to perform the experiment in a chamber fabricated from mumetal; these have recently become available.

All the UPS experiments described in Chapters 5 to 7 were performed with a RFA, and the modified CMA was not actually tested.

CHAPTER 5

GALLIUM PHOSPHIDE

5.0. Introduction

The aim of the work presented in this chapter was twofold: to investigate the electronic structure of clean GaP (110) and to monitor the process of oxygen adsorption on this surface. Adsorption of oxygen was studied both to determine the mechanism of the initial stages of the adsorption process and to help in elucidation of the clean surface structure, since no technique is wholly surface-sensitive and adsorption should affect surface features and leave bulk effects unperturbed. The main method used was UPS, but all the other techniques mentioned in Chapter 4 were employed. The combination of results obtained from several types of experiment is particularly valuable in surface studies.

In the course of these experiments several interesting features were observed which, although not a part of the central theme of this Thesis, are discussed here in some detail; in particular, the bulk band structure of GaP, the assignment of Auger transitions, the nature of plasmon losses and the problems of electron beam effects during oxygen adsorption are considered.

The experimental results are summarized at the end of the Chapter, with some conclusions presented during the Chapter. Further conclusions are drawn in Chapter 8, in conjunction with data from the experiments on InP and GaAs.

5.1. UPS of clean GaP

The electron energy distribution curves (edc's) obtained in the photon energy range 7.4 to 11.6eV are shown in Figure 5.1. The spectra are normalised so that the area under each curve is proportional to the yield of the material at that photon energy. The ordinates are shifted to facilitate presentation of the data; the abscissae represent a reduced scale with energies referred to the valence band maximum.

The yield of GaP, in electrons per absorbed photon, is plotted in

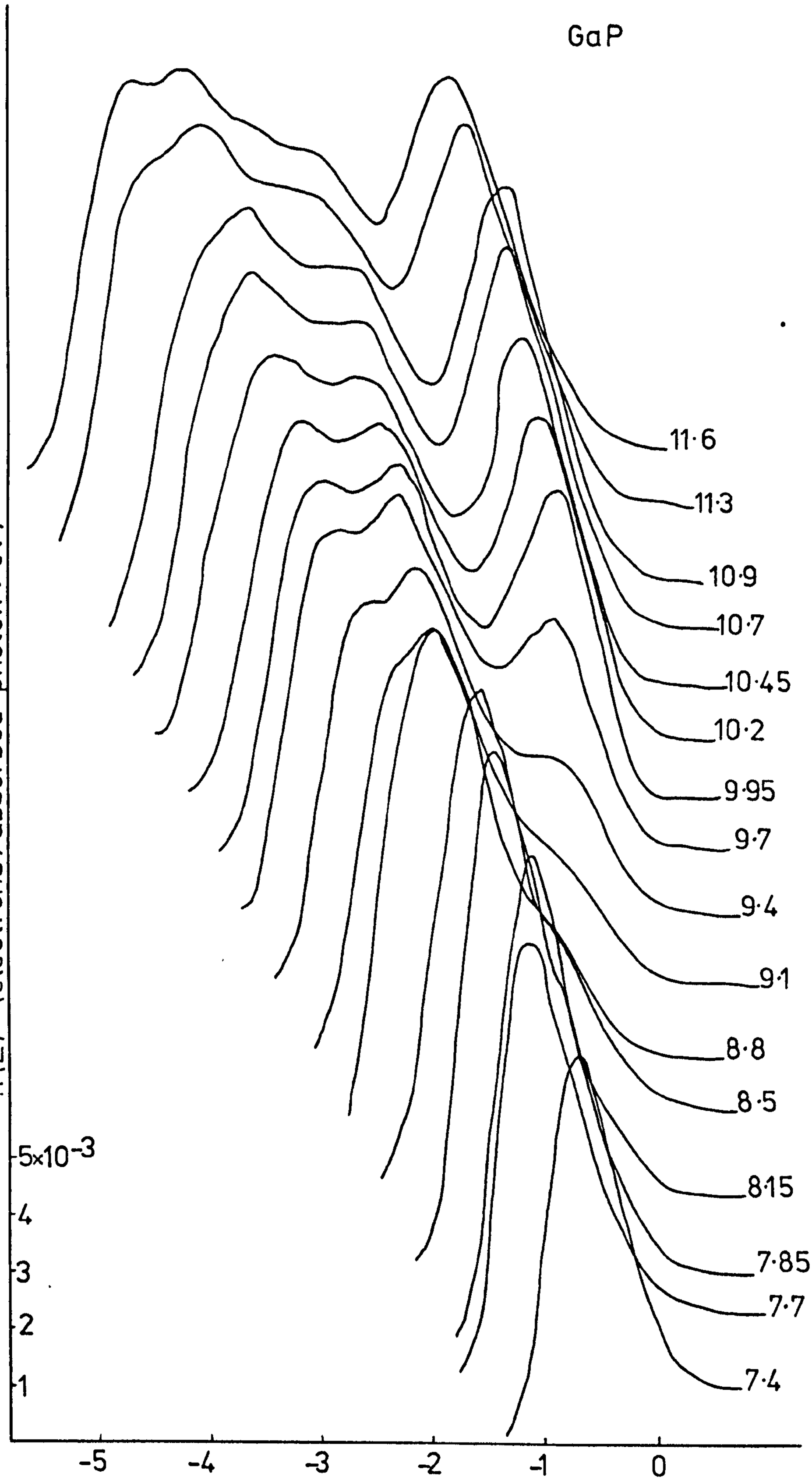

Figure 5.1. UPS electron energy distribution curves from clean GaP (110) in the photon energy range 7.4 to 11.6 eV.

Figure 5.2. This graph is compiled from data taken in two ways: directly, by measuring the total collected current as a function of photon energy, and indirectly, by summing the area under each edc. Results obtained by these two methods are in excellent agreement. Values of reflectivity needed to convert from incident to absorbed photon flux, are interpolated from the compilation by Seraphin and Bennett (1966). The measurements are made absolute by taking the yield of a gold film, evaporated onto the GaP surface; the yield of Au is known (Krolikowski and Spicer 1970) and our results are normalised by these.

Several cleaves were performed, and no significant differences from the data presented in these two Figures were observed. Raw edc's for four of the higher photon energies are shown in Figure 5.3 in order to illustrate the quality of the data: some of the subtle structure visible in the original edc's is lost during the process of normalisation and re-drawing, but all features are included in Figure 5.4.

It is evident that one of the main virtues of photoemission energy distribution data - the enormous quantity of useful data obtained- also leads to problems in presentation and analysis of the results. The most important information to be obtained is the final energy of various transitions and the way in which this final energy changes with photon energy. Bearing in mind that the exact amplitude of a feature is usually unimportant compared with its energy, the essential information on peak positions is extracted and displayed in a form more amenable to analysis in Figure 5.4. The value of photon energy for each edc is added to the initial energy (Figure 5.1) to produce the final energy, referred to the valence band maximum. Shoulders and peaks in an edc are obviously equivalent, but it is more difficult to determine accurately the energy location of a shoulder, particularly on a strongly sloping background. Each group of peaks or shoulders in Figure 5.4 is labelled for ease of reference.

Although, as pointed out in Chapter 3, it is unrealistic to attempt to separate "bulk" and surface contributions to UPS, we here interpret the structure plot of Figure 5.4 in terms of the bulk band structure of GaP

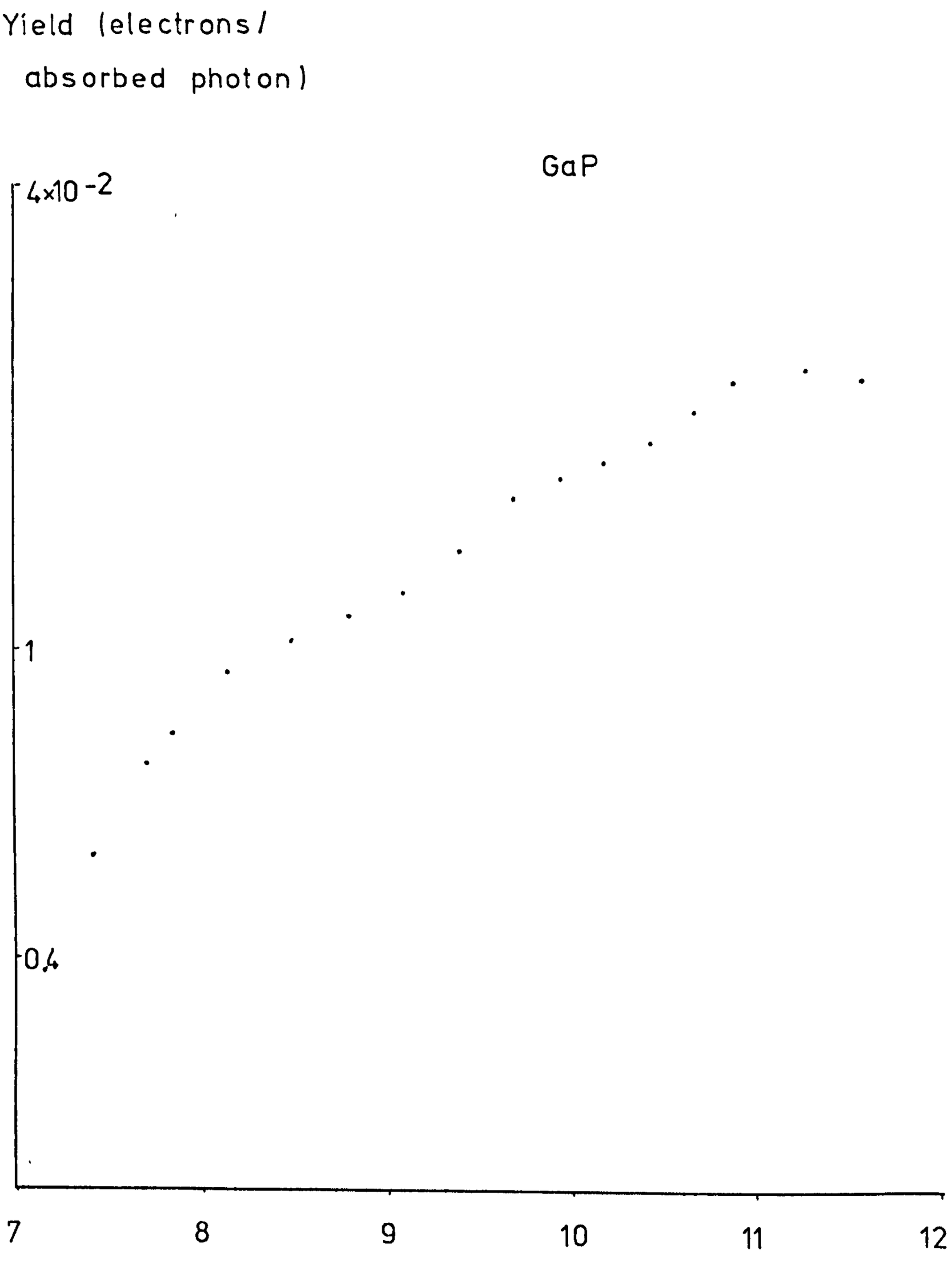

Figure 5.2. Yield versus photon energy for GaP

Figure 5.3. Some raw edc's for GaP

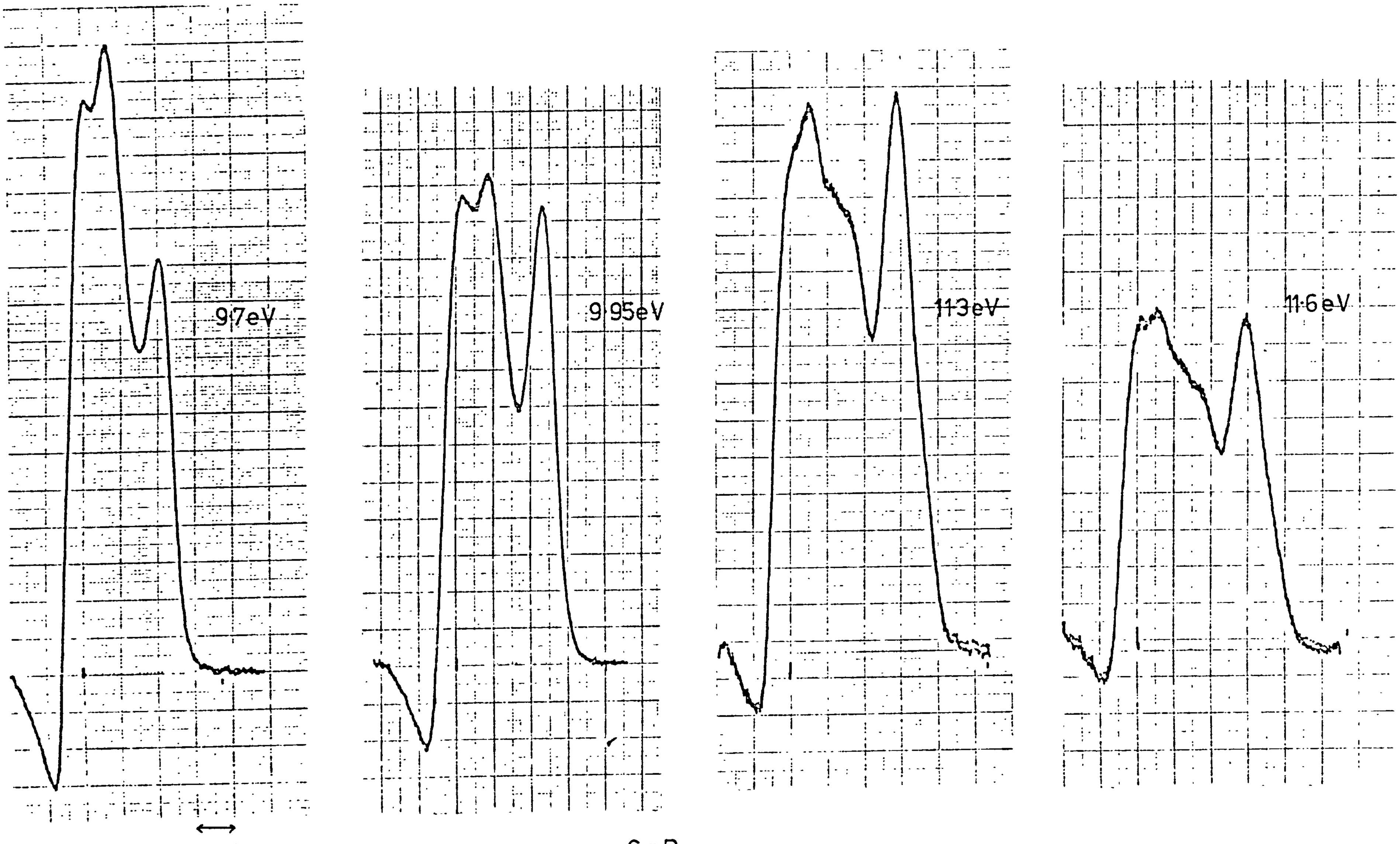

GaP

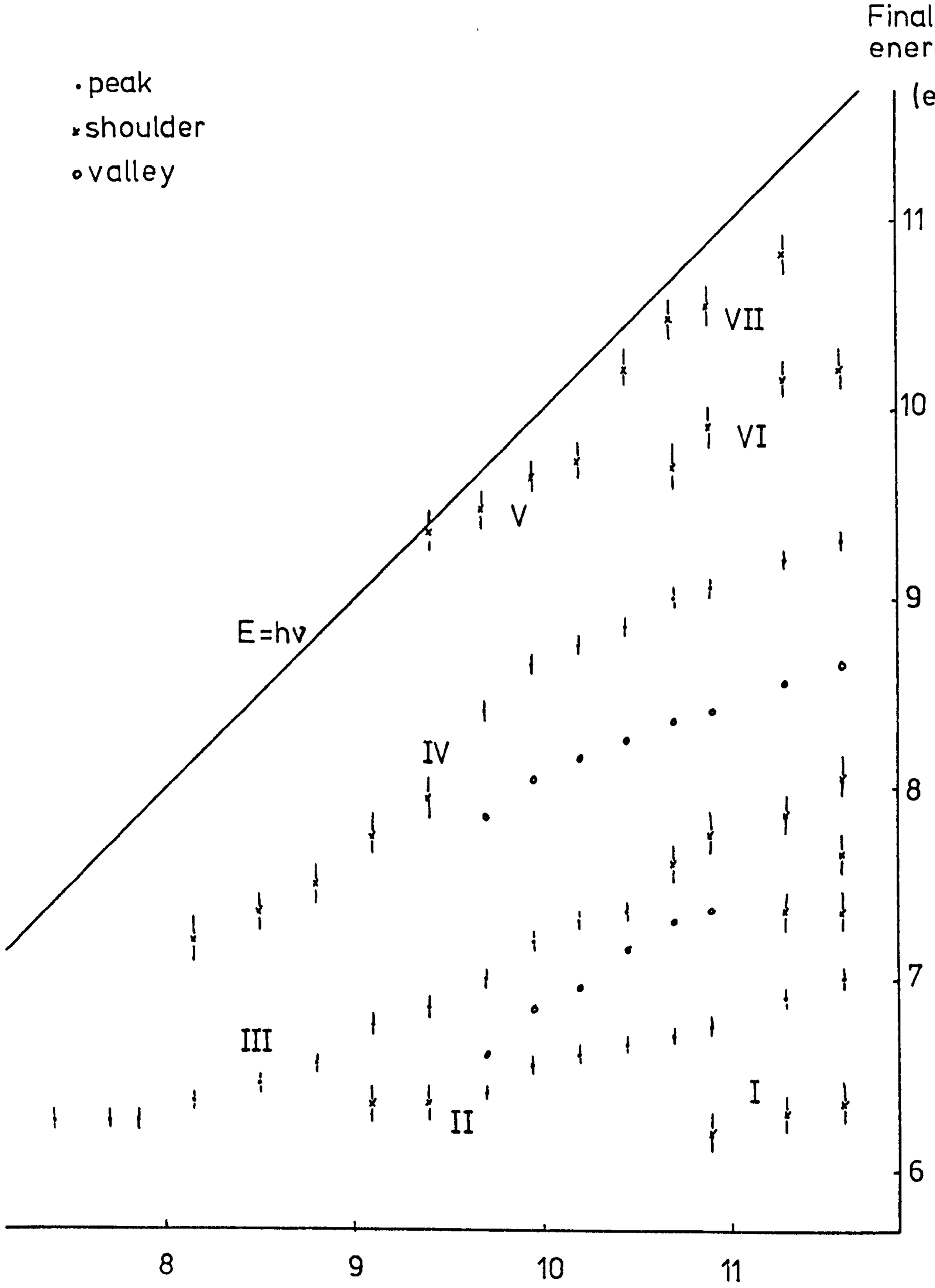

Figure 5.4. Structure plot for GaP, from Figure 5.1.

because it is important to establish whether any observed structure could be due to surface effects. Whilst the eventual aim of UPS measurements might be to provide parameters for construction of a band structure ab initio it is at the moment best to refine band structure calculations by highlighting discrepancies between observed and calculated transition energies. A major drawback in such a procedure is the lack of any published band structure for GaP which extends to energies greater than about 7eV above the valence band maximum. The minimum final energy detectable, owing to the work function, is a little over 6eV and obviously final energies up to $\sim$12eV are required. Fortunately we are able to overcome this problem with the band structure shown in Figure 5.5 , which is an extension of an earlier empirical pseudopotential calculation (Cohen and Bergstresser 1966) contained in an unpublished report (Eden 1967). Spin-orbit interaction, which splits most of the levels and lifts the degeneracy of some E-$\underline{k}$ lines, has been ignored: the effect for GaP is only of the order of 0.05eV (Pollak et al. 1966).

It is obvious that those electrons which have final energies at the Einstein limit E=hν must have originated from states actually at the valence band maximum, i.e. from Γ_{15}^{v} . Since the $\underline{k}$-vectors of the initial and final states must be equal for direct transitions (neglecting phonon interactions) we thus find the energies of Γ points in the conduction bands to be 9.4 eV and 10.4eV. All energies in this section are referred to the valence band maximum, and carry an error $\sim \pm$ 0.1eV). Figure 5.5 gives Γ_{1}^{c} at 9.8eV and Γ_{12}^{c} at 9.3eV, but an empirical OPW calculation (Herman et al.1968) gives Γ_{12}^{c} at 10.5eV and Γ_{1}^{c} at 9.5eV. Although the fine details of point group notation are not really relevant here, the ordering of Γ_{12}^{c} lower than Γ_{1}^{c} appears in conflict with all calculations for all other III-V compounds (e.g. InP(Neumann et al 1975), GaAs (Saravia and Duomarco 1973))so we assume $\Gamma_{12}^{c} > \Gamma_{1}^{c}$ and thus find Γ_{12}^{c} = 10.4eV and Γ_{1}^{c} = 9.4eV. Recent electroreflectance spectra for GaP, taken with synchrotron radiation, gives transitions which probably correspond to Γ_{1}^{c} = 9.38eV and Γ_{12}^{c} = 10.27eV (Aspnes et al 1975), in excellent agreement with our data, and close to the OPW values. The calculated energy of Γ_{12}^{c}

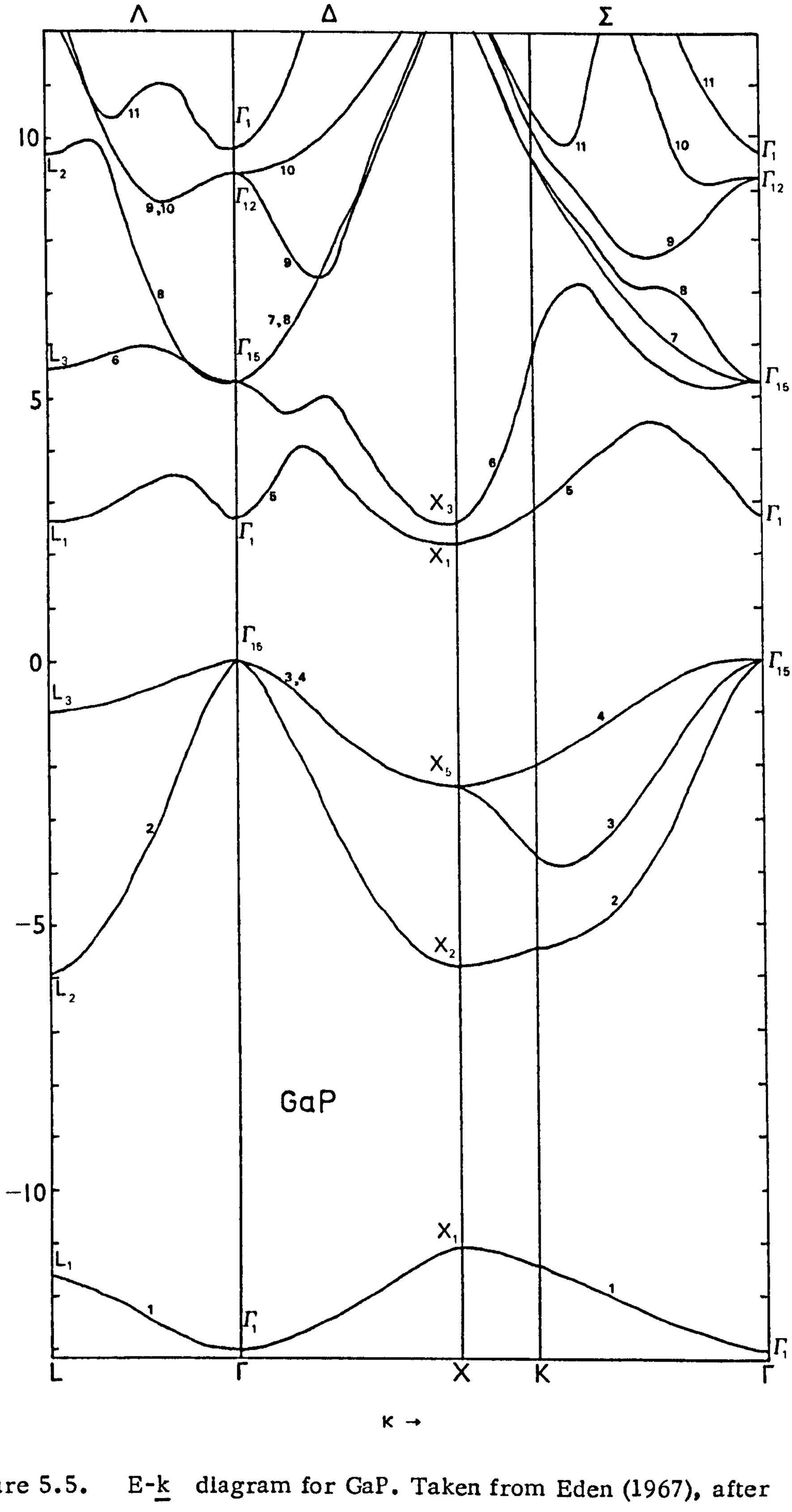

Figure 5.5. E-$\underline{k}$ diagram for GaP. Taken from Eden (1967), after Cohen and Bergstresser (1966)

is said to be very sensitive to small changes in the pseudopotential form factors (Saravia and Duomarco 1973) - although we note that exactly the opposite comment has also been made! (Phillips, quoted as private communication by Aspnes et al 1975) - and it may not be surprising that the OPW calculation gives results in much better agreement.

The identification of Γ points by other techniques (e.g. reflectivity or ELS) is extremely difficult. These transitions are typically very weak because the region around Γ occupies such a small fraction of the Brillouin zone: for example, the volume in $\underline{k}$-space of a sphere around Γ with a radius as much as one-fifth of the distance to the zone edge is still much less than 1% of the volume of the first Brillouin zone. Although this same argument holds for UPS, and the transitions we observe are weak, no other transitions are possible to the same final energies and the unambiguous determination of Γ points is uniquely feasible in UPS. Γ_{15}^{c} and the lower Γ_{1}^{c} are of course below the vacuum level and thus inaccessible in our experiment.

No other structure is as easily identifiable in our structure plot. Three other types of feature, if present, could be readily picked out without detailed reference to a calculated band structure. A flat-band region in the conduction bands will tend to produce a peak in edc's at a final energy equal to the energy of the flat-band region and thus a horizontal straight line in the structure plot. A flat region in the valence bands at an energy E_0 below the valence band maximum will lead to a line $E = h\nu - E_o$ at 45^o in the structure plot. And a region in $\underline{k}$-space with valence band and conduction band parallel so that the final energy changes with constant photon energy will give a vertical line in the structure plot. No features corresponding to any of these three types of structure are seen in our data. Parts of three lines (labelled I, II, III in Figure 5.4) are roughly horizontal at the lowest photon energies at which they appear: I is attributed to scattered electrons, and the flat portions of II and III are probably artifacts caused by their proximity to the photothreshold . The rapidly rising escape probability will tend to shift all peaks in this region to higher energy.

To identify the other groups of structure in Figure 5.4 it is necessary to consider in greater detail the theoretical band structure of Figure 5.5. We have calculated the theoretical curves for all transitions with final energies in the range 6 to 12eV and photon energies from 7 to 12eV: this information is given in Figure 5.6. There is in fact an infinite number of possible lines in $\underline{k}$ -space along which to make such plots. Most band structure calculations concentrate on the three lines denoted Λ (Γ - L), Δ (Γ - X) and Σ (Γ - K - X) and data are sometimes available for the lines X-W and K-W. Because of the symmetry of the first Brillouin zone (Figure 2.2) these lines are especially important in that the energy eigenvalues along these lines, and particularly near the zone edges, tend to reflect a large volume of the Brillouin zone. In the photon energy range accessible to us, direct transitions can occur between the top three valence bands - all bands being numbered from the lowest band upwards in Figure 5.5 - and the conduction bands 6 - 12. The transitions are marked in Figure 5.6 with the numbers of the two bands and the symmetry line. Note that for the purposes of construction of this Figure from Figure 5.5 we have transposed Γ_1^c and Γ_{12}^c and placed them at 9.4 and 10.4 eV respectively, with all bands derived from them retaining unchanged their numbering and dispersion. Inspection of the closely-related band structures for InP (Figure 6.5) and GaAs (Eden 1967) shows this procedure to be reasonable, except that a higher-lying Γ_{12} will have minima a short distance away from Γ : this will tend to produce more kinks in the region of the structure plot with final and photon energies slightly less than Γ_{12} (around 10eV), making this area of Figure 5.6 even more crowded but not substantially changing the shape of the plot.

With the aid of the theoretical structure plot all groups of features can now be identified. To facilitate comparison Figures 5.4 and 5.6 are superimposed in Figure 5.7. Owing to the large number of possible transitions in this region, and the low density of states around Γ, it is difficult to assign features V and VII with certainty, but it appears that the highest energy feature (VII) involves the set of conduction bands (9, 10, 11) around the upper Γ point, the initial state being almost exclusively in the uppermost valence band (4),

GaP

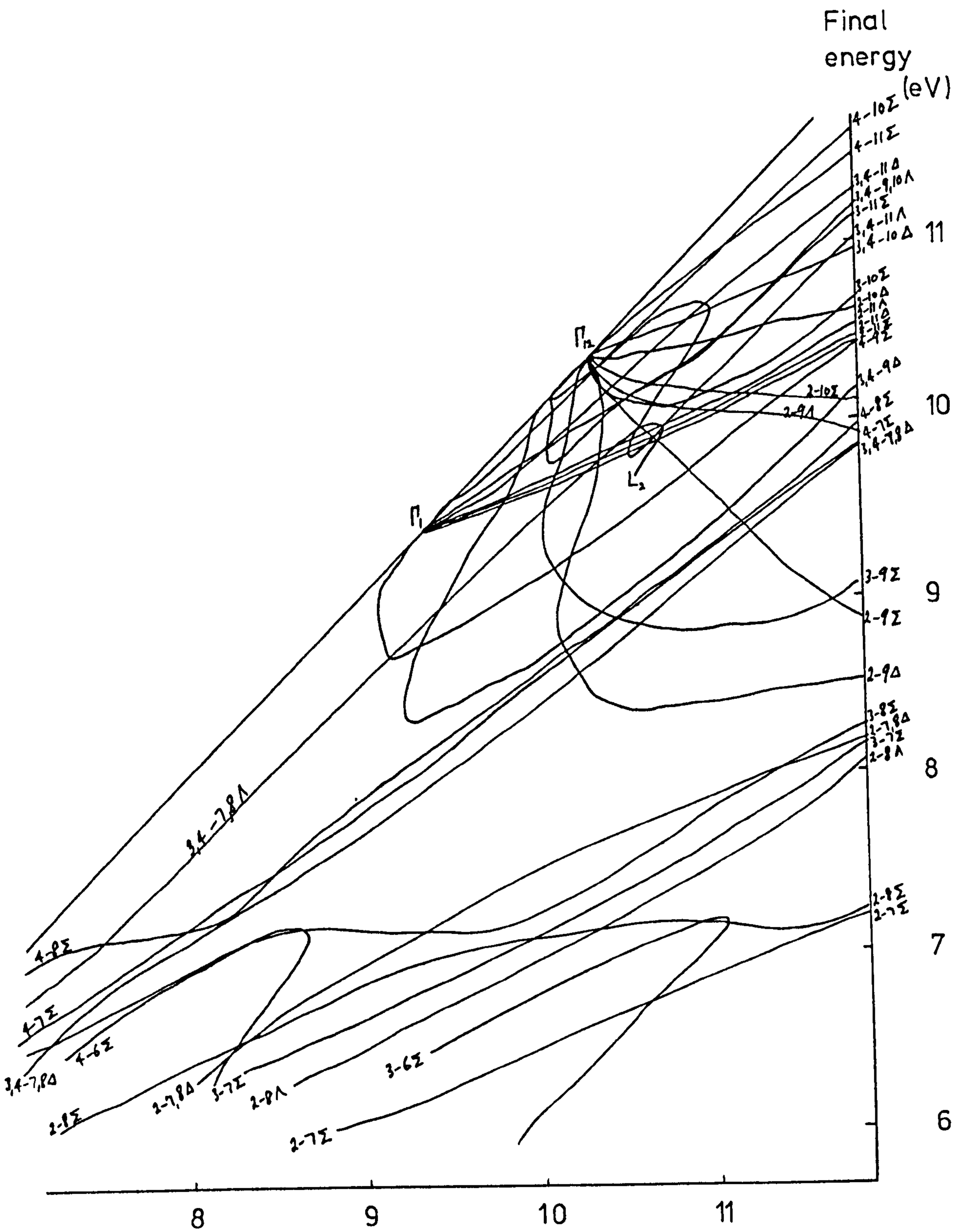

Figure 5.6. Theoretical structure plot for GaP (from Figure 5.5.)

GaP

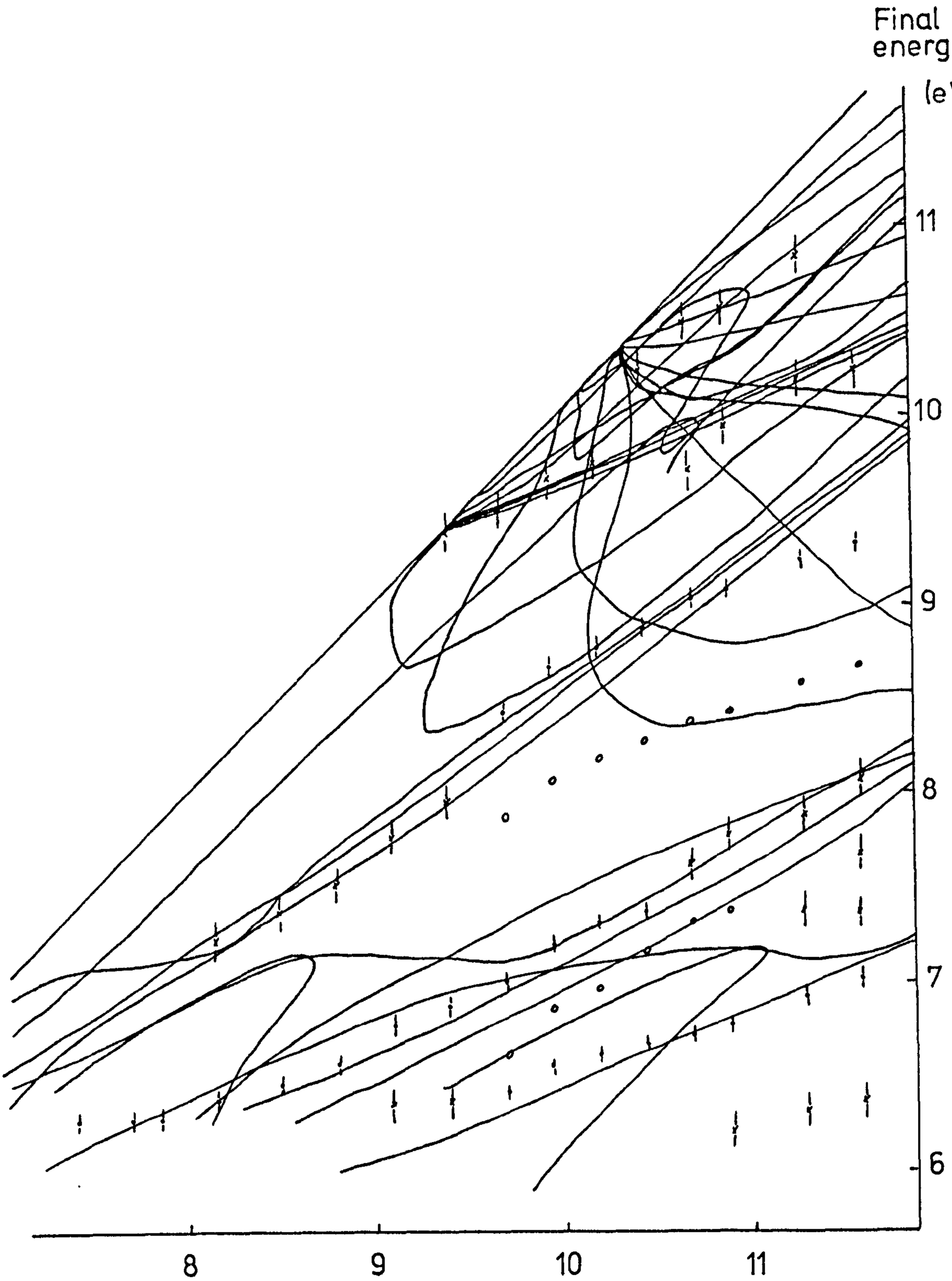

Figure 5.7. Superposition of Figures 5.4 and 5.6.

while the lower-lying feature (V) derives from similar transitions with some contribution from initial states in band 2. Line VI is due almost entirely to transitions from band 2, in this case mainly to bands 10 and 11. The large negative excursion of band 9 in the Δ and Σ directions (it is degenerate with band 10 along $\wedge$) makes the calculated lines involving this level spread widely over the structure plot, thus in effect "diluting" the density of states and making any transitions involving this band much less likely to be observable.

The near-coincidence of several lines, contributing greatly to the effective joint density of states, is responsible for the remaining three features arising from primary electron emission. Transition IV is attributable to initial states in band 4 and final states in bands 7 and 8 along Δ and Σ. This structure comes closest of all those observed to a 45^{o} line, indicating that its initial band (4) is the valence band most nearly flat. Conduction bands 7 and 8 are degenerate along Δ, merging with band 9 towards X, and only narrowly split along Σ; together with the very similar dispersion in these two directions, this produces nearly identical plots in Figure 5.6. However it is by no means obvious from the band structure why this feature should appear so strongly in UPS edc's. To explain this we make further use of the fact that 4-7 transitions have virtually the same relationship of final energy to photon energy along Δ (100) and Σ (110). This suggests that this same form of E-hν dependence might apply for these bands in the entire $<100>$ plane of the Brillouin zone. A similar transition seen in GaAs has been examined in some detail (Spicer and Eden 1968) and it was shown that the constant-energy contours in this $k_z = 0$ plane have almost identical shape for the initial band (4) and the final bands (7, 8, 9) , thus indicating that at any particular photon energy all direct transitions in the $<100>$ plane will yield electrons with very similar final energies and so contribute a sharp peak to the edc. The prediction of such a feature from Figure 5.5 illustrates that even though optical transitions are volume effects in $\underline{k}$ -space, simple comparison plots such as Figure 5.6 making use of the calculated band structure along major symmetry lines can be extremely useful in understanding complicated photo-emission edc data.

Another feature in Figure 5.4 which appears to be due to several contiguous E - hν lines is that labelled III, arising from transitions from bands 2 and 3 to 7 and 8, again mainly in the Δ and Σ directions. If we now consider the edc's of Figure 5.1 it is seen that this peak has maximum intensity in the photon energy range 7.85 to 8.8eV and drops off considerably at higher hν. There is no structure in the density of states of bands 2 and 3 to account for this, but there is considerable enhancement of the conduction band density of states (Kramer et al 1971) at the point of inflection of band 8 along Σ. Again, for the related feature in GaAs (Spicer and Eden 1968) examination of the band 8 eigenvalues throughout the Brillouin zone shows that this point of inflection becomes an actual minimum in the Γ - W and Γ - K' $(1, \frac{1}{4}, \frac{1}{4})$ directions, thus contributing greatly to the conduction band density of states. Figure 5.6 shows the horizontal line corresponding to transitions from band 3 to the flat part of conduction band 8 occurring for photon energies 8.4 to 9.7eV at a final energy of 7.1eV, which is about 0.6eV higher in hν than our strongest peak and also a similar amount higher in final energy, although of course the observed structure does not occur at constant final energy. To resolve this discrepancy we note that the OPW calculation (Herman et al 1968) finds Γ_{15}^{c} at 4.7eV, lower by ~0.6eV than both local and nonlocal pseudopotential values (Cohen and Bergstresser 1966, Chelikowsky and Cohen 1976b) and much closer to the results of 4.81eV from energy derivative reflectance (Stokowski and Sell 1972) and 4.87eV from electroreflectance (Aspnes et al 1975). Now considering some of the differences between Figure 5.5 and Herman's OPW calculation, X_{5}^{v} is almost unchanged, Γ_{15}^{v} is of course identical, band 2 is the same and band 3 has greater curvature, with its minimum about 0.3eV lower, but differing little until close to K, so there is almost no change in the initial states of transition III. So in line with this calculation, if we lower Γ_{15}^{c} by 0.6eV and make the assumption that all bands emanating from Γ_{15}^{c} are linearly shifted, which is not unreasonable close to Γ, the lower energy part of the 3-8 Σ transition is indeed moved almost into coincidence with our data, and the region with high density of states corresponds to the

strongest peak in the edc's.

The feature designated II is obtained from transitions from band 2 along Σ. Figure 5.6 shows only 2-7 Σ transitions along this line, but , following the above argument for lowering Γ_{15}^{c} , 2-8 Σ transitions will also contribute in this region. This peak has its maximum intensity in the edc's taken with $h\nu \sim 10.7$-10.9eV, giving a final energy around 6.7eV, in fair agreement with the revised value for the minimum in band 8 along Σ discussed above. The threshold function may well distort this peak at lower photon energies. The shoulder labelled I does not correspond to any structure derived from the band structure and is attributed to scattered electrons.

There has been no previous published UPS work on GaP in this photon energy range.

Energy distribution curves for $3 \leq h\nu \leq 6$ eV have been obtained from GaP covered with caesium (Fischer 1966), almost all of which comprise one very broad peak, but are said to be in good agreement with the band structure of Cohen and Bergstresser (1966). The problems of sample preparation suffered by Eden (1967) probably invalidate the data collected. Good quality single crystals were not available so samples of GaP were epitaxially grown on GaAs substrates and cleaning was attempted merely by heating the specimen. It is noted that care was necessary to avoid visible evidence of gallium accumulation on the surface and that the band-bending region was very thin, leading to distortion and smearing of the edc's at higher energies. The edc's obtained do not resemble those presented in Figures 5.1 and 5.3, being dominated by a large stationary peak at a final energy of ~ 7.0eV with an accompanying shoulder at 6.5 eV. These may be due to the effects of gallium and surface-segregated impurities. Some electrons were observed at higher energies and a structure plot was compiled showing, besides the two horizontal features, transitions corresponding very roughly in shape to our III, IV and VII but with energies different by up to 1eV. Some of these fitted the band structure of Cohen and Bergstresser to within 0.5eV.

Because of the combined problems of contamination and severe band-bending, these results may not be reliable.

There are several interesting general points raised by the direct transition analysis. Perhaps the most outstanding is the quality of the agreement between the experimental results and theoretical bandstructures: in fact on balance the fit is better than could realistically be expected, having regard to the experimental error bars and the theoretical uncertainty. It is unfortunate that no extended plot is available of the OPW calculation of Herman et al,for their empirically adjusted OPW values seem to fit our data rather more satisfactorily than the empirical pseudopotential results of Cohen and Bergstresser. It is striking that both these methods, fitted to just three points near the fundamental bandgap, predict to within fractions of an eV levels up to 10eV distant from the band edges. In view of the short electron escape depths expected (Figure 3.2) it may be felt surprising that the bulk electron states influence the UPS data so greatly: it is in fact remarkable that electron states characteristic of the bulk continue apparently unperturbed right up to the surface.

The value of having an energy band diagram with which to compare the data is emphasized by consideration of the three most prominent edc peaks (II, III and IV in Figure 5.6). All have been shown to arise from complex groups of transitions which would be very difficult to predict without such a calculation. In all the discussion of these data, it has been assumed that the optical transitions are direct. The analysis in terms of the bulk band structure shows that this is correct. The mere fact that the edc's change in shape with photon energy and do not replicate the valence band density of states indicates $\underline{k}$-conservation. Transition IV also illustrates this well: the densities of state of both the initial and final bands are smooth functions of energy, spread out over a wide range of energy. But optical transitions between these two bands produce a sharp peak in the energy distribution because of the similarity in shape of the constant-energy contours in the initial and final bands.

5.2. UPS of GaP with $15 \leq h\nu \leq 35$ eV

Spectra obtained at Leicester with a rare-gas discharge lamp are given in Figure 5.8. Figure 5.9 shows a family of edc's measured with synchrotron radiation in the photon energy range 15 to 35eV. The data of Figure 5.8, after subtraction of a smoothly varying background, are presented in Figure 5.10, together with a density of states curve from the nonlocal pseudopotential band structure calculation of Chelikowsky and Cohen (1976b). It is seen that, although the essential features are roughly reproduced in energy, there are large discrepancies, particularly in the intensity of the features. One of the possible interpretations of the differences has been discussed by us before (Norman and Williams 1976 -see Appendix). We draw here on a tight-binding calculation for GaAs (Chadi and Cohen 1975b) which shows that the orbital character of the top two valence bands is entirely p-like, whereas the lowest valence band is s-like with the charge located around the group V atoms. The second valence band is mainly s-like around Ga and p-like around the group V atoms, with a "mean" of approximately 60% s-like character. The necessity of considering the different photoionisation cross-sections for initial states of different orbital symmetry has recently beem emphasized (Williams 1976) and I originally proposed this explanation for the discrepancy between the predicted density of states and observed edc (Norman and Williams 1976). It is now recognised that the variation with energy of photoionisation cross-sections is very similar to the results of Hartree-Fock calculations for atomic species (Kennedy and Manson 1972), and it now seems more likely that the surfaces studied here were not perfectly clean, and the maximum in the edc is due to emission from the 2p levels of adsorbed carbon and oxygen. The main change observed on exposure to 2×10^5 LO_2 is an increase in the broad peak centred at $\sim$ -6eV.

Notwithstanding the possibility of contamination it is interesting to note that the edc for 16.8eV bears much closer resemblance to the theoretical density of states than that obtained at 21.2eV. This is a little

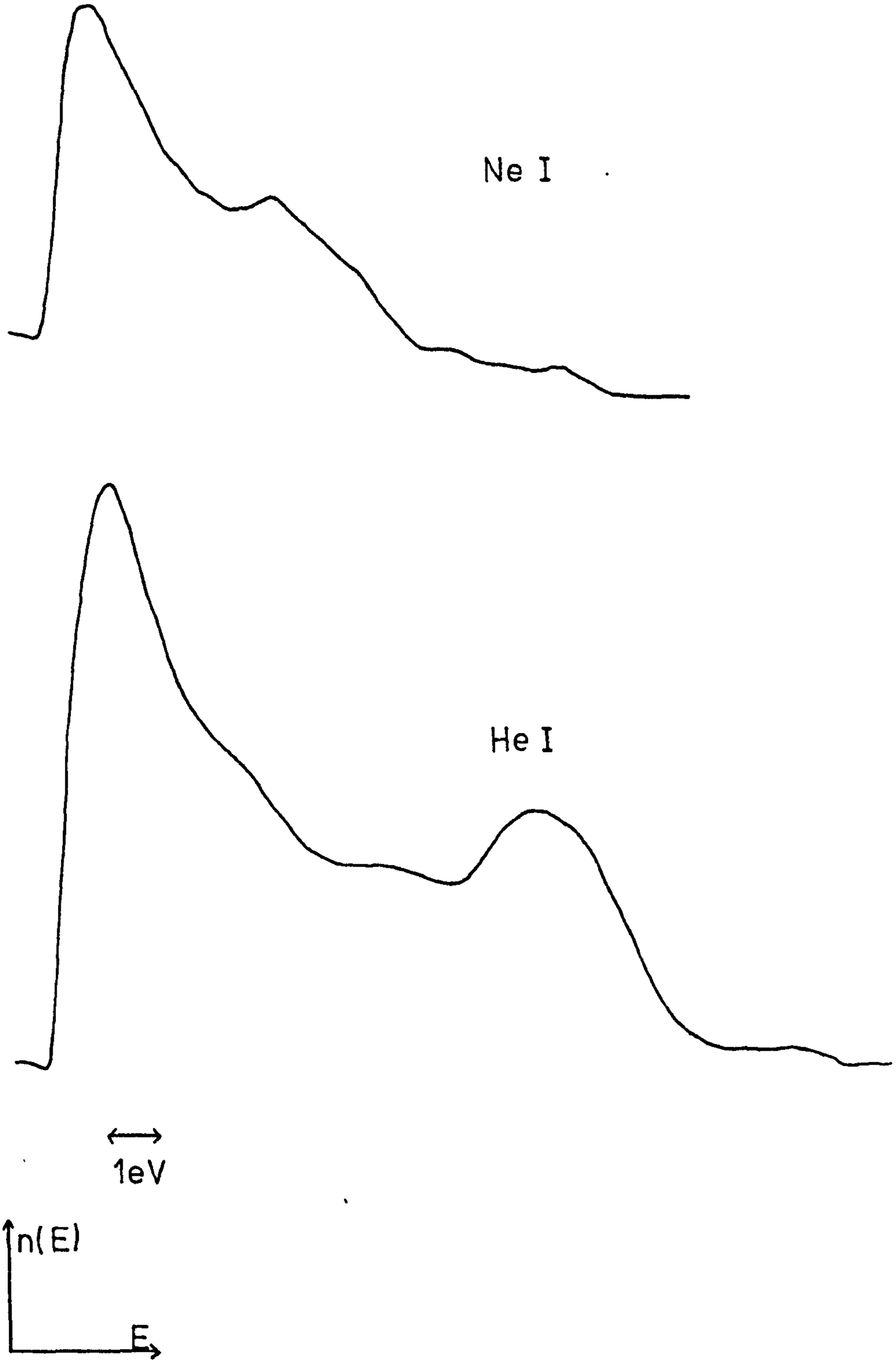

Figure 5.8. NeI and HeI edc's for GaP.

Figure 5.9 Edc's for GaP in the photon energy range 15 to 35eV

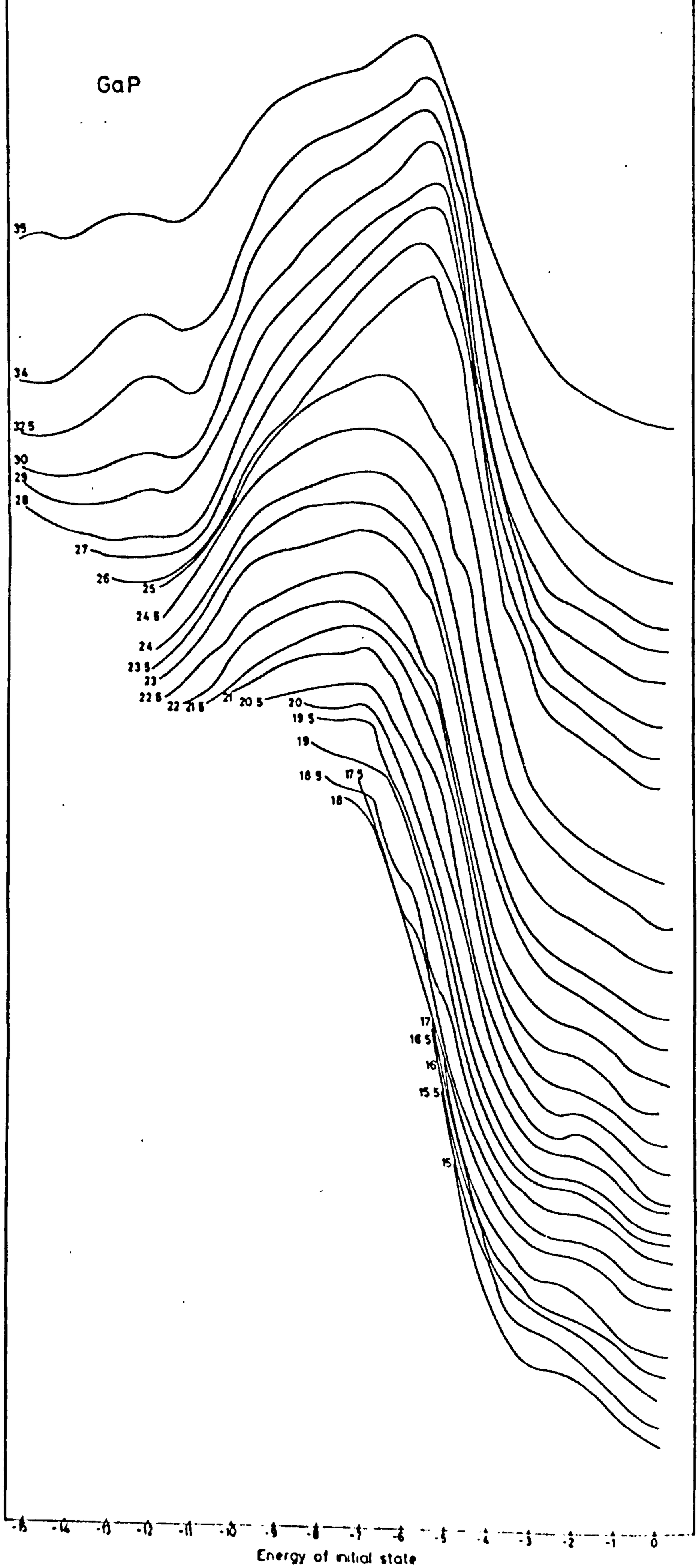
GaP
39
36
32 5
30
29
28
27
26
25
24 5
24
23 5
23
22 5
22
21 5
21
20 5
20
19 5
19
18 5
18
17 5
17
16 5
16
15 5
15
No of photoelectrons
-13
-12
-11
-10
-9
-8
-7
-6
-5
-4
-3
-2
-1
0
Energy of initial state

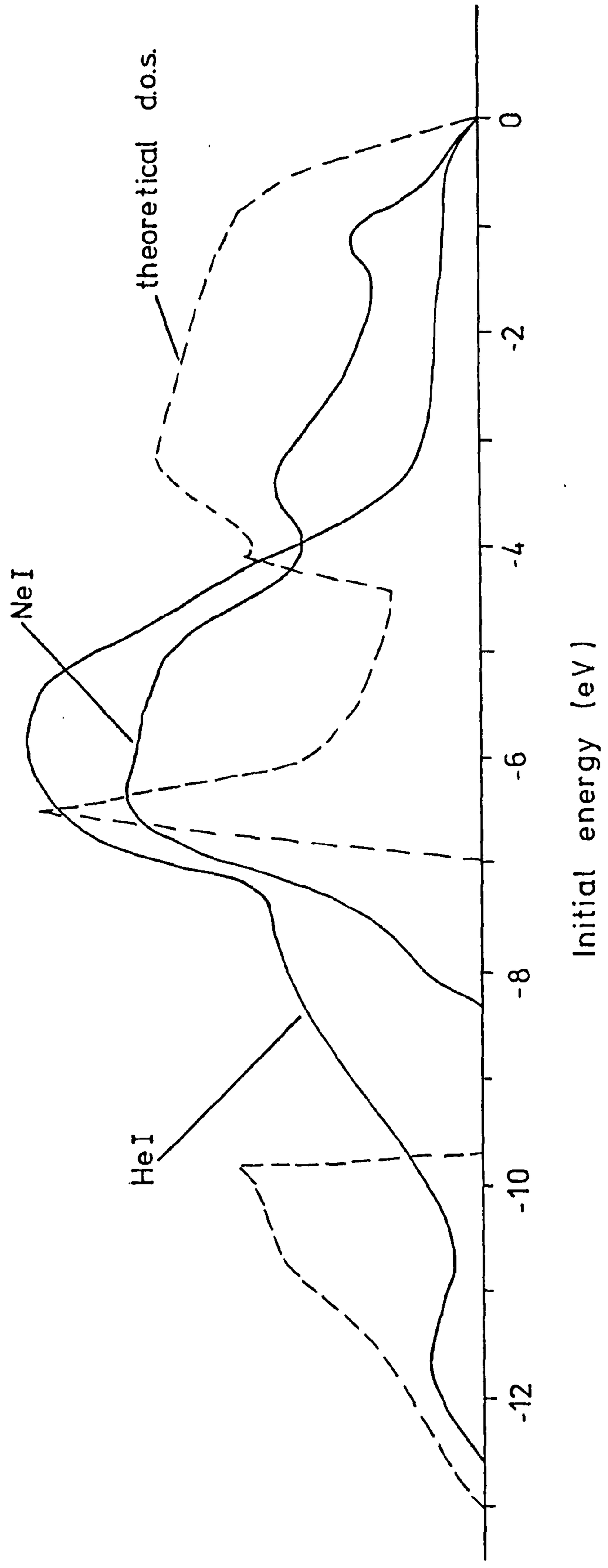

Figure 5.10. Data of Figure 5.8. after subtraction of a smoothly varying background, and theoretical valence band density states (Chelikowsy and Cohen 1976b)

surprising in view of the arguments presented in Chapter 3 on the progression towards an X-ray limit. Two possibilities exist : the shorter escape depth expected at the higher energy will tend to emphasize surface effects, thus increasing emission from the adsorbed contaminants at the expense of the clean surface; we must also consider the question of photon-induced Auger emission. He I (but not Ne I) is energetic enough to ionize the Ga 3d core levels and thus Ga M_4VV Auger transitions are possible : such transitions, with a kinetic energy of $\sim$ 10eV, have been observed in GaP (Morgan and Van Velzen 1973) and would correspond to an initial energy $\sim$ 6eV (for $h\nu$=21.2eV) in Figure 5.8. Similar complications due to Auger emission have been described previously (Eastman et al 1974).

The few published UPS data on GaP give vastly differing results for the valence bands. The edc's obtained at 21.2eV are shown in Figures 5.11. The results for cleaved (110) GaP are from Eastman et al (1973) at a photon energy of 20eV, the sputtered curves from Shevchik et al (1974) and the (111) and ($\bar{1}\bar{1}\bar{1}$) data from Jacobi and Ranke (1976). We have omitted the spectrum of Leonhardt (1975) because it is not clear whether He I or He II radiation was used. It is evident from these spectra that considerable variation has been recorded . This may be attributable to the various surface preparation techniques used. The sputtered specimens (Shevchik et al) are said to be not stoichiometric, and excess gallium is evident in their XPS data. It is possible that the samples of Jacobi and Ranke are similarly affected, since their definition of stoichiometry via AES peak heights is necessarily somewhat imprecise. Of course it is quite reasonable to expect there to be differences in the spectra recorded from different crystal faces.

We have obtained edc's at 20eV in the course of our partial-yield work (see following section) which are very similar to that presented by Eastman et al. Small differences between spectra obtained by different workers with synchrotron radiation may be explicable by polarization effects, or different angles between incident beam, sample and analyser. Synchrotron

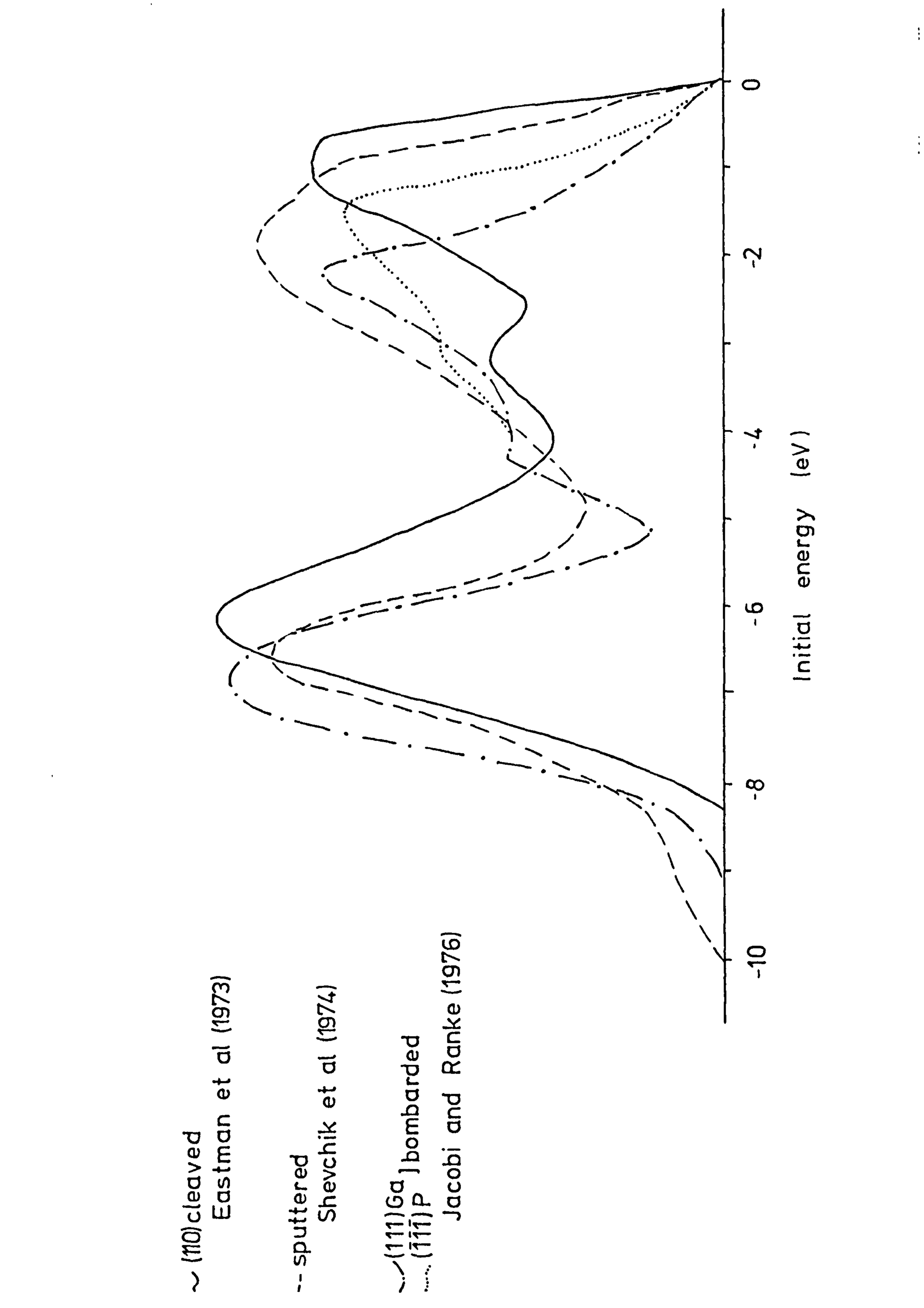

Figure 5.11. UPS data for GaP obtained by different workers

radiation-excited UPS has been used to determine the binding energies of the Ga $3d_{5/2}$ and $3d_{3/2}$ core levels. We find these levels to be situated 18.4 ± 0.05 and 18.9 ± 0.05 eV below the valence band maximum. A compilation of XPS and UPS determinations of these values is given in Table 5.1.

5.3. Surface electronic structure

Although all the features found in GaP edc's can be explained in terms of transitions between bulk energy levels, it is necessary first to consider whether a surface state could also be responsible for any of the observed structure. Since surface states are localized, and do not match to bulk wavevectors (Chapter 2.4), conservation of $\underline{k}$ is not an important selection rule : a surface state peak should thus move synchronously with photon energy and maintain a constant initial energy with respect to the valence band maximum. Three features in Fig.5.4 appear to lie on lines of constant initial energy for a few photon energies : the shoulder at $E_i \approx -1.3$eV ($8.5 \leq h\nu \leq 10$eV), the feature at $E_i \approx -3.1$eV ($10.4 \leq h\nu$ 10.9eV) and the shoulder close to $E = h\nu$ for $9.4 \leq h\nu \leq 11.3$ eV. It appears from the structure plot that the first two of these features naturally evolve from, and develop into, structure which is present for all possible photon energies (transitions IV and III respectively), and it is unlikely on this basis that they represent surface states in the narrow regions selected, but there are other reasons for rejecting such a suggestion. One is related to this restricted photon energy range. As $\underline{k}$-conservation is not necessary for a surface state, it should appear in edc's at all photon energies, since there is an available final state in some k -direction at all values of $h\nu$. It does not seem possible that either of these peaks could be obscured by an adjacent bulk-derived feature. The $E_i \sim 3.1$ eV feature is flanked by prominent valleys which, if it were to continue at other photon energies, could not conceal this structure. Adsorption of gases onto the surface is expected preferentially to affect surface states, small exposures to oxygen removing the filled

TABLE 5.1.

Binding energies of Ga $3d_{5/2}$ and $3d_{3/2}$ in GaP

Referred to E_V	Referred to E_F	Authority
18.4	18.9	this work
	18.66	Lane et al (1972)
	19.33	Lane et al (1972)
	19.2	Gudat et al (1972)
	19.7	Leonhardt et al (1973)
18.55		Ley et al (1974)
	18.7	Ley et al (1974)
18.6	19.0	Shevchik et al (1974)
18.4		Eastman & Freeouf (1975)
	19.4	Nefedov et al (1975)

surface states on Si(111) and Ge (111) completely. Exposure of GaP (110) to oxygen (see Chapter 5.5) produced no significant change in edc structure at energies greater than $E_1 \sim -3eV$, and all the features mentioned remained visible even at the highest oxygen exposure used. Several calculations of surface states for III-V compounds find a strong filled surface state within $\sim 0.5eV$ of the valence band maximum. The series of shoulders at $E_1 \sim 0.1eV$, seen only for $9.5 \leq h\nu \leq 11.3eV$ is unlikely to be due to surface states for three reasons: the limited photon energy range in which it is seen, its persistence after oxygen exposure, and its positive identification as being due to Γ bulk transitions. Thus we conclude that there is no sharp structure due to filled surface states overlapping the bulk valence bands.

Note that we have not demonstrated that filled surface states below the valence band maximum do not exist, but that any surface states present have no sharp structure. Such states may be spread throughout the energy range of the balence band, or they may be strongly mixed with valence band states.

It is easy to obtain an order-of-magnitude estimate of the limits of detectability of filled surface states. The upper valence bands of GaP are about 6eV wide and GaP contains $\sim 8 \times 10^{22}$ valence electrons.cm^{-3}. If we take an average value of electron mean-free-path to be 25Å, the average bulk density of states sampled by UPS becomes $\sim 3 \times 10^{15}$ states.cm^{-2}.eV^{-1}. Similarly we can obtain a density of filled surface states, taking two filled states per surface phosphorus atom and a surface state band $\sim 1eV$ wide, of $\sim 9 \times 10^{14}$ states.cm^{-2}.eV^{-1}. Such a density, about one-third of the bulk density of states, should be readily detectable.

Thus we have shown that no structure is observed in edc's which cannot readily be attributed to transitions between extended valence and conduction bands. This was a major disappointment of this study, which was started at a time when several theoretical calculations (see Chapter 2.4) showed that surface states were expected above or at the valence band maximum,

and had indeedjust been reported in Si (111) (Wagner and Spicer 1972) and on the cleavage faces of Si, Ge and GaAs (Eastman and Grobman 1972). Although filled states in the bandgap of the elemental semiconductors have been observed by many workers, it appears that this result on GaAs must have been entirely erroneous: careful experiments on several III -V compounds have failed to show any filled states within the bulk bandgap, even with exceptionally good cleavage faces or intentionally poor cleaves. The authors of this earlier report later admitted the result to be irreproducible (Eastman and Freeouf, 1974).

Although emission from filled states is the most direct UPS demonstration of surface states, the existence, energy position and density of surface states can still be determined in several ways by UPS. We have performed partial yield measurements, using synchrotron radiation, on cleaved n-type GaP (110) surfaces, some results of which are presented in Figure 5.12. The resemblance between the shape of the partial-yield spectra and the bulk photoabsorption spectra (Gudat et al.1972) emphasizes that photoemission yield measurements sample a type of absorption coefficient (Gudat and Kunz 1972) with considerably enhanced surface sensitivity owing to the short electron escape depth. The data of Gudat et al. are shifted by 1eV to higher photon energies to facilitate comparison of the spectra. The increase in partial-yield intensity occurring at $h\nu \sim 24$ eV ($E^{*} = 6$eV) and $h\nu \sim 25$eV ($E^{*} = 7$eV) is due to the onset of emission direct from the Ga 3d core levels. After contamination in poor vacuum, the same type of curve is obtained, but the shoulder between 19 and 21eV disappears, and a rather differently sloping background is found. This difference in the general background shape makes it difficult merely to subtract the spectra from contaminated and clean surfaces: instead, I present in Figure 5.13 curves derived by taking three linear background sections as indicated in Figure 5.12. This procedure is obviously inexact, but gives a reasonably good fit (particularly at the low energy end) and serves to illustrate the form of the

Figure 5.12. Photoemission partial-yield spectra for GaP (110), at two different values of final state energy (E^*). The curve for absorption coefficient (α) is from Gudat et al (1972).

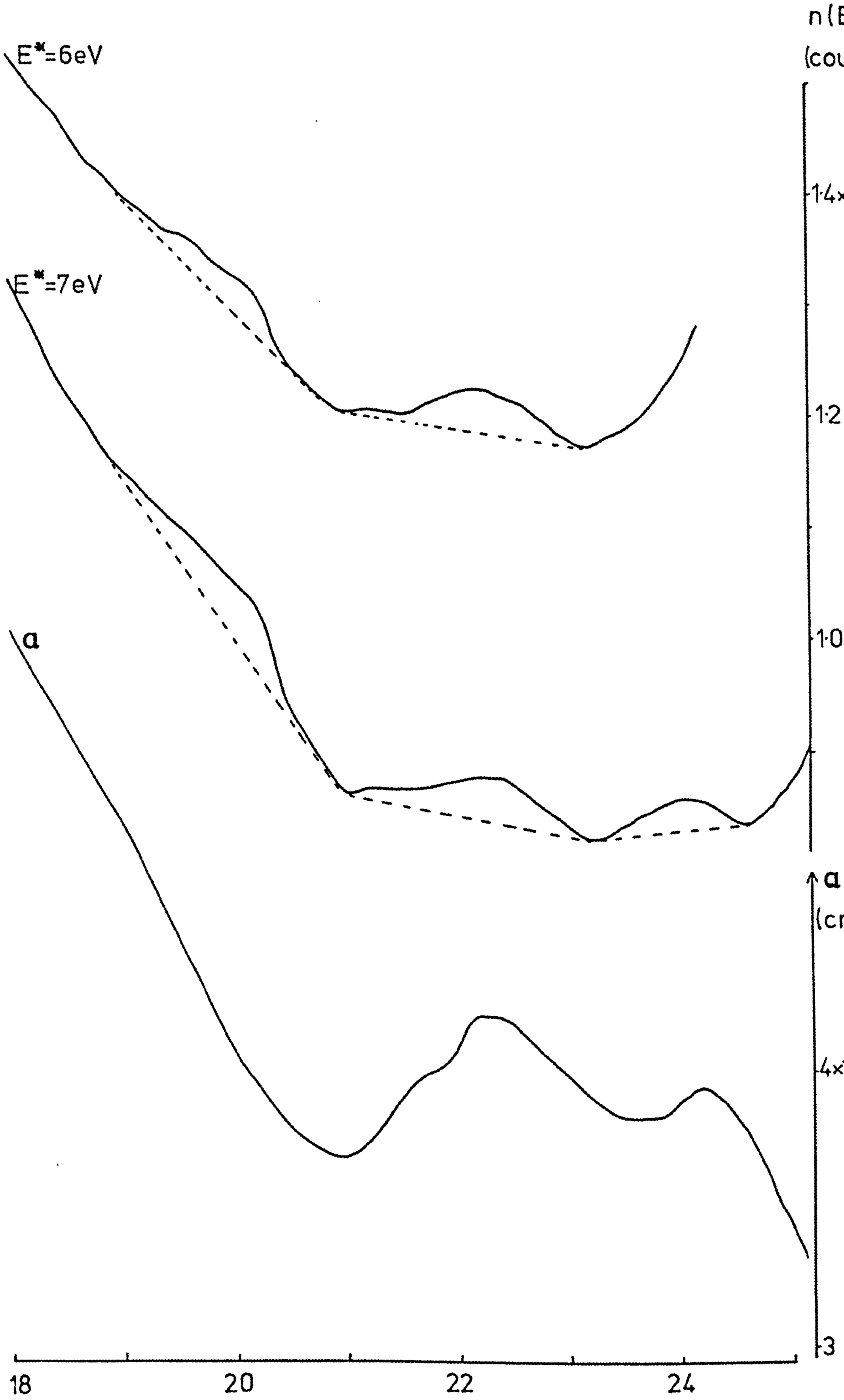
E*=6eV
E*=7eV
a
n(E)
(counts
1·4×10 5
1·2
1·0
a
(cm-1)
4×10 5
3
18
20
22
24
Photon energy (eV)

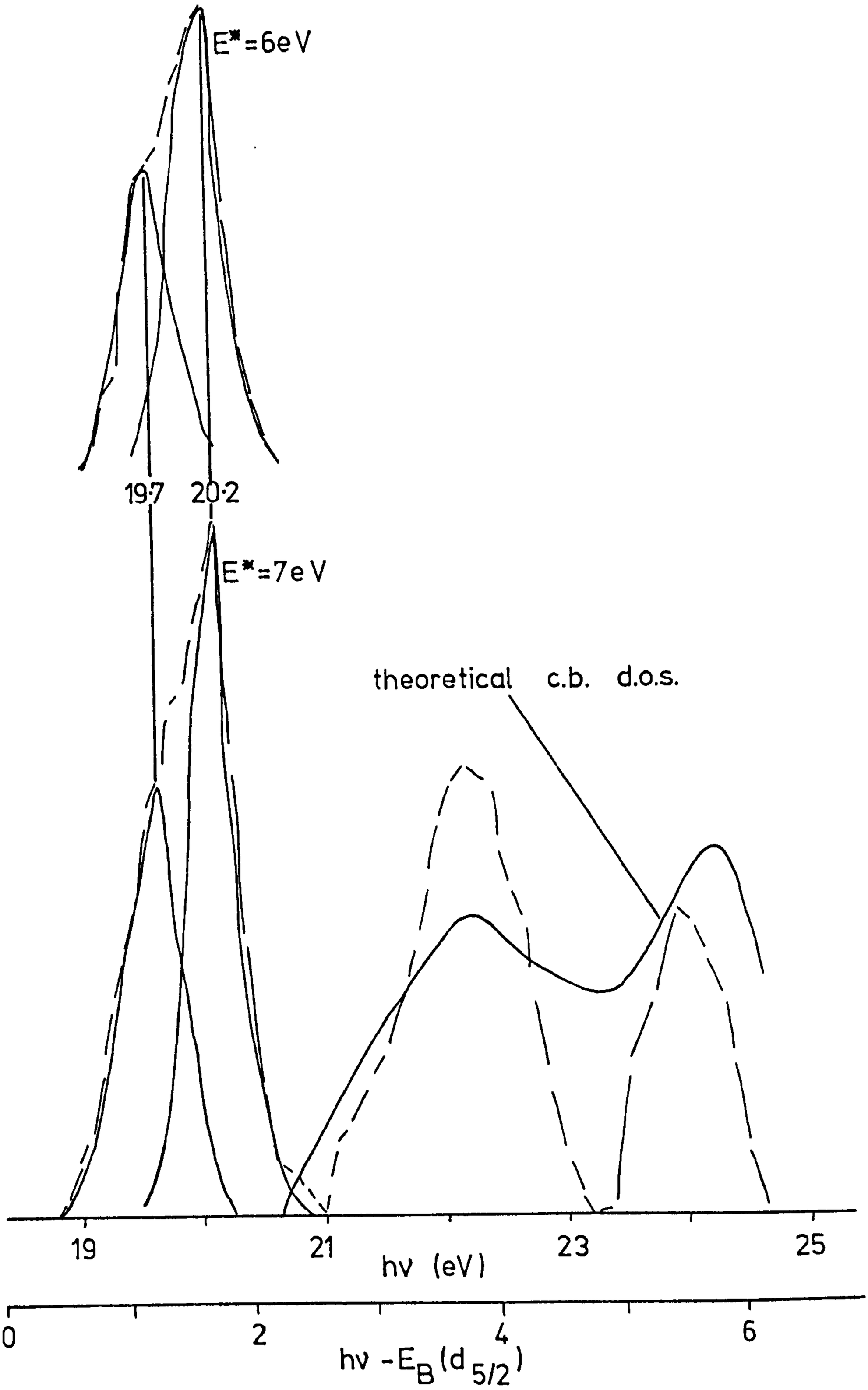

Figure 5.13. Data of Figure 5.12 after subtraction of background. Deconvolution of the features between 19 and 21eV into two Gaussians is indicated. Also included is a theoretical calculation of the conduction band density states (Chelikowsky et al 1973).

energy dependence. The two higher energy peaks reproduce well the major features in the conduction band density of states (c.b. d.o.s.) from the calculations of Chelikowsky et al (1973) and others.

The broad peak at photon energies of 19-21eV is attributed to an empty band of surface states. This peak is readily resoluble into a doublet peaking at 19.7 and 20.2eV, corresponding exactly to the 0.5eV splitting found between the Ga $3d_{5/2}$ and $3d_{3/2}$ levels, and locating the final state of this feature at 1.3eV above the valence band maximum. This feature is identified as a surface state in several ways: its energy position, well within the bulk bandgap, is consistent with this interpretation. Partial-yield spectra taken for various values of secondary electron energy E^* show that the intensity of this feature increases relative to that of the conduction band as E^* is increased. Since the electron escape depth decreases with increasing energy (up to $\sim$ 20eV) this technique should reveal better surface effects as E^* increases. The sensitivity to contamination of the peak at 1.3 eV also suggests an explanation in terms of surface states: none of the other features shows such reaction to adsorption. A similar feature 1.2 eV above the valence band maximum, has been observed in other partial-yield measurements (Eastman and Freeouf 1975, Gudat and Eastman 1976) and described as an empty surface state.

This interpretation may be disturbed by excitonic effects. A core surface exciton associated with the Ga dangling bond in GaAs has been seen (Lapeyre and Anderson 1975) and postulated for several other III-V compounds (Gudat and Eastman 1976). However, an excitonic energy of at least 1.4eV (allowing for the width of $\sim$ 0.45eV FWHM) would be needed to remove completely the surface state band from the bulk bandgap as seen in our partial-yield data. There is considerable disagreement over the value of the bulk core level to conduction band excitonic binding energy in GaP:Aspnes et al. (1975) estimated a value of <0.15eV but 0.8 eV is suggested by Thiry et al. (1976). In general, it would be expected that excitonic binding energies for transitions involving empty surface states would be larger than for the bulk because the surface states are well-localized and there is less dielectric screening at the surface.

A lower bound of $\sim$ 0.6eV has been given for the surface state excitonic binding energy in GaAs (Gudat and Eastman 1976). Thus it is possible that the surface state seen in our partial-yield spectra is actually degenerate with the bulk conduction band but lowered in emission energy by a surface excitonic effect.

Several other aspects of these measurements are worthy of comment. Since the partial-yield spectra reveal transitions from well-localized Ga levels with d-symmetry, the orbital nature of the final state can be deduced. Application of the optical selection rules shows that the surface state seen here must have p- or f-orbital character. Any partial f-wave character is probably negligible (Freeouf 1976) and in any case the cross-section for d $\rightarrow$ f transitions will be very much smaller than for d $\rightarrow$ p transitions owing to the unfilled 4p shell around the Ga atom from which this state is derived (Brian Holland, personal communication) ; so we conclude that the Ga dangling-bond has predominantly p-symmetry. ELS results were interpreted as showing s-orbital character for the empty surface state on GaAs (Ludeke and Koma 1975b), but it appears that the dipole approximation may not hold at the low electron energies used. Incidentally, the selection rules mean that we cannot probe final states with s- or d-symmetry by excitation from the Ga 3d levels.

Differences occur between the peak values of core level to conduction band transitions observed by photoabsorption and photoemission partial-yield. These values are tabulated, together with theoretical energies of peaks in the conduction band density of states for GaP, InP and GaAs in Table 5.2. No systematic variation is found, but the differences are probably related to the differences between bulk and surface-enhanced core excitons as discussed above. Very large surface excitonic effects ($>$ 2eV) have very recently been reported for silicon (Margaritondo and Rowe 1977). It is interesting to note that the adsorption data of Gudat et al (1972) were shifted in energy in the publication by Eastman and Freeouf (1974) as as to coincide

TABLE 5.2

Comparison of energies of conduction band features revealed by photoemission partial-yield, absorption and theory

GaP		InP		GaAs		
18.4	18.9 *	16.9	17.65†	18.6	19.1‡	Core levels
22.15	23.85	18.8	19.9 †	21.3	22.4‡	partial-yield photoemission
20.6-20.9	23.1-23.3 #	18.8	19.7 #	20.6-21.0	22.9 - 23.0 #	absorption
22.2	23.6 □	19.8	21.6 ±	21.75	23.6 ⊙	theoretical conduction band density of states
22.2	24.0 ©	20.2 ⊙				

* this work (Chapter 5.3)

† this work (Chapter 6.3)

‡ Eastman and Freeouf (1974)

Gudat et al (1972)

© Chelikowsky and Cohen (1976 b)

□ Kramer et al (1971)

± Neumann et al (1975)

with their partial-yield conduction band peaks; no mention has been made of any justification for this.

Finally, we discuss the magnitude of the surface state derived peaks. The curve for E^* = 7eV displays a peak value (for the surface state transition from the $3d_{3/2}$ level) about 12% above the background. While this is not large, this peak magnitude is somewhat greater than that obtained by Eastman and Freeouf (1974) in their first partial-yield work on GaAs and about ten times greater than surface-derived features found for II-VI compounds (Bauer et al. 1977). It seems that such relatively small peaks are typical for the compound semiconductors. The ratio of the intensities of the peaks arising from the Ga $3d_{5/2}$ and $3d_{3/2}$ levels is observed to be $\sim$ 0.65:1, almost exactly the reverse of the ratio 6 : 4 expected from the degeneracies of the levels ($2\ell + 1$) in a single-particle excitation picture. Freeouf (1976) showed that this inversion may reasonably be explained by considering exchange interactions between the excited electron and the nine d-electrons remaining in the core. Other many-body effects may be important.

5.4. Band bending

The existence and energy position of bands of surface states can be inferred from observations of the position of the Fermi level at the surface as the bulk doping is varied. The bulk Fermi level position is determined by the type and concentration of bulk impurities according to familiar formulae: in particular for non-degenerate n-type semiconductors

$$E_C - E_F = kT \quad \ell n \frac{N_C}{N_D}$$

where the concentration of donors is N_D ($\gg N_A$), and N_C is the effective density of states in the conduction band. The presence of surface states modifies this relationship near the surface: the Fermi level is pinned by bands of surface states, and the bulk bands bend to maintain the bulk Fermi level position (Figure 5.14).

Figure 5.14. Illustration of band bending at the surface of an n-type semiconductor.

E_{vac} = vacuum level

E_c = conduction band minimum

E_f = Fermi level

E_g = bulk bandgap

E_v = valence band maximum

χ = electron affinity

φ = work function

Φ = photothreshold

V_{bb} = band bending voltage

L = Debye band bending length

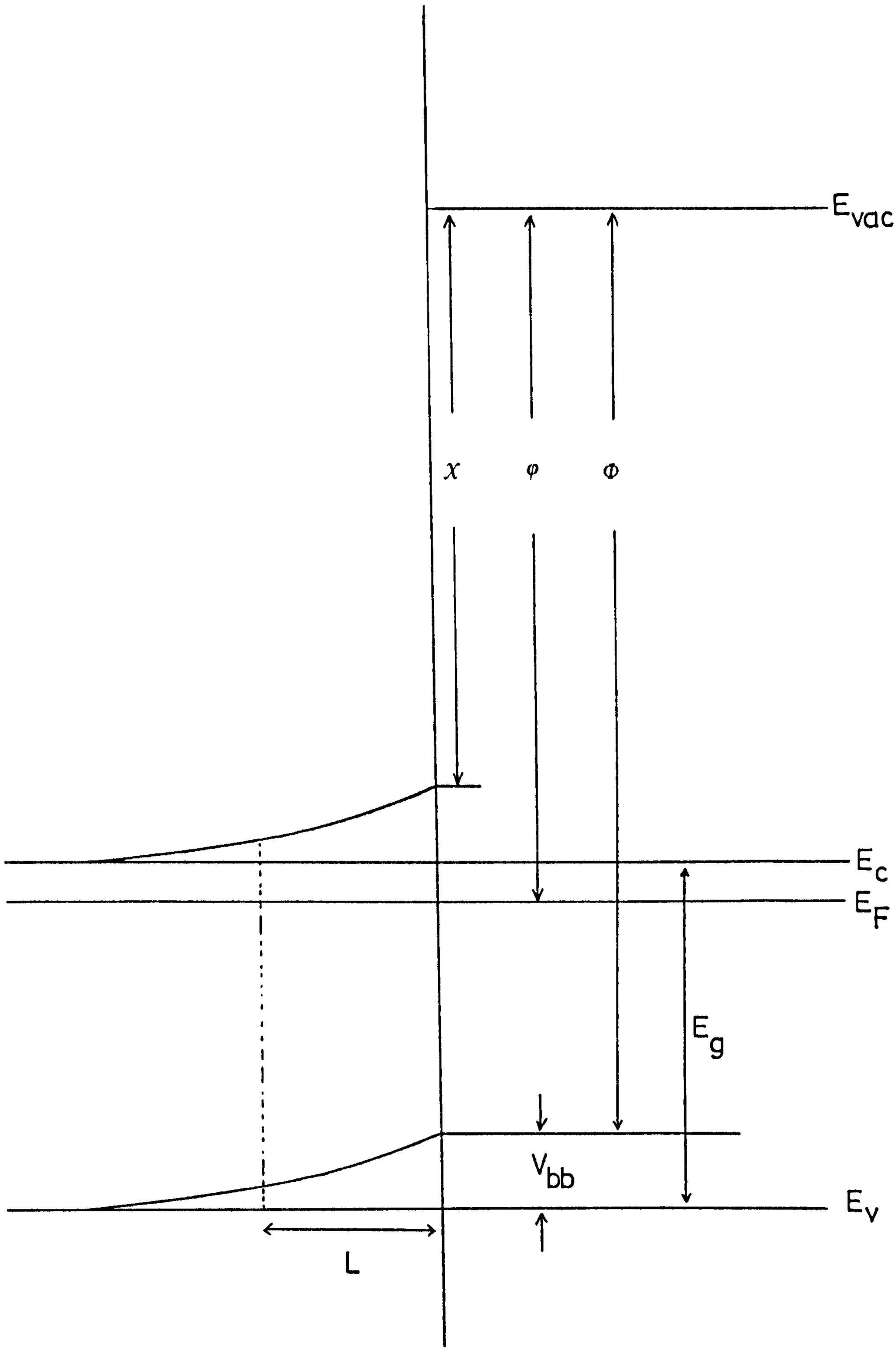
E_{vac}
χ
φ
Φ
E_c
E_F
E_g
V_{bb}
E_v
L

Obvlously, to achieve pinning,there must be some electrons at the bottom of the "empty" surface state band: in principle emission from these states could be seen in UPS. Assuming complete carrier depletion in the band bending region, we can calculate the total amount of charge on the surface needed to compensate the space charge from the equation

$$Q_{ss}^{2} = \frac{2\varepsilon\varepsilon_o N_D V_{bb}}{e}$$

where Q_{ss} is the surface charge, ε the dielectric constant of the semiconductor, ε_o the permittivity of free space, N_D the donor concentration, V_{bb} the band bending in eV and e the electronic charge. Using the band bending value 0.5eV, we find the surface charge in the empty surface state band to be $\sim 1\text{-}2.5 \times 10^{11}$ electrons.cm^{-2}. From the previous estimate of the limits of detectability of filled surface states, again assuming two empty states per surface gallium atom, we find that $\sim$ 0.01-0.03% of the surface states are filled to pin the Fermi level. Even if the lower edge of the empty surface state band were very abrupt, it is very unlikely that such a low density of states could be detected by photoemission.

Perhaps the easiest way to test for surface states within the bulk bandgap is to observe the variation of band bending as the concentration and type of impurity is altered. In particular the difference in Fermi level between highly-doped (but not degenerate) n-type and p-type specimens would be equal to the bandgap in the absence of surface states. Unfortunately no p-type material was available to us. The material used was Czochralski-grown by the Plessey Co.Ltd. and measured, by Hall effect, to have an excess donor concentration in the range 2×10^{15} to 1×10^{16} cm^{-3}. We calculate N_C for GaP to be $\sim 5 \times 10^{19}$ cm^{-3} and so $E_C - E_F \sim 0.22$ to 0.26eV. Taking the mean value of 0.24eV gives $E_F - E_V = 2.00$eV at room temperature.

With just this one type of bulk doping it is still possible to detect the presence of empty surface states by measuring the surface Fermi level. This was done routinely in each experiment by observation of the Fermi level of an evaporated film of gold. For the first experiment this was measured both from

gold evaporated onto a separate plate which could be moved under the collector and from a film of gold evaporated over the GaP sample itself: identical results were obtained showing that no charging or any other unexpected effect was in fact occurring. The use of the plate had the disadvantage of requiring a gap in the shielding underneath the collector, which could have distorted the edc's from the semiconductor: a mixture of these two methods was used for subsequent experiments. The Fermi level of gold is easily seen in edc's ,and thus a scale is established relating the retarding voltage to the Fermi level of a sample. From the structure plot of Figure 5.4 it is seen that there is emission from near the valence band maximum for some photon energies in the range 9.4 to 11.3eV : thus the difference $E_F - E_V$ may be calculated. From a weighted average of fourteen direct measurements and many more indirect determinations - making allowance for the difference between the valence band maximum and the highest initial state from which emission is observed - a value of $E_F - E_V = 1.50 \pm 0.1$eV is obtained . No systematic variation with different cleaves was observed . We thus have $V_{bb} = 0.50 \pm 0.1$eV.

The depth within the crystal to which this band bending extends is of interest, but is difficult to measure or calculate accurately. If we take the approximation that the bands bend exponentially, such that

$$V - V_{bb} = V_{bb} \exp(-z/L)$$

where L is the Debye length, given by

$$L = \left(\frac{\epsilon \epsilon_o kT}{e^2 N_D} \right)^{\frac{1}{2}}$$

we find L is in the range 850 to 380 Å for GaP with a donor concentration between 2×10^{15} and 1×10^{16} cm^{-3}. This depth is several times greater than the electron escape depth at the photon energies used here, so, with this lightly-doped material it is unlikely that band bending will significantly distort the edc's. For example, if we take an escape depth of $\sim$ 50 Å, L $\sim$ 500 Å and $V_{bb} \sim 0.5$eV , then $(V - V_{bb})_{z = 50Å} \sim 0.45$eV: the mean band bending

over the mean electron escape depth is within 10% of its value at the surface.

Further information on surface band bending can be obtained from the widths of edc's. If W is the edc width then $h\nu - W$ gives the energy separation between the vacuum level and the highest filled level from which transitions are possible at that photon energy . Making allowance for the fact that this may not correspond to the valence band maximum, by taking the lowest value consistently obtained , we find a mean value of $E_{vac} - E_v = 5.55 \pm 0.2$eV. In the absence of band bending this should be equal to the bulk photoelectric threshold Φ. A calculation of Φ from the bond-orbital method, which gives excellent agreement with experimentally obtained values for fourteen other semiconductors, predicts $\Phi = 6.15 \pm 0.2$eV (Çiraci and Bell 1974) . If we accept this value, our figure of $E_{vac} - E_v = 5.55$eV gives an upward band bending of 0.60 ± 0.4eV, in agreement with the value of 0.50 ± 0.1eV obtained from measurements of the Fermi level position . The photoelectric threshold of p-type GaP has very recently been measured and found to be ~ 6.04eV (Huijser et al 1977). From this experiment a figure of $\chi \sim 3.75$eV is given: use of this estimate with our value of $E_{vac} - E_v$ indicates that emission extends to 1.80eV below E_c , i.e. $V_{bb} \sim 0.44 \pm 0.2$eV. These values are very imprecise, and the principle of combining surface parameters from different samples is rather dubious, but the figures obtained lend tenuous support to the values obtained directly from our measurements.

5.5. Oxidation of GaP , studied by UPS

Oxygen exposures were made in steps of fractions of a decade in the range 1 to $\sim 10^7$ Langmuirs on several clean cleaved GaP surfaces. A selection of data is given in Figure 5.15: these spectra are given on the same vertical scale, and are plotted against retarding voltage to emphasize the changes in the leading edge of the edc's. Since the width of an edc is directly related to the electron affinity E_g by the expression $W = h\nu - \chi - E_g$ (Figure 5.14) it is easy to calculate the change $\Delta\chi$ induced by adsorbed oxygen: the variation of $\Delta\chi$ with oxygen exposure is given in Figure 5.16. The change in yield is obvious in Figure 5.15 and this is plotted in Figure 5.17.

Figure 5.15. Edc's from GaP (110) with various exposures of oxygen

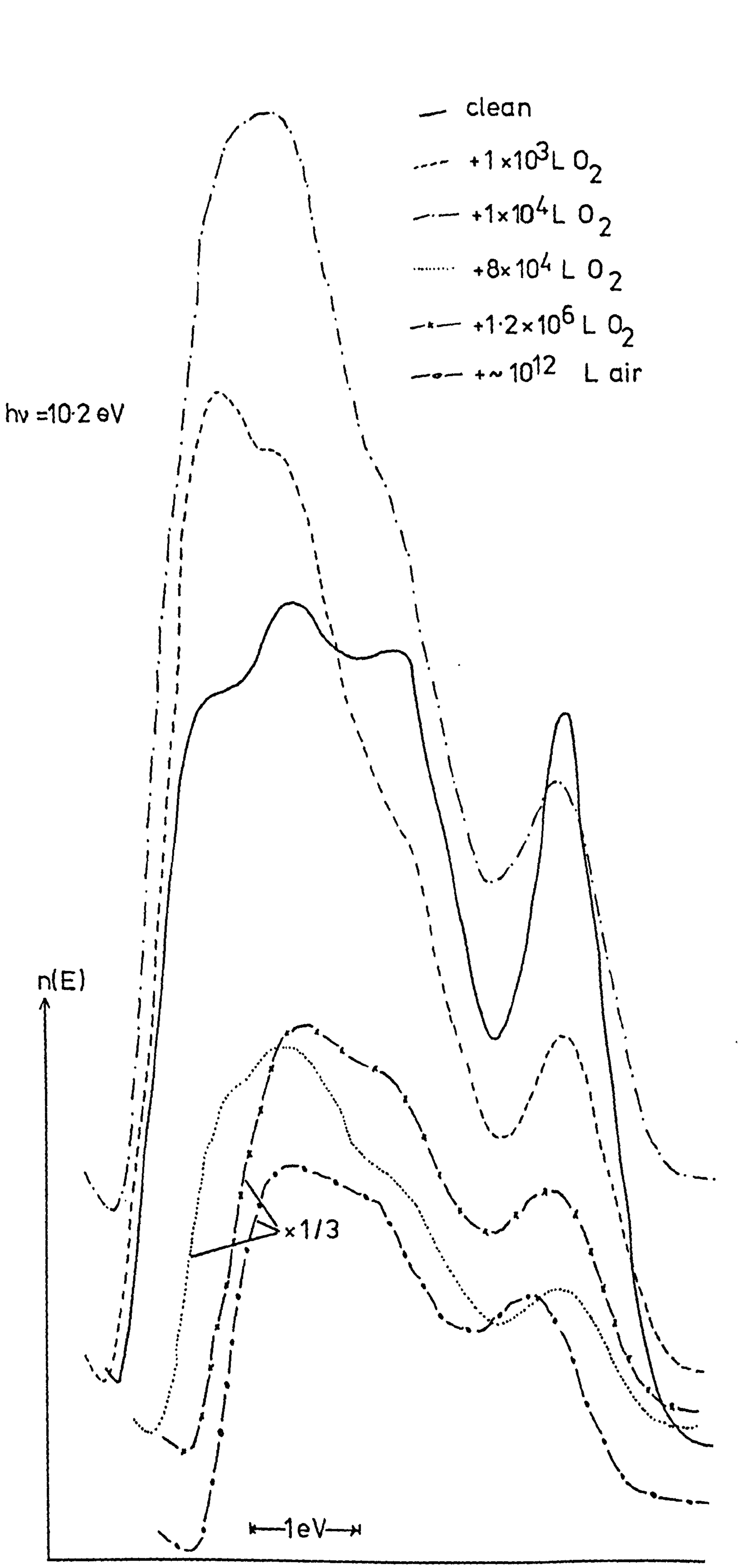
clean
+1×10³L O₂
+1×10⁴L O₂
+8×10⁴ L O₂
+1·2×10⁶ L O₂
+~10¹² L air
hν =10·2 eV
n(E)
×1/3
1eV
Retarding voltage

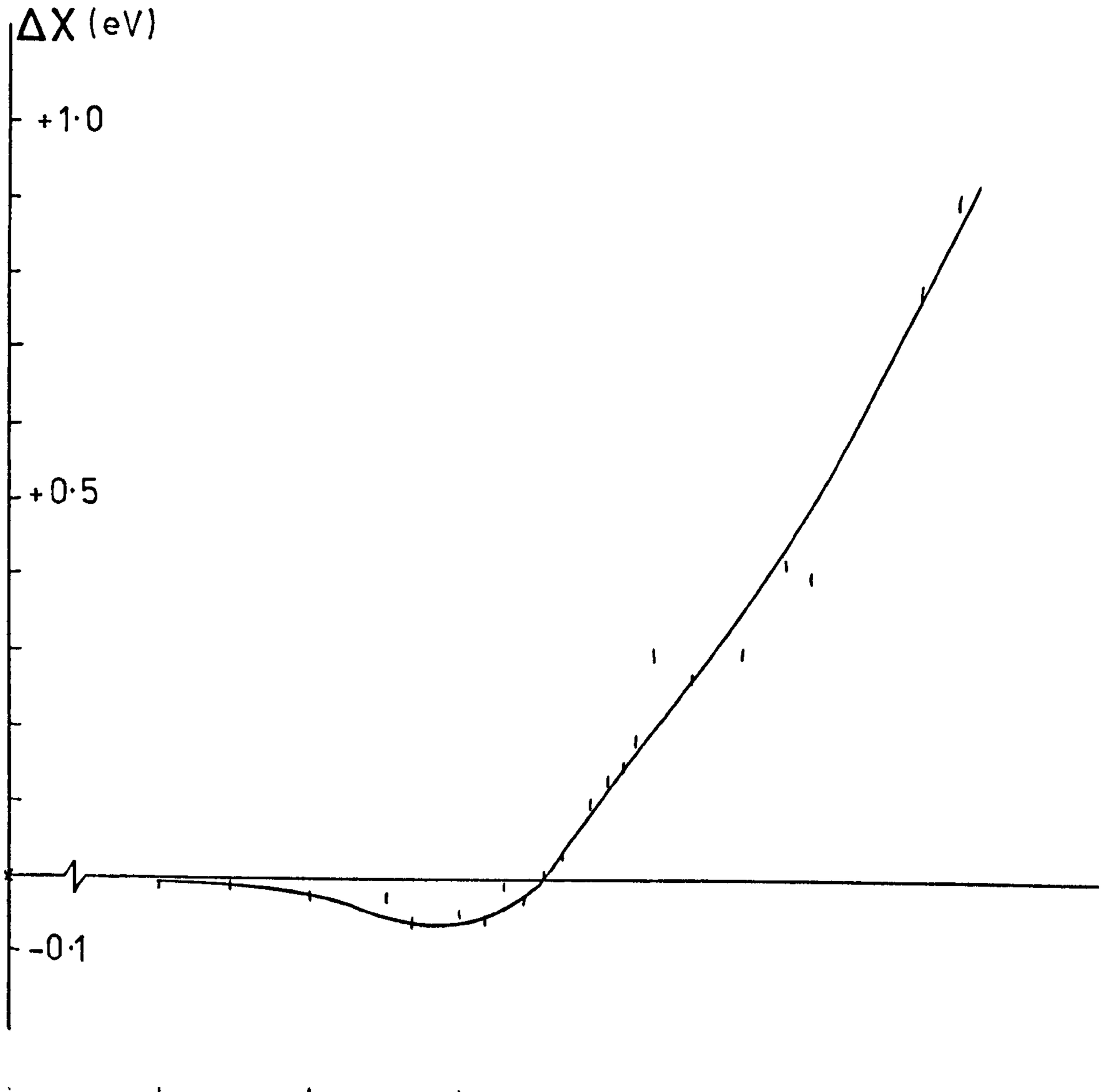

Figure 5.16. Change in electron affinity ($\Delta\chi$) of GaP as a function of oxygen exposure.

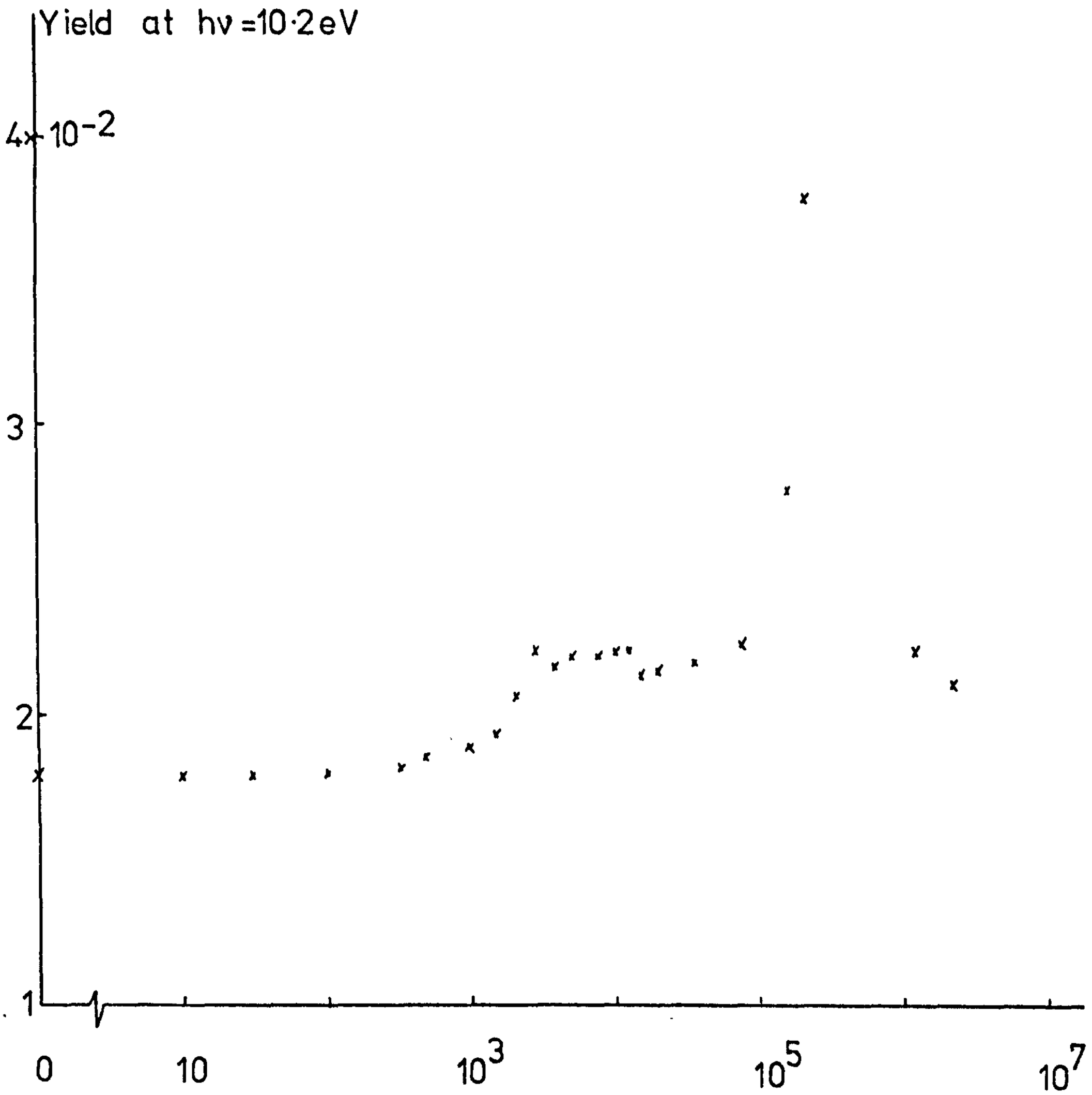

Figure 5.17. Change in yield of GaP as a function of oxygen exposure

It must be pointed out that the exposure of oxygen needed to induce these changes varied from one experiment to another by as much as a factor of one hundred. These variations occurred between different runs, and not within a run; we attribute this effect to the creation of excited oxygen species (which may be ions, atomic oxygen, ozone, molecular oxygen in excited form etc.) by the ionisation gauge and ion pump. Pianetta et al (1976) found that excitation of oxygen by hot filaments or discharges decreased the exposure of oxygen required for half-monolayer coverage on GaAs by a factor of $\sim 10^4$, although GaSb was not similarly affected. Poor reproducibility of oxygen exposures has been reported before (Ibach and Rowe 1974a, Jacobi and Ranke 1976). Obviously this makes it impossible to quote any values for sticking coefficient, but the effects of increasing oxygen exposure can still be followed.

The changes in electron affinity are interesting. Around $10^3 LO_2$ χ decreases slightly, suggesting the possibility of a long-range interaction with the oxygen going beneath the surface; oxygen ions on the surface would provide a negative dipole and thus increase the electron affinity. This is in fact what happens at higher exposures, with χ increased by nearly 1eV after $\sim 2 \times 10^6 LO_2$. A similar slight decrease in electron affinity was observed but discounted for GaAs (Gregory and Spicer 1976b), but has very recently been reported during the oxidation of GaSb (Chye et al 1977).

The changes in yield with increasing exposure are complex. The small increase at very low exposures is probably caused by the drop in electron affinity: the larger increase in yield, at around $2 \times 10^3 LO_2$, coincides roughly with the minimum work function. Alternatively, there may be a slight drop in reflectivity. The effect of adsorbates on the reflectivity of semiconductors has apparently not been studied, probably because this parameter is normally rather insensitive to surface condition. The massive growth of the yield after $10^5 LO_2$ has several possible explanations. Emission direct from the 2p levels of the adsorbed oxygen is certainly increasing, and there may well be an increase in the electron-electron scattering length or the formation of a surface oxide

with a large bandgap. The latter factors must be involved to some extent, since there is an increase in emission of high-energy electrons (visible in the lower curves of Figure 5.15). The sharp drop in yield at the highest exposures can be attributed entirely to the increased work function.

No change in Fermi level position was detected during any of the controlled oxygen exposure experiments , E_F remaining pinned about 0.5eV below the conduction band edge. The only exception to this occurs in the curve shown in Figure 5.15 taken after the chamber had been accidentally let up to atmosphere, giving an exposure around 10^{12}L. Unfortunately the Fermi level of the sample after this treatment was not checked, but it is seen that all the structure in the edc has been shifted by 0.3eV to lower energy and the width of the edc is 0.9eV less than for the clean sample. If we suppose that the relationship between retarding voltage and Fermi level is unchanged by the massive air exposure, it appears that the bands are unbent by 0.3eV, leaving a residual band bending of 0.2eV. We recall here the earlier result that the UPS electron probe depth is very much less than the width of the band-bending region, so all structure is shifted linearly with the surface bands. We suggest that the bands become pinned by extrinsic surface states induced by the adsorbed contaminants.The increase in electron affinity of 0.9eV is the same as that found for the largest controlled exposure of oxygen ($\sim 2 \times 10^6 LO_2$).

Finally, we discuss the bonding of oxygen to surface atoms. The insensitivity of the Fermi level position to adsorbed oxygen indicates that the empty surface states, derived from Ga atoms, are little affected (unless, by chance, extrinsic states caused by the adsorbate happen to have the same energy as the intrinsic states). It seems that this result is due to oxygen combining with the two surface P electrons, reducing the energy of those electrons and removing the filled band while leaving the empty surface band, and thus the surface Ga atoms, largely unmodified. This argument suggests that the first stages of oxidation involve bonding to P atoms. From Figure 5.15 it is seen that there is no preferential removal of valence band structure,

and this is confirmed by edc's taken at different photon energies -Figure 5.18 gives typical examples. It seems that the only visible effect of oxygen in the valence band region is the growth of the O 2p level at higher exposures:this gives no positive indication of the oxygen bonding site so we make use of other results for the GaAs - oxygen system.

The adsorption of oxygen on different faces of GaAs has been considered by many workers over the past ten years. There seems little doubt that oxygen is dissociatively adsorbed, as oxygen atoms (Arthur 1967) but there is considerable dispute over whether bonding is predominantly to the Ga or As surface atoms. One UPS experiment on the adsorption of oxygen on GaAs (110), the results of which have been published many times (Pianetta et al 1975, Spicer et al 1976a, Lindau et al 1976b, Spicer et al 1976b, Pianetta et al 1976, Spicer et al 1976c, Lindau et al 1976c, Lindau et al 1977) shows that a large chemical shift (2.9eV) occurs in the As 3d level on light oxidation with no accompanying peak shift (but an increase in width) of the Ga 3d level. On heavy oxidation a total As 3d shift of 4.5eV is observed, together with a 2eV shift in the Ga 3d level. This is interpreted to mean that the first stages of oxygen adsorption involve exclusively the As dangling bonds, and only on heavy oxidation are the Ga-As bonds broken. It is unfortunate that these authors have not considered in any of their publications the different ESCA shifts observed between the elements and the oxides of gallium and arsenic : shifts have been reported to be twice as large for As as for Ga (Wagner and Biloen 1972). Of course what really matters is the difference in chemical shift between GaAs and oxidized GaAs, not the bare elements, and this will to some extent reflect the variations in charge density around the two species of surface atom in the clean and oxidized state. However, we note that the surface Ga atoms in GaAs have already suffered a chemical shift to the more electronegative As atoms in the formation of the compound, and we may thus expect a smaller shift in the Ga levels on oxidation than in the As levels. It is clear that the larger As shift is not necessarily a definitive indication of predominant anion bonding.

Figure 5.18. Edc's at different photon energies for GaP + 2.25×10^5 LO_2

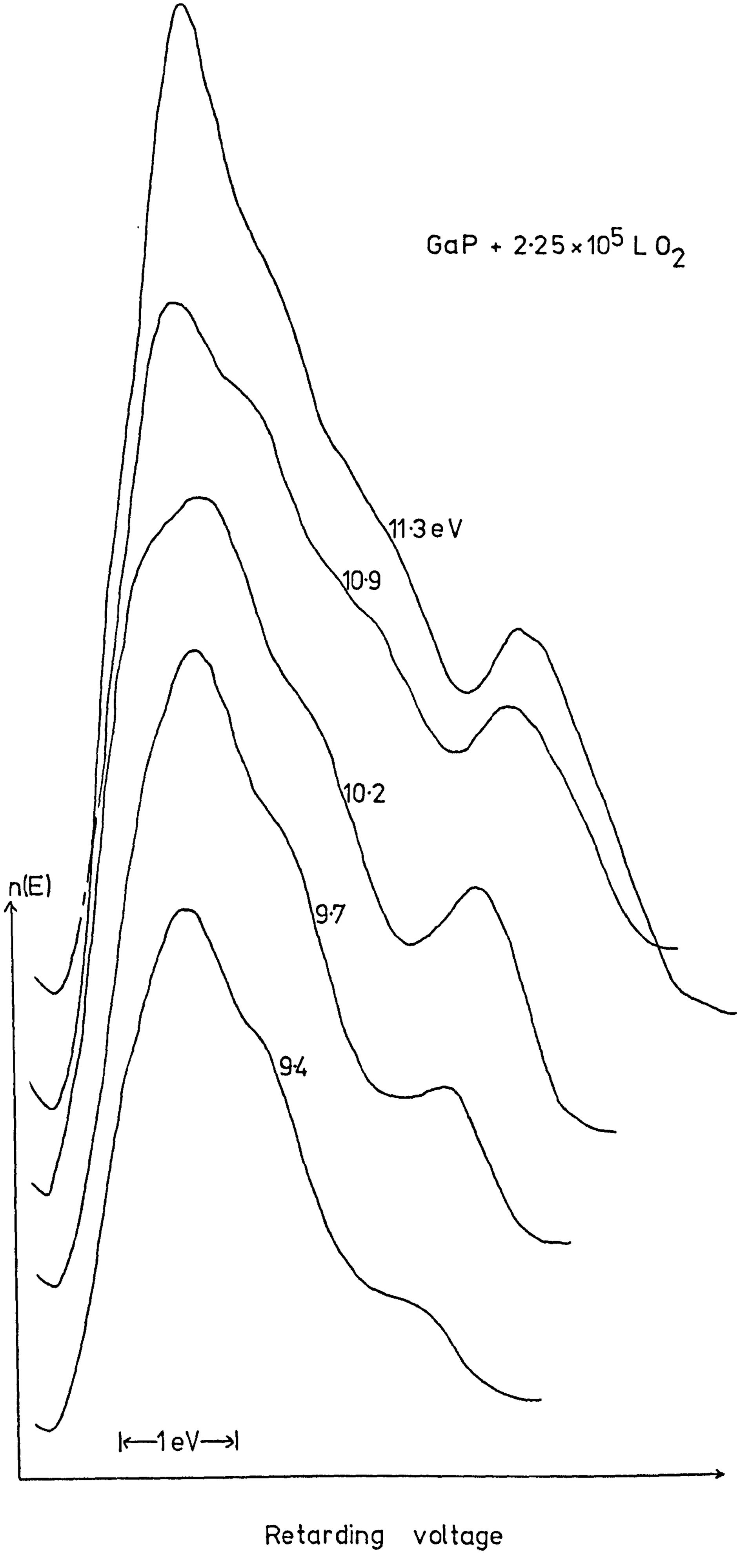
GaP + 2·25×10^5 L O2
11·3 eV
10·9
10·2
9·7
9·4
n(E)
|←1 eV→|
Retarding voltage

ELS results suggest that oxygen is chemically bonded only to the Ga atoms, with As apparently not playing a direct role in the oxidation process. This conclusion is reached from data on GaAs (100), (111), ($\bar{1}\bar{1}\bar{1}$) and (110) surfaces (Ludeke and Koma 1975a, 1976) where ELS structure derived from Ga 3d core level excitations is affected by oxygen before any effect is seen on transitions originating with the As 3d level. At increased exposures As-O bonding becomes important and a model to account for these results has very recently been proposed (Ludeke 1977). A very recent AES determination (Ranke and Jacobi 1977) also shows oxygen bonding to Ga surface atoms at an earlier stage than As-O bonds.

In view of the confusion regarding GaAs it is obviously unwise to attempt to generalize any results to other III- V compounds but it appears that our result that the first stage of the oxidation of GaP involves P-O bonding may be only partially correct, and Ga-O bonds may be formed as well. It is possible that formation of extrinsic states hinders the observation of changes in the Ga dangling bond states.

5.6. AES/LEED/ELS of Clean GaP

After the cleaning procedure detailed in Chapter 4.2 had been carried out, LEED indicated an unreconstructed surface giving a (1 x 1) pattern. Plate IX (a) and IX (b) show photographs of LEED patterns obtained at 94eV and 91.5V respectively. The 0^{o} azimuth is oriented about 40^{o} away from vertical in all the photographs.

The Auger electron spectra of GaP (110) are given in Figures 5.19 and 5.20. The values of the energies of Auger peaks are tabulated in Tables 5.3 and 5.4 , together with my assignment of the transitions giving rise to the peaks.

The identification of the main peaks has been discussed earlier (Morgan and van Velzen 1973), but it appears that some of the weaker structures have not been correctly interpreted. As has been suggested in the case of

Plate IX LEED patterns from GaP (110)

(a) clean; E_p = 94V

(b) clean; E_p = 91.5V

(c) after exposure to ~ 1 x 10^5 LO_2 ; E_p = 94V.

(d) after heating in oxygen; E_p = 94 V.

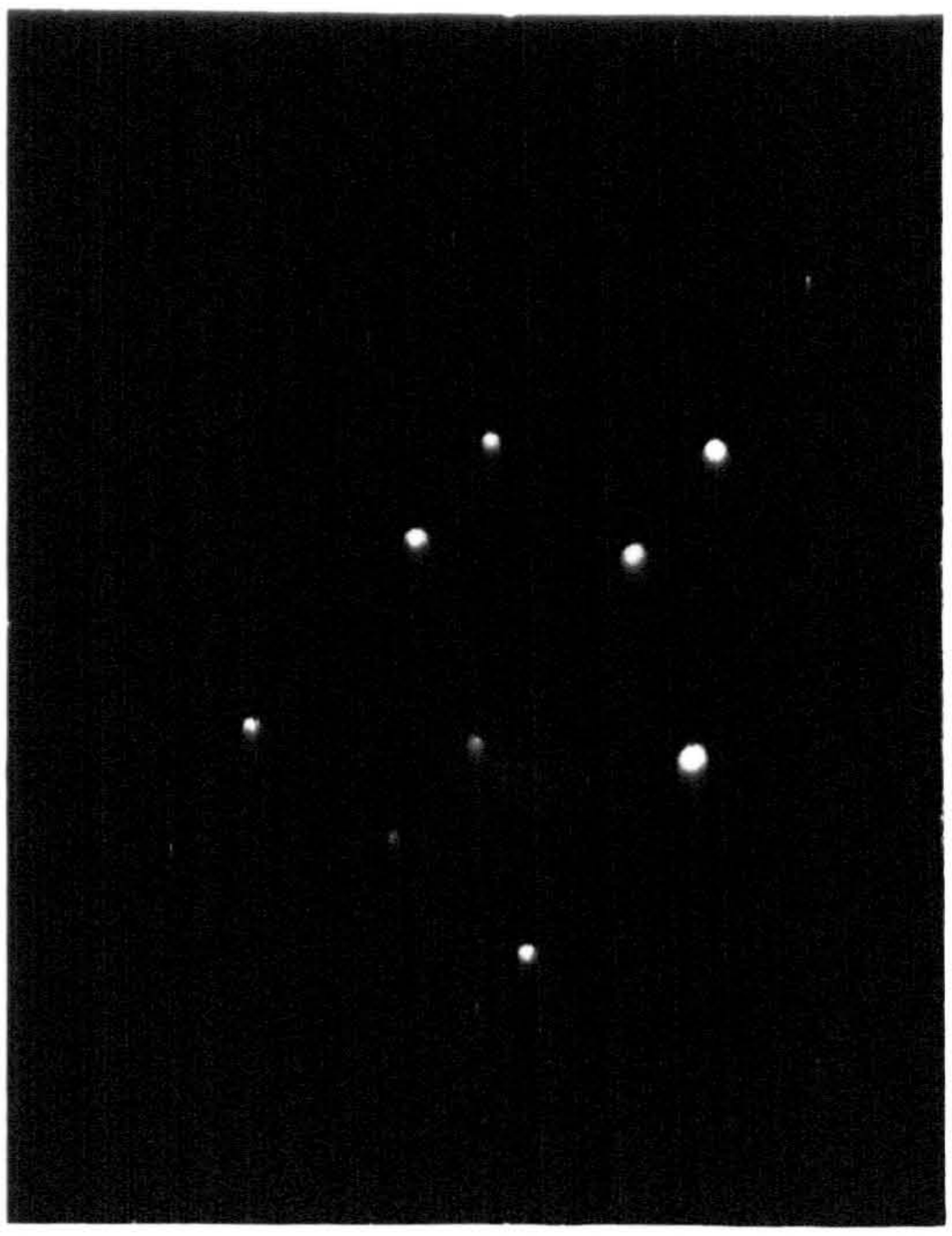

a

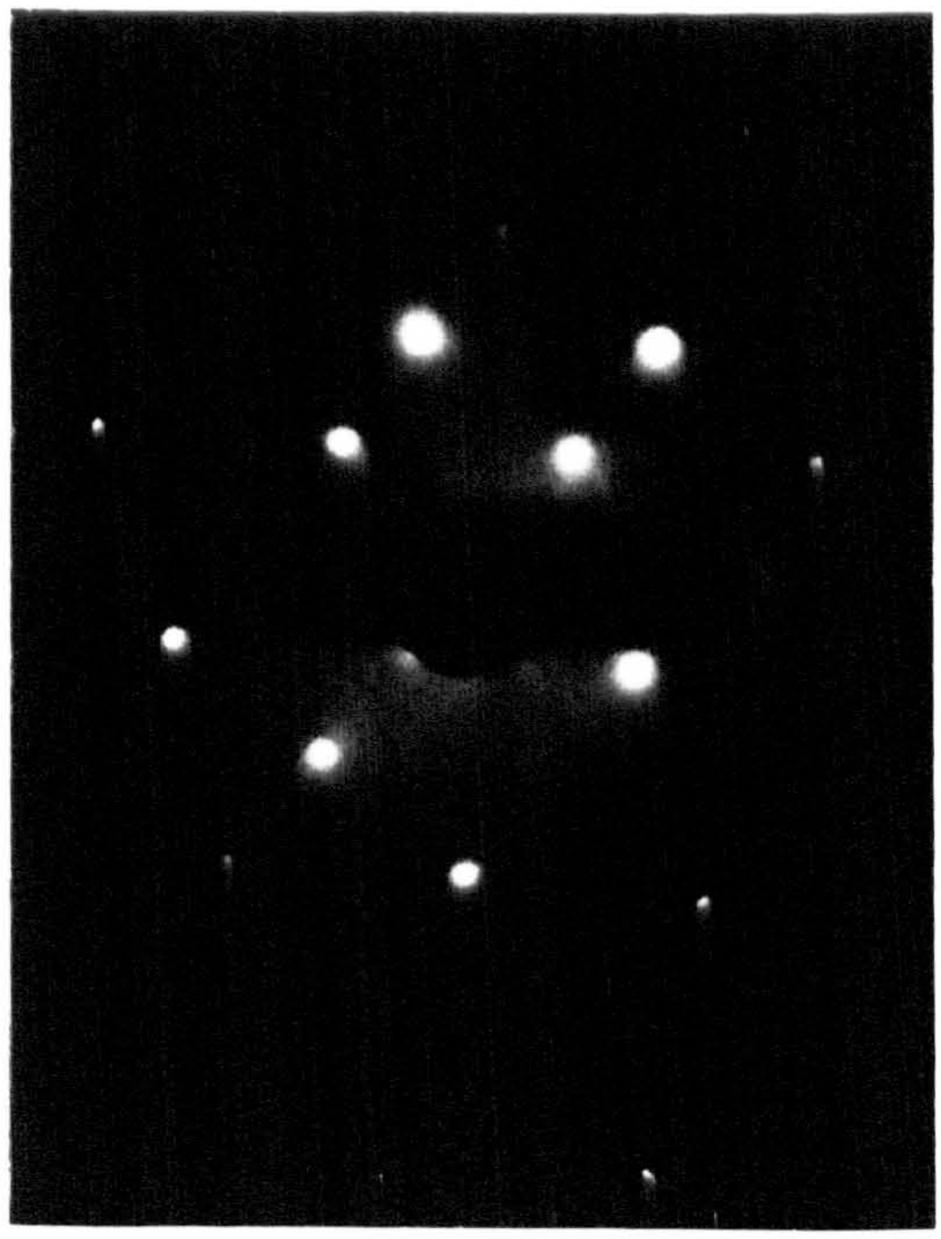

b

c

d

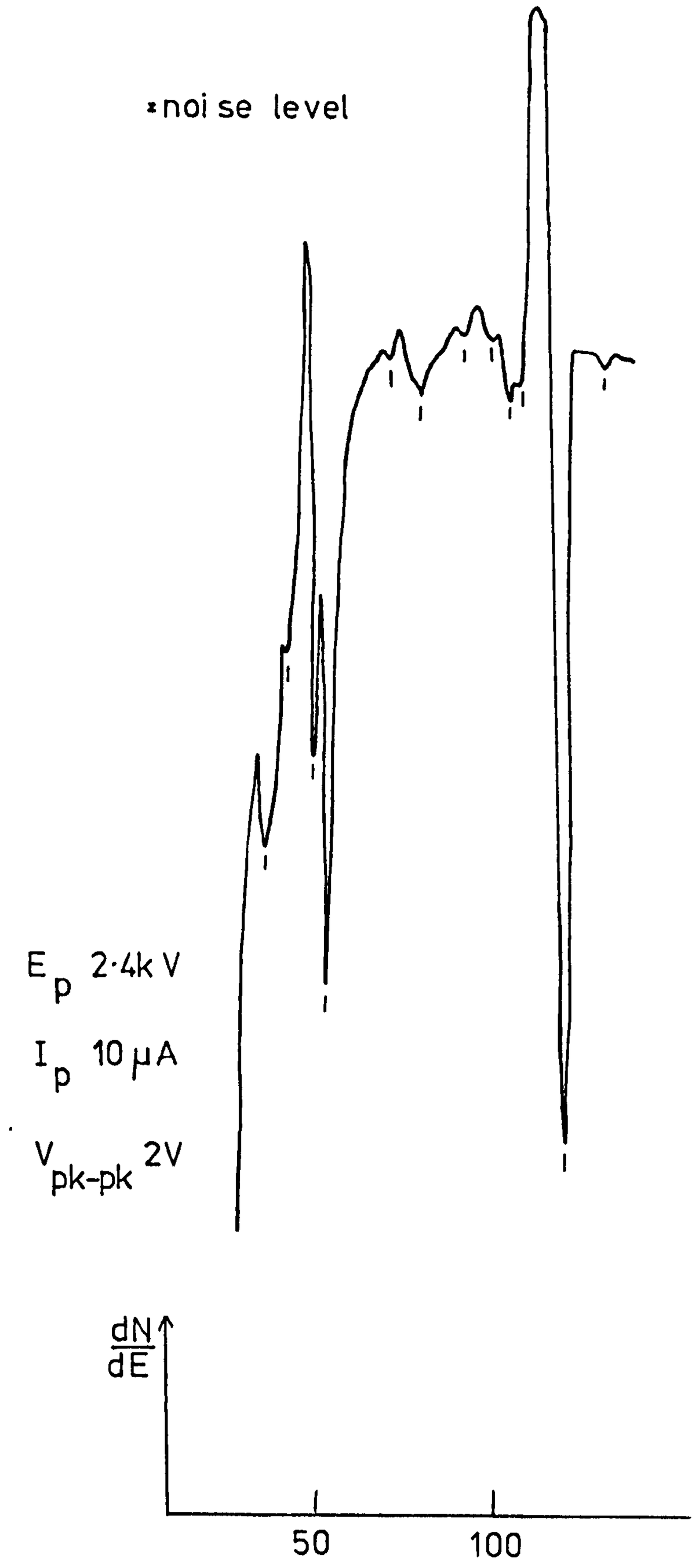

Figure 5.19. Low-energy Auger electron spectrum of GaP (110)

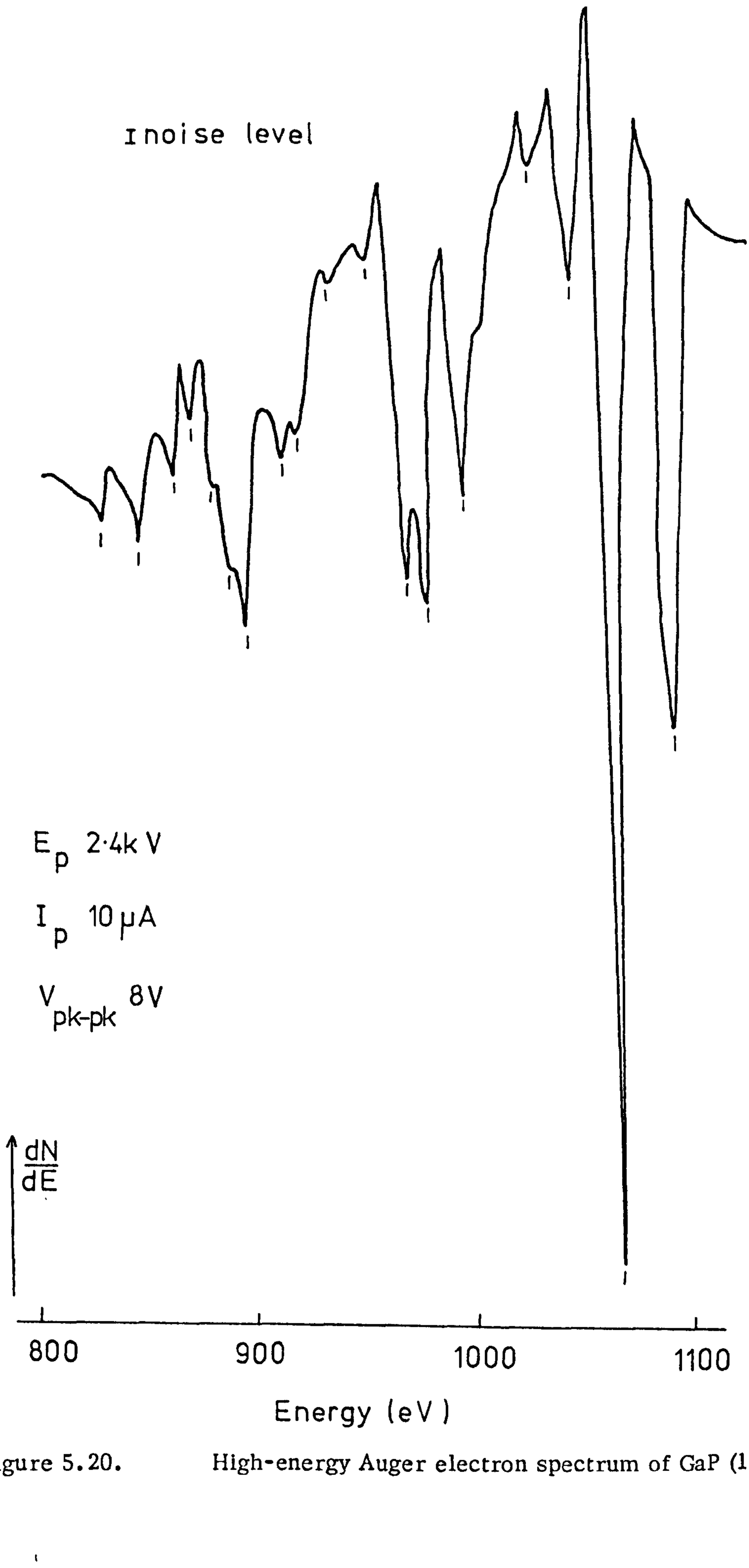

Figure 5.20. High-energy Auger electron spectrum of GaP (110)

Table 5.3

Energies and identification of low-energy GaP Auger peaks

Energy (eV)	Transition
39.5	P $L_1 L_{2,3} V$
43	surface plasmon loss from 54eV
50	Ga $M_3 M_{4,5} M_{4,5}$
54	Ga $M_2 M_{4,5} M_{4,5}$
72 – 80	Ga $M_{2,3} M_{4,5} V$
94 – 100	Ga $M_{2,3} VV$
105	Ga $M_1 M_{4,5} M_{4,5}$
108	surface plasmon loss from 119.5eV
119.5	P $L_{2,3} VV$
133	Ga $M_1 M_{4,5} V$

TABLE 5.4.

Energies and identification of high-energy GaP Auger peaks

Energy (eV)	Transition
827	$L_3M_{2,3}M_1$
844	$L_3M_1M_{2,3}$
860	$L_2M_{2,3}M_1$
871	$L_2M_1M_{2,3}$
876	bulk plasmon loss from 893.5 eV
893.5	$L_3M_{2,3}M_{2,3}$
914 } 919 }	$L_2M_{2,3}M_{2,3}$
933	2 x bulk plasmon loss from 969 eV
951	bulk plasmon loss from 969 eV
969	$L_3M_{4,5}M_{2,3}$
982	$L_3M_{2,3}M_{4,5}$
996.5	$L_2M_{4,5}M_{2,3}$
1005	$L_2M_{2,3}M_{4,5}$
1030	2 x bulk plasmon loss from 1067 eV
1049	bulk plasmon loss from 1067 eV
1067	$L_3M_{4,5}M_{4,5}$
1092	$L_2M_{4,5}M_{4,5}$

All from Ga atom

zinc (Schön 1973) it seems unlikely that the $M_{2,3}$ levels, whose spin-orbit splitting is less than 4eV, could be resolved at energies around 1keV, especially with a modulating voltage of 10V, as used by Morgan and van Velzen. This leads to different designation of the four levels at 969, 982, 996.5 and 1005 eV : Morgan and van Velzen gave these as $L_3M_2M_4$, $L_3M_3M_4$, $L_2M_2M_4$ and $L_2M_3M_4$, whereas a more realistic assignment is $L_3M_{4,5}M_{2,3}$, $L_3M_{2,3}M_{4,5}$, $L_2M_{4,5}M_{2,3}$ and $L_2M_{2,3}M_{4,5}$. The previous identification required vastly differing $M_{2,3}$ separations for the two pairs of peaks considered here.

Similar arguments, based on the separation of the $L_{2,3}$ levels, lead us to disagree with the identification of the levels at 827 and 844eV: the $L_{2,3}$ splitting is about 27eV and it seems that the labels of $L_3M_{2,3}M_1$ and $L_3M_1M_{2,3}$ are preferable to those of $L_3M_1M_3$ and $L_2M_1M_2$ previously suggested. There is little dispute about the low-energy Auger peaks except again over the $M_{2,3}$ splitting. Apart from the well-defined peaks at 50 and 54eV, which involve the well-localised gallium 3d electrons, the next four peaks, arising from a Ga $M_{2,3}$ hole, at 72, 80, 94 and 100eV involve valence electrons and hence are broadened sufficiently for definite identification of the split M_2 and M_3 levels to be somewhat unlikely. We prefer an alternative explanation for the peak at 39.5eV : the intensity ratio is too large, and the energy difference too small, for this to be a bulk plasmon loss from the 54eV peak. This is likely to be a phosphorus $L_1L_{2,3}V$ transition. The energy of such a transition is difficult to calculate accurately as the difference between the $L_{2,3}$ levels of the (Z) and (Z + 1)- element is large (36eV), and so the energy of the Auger peak depends critically on the approximation used to correct for the energy level shift by the initial hole ionization.

A very recent publication (Jacobi and Ranke 1976) has made observations broadly similar to the above, and reports an extra peak at 115eV and an alternative explanation for the feature we find at 108 eV. These peaks are described in terms of transitions involving the phosphorus atoms

and the valence electrons: since the phosphorus is the more volatile surface constituent, these types of transition would be expected to be sensitive to the condition of the surface, and it may well be that differing surface preparation techniques lead to slightly different Auger electron spectra.

No effects of the electron beam were found on the clean (110) face of GaP, even after prolonged irradiation. This finding conflicts with the observations on the (100) face (Bayliss and Kirk 1975). It appears that the cleaning procedure employed by these authors did not include annealing, and so it is unlikely that the surfaces prepared were properly stoichiometric: indeed, they (Bayliss and Kirk 1976) reported several different surface phases on the (100) faces of GaP, InP and GaAs. The presence of large amounts of imbedded argon and residual carbon in their "clean" Auger spectrum also casts some doubt on the results. However, we note that such impurities may be expected to stabilize a surface, and also phosphorus was observed in the residual gas of their system, which certainly indicates a considerable degree of dissociation. It is also worth remarking that the (110) face should be more stable than any other, and it may not therefore be surprising that no preferential dissociation of our surface was found.

Electron energy loss spectra from GaP at three different primary beam energies of the glancing-incidence gun are given in Figure 5.21. Whilst not quite as spectacular as losses obtained from some free-electron like metals, the bulk plasmons are clearly visible, and multiple losses of up to four plasmons can be seen. To enhance small structures on the large varying background we have used the derivative of n(E). Note that, for the differentiated curves, we have taken the minima in $dn/_{dE}$ as the positions for the features found, instead of the energies where $dn/_{dE} = 0$. However, we have also measured the loss energies from the minimum in the differential of the elastic peak, and thus little error is expected : if all peaks in n(E) have the same width, and the modulation voltage is sufficiently small, our procedure is exact.

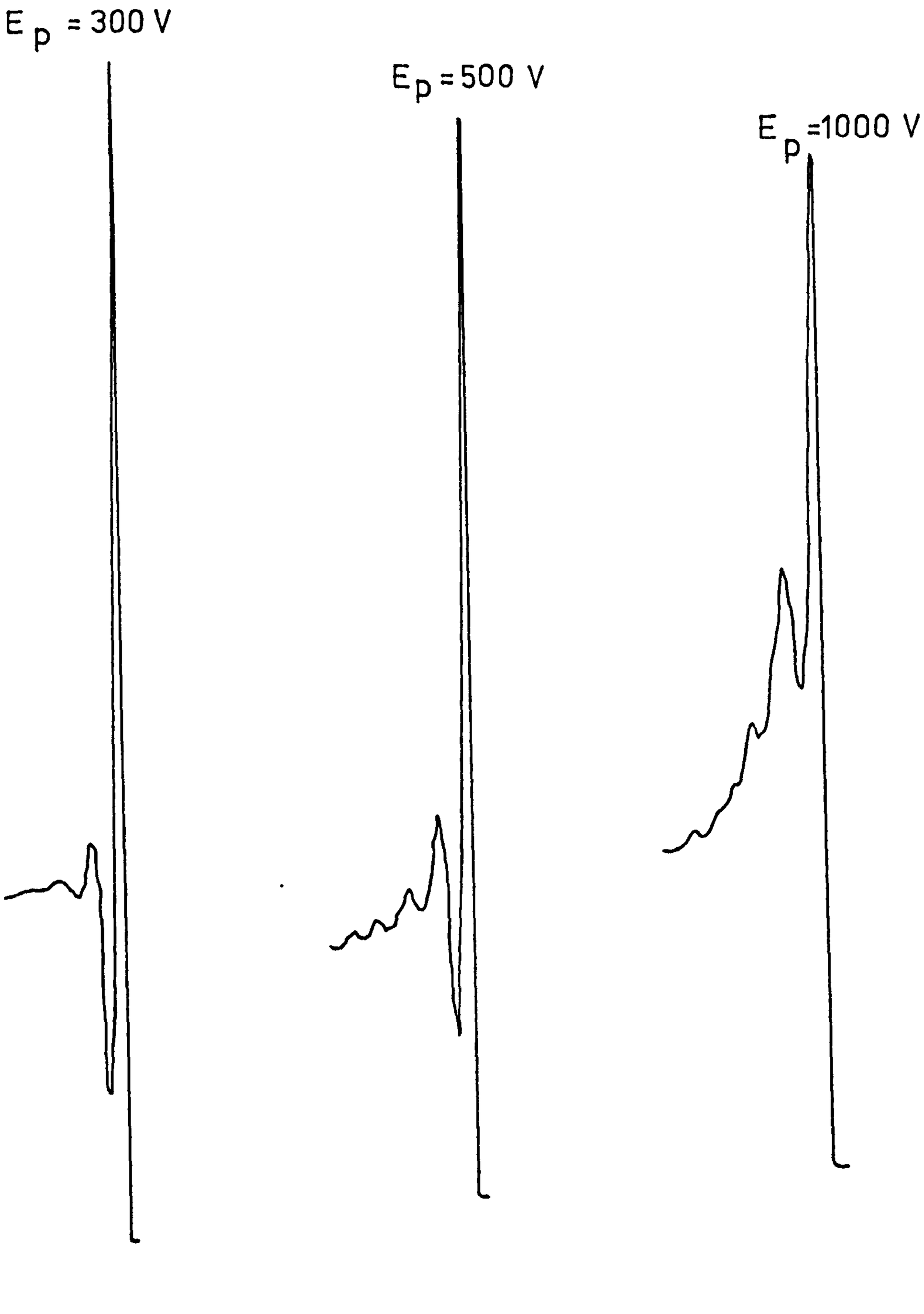

Figure 5.21. Electron energy loss spectra from GaP (110) at three different primary electron energies

Differentiated curves are shown in Figures 5.22 and 5.23 for normal- and glancing-incidence electron beams respectively. The energies of prominent features are listed in Tables 5.5 and 5.6 , together wtih designations of the possible transitions giving rise to these energy losses. It is seen that there is little resemblance between the spectra obtained at normal- and glancing-incidence, the latter strongly emphasizing surface features. Most of these losses have been identified and discussed previously (Morgan and Van Velzen 1973) but a few comments are necessary. Many of the features are broad, and cannot be placed to better than ± 0.2eV; however, we find a lower value of surface plasmon energy than quoted previously (11.2eV). It is unfortunate that the shape of the $^{dn}/_{dE}$ curve makes it impossible unambiguously to separate a contribution from the double surface plasmon loss; attempts to differentiate this spectrum were not successful owing to problems with noise and phase equalisation. The bulk plasmon energy of ~ 16.3eV is very close to the value of 16.6eV calculated from the free-electron model: although semiconductors, with mostly covalent bonding, are not normally considered to be so, they are free-electron-like in the sense that strong interband transitions occur mainly at energies less than the free electron plasmon energy. The small feature at ~ 3.65eV, not seen in normal-incidence spectra but reproducibly present in all glancing-incidence spectra, is attributed to a transition involving surface states: it may be from filled surface states to the conduction band, from the valence band to empty surface states or possibly from filled to empty surface state bands. Such a transition was indirectly obtained from ellipsometric measurements (Morgan 1974) on clean and adsorbate-covered GaP surfaces. It has been pointed out that these results could be explained in terms of the perturbation of the surface electric field by the adsorbate (Lukeš 1975) but such an interpretation is not valid for our electron-loss measurements. We remark here on several observations which support our assignment :(i)this feature is present only in the glancing-incidence spectra, which emphasize surface effects, and is not seen in the normal-incidence spectra :(ii) it is

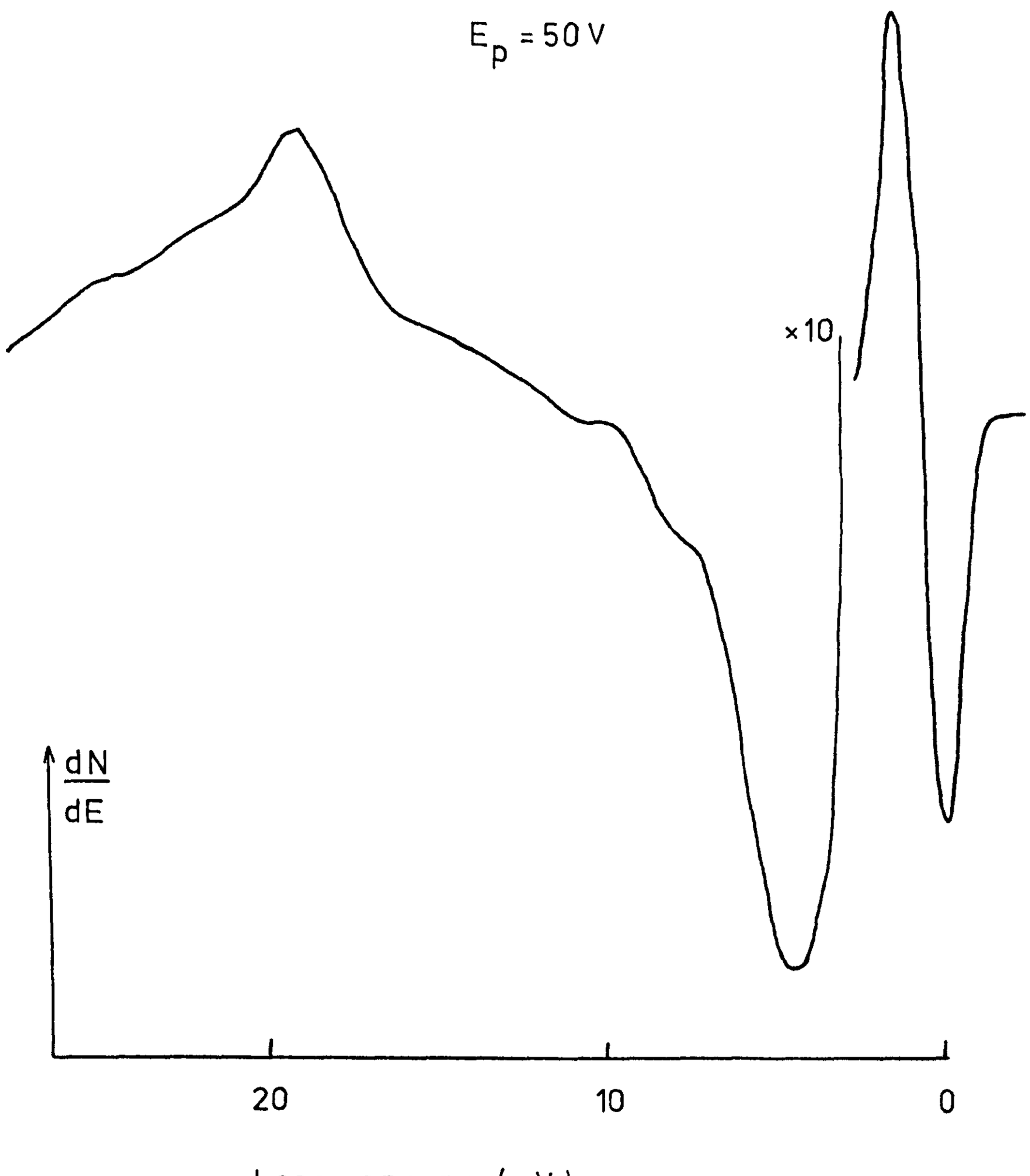

Figure 5.22. Electron energy loss spectrum taken with normal-incidence electron gun.

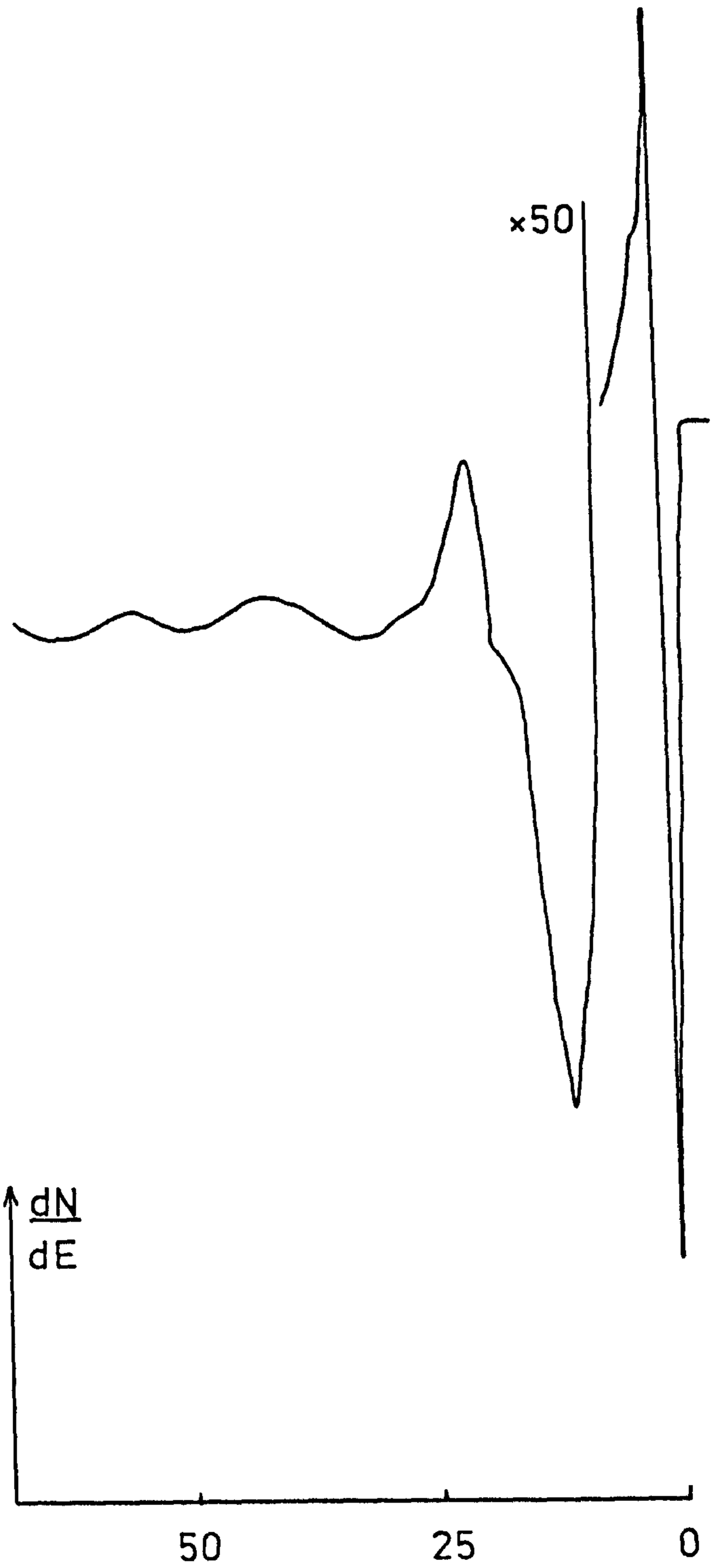

Figure 5.23. Electron energy loss spectrum with glancing-incidence electron gun.

TABLE 5.5.

Loss energies from clean GaP; normal incidence electrons.

Energy (eV)	Identification
4.4 – 7.9	interband transitions
10.3 - 10.7	surface plasmon
15.4 - 16.0	bulk plasmon
20.5 - 20.9 – 23.9	Ga 3d core to conduction band transitions

TABLE 5.6

Loss energies from clean GaP; glancing incidence electrons

Energy (eV)	Identification
3.65	surface state transition
9.7 - 10.5	surface plasmon
16.0 - 16.6	bulk plasmon
23.9, 25.9	Ga 3d core to conduction band transitions
32.5	2 bulk plasmons

not seen after oxygen adsorption (Figure 5. 26) ; (iii) this feature becomes less prominent as the electron energy is increased. It is expected that the electron,mean-free-path will increase steadily as the energy is increased from 300eV, and thus surface sensitivity will diminish. Loss of focus prevented the use of lower primary energies than 300eV, so this energy-dependence could not be fully tested. A weak feature seen at ~ 3.1eV in ELS of GaAs (110) has recently been attributed to a transition between bands of surface states (Ludeke and Koma 1976), although this had not been seen earlier (Froitzheim and Ibach 1975).

It must be remarked that a transition between bands of surface states would be surprising if, as indicated by most theoretical studies, the filled states are localized on the P atoms and the empty states on the Ga atoms. In the case of complete localization the wavefunctions will be orthogonal and thus transitions are forbidden. It is still possible for such transitions to exist if the localization is not complete and there is some overlap of wavefunction; alternatively, hybridization with bulk states may allow inter-surface state transitions or transitions between surface and bulk states.

5.7. Oxidation of GaP , studied by AES/LEED/ELS

It has been recognised for some time that the electron beam used for AES or LEED studies may perturb the system under investigation. This effect has been shown to be particularly severe in the case of adsorption on semiconductors, where electron-assisted adsorption has been reported in several systems, for example, O_2 on Si (111) (Coad et al 1970), CO and O_2 on Si (111) (Kirby and Lichtman 1974), O_2 on GaAs (111) and ($\bar{1}\bar{1}\bar{1}$) (Ranke and Jacobi 1975) and O_2 on Ge (111) (Margoninski 1976). However, several other studies have shown no electron-beam effects. No influence of electron irradiation on the oxidation of cleaved GaAs (110) faces was found (Dorn et al 1974) and it may be thought that the surface concentration of adsorbed oxygen is small on the cleavage faces. Lüth and Russell (1974) , in their ELS measurements of clean and oxygen-covered GaAs (110) surfaces,

turned off all filaments during oxygen admission, but make no comment on the possible effects of their low-energy electron gun on the oxidised surface. The oxidation of (110) slices of GaP was investigated by Morgan and Van Velzen (1973), who specifically state that they made no measurement of the influence of the electron beam on the oxidation, and in a similar study of InP (110) Williams and McGovern (1975) observed some effects at high beam current densities. Electron-beam effects were not mentioned in another publication on ELS of oxygen-exposed GaAs surfaces (Ludeke and Koma 1975 a, 1976.). Thus although some puzzling conflicts of evidence exist in the literature, it is obviously wise to beware of possible difficulties.

We note here that another possible problem, preferential adsorption of the residual gases in the vacuum system, is unlikely to cause trouble on GaP. Careful study of the chemisorption of many gases on crushed GaP crystals (providing a very large area of mainly (110) surfaces) revealed that adsorption of H_2, CO, CO_2 and CH_4 proved negligible (Van Velzen and Morgan 1973). It is fortunate that none of the usual residual gases of a baked, ion-pumped system actually sticks to GaP (110).

Considerable precautions were taken in an attempt to minimize the anticipated problems of electron-stimulated adsorption. The pressure of oxygen during exposure could be monitored in three different ways: with a nude Bayard-Alpert ionisation gauge, with the Q7 quadrupole mass spectrometer or simply by measuring the current drawn by the main ion pump of the system. Only the Q7 had a direct line-of-sight to the specimen. It was established that no significant differences were observed between the adsorption characteristics when the pressure was measured by each of these methods. Oxygen adsorption was carried out at pressures between 1×10^{-6} Torr and 2×10^{-4} Torr, care being taken always to maintain a dynamic equilibrium with a controlled flow of gas through the system.

An Auger electron spectrum from clean GaP is shown in Figure 5.24 (a), and Figure 5.24 (b) gives the oxygen and carbon peaks from a scan taken immediately after the oxygen had been pumped from the system following an

Figure 5.24. Auger electron spectra from GaP

(a) clean GaP. (b) -(e) GaP exposed to 3×10^5 L O_2.

(b) immediately after beam turned on

(c) after irradiation by beam for one hour

(d) different position on sample, not previously irradiated by beam

(e) after beam had irradiated reverse side of sample for two hours.

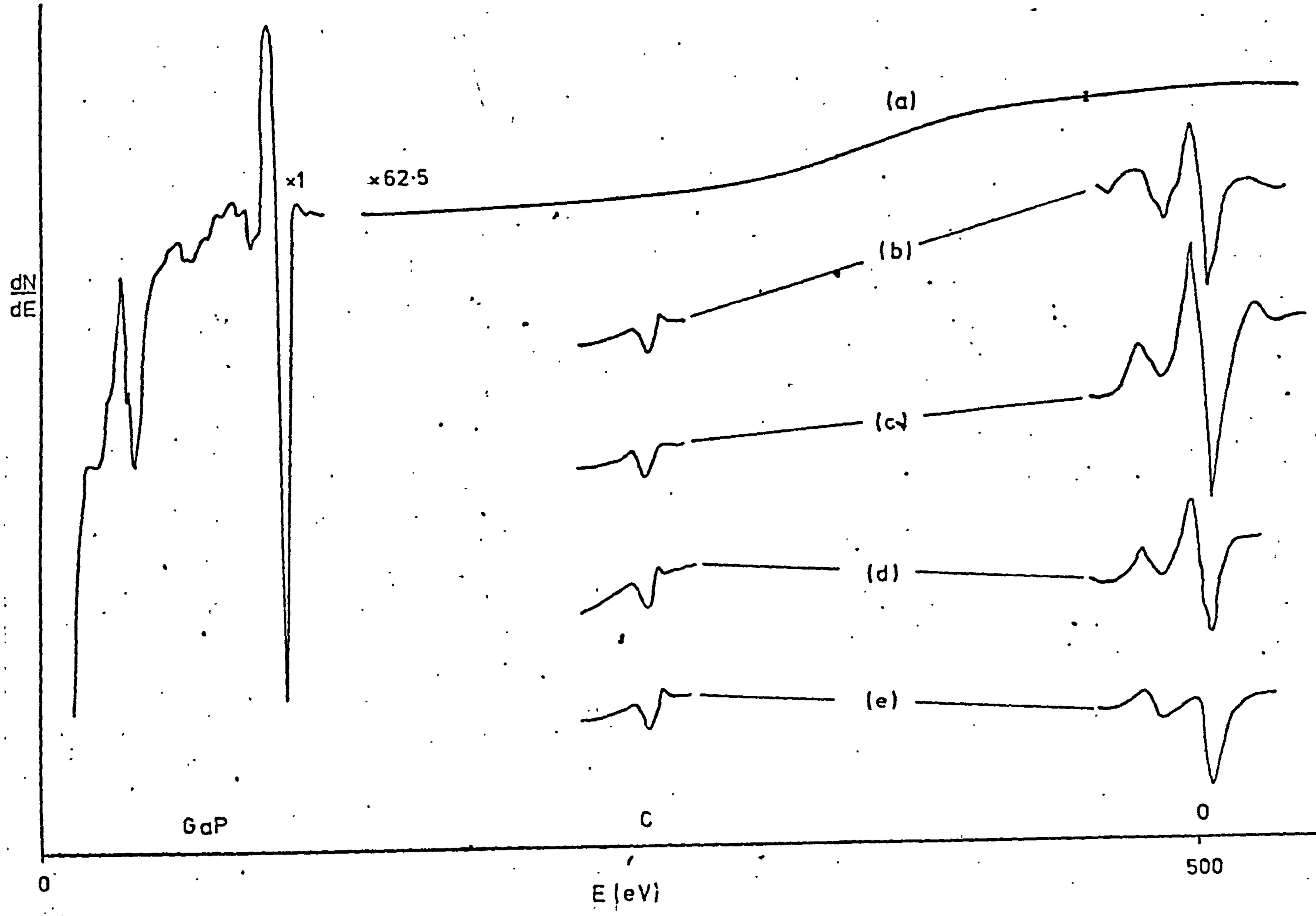
dN/dE
×1
×62·5
(a)
(b)
(c)
(d)
(e)
GaP
C
O
0
500
E (eV)

exposure of 2×10^{-4} Torr for 25 minutes, a total of 3×10^{5} Langmuirs O_2. We do not give, in this section, the remainder of the Auger spectrum. After this scan had been taken, the entire scan taking $\sim$ 7 minutes, a raster across the sample revealed an elliptical area, clearly distinguishable from the rest of the crystal surface, where the beam had hit the sample at glancing incidence. When the beam was left on this spot for one hour, the oxygen Auger peak increased considerably, as shown in Figure 5.24 (c). A further Auguer scan of a fresh area, which had not been exposed to the electron beam either in its clean or partially oxidised state, revealed a much lower concentration of oxygen (Figure 5.24 (d)). It is seen that there is a small carbon Auger peak in the spectra of oxidised GaP. This was always observed on oxidised samples, and its magnitude was found to be almost independent of oxygen exposure and duration of electron-beam irradiation. It seems that this is a result of the cracking of the initial oxide by the electron beam; a similar study of oxidised silicon showed that small amounts of carbon tended to stabilize the oxide and prevent further beam-induced dissociation (Thomas 1974).

We have tested, and can reject, the possibility that a part of the surface is in some way pre-conditioned by the electron beam during AES before admission of oxygen. When each Auger electron spectrum, both before and after oxidation, was taken from a part of the surface which had not previously been exposed to the electron beam, results were obtained which were identical to those of Figure 5.24 (a-d).

However, it was observed that the first area to be studied after each admission of oxygen yielded a higher oxygen Auger peak than each subsequent scan on a fresh area. We eliminated the possibility that this apparent time-dependence was due to residual oxygen in the chamber, which would be gradually pumped away, by waiting approximately 30 minutes after oxygen exposure before turning on the electron gun. This time was sufficient for the chamber pressure to fall below 2×10^{-10} Torr, and for the partial pressure of oxygen to fall below the detection limit of the Q7 quadrupole mass spectrometer. The pressure fell only very slowly after this time, yet the dramatic variation of oxygen Auger peak height was still observed.

By monitoring the current drawn by the filament of the electron gun and the current incident on the sample (measured with a small attractive bias on the sample) it was found that, with a constant heater current, the emitted current rose rapidly for about the first twenty to thirty minutes after the gun was switched on, and then remained constant. This pattern was repeated after each cycle of oxygen admission.

A further set of experiments was performed in which the sample was rotated away from the electron gun and the beam allowed to hit the back of the sample holder for between two and four hours after each oxygen exposure. After this procedure had been followed prolonged exposure of the oxidised GaP surface to the electron beam led to no significant change in the oxygen Auger peak. This means that we can rule out the occurrence of beam-stimulated surface diffusion of oxygen into the area irradiated by the beam. Incidentally, the possibility of electron-stimulated desorption of oxygen or oxides from the surface can also be discussed. A typical Auger electron spectrum, obtained in this manner from GaP which had been exposed to 3×10^5 L oxygen, is given in Figure 5.24(e).

Our observations, which have been described by us in some detail elsewhere (Norman and Skinner 1977 - see Appendix), can be explained by adsorption of oxygen into the lanthanum hexaboride filament coating and absorption into the porous ceramic holder which supports the filament. During the first twenty to thirty minutes of running the electron gun, the oxygen will be driven off the filament, and the emission current rises as the poisoning effect of the adsorbate is reduced. For several hours after that, the oxygen will gradually diffuse out of the ceramic filament holder, which is heated only indirectly. All the oxygen molecules may be ionised by the electron beam and thus become 2.4keV oxygen ions directed towards the sample. It is not clear what effect the focussing lens and deflection plates of the electron gun will have on such oxygen ions, but it seems likely that a large proportion of this flux may reach the sample, although such an ion beam may not be well-focussed. At energies of 2.4keV many ions may cause significant surface

damage and could be implanted into the sample. Penetration depths of higher energy ions (≥ 10keV) have been studied extensively (Mayer et al 1970) but at the energy of interest to us there are no ion range data available. However, a recent estimate for argon ions in silicon (Johannessen et al 1976) would indicate a probable penetration depth of about three monolayers at ~ 2.4keV. Calculation of ion flux is impossible since the number of molecules of oxygen adsorbed onto and dissolved in the filament coating and its supports is unknown. Nevertheless, the surface area of these parts is many times greater than the area of the semiconductor surface which is probed by the electron beam (~1 mm^2) and the sticking coefficient for molecular oxygen on the components of the filament is likely to be greater by several orders of magnitude than for the unreactive GaP (110) surface; hence, there will be enough oxygen released from the gun towards the sample to produce several monolayers of oxygen on or within the surface.

These findings obviously mean that very great care should be taken to outgas the electron gun thoroughly after each oxygen exposure: it seems that it is necessary to run with the beam directed away from the sample for between two and four hours before reliable results on the oxidised GaP face can be obtained. Unfortunately, the full implication of this was not realized until these studies had almost been completed, and the results presented undoubtedly do contain an element of this type of ion-bombardment. However, each spectrum was taken approximately half-an-hour after the end of each cycle of oxygen exposure, after all traces of oxygen had been pumped from the system, and so it is believed that comparison between our spectra are probably valid.

LEED indicated that adsorption of oxygen induced no extra spots or reconstruction, but just a uniformly increased background . Plate IX (c) shows a LEED pattern obtained at 94eV (the same as Plate IX (a))after admission of ~ 1×10^5 L O_2 .

The effect of increasing oxygen exposure on the Auger spectra is given in Figure 5.25. The only change observed in the high-energy gallium-derived Auger peaks (800-1100eV) was a monotonic attenuation of all peaks with

Figure 5.25. Auger electron spectra from GaP with increasing oxygen exposure.

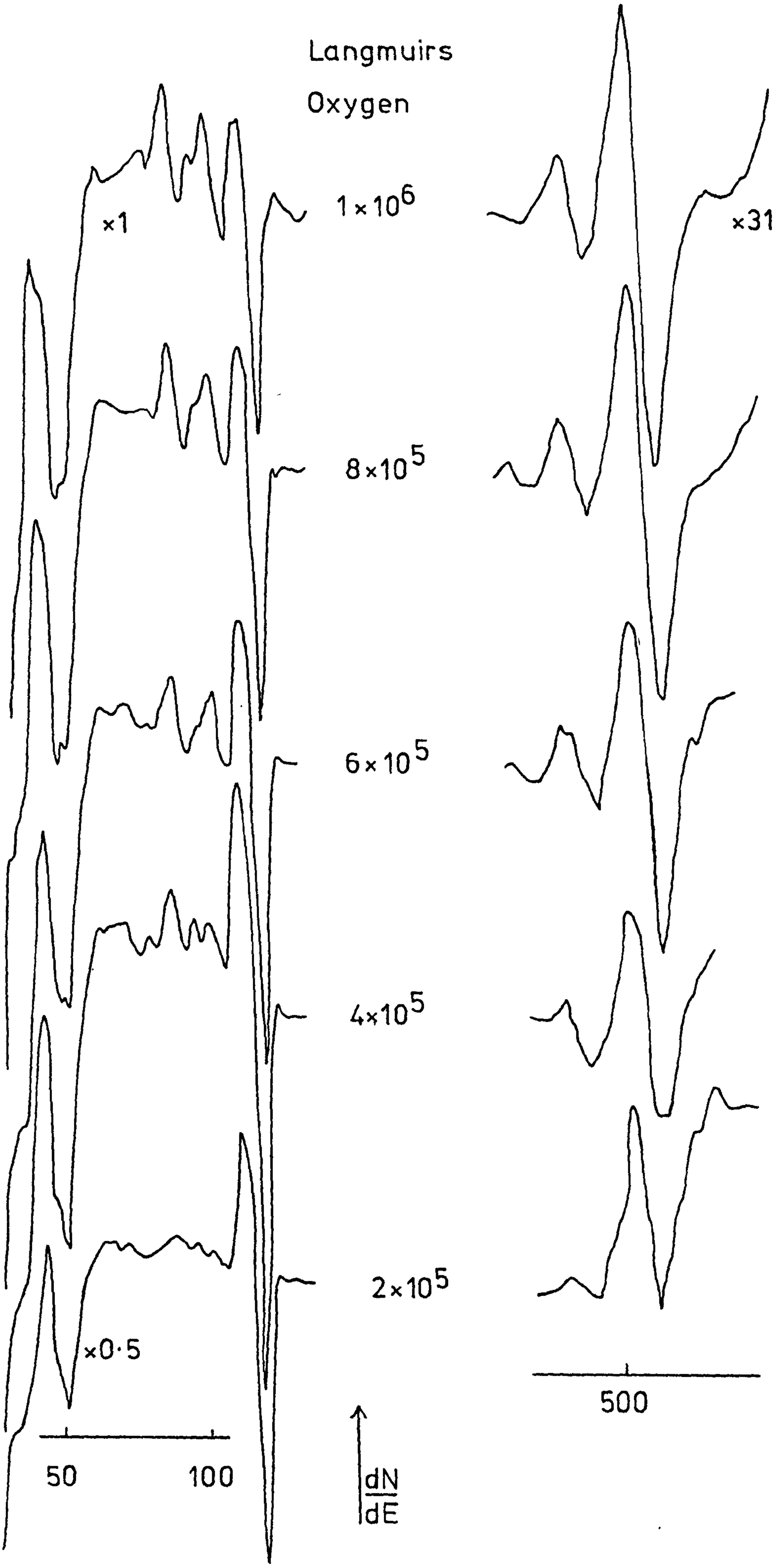
Langmuirs
Oxygen
×1
1×10^6
×31
8×10^5
6×10^5
4×10^5
2×10^5
×0·5
50
100
500
dN/dE

increasing oxygen coverage: the peaks attributed to bulk plasmon losses are almost extinguished, but none of the other peaks is preferentially affected. It is clear that the P(119) : Ga (54) ratio decreases with increasing oxygen coverage; it is not possible, however, to plot this relationship in a sensible way because the phosphorus 2p level becomes involved in other transitions which appear at 94 and 108eV. The weaker Ga peaks at 72, 80, 100 and 108eV gradually disappear but the stronger peaks at 50 and 54eV persist. No extra features are found at intermediate oxygen exposures. After the 100eV Ga M_{23} VV peak disappears (Figure 5.25; $6 \times 10^5 LO_2$ exposure) a weak shoulder at 99eV grows, and also a small peak at 85eV appears - these being strongest after $3 \times 10^{10} LO_2$ exposure.

Several possible explanations for the origin of the peaks at 94 and 108eV and shoulders at 85 and 99eV may be considered. Diffraction of excited secondary electrons on their way out of the crystal has been described (McDonnell et al 1973). Such scattering is, however, unlikely to be induced by an adsorbate layer which has been shown by LEED to be disordered (Plate IX (c)). These peaks could still be designated phosphorus $L_{2,3}VV$ transitions if the adsorption of oxygen has caused a great change in the density of states at the surface. A shift of $\sim$ 6eV in the maximum of the density of states could explain an Auger energy shift from 119.5eV to 108eV. However, there is no evidence for such a change: the UPS results show no dramatic change, and the Auger peaks from Ga atoms involving the valence band are not shifted. The peak at 94eV cannot be accommodated in such a scheme, moreover. The weak shoulder visible at 108eV in the clean GaP spectrum was attributed to a surface plasmon loss from the main 119.5eV peak. It is extremely unlikely for this explanation to hold for the large 108eV peak after adsorption of oxygen.

The interpretation for the peaks at 94eV and 108eV which I believe to be correct involves the concept of cross-transitions between levels on the phosphorus and oxygen atoms. Interatomic Auger transitions have been invoked to explain peaks found in the oxidation of alkali metals (Janssen et al 1974)

and in several highly-ionic compounds (Citrin et al 1976). It seems that the first suggestion of the use of such transitions was for this same system of oxygen on GaP (Morgan and Van Velzen 1973), where the 94eV peak is explained as a $PL_{2,3}OL_1V$ transition - a designation with which we disagree, however. Extra peaks observed on the oxidation of InP have been described in similar terms (Williams and McGovern 1975).

The energies calculated for various possible transitions and observed peak positions are given in Table 5.7. The two values of theoretical energy are from calculations both with and without correction of the electron energy levels for the ionization of the core hole, according to eqs.(3.1) and (3.2). It is seen that better agreement with observation is obtained if it is assumed that there is no relaxation of energy levels.This may be reasonable in the case of interatomic Auger transitions since the screening between shallow oxygen levels and the phosphorus core hole will undoubtedly be greater than between levels all on the phosphorus atom.

All our observed Auger electron peaks for GaP with adsorbed oxygen are thus explained except for the feature of 85eV. To assist in assigning this peak, we consider here the electron loss spectra.

The energy-loss spectrum obtained after an exposure of $3 \times 10^{10} LO_2$, shown in Figure 5.26, exhibits several changes from that obtained on clean GaP (Figure 5.23). The shoulder at 3.65eV, tentatively ascribed to transitions between filled and empty bands of surface states, is not visible, and the main dip in the spectrum now occurs at around 9.0eV, with the surface plasmon loss at $\sim$ 10.5eV no longer seen. The other peaks, with their assignments given in Table 5.8, show little change.

I attribute the new loss at $\sim$ 9eV to an interface plasmon. From the discussion in Chapter 3.4, such plasmons have an energy $\hbar\omega_1$ given by the expression

$$\hbar\omega_1 = \frac{\hbar\omega_p}{\sqrt{1+\varepsilon}}$$

where ε is the bulk dielectric constant of the medium bounding the solid. It

TABLE 5.7.

Observed and calculated Auger transitions for GaP with adsorbed oxygen

Transition	calculated energy (eV)*	observed energy (eV)
$PL_{2,3}VV$	119	119.5
$PL_{2,3}OL_{2,3}V$	114 - 115	not seen
$PL_{2,3}OL_{2,3}OL_{2,3}$	109 - 111	108
$PL_{2,3}OL_{1}V$	93 - 98	99
$PL_{2,3}OL_{1}OL_{2,3}$	88 - 93	94
$PL_{2,3}OL_{1}OL_{1}$	67 - 77	75

* The two theoretical values of energy are from calculations both with and without correction of the electron energy levels for the ionization of the core hole.

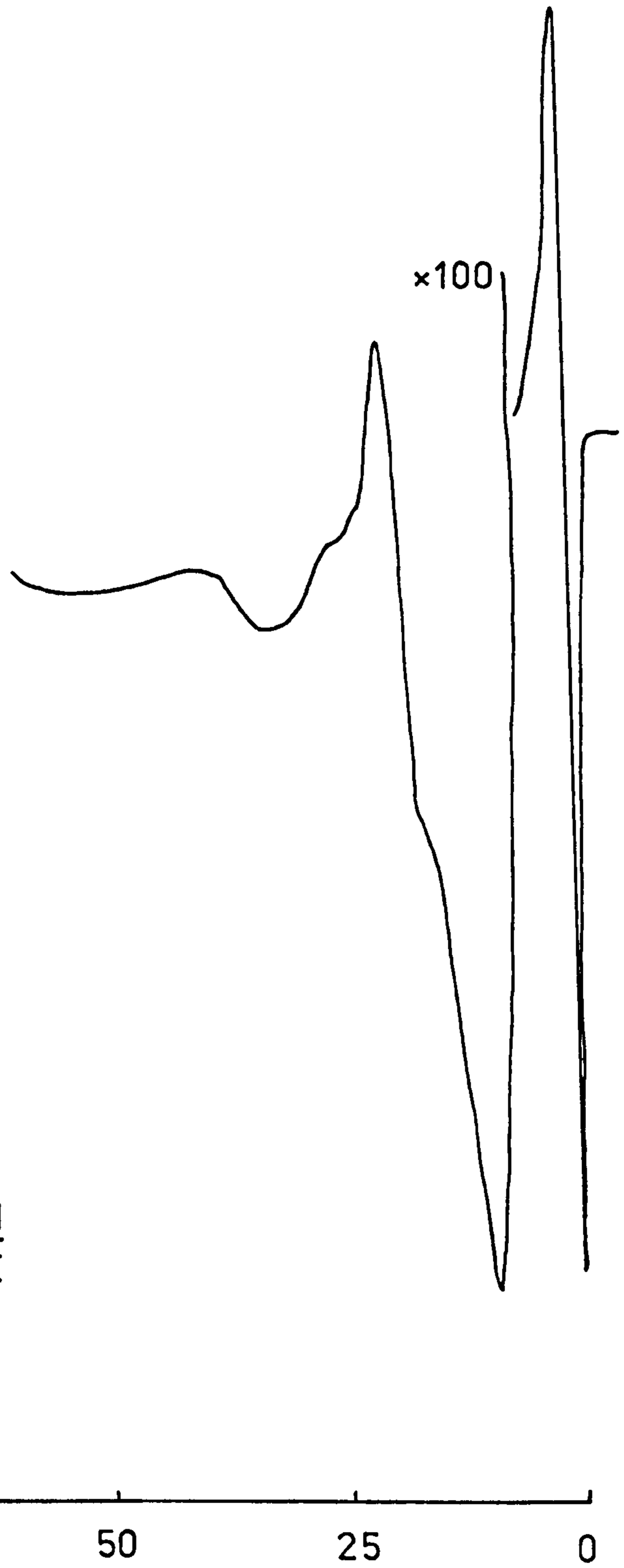

Figure 5.26. Electron energy-loss spectrum of GaP + 3 x 10^{10} LO_2, taken with glancing-incidence electron gun

TABLE 5.8

Loss energies from GaP with adsorbed oxygen ; glancing incidence electrons

Energy (eV)	Identification
8.8 - 9.1	interface plasmon
16.0 -16.6	bulk plasmon
23.4	Ga 3d core to conduction band
25.2	transition
32.8	2 bulk plasmons

is important to note that it is predicted that there is not a gradual shift in energy from $\hbar\omega_s$ to $\hbar\omega_i$ as the adsorbate coverage increases, but plasmons are found at the two frequencies, with the proportion at the shifted energy increasing (Stern and Fernell 1960). Taking our values 16.0 - 16.6 eV for $\hbar\omega_p$ and 8.8 - 9.1eV for $\hbar\omega_i$, we find $\epsilon \sim 2.1 - 2.6$. It is impossible to measure the dielectric constant of such a very thin "oxide" film, and indeed it is likely to fluctuate greatly near a surface (Feibelman 1975), but we note that similar shifts on oxidation have been observed on aluminium (Powell and Swan 1960). Of more relevance is the report (Mityagin et al. 1972) of the decrease of the surface plasmon energy in GaAs from 11 to 8eV as the surface was allowed to contaminate in poor vacuum. Similar losses at 8.2eV have been seen in dirty GaP under high-energy ion bombardment (Benazeth et al. 1972) and in optical reflectivity (Martin et al. 1973). A very strong loss at 8.2eV, dominating the electron-loss spectrum, was found during the adsorption of oxygen on n-type GaAs (110) but not on p-type material (Lüth and Russell 1974). The authors were unable to explain this new loss energy or the difference in behaviour between samples of different residual conductivities but a similar shift in the surface plasmon loss energy of silicon during oxidation has been described by a dielectric-scattering theory (Ibach and Rowe 1974a) which assumes a frequency-dependent dielectric constant and finds a coverage-dependent shift in plasmon energy. Although we recorded only one electron energy loss spectrum at an intermediate coverage, corresponding to about half the oxygen coverage of the curve of Figure 5.26, no evidence was found of a gradual shift in surface plasmon frequency; this interjacent curve shows just an admixture of the losses at $\sim$10.5eV and $\sim$9eV.

The designation of the 9eV loss as an interface plasmon enables us to identify the small Auger peak at 85eV and propose an alternative explanation for the shoulder at 99eV, with both being 9eV losses from the strong interatomic transitions at 94 and 108eV. These loss peaks grow approximately linearly with the interfacial peaks, and the designation $PL_{2,3}OL_{2,3}OL_{2,3}$-$\hbar\omega_i$ is possibly more satisfactory for the feature at 99eV than the $PL_{2,3}OL_1V$

transition given in Table 5.7. The $PL_{2,3}OL_{2,3}V$ loss is not seen, and the UPS results suggest a general weakening of GaP valence band structure with increasing oxygen exposure, so it may be reasonable to expect a decrease in features involving the GaP valence bands with a corresponding increase in those in which oxygen levels participate.

It has long been expected that plasmons can be produced in XPS in two different ways: "intrinsic" plasmons may be created during the photoexcitation process, while "extrinsic" plasmons are formed by electron collisions during the passage of the excited electron to the surface (see e.g., Langreth 1973). Similar mechanisms apply to surface plasmons and to plasmons produced in other electron spectroscopies. Obviously extrinsic plasmons should be created by any energetic electron passing through the medium: in our particular system, extrinsic interface plasmons should be produced by the 119.5eV electrons from $L_{2,3}VV$ transitions in phosphorus atoms immediately next to the interface but not involved in bonding to oxygen. Such a plasmon loss at $\sim$ 110.5eV is not observed in any of the spectra from GaP with adsorbed oxygen, even where the losses at 85eV and 99eV are large. We interpret this as evidence that the interface plasmons are intrinsic, that is that they are produced as part of the process of Auger electron excitation rather than during the actual emission. It is normally considered that intrinsic and extrinsic plasmons cannot be distinguished, partly because of interference between the two effects.

It is tempting to speculate further that, since the interface plasmons are not seen as losses from the $PL_{2,3}VV$ peak while they do appear as losses from the $PL_{2,3}OL_{2,3}OL_{2,3}$ and $PL_{2,3}OL_{1}OL_{2,3}$ peaks, the mechanism for production of these plasmons involves the higher electron levels and not the initial core hole.

In order to test further the hypothesis of oxygen-ion implantation by the electron beam, a small amount of deliberate oxygen ion bombardment was attempted. The chamber was let up to $\sim 8 \times 10^{-5}$ Torr and the ion gun run for one hour at 480V (the maximum voltage possible). The results are

given in Figure 5.27 , where it is shown that a difference was still observed between the central area, which still showed slightly darker on the raster scan (although now hardly discernible from the rest of the surface), and another area which had not previously been exposed to the electron beam. If this figure is compared with Figure 5.28, obtained after the massive oxygen exposure of $\sim 3 \times 10^{10}$ Langmuirs, it is seen that there are significant changes in the GaP peaks, but almost no change in the oxygen Auger peak height. In fact, for the central "dark" area, the oxygen Auger peak height is identical to Figure 5.27, but for the un-irradiated area, the oxygen Auger peak has increased by $\sim$ 30%. This suggests that the electron-beam implantation had already saturated the sample with oxygen, within the Auger electron probe depth: we estimate, again based on thework of Johannessen et al (1976), the penetration depth of 480eV oxygen ions to be about one monolayer. The changes in the GaP peaks are strange: the main Ga $M_3M_{45}M_{45}$ peak at 50eV is reduced in peak-to-peak magnitude by 30% and the $PL_{23}VV$ peak at 119eV is reduced to only 40% of its amplitude in Figure 5.28, but the peaks at 94 and 108eV, attributed to interatomic Auger transitions, do not change at all. However, the carbon Auger peak, which had remained at the low value shown in Figure 5.24 (b-e), is removed entirely by the oxygen ion bombardment, both from the central "dark" area and from the rest of the surface. It is possible that the carbon contamination, although apparently slight, was in fact modifying the adsorption characteristics. We add here that a small peak at 114.5eV appears in Figure 5.27. This is attributed to the $PL_{2,3}OL_{2,3}V$ transition, given in Table 5.7 but not observed in other experimental spectra.

It is interesting to observe that the Auger electron spectra of the sample exposed to $3 \times 10^{10} LO_2$, or oxygen-ion bombarded, do not resemble the spectrum obtained from a chemically oxidised sample. Figure 5.29 shows such a spectrum, from a slice which had not been etched in bromine/ methanol before loading into the system, but had otherwise followed the standard pumping, bakeout, Ar^+ ion bombardment and annealing stages. This spectrum now looks very similar to that obtained by Morgan and Van Velzen (1973) from an oxidised sample. The fact that much larger peaks

Figure 5.27. Auger electron spectra from GaP after oxygen ion bombardment. Central area had previously been exposed to electron beam, "fresh" area had not previously been exposed.

"fresh" area

×1

×31

central area

50

100

500

Figure 5.28 Auger electron spectra from GaP + $\sim$ 3×10^{10} LO_2 . Central area and "fresh" area as in Figure 5.27.

"fresh" area

×1

×31

central area

50

100

500

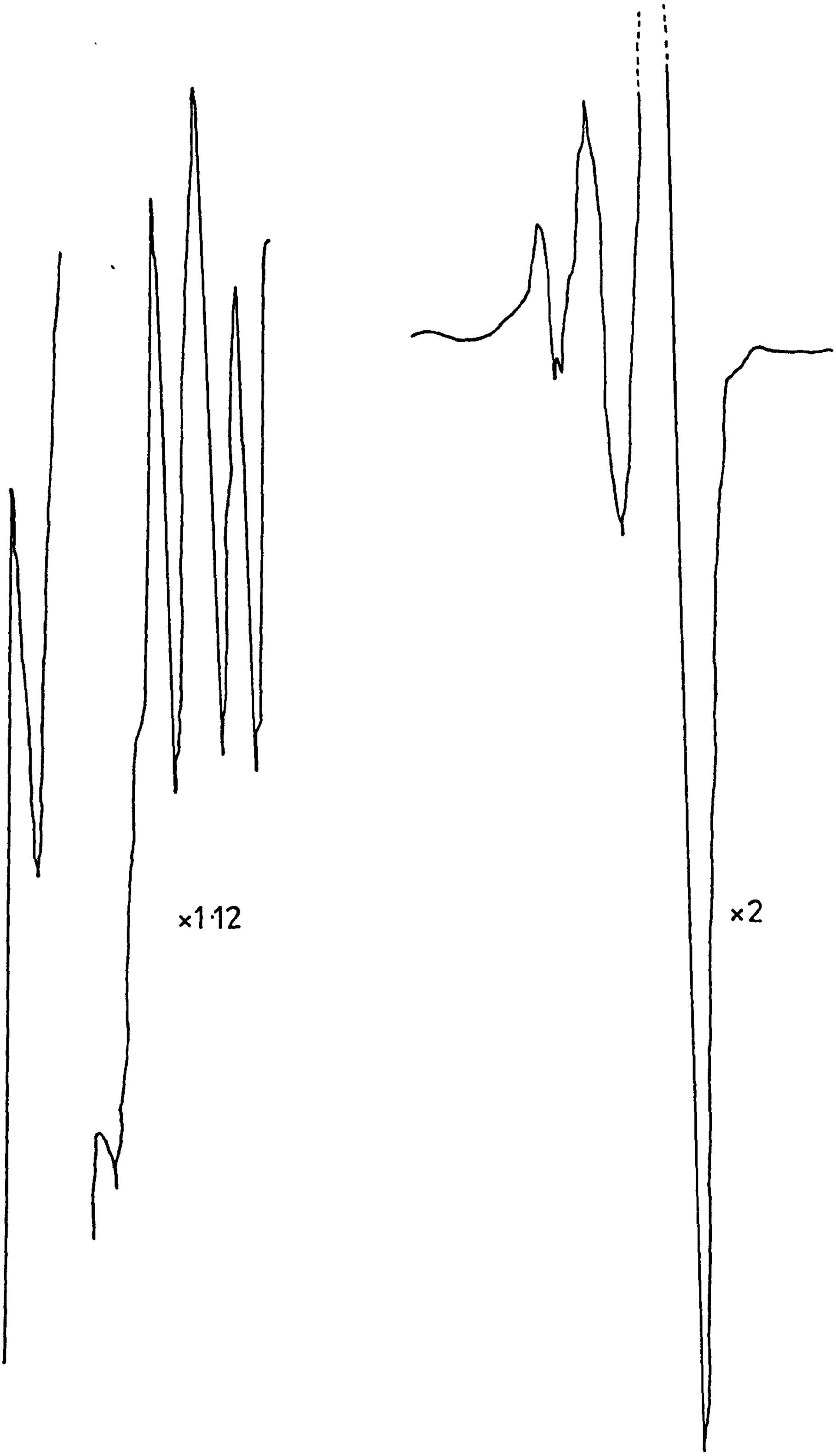

Figure 5.29 Auger electron spectrum from uncleaned GaP.

at 94 and 108eV (relative to the 119eV peak) can be achieved by chemical oxidation tends to confirm the designation of these peaks as arising from interatomic transitions. Since the spatial overlap of the initial hole wavefunction will be small, only those phosphorus atoms with nearest-neighbour oxygen atoms will contribute to these transitions: in the case of an adsorbed overlayer, this means just the phosphorus atoms on the surface. With chemical oxidation, diffusion of oxygen atoms into the bulk is likely, instead of simple adsorption, and so there may be many more oxygen and phosphorus atoms in close proximity within the Auger electron escape depth. If the estimate of one monolayer for the penetration depth of 480eV oxygen ions is approximately correct, it is not surprising that the oxygen ion bombardment did not increase the amplitude of the interatomic transitions.

The extinction of the interface plasmon loss features at 85 and 99eV can be similarly explained. If oxygen diffuses into the bulk, there is no interface between the bulk crystal and an adsorbed overlayer which may support plasmon creation.

The effects of heating the sample tend to confirm the explanations suggested here. A sample which had been exposed to $1 \times 10^{6} LO_2$, giving the Auger spectrum of Figure 5.25, was then heated to $\sim 500^{o}C$ for one hour in a vacuum of $\sim 1 \times 10^{-9}$ Torr. The LEED pattern became much more sharp, and the Auger spectrum reverted to a form very similar to that obtained for an exposure of $1 \times 10^{4} LO_2$: the oxygen Auger peak-to-peak height was reduced by a factor of 2.2 , the phosphorus (119.5eV) peak-to-peak height increased by a factor of 6.4, and all evidence of cross-transitions disappeared completely. The adsorbed oxygen presumably has not diffused into the crystal, which would have produced enhanced cross-transitions, but has been thermally desorbed.

Heating in oxygen produced no such dramatic effects. A sample which had been exposed to $2 \times 10^{5} LO_2$ was heated to $\sim 500^{o}C$ for thirty minutes in an atmosphere of 1×10^{-4} Torr O_2. The Auger electron spectrum changed very little: the oxygen Auger peak-to-peak height was increased by 20%, the

phosphorus decreased by 10%, and interatomic transitions became very slightly more prominent. The LEED pattern obtained, again at 94V, is given in Plate IX (d). No change in symmetry is observed. We note that the (111) face of GaP, which exhibits a (1 x 1) structure when clean, formed a $(\sqrt{3} \times \sqrt{3})30^{\circ}$-O pattern after exposure to $1.2 \times 10^{4} LO_2$ at $350^{\circ}C$ (Mityagin et al 1973b). The same authors have also reported a (111) GaP (2 x 2) pattern stabilised by residual carbon (Mityagin et al 1973a).

AES has been used to study the result of different techniques of oxidation of GaP (111) (Oda and Sugano 1974). Substrates exposed to an oxygen plasma, estimated to produce an oxide layer $\sim$ 400 Å thick, showed only peaks directly attributable to gallium transitions. Slices thermally oxidized, at a temperature of $900^{\circ}C$, had Auger electron spectra totally dominated by the P-O interatomic transitions at 94 and 108eV. Finally, they reacted GaP with a hot solution of hydrogen peroxide and formed an oxide layer about 1500 Å thick which AES apparently showed to produce only transitions due to gallium atoms; GaAs similarly treated gave an identical spectrum with all peaks shifted by $\sim$ 3.5eV. However, these authors are unable to assign some of the features: we suggest that, allowing for the 5.7eV shift between gallium metal and gallium oxide (Schön 1973), their four unidentified peaks can all be Ga-O interatomic transitions at 64eV ($GaM_{2,3}OL_1 OL_1$), 77eV ($GaM_{2,3}OL_1 OL_{2,3}$), 87eV ($GaM_{2,3}OL_{2,3}OL_{2,3}$) and 102eV ($GaM_{2,3}OL_{2,3}V$). These results lend weight to the hypothesis that small quantities of oxygen are adsorbed on the surface, bonding to phosphorus atoms. Further exposures, including heating in oxygen, produce diffusion of oxygen into the lattice, with bonding still being to phosphorus atoms. We find that chemical oxidation gave similar results, with large P-O interaction, but the Japanese workers obtained spectra showing no phosphorus at all, and bonding to gallium atoms. Thermal oxidation at high temperatures has been demonstrated to produce a major phase of $GaPO_4$ and a small amount of Ga_2O_3 (Rubenstein 1966). It may be that the solution of hot H_2O_2

dissolves any gallium phosphate leaving gallium oxides.

A semi-quantitative calibration of oxygen average versus oxygen exposure may be obtained from Figure 5.30. The oxygen Auger peak-to-peak height is here plotted against the exposure, on logarithmic scales. It is expected that there will be a break of slope on such a plot, corresponding to an initial saturation coverage; adsorption continues more slowly on top of an oxygen overlayer, assuming there is no diffusion of oxygen into the GaP lattice. It has been shown that the saturated adsorption phase consists of approximately 60% of a monolayer of oxygen atoms for GaP (110) (Van Velzen and Morgan 1973) and for GaAs (110) (Dorn et al 1974); a monolayer consists of two oxygen atoms for each surface molecule of GaP. All the exposures up to and including $1.3 \times 10^{6} LO_2$ fit reasonably well onto a straight line, and although there is only one point at a very large exposure, it is possible to draw the two limiting straight lines through this point, and thus determine that the exposure corresponding to the break of slope is between $1.3 \times 10^{6} LO_2$ and $2.5 \times 10^{6} LO_2$. Provided that this result is used with considerable caution, we may thus roughly convert our oxygen exposures to oxygen coverages. The overall result, that about 1 Torr.sec of oxygen is needed to produce a saturated adsorption coverage, is not surprising in view of our Auger electron spectra: careful exposure to small doses of oxygen (1×10^{4} L) made almost no difference, and only at exposures greater than $1 \times 10^{5} LO_2$ were significant changes recorded.

It is obvious that a plot of this form implies a continuously varying value of sticking coefficient s. We find $s \sim 8 \times 10^{-6}$ at 0.1 monolayer coverage, $s \sim 2 \times 10^{-6}$ at 0.6 monolayer and $s \sim 1 \times 10^{-10}$ at 0.8 monolayers. Such very low figures are typical of III-V semiconductors, although variations of one or two orders of magnitude between different determinations of s seem usual.

Figure 5.30. Oxygen Auger peak-to-peak height as a function of oxygen exposure.

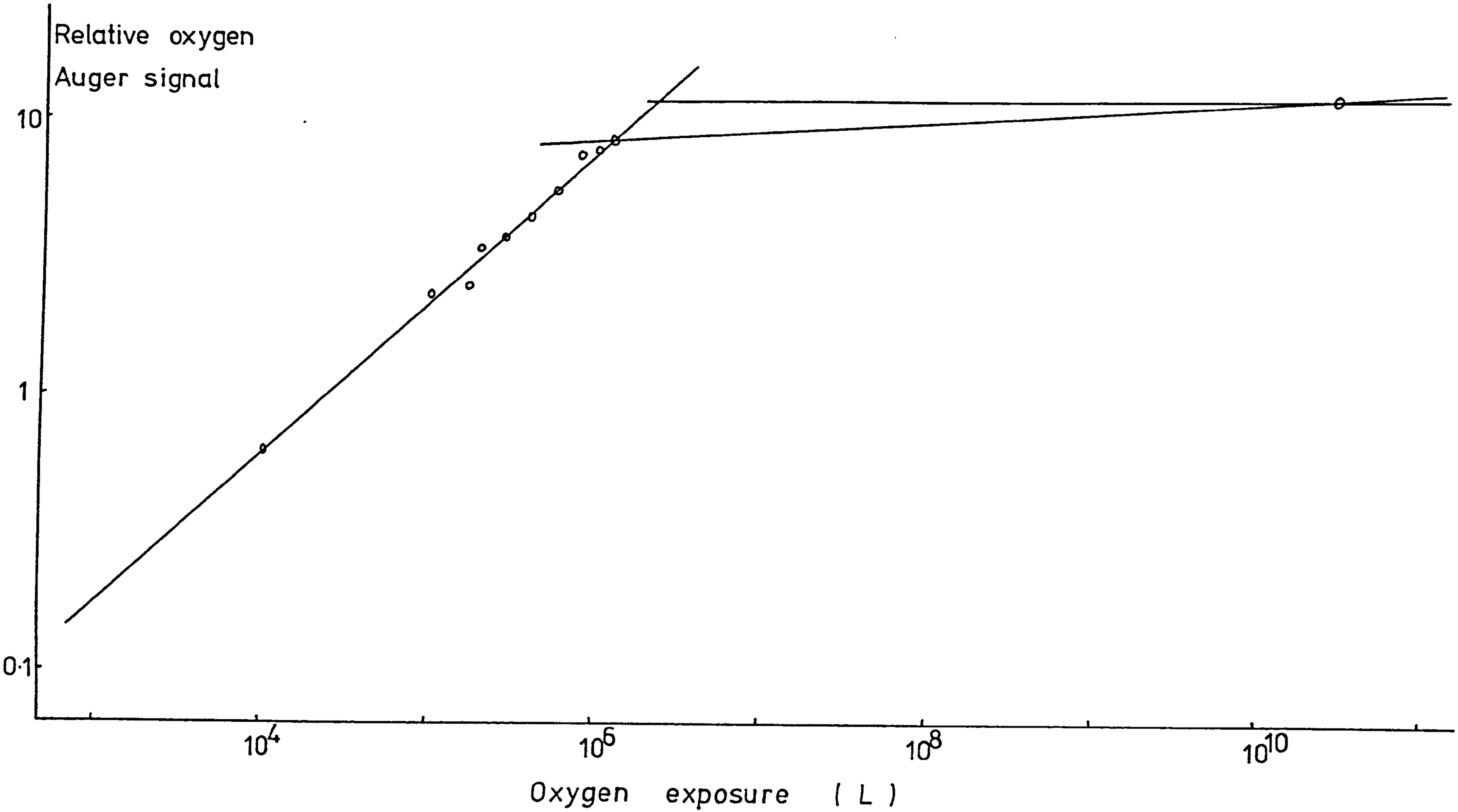
Relative oxygen
Auger signal
10
1
0·1
10^4
10^6
10^8
10^{10}
Oxygen exposure (L)

Figure 5.30.

5.8. XPS of GaP

Spectra of clean cleaved GaP, obtained with AlKα and MgKα exciting radiation, are given in Figures 5.31 and 5.32 respectively. The need to use two different photon energies in order to sort out which peaks are due to Auger electrons and which to core electrons is well illustrated here: with the MgKα X-rays at 1253.6eV peaks arising from the C 1s (284eV), P 2s (189eV) and Ga 3s (160eV) levels are all very close in kinetic energy to Auger transitions of Ga (970eV $\sim L_3M_{45}M_{23}$; 1065eV $\sim L_3M_{45}M_{45}$; 1094eV $\sim L_2M_{45}M_{45}$). Fortunately Al Kα radiation at 1486.6eV allows the separation of these overlapping lines. The core levels and Auger transitions observed are listed in Tables 5.9 and 5.10. Auger transitions are marked with an arrow (↓) in Figures 5.31 and 5.32 and core levels are indicated by a line (|).

The spot size of the X-ray source is rather large, and thus some electrons are excited from the aluminium sample holder: this is responsible for the O1s,C 1s and Al 2p lines observed.

Exposure to amounts of oxygen ranging from 2×10^3 L to 1×10^5 L made no noticeable difference to the X-ray photoelectron spectra, except for a large increase in the oxygen signal. This somewhat surprising result can presumably be explained by considerations of escape depth. At the electron kinetic energies measured here, the mean-free-path may well be as great as 20 or 30 Å, and thus sensitivity to reactions involving only the top monolayer or two of the surface will be low.

Interestingly, argon ion bombardment, removing an estimated 100 Å from the surface, changed the XPS curves appreciably. Figure 5.33 shows the portions of both AlKα and MgKα-excited spectra with the highest kinetic energy. Both the phosphorus core levels have intensities reduced by approximately a factor of two, whereas all the features associated with Ga (both Auger and core electrons) are unaffected. The P 2p level at 129eV now has two satellite peaks, at 135eV and 141eV. None of the possible explanations for this feature seems reasonable. Although there is undoubtedly

Figure 5.31. X-ray photoelectron spectrum of GaP obtained with Al K α radiation. Auger transitions are indicated by an arrow (↓) and core levels by a line (|).

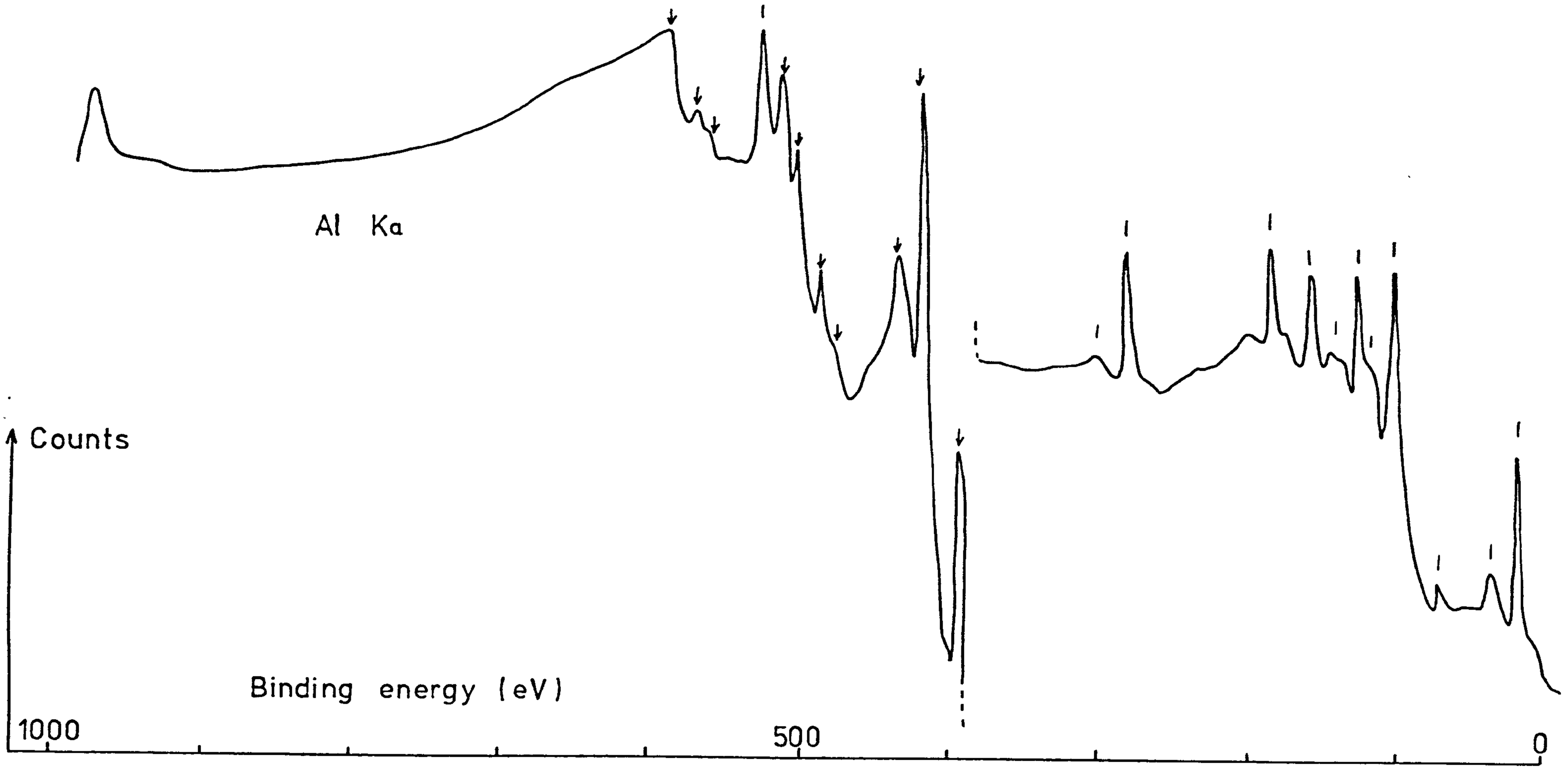
Al Ka
Counts
Binding energy (eV)
1000
500
0

Figure 5.32. X-ray photoelectron spectrum of GaP obtained with Mg Kα radiation

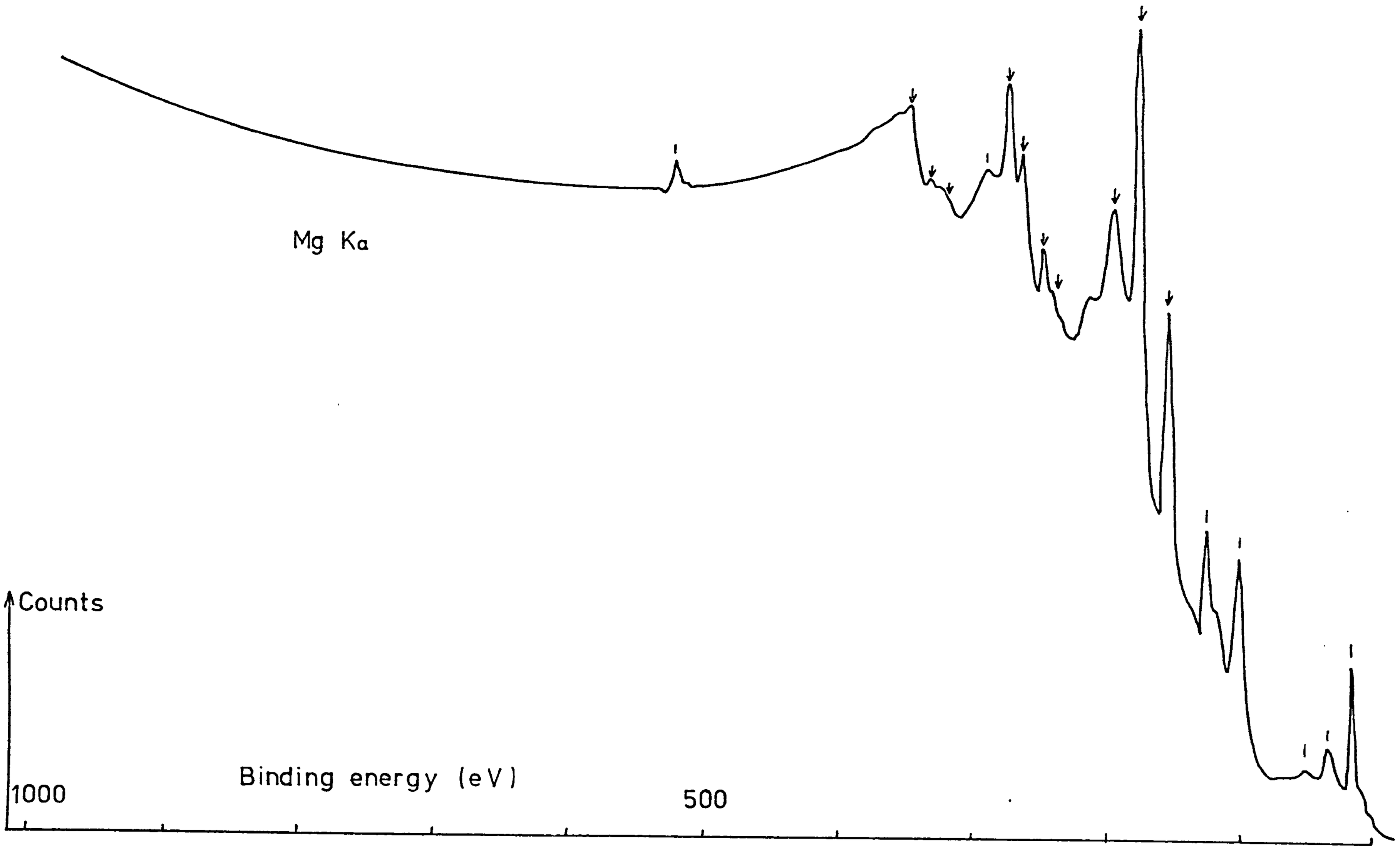
Mg Kα
Counts
1000
Binding energy (eV)
500

TABLE 5.9

Core levels observed with Al Kα- and Mg Kα- excited XPS from GaP(110)

Binding energy (eV)	Identification
534	O 1s
306	bulk plasmon loss from 288eV
288	C 1s
190	P 2s
163	Ga 3s
144	bulk plasmon loss from 129eV
129	P $2p_{\frac{1}{2},\frac{3}{2}}$
119	Al 2s
105	Ga $3p_{\frac{1}{2},\frac{3}{2}}$
71	Al $2p_{\frac{1}{2},\frac{3}{2}}$
53	2 x bulk plasmon loss from 19eV
36	bulk plasmon loss from 19eV
19	Ga $3d_{\frac{3}{2},\frac{5}{2}}$

TABLE 5.10

Auger transitions of Ga observed in XPS of Ga P

Kinetic energy (eV)	Transition
1094	$L_2M_{4,5}M_{4,5}$
1069	$L_3M_{4,5}M_{4,5}$
1052	bulk plasmon loss on 1069eV.
1007	$L_2M_{2,3}M_{4,5}$
997	$L_2M_{4,5}M_{2,3}$
981	$L_3M_{2,3}M_{4,5}$
971	$L_3M_{4,5}M_{2,3}$
924 / 915	$L_2M_{2,3}M_{2,3}$
896	$L_3M_{2,3}M_{2,3}$

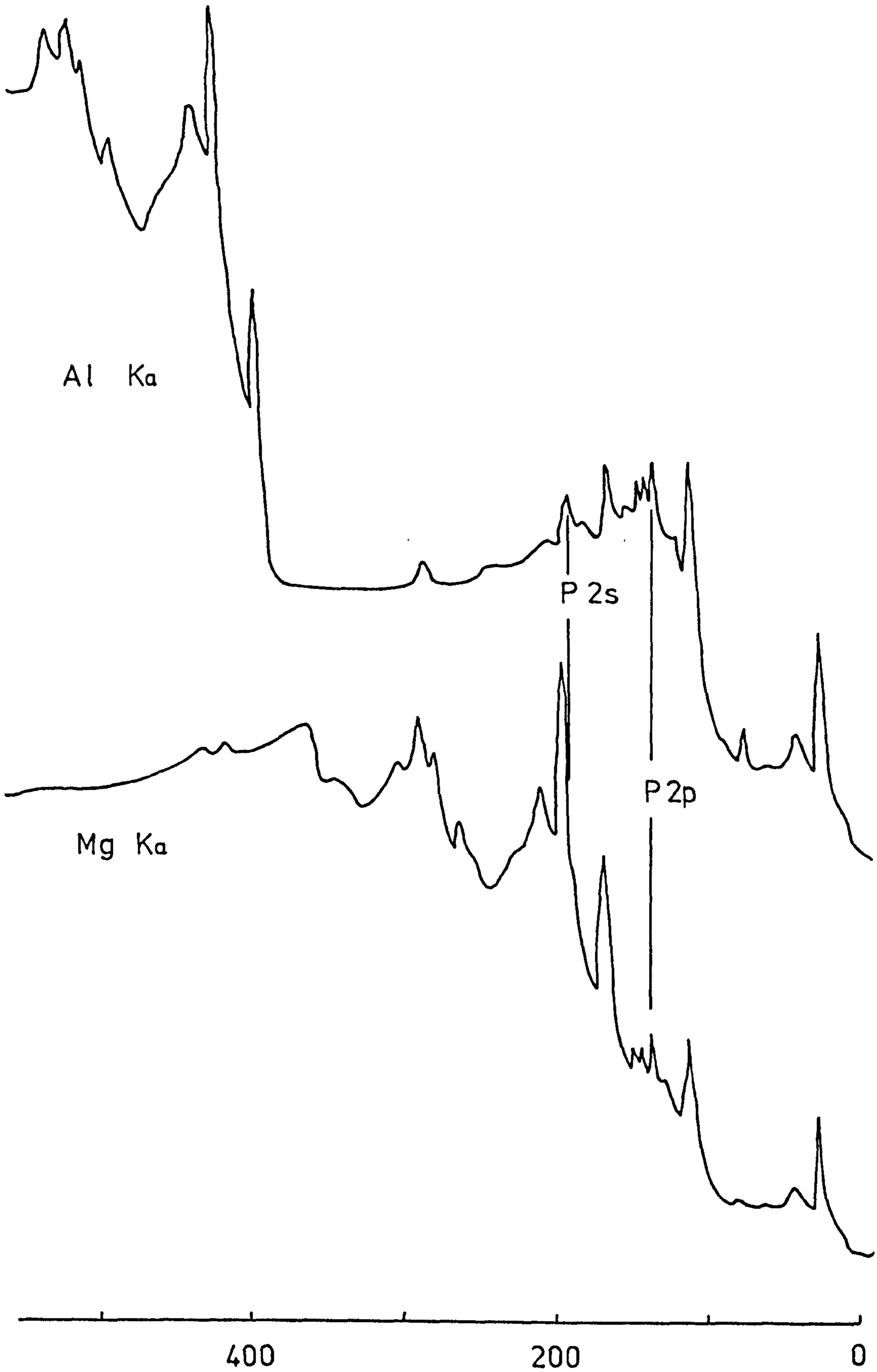

Figure 5.33. AlKα- and Mg Kα -excited spectra of GaP after argon ion bombardment.

some argon imbedded in the surface, it is barely detectable in the AlKα spectrum and not visible above background with MgKα excitation.

5.9. Summary

UPS electron energy distribution curves of GaP taken with photon energies between 7 and 12eV have been interpreted in terms of direct optical transitions with the aid of theoretical bulk band structures. More satisfactory agreement was found with the empirically adjusted OPW calculations of Herman et al than with the empirical pseudopotential results of Cohen and Bergstresser. Work at higher photon energies suffered problems with contamination. No effects attributable to filled surface states were seen in UPS but a band of empty surface states pins the surface Fermi level at about 0.5eV below its bulk value. This empty surface state was also observed with synchrotron radiation-excited partial-yield spectroscopy: the peak energy of the surface state band determined by this technique is $\sim$ 0.3eV lower than the pinning level but this simple single-electron energy may well be reduced below its true value by core-hole to surface state excitons. ELS shows a weak transition probably arising from a filled band of surface states. Adsorption of oxygen neither changes the Fermi level pinning nor removes any structure from the edc's; no core level shifts were detected with XPS. GaP (110) is very unreactive to oxygen, exposures around 1 Torr.sec being needed to change the UPS and AES spectra. Heavy oxidation raises the electron affinity by $\sim$ 1eV, increases the photoelectric yield by a factor of two to three, and produces Auger electron peaks attributed to interatomic transitions between phosphorus and oxygen. Electron energy loss spectra show the removal of the surface state feature and the replacement of the surface plasmon excitation at 10.5eV by an interface plasmon at $\sim$ 9eV. LEED indicated that oxygen adsorption produced no change in surface structure, the (1 x 1) pattern from clean GaP persisting with an increase in background intensity implying a disordered surface oxide. Considerable problems with using electron -stimulated spectroscopies to study the adsorption of oxygen were encountered and explained.

CHAPTER 6

INDIUM PHOSPHIDE

6.0. Introduction

The experiments performed on InP (110) had the same purpose as those on GaP : to further the understanding of the electronic structure of the clean surface and to examine the nature of the process of oxygen adsorption. The sole technique used in this investigation was UPS, both at low energies ($7 \leq h\nu \leq 12$eV) with a hydrogen discharge light source , and at higher energies ($16 \leq h\nu \leq 32$ eV) using synchrotron radiation.

In view of the increased use of InP as a microwave emitter, it is also of considerable interest to examine in some detail the bulk conduction band structure. The levels actually involved in the oscillation mechanism are below the vacuum level, and inaccessible in conventional UPS, but determination of the energies of higher conduction bands may help in refinement of theoretical band structures.

A summary of the experimental results is presented at the end of the Chapter, with some interim conclusions in the course of the Chapter but the main conclusions postponed to Chapter 8.

6.1. UPS of clean InP

Hydrogen-lamp edc's ($7.4 \leq h\nu \leq 11.3$eV) are presented in Figure 6.1. Some raw data are given in Figure 6.2, indicating that the quality of the data is as good as for GaP. The photoelectric yield of InP is plotted in Figure 6.3. All the remarks made for GaP (Chapter 5.1) on plotting, reflectivity, normalisation and reproducibility apply equally to InP. The data of Figure 6.1 are reduced to the structure plot of Figure 6.4. Many more features are marked than were visible in GaP, particularly at the higher photon energies. The reason for this is illustrated by Figure 6.2 : some peaks are much broader than in GaP, and often tend to be resoluble into a peak and an associated shoulder.

Figure 6.1. UPS electron energy distribution curves from clean InP (110) in the photon energy range 7.4 to 11.3 eV

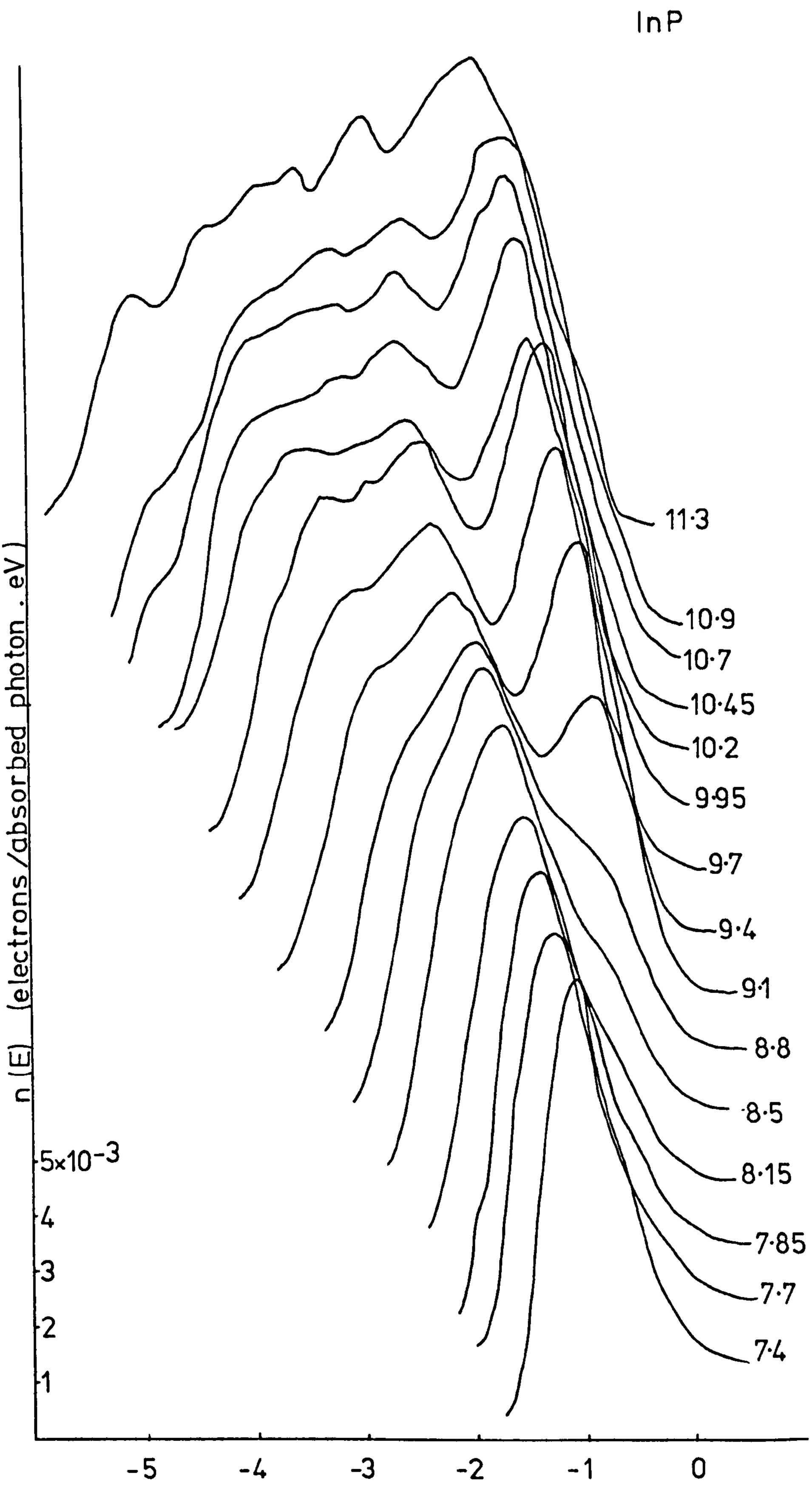
InP
11·3
10·9
10·7
10·45
10·2
9·95
9·7
9·4
9·1
8·8
8·5
8·15
7·85
7·7
7·4
n (E) (electrons / absorbed photon . eV)
5×10⁻³
4
3
2
1
-5
-4
-3
-2
-1
0
Initial-state energy (eV)

Figure 6.2. Some raw edc's for InP.

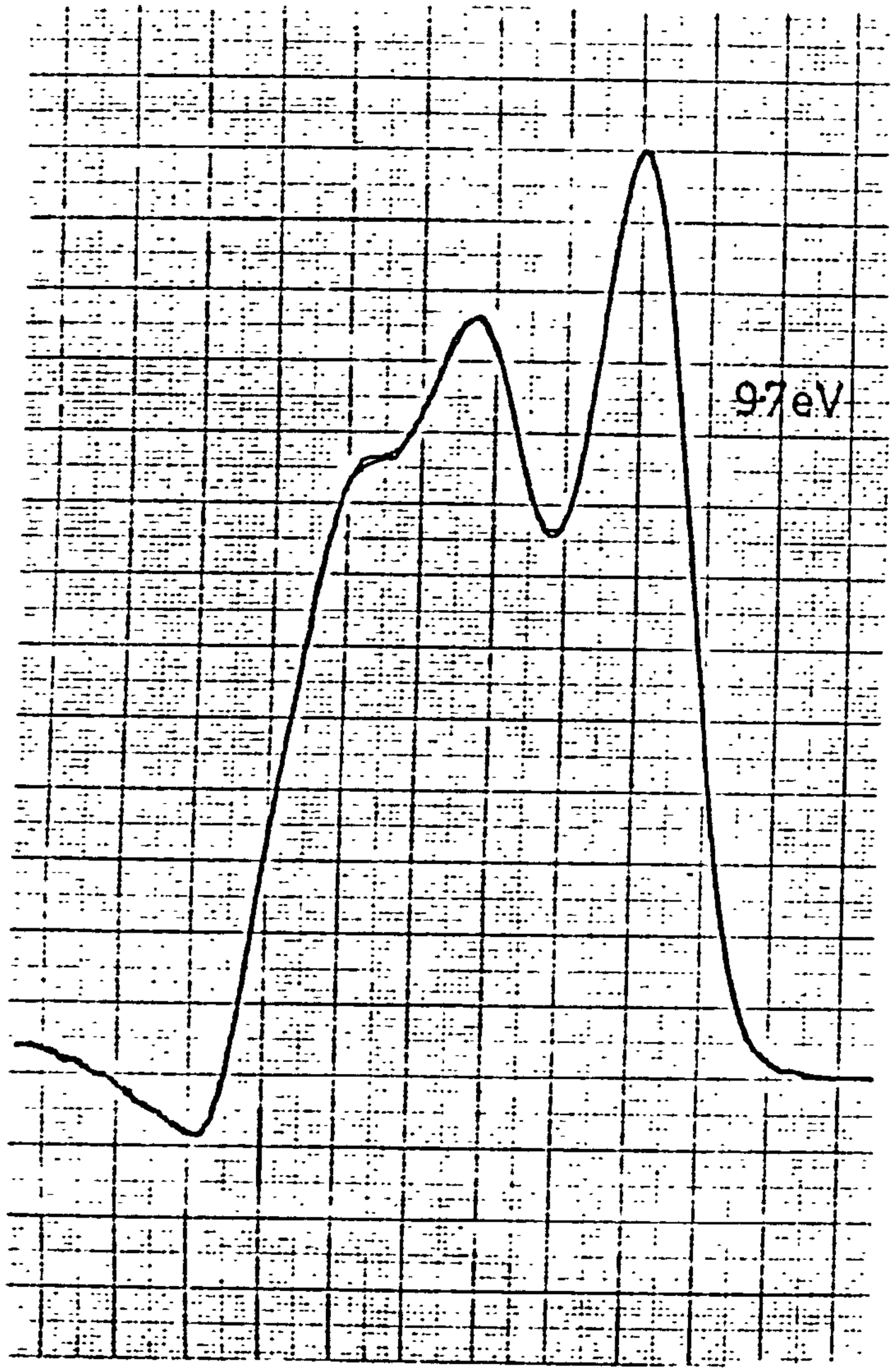

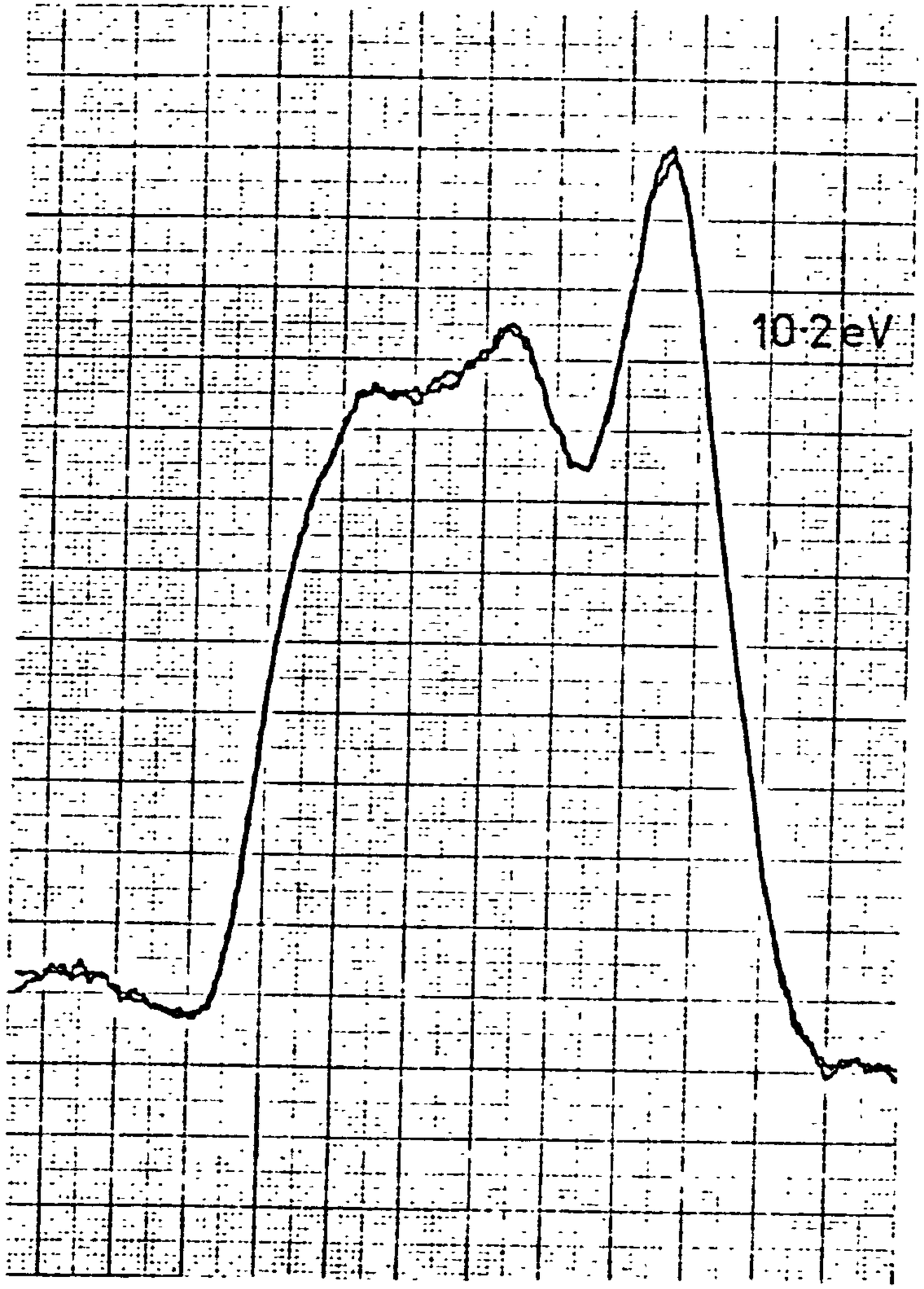

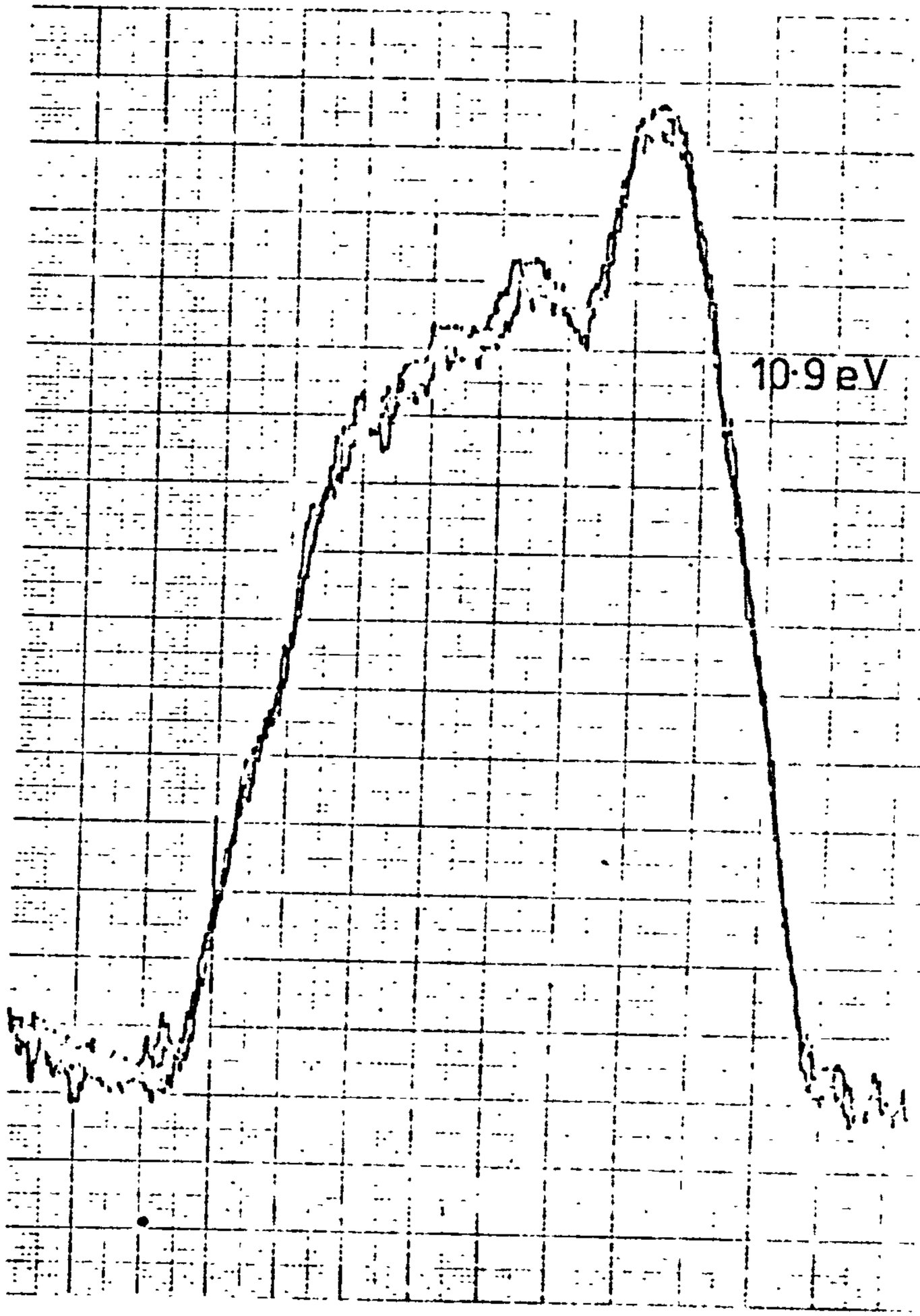

InP

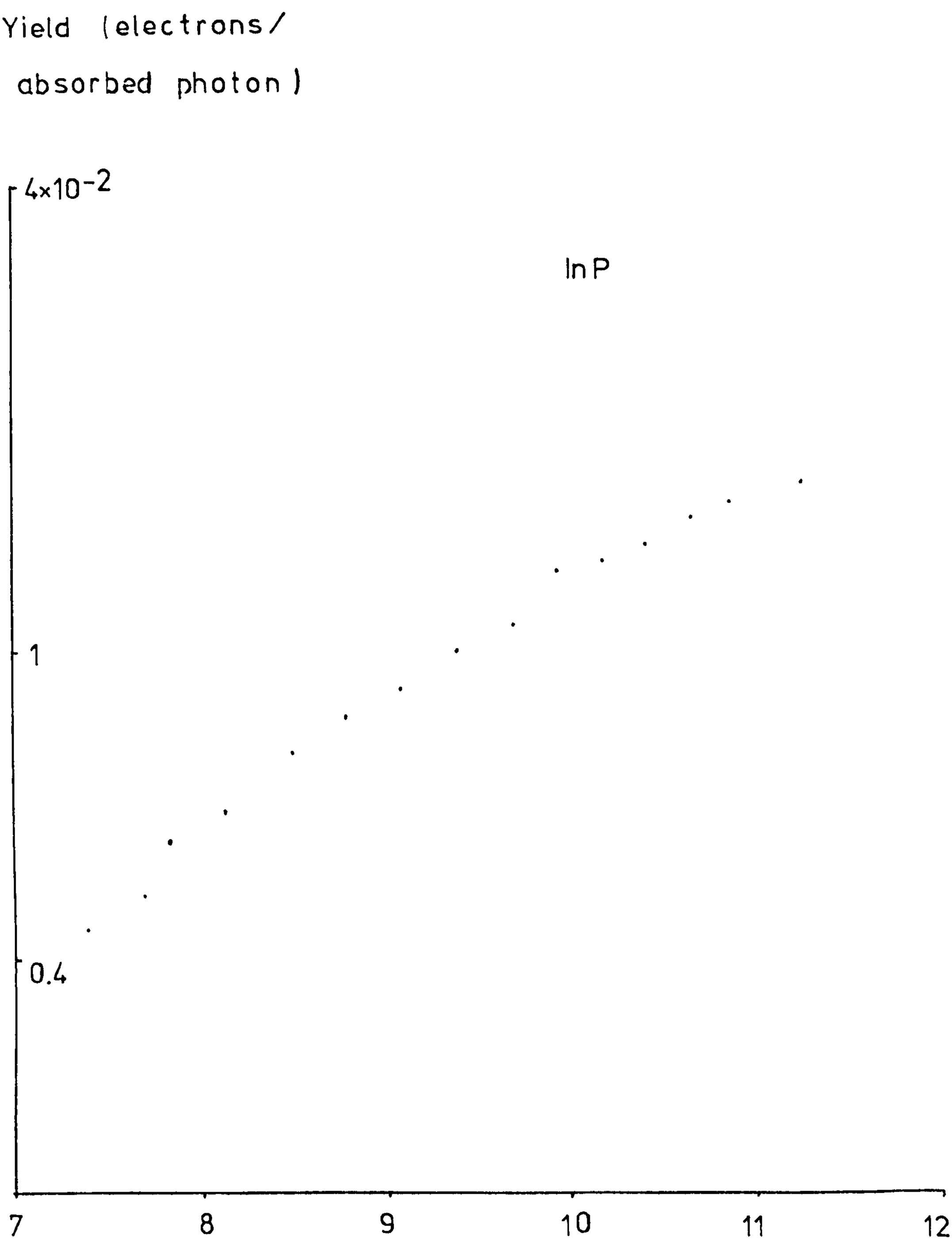

Figure 6.3. Yield versus photon energy for InP

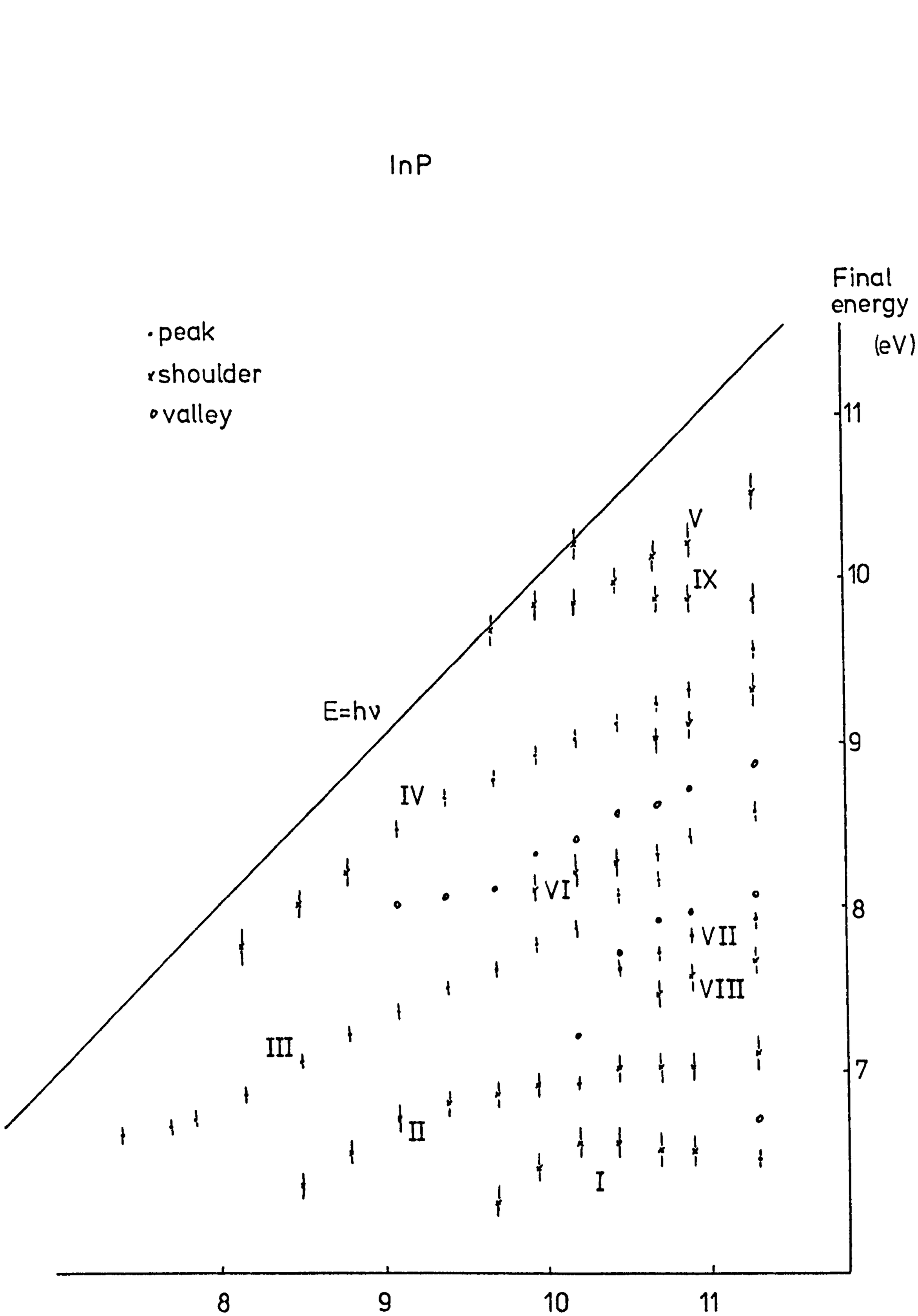

Figure 6.4. Structure plot for InP, from Figure 6.1.

The curve of yield against photon energy up to 11.3eV is almost featureless (Figure 6.3). Data very recently given by Chye et al. (1976) show a similar form, with all values about 20% lower than ours, and a broad maximum around 10eV. As discussed in Chapter 4.1, deterioration of the transmission of LiF windows is most pronounced at higher energies and so the calibration of photon flux, necessary for calculation of the absolute yield, becomes less reliable towards 11eV. It is not possible to state which of these two sets of data is more likely to be correct.

From Figure 6.4 we can immediately see that there are conduction band Γ points at $\sim$ 9.7 and $\sim$ 10.2eV and that there is no structure corresponding to flat valence bands or parallel initial and final bands. The features labelled I and II lie roughly horizontal for most of the photon energy range in which they are visible. Structure II is attributed to transitions to a conduction band with zero dispersion and will be considered later in more detail. Feature I probably arises from scattered electrons. For identification of the other features following more complex E- $h\nu$ lines, a theoretical bulk band structure must be consulted.

Interpretation of Figure 6.4 in terms of the theoretical bulk band structure of InP raises the same problems as were encountered with GaP. The only published band structure which extends to conduction band energies greater than $\sim$ 7eV is the extension (including $\underline{k}.\underline{p}$ interpolation) of the empirical pseudopotential results of Cohen and Bergstresser (1966) by Neumann et al (1975) which is shown in Figure 6.5. The upper Γ points from this calculation are almost 2eV lower than the values we find, Γ_1^c being given as $\sim$ 7.9eV and Γ_{12}^c as $\sim$ 8.4 eV. We note here the comment of Chye et al (1976) that emission from the InP valence band maximum was observed only for $h\nu = 10.2 \pm 0.5$eV, in agreement with our data. A tabulation of critical-point energies from an empirically adjusted OPW calculation (Herman et al 1969) gives $\Gamma_1^c = 9.5$eV and $\Gamma_{12}^c = 10.2$eV, very close to our observed values. Some of the levels near the bandgap obtained in this

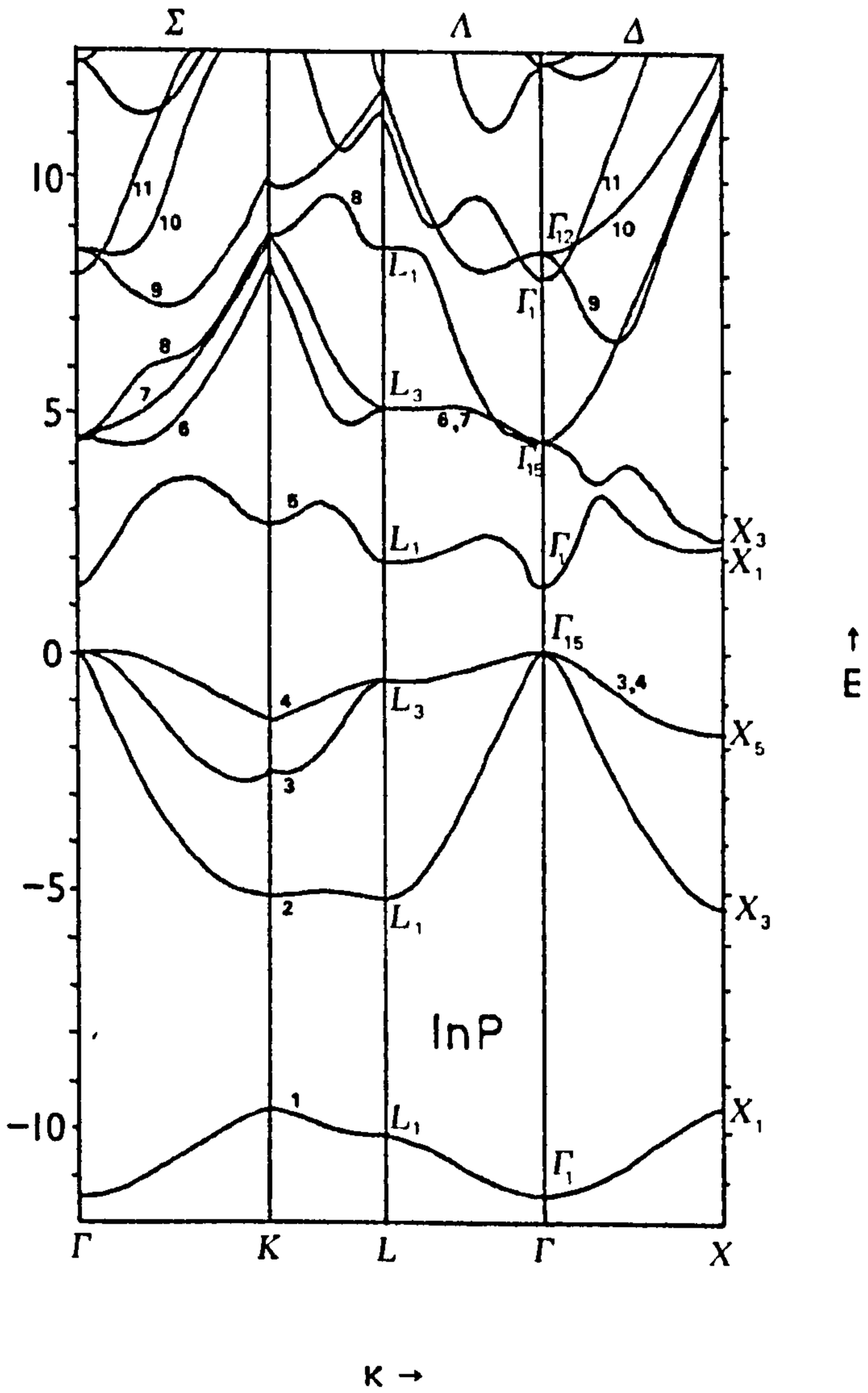

Figure 6.5. E-$\underline{k}$ diagram for InP, taken from Neumann et al (1975)

calculation were adjusted slightly in a later publication (James et al 1970) so it is possible that the small change in parameters will affect the higher conduction band also. Unfortunately these revised data are not available.

A structure plot was constructed from the band structure of Neumann et al. with the two upper Γ points and all the bands derived from them linearly shifted to fit our experimental values. This approach worked well for GaP, but the plot obtained for InP bears little resemblance to the experimental plot of Figure 6.4. Nevertheless, this theoretical structure plot is shown, with the experimental points superimposed, in Figure 6.6. to aid discussion of the assignment of critical points more in keeping with our data. It was noticeable that the set of E - $h\nu$ lines due to transitions between bands 2 and 10, going away from Γ_1^c, produced a much better fit to the series of weak shoulders (V) when Γ_1^c was lowered by about 0.1eV (to $\sim$ 9.6eV), and this has been done in Figure 6.6 : no edc was taken between $h\nu$ = 9.4eV, where the high-energy shoulder is not visible, and $h\nu$ = 9.7 eV, where it is seen. Note that these shoulders grow in strength with increasing photon energy, as follows from the arguments in Chapter 5.1 about the weakness of the contributions from the volume of the Brillouin zone near Γ : increasing $h\nu$ here corresponds to probing regions of $\underline{k}$ -space nearer to the zone edges. Although there is no obvious similarity between theory and experiment in Figure 6.6 , it must be pointed out that nowhere are experimental points more than $\sim$ 1eV apart, and thus an appearance of disagreement may be gained with bands wrong by only $\sim$ 0.5eV; in view of the computational complexity, accord within such limits might be felt satisfactory. However, several of the observed and calculated E-$h\nu$ lines diverge greatly, and we should assess alternative assignments. To assist this, critical-point energies abstracted from several calculations are tabulated in Table 6.1.

A complicating factor with some levels is spin-orbit interaction. This was not a difficulty with GaP, but the heavier cation of InP produces

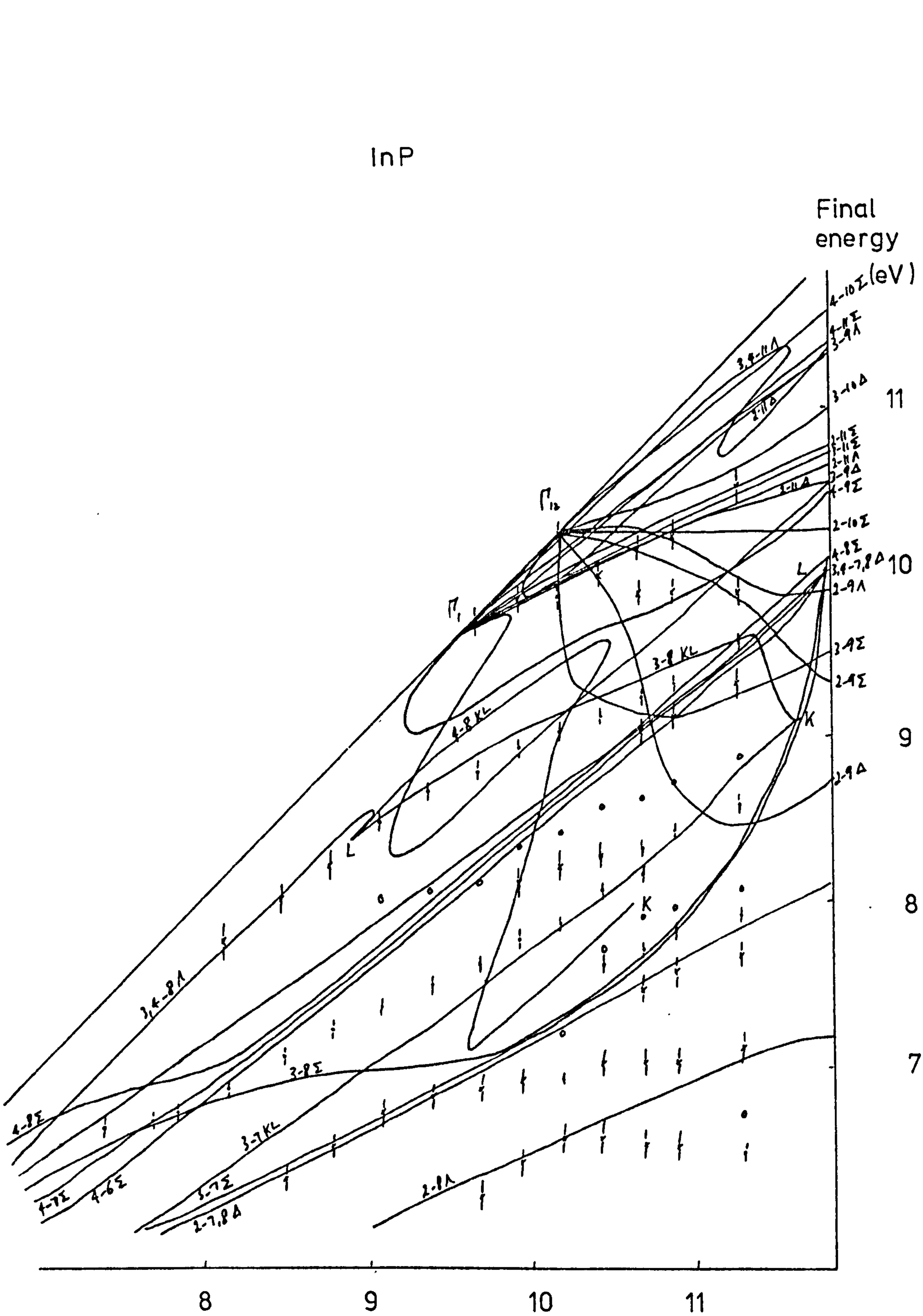

Figure 6.6. Theoretical structure plot for InP, taken from Figure 6.5, with experimental points from Figure 6.4 superimposed.

splittings > 0.2eV in Γ_{15}^{c} and Γ_{1}^{v} for instance. The single point group notation, not now strictly applicable, is retained for ease of comparison with GaP and with calculations which neglect the splitting. Many calculations ignore this effect, and we shall attempt to use the weighted mean values where possible. We point out, however, that spin-orbit splitting may well account for the observed combinations of peak and shoulder mentioned earlier . For example, structure IV (Figure 6.4) which analogy with GaP would attribute mainly to transitions from band 4 to bands 7 and 8 along Σ and Δ, is accompanied at the highest photon energies by a shoulder separated from the peak by $\sim$ 0.2eV, which is almost exactly equal to the theoretical splitting of bands 7 and 8 along Σ. Peaks VII and shoulders VIII, with the same splitting, may have a similar explanation.

Although the calculation of Neumann et al. yields disparate results from our experimental values, we can hope to proceed from this theory to a satisfactory explanation of the data by empirically adjusting the critical point energies using as a starting point the information in Table 6.1. Since the band structures of all III-V compounds are structurally similar, differing only in detail, comparison with the results from GaP will also help, particularly in selecting those regions of $\underline{k}$-space which contribute disproportionately to the edc's.

The feature labelled II is probably due mainly to transitions from band 2 to band 8 along Σ. The extensive horizontal portion at a final energy of 6.9 - 7.0eV corresponds to the flat part of band 8, given by Neumann et al. at $\sim$ 6.1eV; the incomplete empirically adjusted OPW calculation presented by James et al (1970) shows this feature at about 7 eV. This particular band joins the lower Γ_{15}^{c} and X_{5}^{c}, both being points about whose energy there is little agreement: for example, the calculated energy difference varies from 4.5eV (Herman et al 1969) to 7.1eV (Neumann et al. 1975). Of all the symmetry points within 5eV of the band edges Γ_{15}^{c} is the most sensitive to small changes in pseudopotential form factors (Cohen and Bergstresser 1966).

By analogy with GaP we expect line III to be due to Σ transitions from band 3 to bands 7 and 8, and feature IV similarly from the coincidence of transitions from the degenerate bands 3 and 4 to 7 and 8 along Δ and from band 4 to bands 7 and 8 along Σ. Since all these transitions involve E -$\underline{k}$ lines joining Γ_{15}^{v} to X_5^{v} in the valence bands and Γ_{15}^{c} to X_5^{c} in the conduction bands, they are especially sensitive to the energies of just these few points. As mentioned in the previous paragraph, there is no theoretical agreement over the energies of Γ_{15}^{c} and X_5^{c}: Table 6.1 shows better accord over X_5^{v}, which is said (Cohen and Bergstresser 1966) to be the level least affected by small changes in pseudopotential form factors. Whilst our results are entirely consistent with a value for X_5^{v} around -1.8 to -2.0eV, it is difficult to fit our transitions III and IV satisfactorily unless bands 3 and 4 are more nearly flat than the calculations indicate. Feature IV first appears as a series of shoulders only $\sim$ 0.5eV below the E = hν line and thus the initial states must be within 0.5eV of the valence band maximum. This portion of the structure plot could to some extent be explained by the distorting effect of the large background in the edc's, which tends to increase the apparent energy of a shoulder, but IV develops into a distinct peak by hν = 9.1eV with a final energy still only 0.65eV below E = hν. It is possible that this feature derives from abother set of transitions involving a much flatter valence band, for instance the degenerate bands 3 and 4 along Λ. There is, however, no suitable final state for this transition to give an E - hν line similar to our line IV. Furthermore, a direction with bands 3 and 4 not degenerate is needed in order to explain features III and IV, both of which are higher in energy by up to 0.5eV than the theoretical structure plots. There remains the chance that there is a volume of $\underline{k}$-space having high density of states which is not represented by the major symmetry lines, but the most probable conclusion from our data is that the top valence band is almost flat along Σ and Δ for about two-thirds of the distance to the zone edge, with an increase in dispersion near to X. The energy of X_5^{c} cannot be positively identified since the splitting X_5^{c} - X_5^{v} is slightly beyond our

available photon energy range, difficulties with the decrease in transmission of the LiF window having prevented the use of $h\nu > 11.3$eV in the series of experiments on InP. The convergence of lines III, IV and IX points to a value of final energy for X_5^c around 9.8eV at a photon energy of 11.7eV. This would indicate $X_5^v \sim -1.9$eV, close to the mean of the theoretical values. Features III and IV then have similar explanations to their counterparts in GaP, namely transitions from bands 3 and 4 respectively to bands 7 and 8 along Σ, with some contribution to IV from 3,4 - 7,8 Δ transitions. Since X_5^c and Γ_1^c are so similar in energy, band 9 joining these points may be fairly flat and thus a probable identification for feature IX is a set of transitions to this final band.

It is difficult to identify the remaining features VI, VII and VIII, because they appear for such limited energy ranges. The series of shoulders labelled VI may well be due to transitions along the line joining K and L between bands 3 and 8. The portion of band 3 around K is known to have a high density of states and it seems probable that the same is true of the maximum in band 8 along this direction. This would explain why feature VI is seen only in a narrow energy range. Note that for this explanation to hold we must lower this local maximum in band 8 by about 1.3eV from the value given by Neumann et al; following the previous practice of linearly shifting the band will lower L_1^c to 7.1eV almost exactly equal to the adjusted OPW value (Table 6.1). The fact that bands 3 and 8 are both fairly flat between K and L suggests that this may hold over a large part of the hexagonal face of the Brillouin zone, thus increasing the possibility of such transitions. Lines VII and VIII may be the spin-split contributions from 2 - 7, 8 Δ transitions, although it is not clear why such a feature is not seen at lower photon energies since none of the bands involved has any singularity. A more plausible interpretation involves transitions from band 3 to bands 6 and 7, again along the KL direction. Unfortunately the lack of any sufficiently accurate band structure hampers the identification of these weaker features.

TABLE 6.1

THEORETICAL ENERGY LEVELS IN InP

Γ_{15}^{c}	11.9	11.5	12.3	
Γ_{12}^{c}	10.3	10.2	8.4	
Γ_{1}^{c}	9.6	9.5	7.9	
Γ_{15}^{c}	5.3	5.2	4.5	4.92 4.64
Γ_{1}^{c}	1.4	1.4	1.4	1.50
Γ_{15}^{v}	0.0	0.0	0.0	0.00 -0.21
Γ_{1}^{v}	-11.1	-11.1	-11.4	-11.42
X_{5}^{c}	9.8	10.4	11.6	
X_{3}^{c}	3.2	3.1	2.5	2.97
X_{1}^{c}	2.3	2.0	2.3	2.44
X_{5}^{v}	-1.7	-1.8	-1.7	-2.06 -2.09
X_{3}^{v}	-4.5	-4.5	-5.3	-6.01
X_{1}^{v}	-9.7	-9.5	-9.6	-8.91
L_{1}^{c}	7.7	7.2	8.4	
L_{3}^{c}	5.8	5.6	5.2	5.70 5.58
L_{1}^{c}	2.4	2.4	2.0	2.19
L_{3}^{v}	-0.6	-0.6	-0.6	-0.94 -1.09
L_{1}^{v}	-4.6	-4.7	-5.1	-5.84
L_{1}^{v}	-10.1	-10.0	-10.0	-9.67
	*	*	†	‡

* empirically adjusted OPW calculations based on two different values of X_{1}^{c} (Herman et al 1969)

† empirical pseudopotential (Neumann et al 1975)

‡ non-local pseudopotential (Chelikowsky and Cohen 1976b)

Some UPS electron energy distribution data for clean InP in this photon energy range have very recently been published (Chye et al.1976) but the interpretation is limited to the identification of a Γ point and the observation that "all the structures in the edc's appear to arise from bulk direct transitions since the initial and final state energies change with photon energy." The edc's presented closely resemble those of Figure 6.1 but apparently have worse resolution. Some edc's with $3.0 \leq h\nu \leq 6.2$ eV for roughly cleaved InP covered with caesium have been presented with little explanation (Fischer 1966) and the photoelectric yield interpreted as showing some features similar to reflectivity spectra. These results were later re-interpreted in terms of bulk imperfections (Fischer 1968). This early work was undoubtedly handicapped by the rather poor quality of the single crystals then available. A structure plot constructed from edc's from caesiated InP with photon energies up to 6eV has been used by James et al.(1970)to assist the production of an OPW calculation of the bands near the bulk bandgap.

6.2. UPS of InP with $16 \leq h\nu \leq 32$ eV.

A family of edc's measured with synchrotron radiation in the photon energy range 16 to 32eV is given in Figure 6.7. These higher photon energy spectra exhibit completely different characteristics from the low energy data of Figure 6.1. Although there is considerable modulation of the intensity of the spectral features, there is almost no change in the position of peaks as the photon energy is varied. To illustrate this, the positions of prominent features are plotted against photon energy in Figure 6.8. Similar work on germanium also showed that no structure moves by more than 0.5 eV in the photon energy range $16 \leq h\nu \leq 23$eV (Grobman et al 1974,1975). In one sense, the X-ray limit has already been reached at these relatively low photon energies; the edc's do not resemble those obtained in XPS,but the spectra reflect mainly initial state and transition probability effects.

Figure 6.7 Edc's for clean InP in the photon energy range 16 to 32 eV.

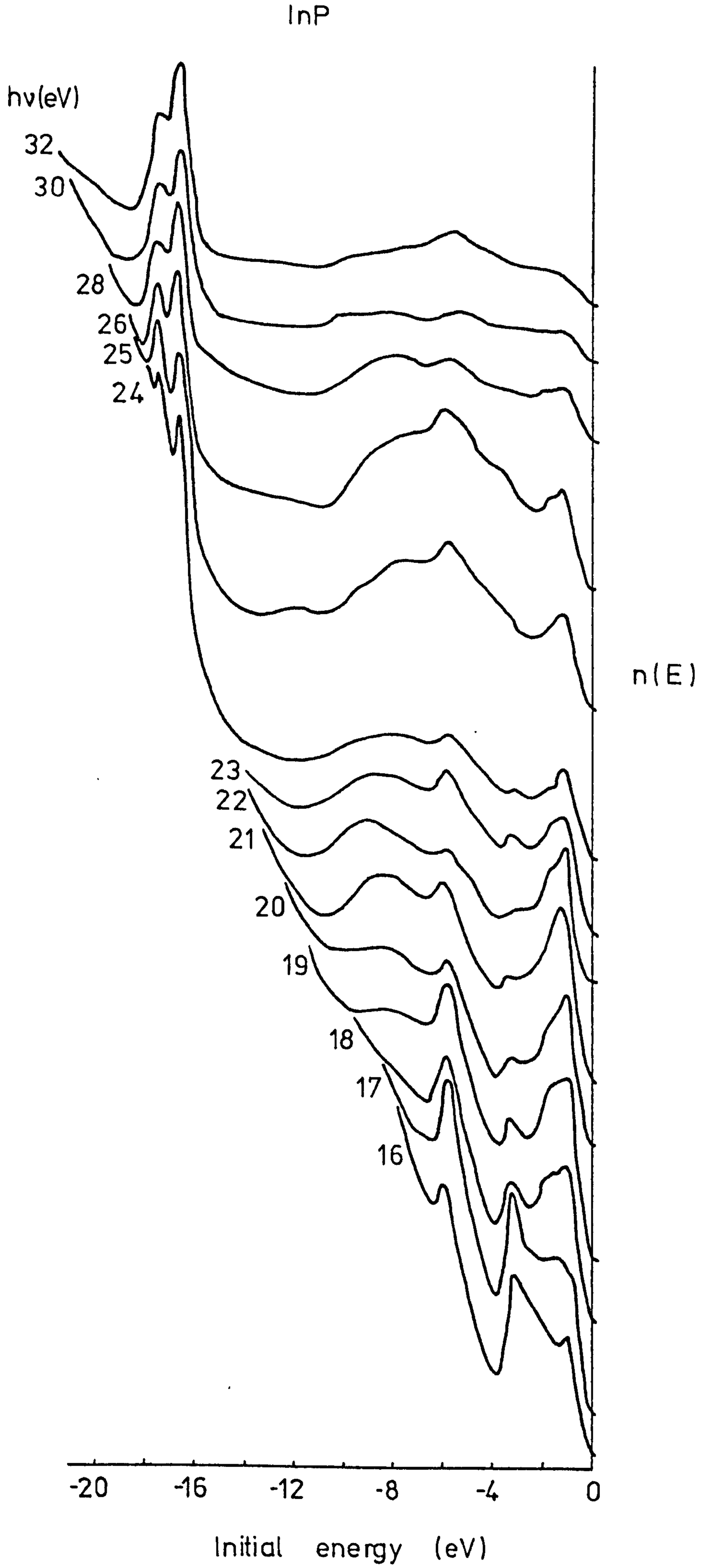
InP
hν(eV)
32
30
28
26
25
24
23
22
21
20
19
18
17
16
n(E)
-20
-16
-12
-8
-4
0
Initial energy (eV)

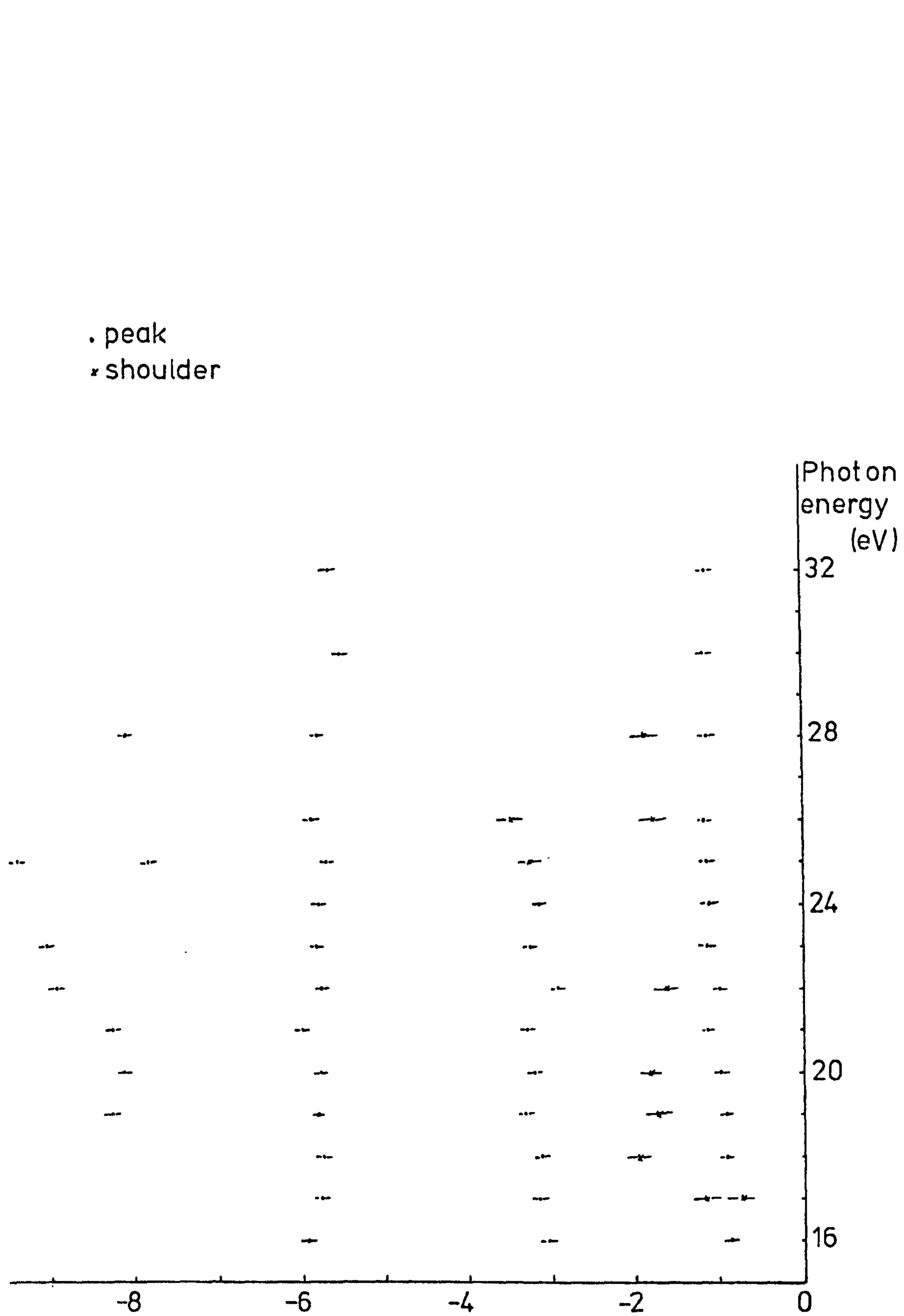

Figure 6.8. Structure plot for InP, from Figure 6.7.

The apparent availability of final states over most of $\underline{k}$-space, the inapplicability of current band structure techniques to calculation of states far above the vacuum level and the increasing surface sensitivity at higher electron energy all make it unprofitable to attempt to apply a direct-transition analysis to these data. Instead, by comparison with calculations of the valence band density of states we can hope to extract values of the critical point energies in the valence bands.

This approach has been used before for InP, both for XPS (Vesely and Kingston 1973, Ley et al 1974) and UPS (Shevchik et al 1974) but several aspects of these investigations appear unsatisfactory. The crystals of Vesely and Kingston were argon ion bombarded -but not annealed- and measured at a pressure around 2×10^{-6} Torr, with a considerable fraction of a monolayer of carbon and oxygen contamination visible. They used un-monochromated Mg Kα X-rays, and emission from the In 4d levels induced by the Mg K$\alpha_{3,4}$ satellite lines completely overwhelms the valence band spectrum: this measurement therefore relies very heavily on the method of deconvolution of this structure. From the results given in Chapter 5.8, it seems extremely unlikely that stoichiometric surfaces can be generated solely by bombardment. In the work of Ley et al. crystals were cleaved in an inert atmosphere before insertion into the spectrometer operating at a pressure around 3×10^{-8} Torr. Using monchromated Al Kα X-rays about ten hours was necessary to accumulate satisfactory statistics for the valence band spectra, during which time large quantities of contaminants were adsorbed. In view of the relatively long electron mean free paths expected at energies $\sim$1500eV surface contamination may not be as serious as in UPS. The measurements of Shevchik et al. were performed on sputtered films, which are said to contain an excess of the metallic component. This may be the reason why, for instance, the value of binding energy for the In $4d_{5/2}$ level in their InP (17.1eV) is

identical to that of indium metal, and also suggests an explanation for a peak in their He I spectrum which is attributed to an Auger transition. Figure 6.7, with the benefit of tunable photon energy, shows no such peak at constant kinetic energy. Notwithstanding these problems, significant differences are found between XPS and UPS determinations of the valence band density of states, although InP has not previously been studied by synchrotron radiation excited UPS.

There is some difficulty in defining the exact energy positions of several of the critical points in XPS, since the inherently poor resolution of this technique greatly broadens the fine structure in the theoretical density of states. This is not a significant problem with our data, and most of the uncertainty in energies is due to the small changes in position with photon photon energies which do occur (Figure 6.8). The energies determined in this work are tabulated in Table 6.2, together with values from XPS experiments, and several theoretical calculations. Our data for the lowest valence band (X_1, L_1, Γ_1) are probably not very reliable, for several reasons. This band has s-symmetry, and such states have relatively low photoionization cross-sections at low energy; although all cross-sections are considerably lower at XPS energies, those for s-states fall more slowly than for states with different orbital character and thus s-like bands are revealed better in XPS. Particularly for the deepest valence band, which exhibits little dispersion and thus appears rather core-like, final-state relaxation will tend to cause features to move to higher emitted energies. This of course occurs equally for XPS and UPS, but does mean that the energies determined by photoelectron spectroscopy are not strictly interpretable in terms of the single-electron density of states. Another problem with states far from the bandgap is that the lifetime of the hole state decreases with distance from the Fermi level and so the deepest band is broadened more than shallower levels. The gap $X_1^V - \Gamma_1^V$ is between 1.4 and 1.8eV according to the various theories, but is observed at 2.1 ± 0.7eV (XPS) and 2.8 ± 1.0eV (our work). In contrast, the next highest critical points,

TABLE 6.2.

Valence-band energies in InP. Comparison of our values with those determined by XPS, and several theoretical calculations. All energies in eV, referred to Γ_{15}^{v}

L_3^v	1.0 ± 0.1	1.0 ± 1.3	0.8	0.6	0.7	0.7	0.6	1.02	1.0
X_5^v	1.75 ± 0.15	2.0 ± 0.2	2.0	1.7	1.6	1.8	1.7	2.07	1.9
W_2^v	3.1 ± 0.15	2.5 ± 0.2							
Σ_{1min}^v	3.5 ± 0.2	3.2 ± 0.2	3.0	3.0		2.75	2.6		
L_1^v	5.80 ± 0.05	5.9 ± 0.2		4.5		4.85	5.1	5.84	4.9
X_3^v	6.10 ± 0.05			4.6	4.6	5.0	5.3	6.01	5.3
X_1^v	7.6 ± 0.5	8.9 ± 0.3		9.7	9.2		9.6	8.91	9.7
L_1^v	9.0 ± 0.3	10.0 ± 0.3		10.1	9.7		10.0	9.67	10.1
Γ_1^v	10.4 ± 0.5	11.0 ± 0.4		11.1	10.8		11.4	11.42	11.1
	*	†	Δ	#	+	o	ξ	x	□

* this work

† XPS (Ley et al 1974)

Δ empirical pseudopotential (Cohen and Bergstresser 1966)

\# empirically-adjusted OPW (Herman et al 1969, James et al 1970)

\+ relativistic OPW (Ortenburger and Rudge 1972)

o empirical pseudopotential (Varea de Alvarez et al 1972)

ξ empirical pseudopotential (Neumann et al 1975)

x non-local pseudopotential (Chelikowsky and Cohen 1976b).

□ bond-orbital method (Pantelides and Harrison 1975).

X_3^v and L_1^v, fall almost 1eV lower than predicted by all calculations except the non-local pseudopotential method (Chelikowsky and Cohen 1976 b), which was specifically adjusted to fit the XPS data. The minimum in band 3 along Σ ($\Sigma_{1\,min}^v$), prominent in UPS, also appears lower than predicted. It is difficult to assign the peak at $\sim$ 3.1eV, particularly noticeable at hν = 16 and 17 eV, to any of the calculated critical point energy levels. The peak in the density of states to which this corresponds has been attributed in similar compounds to the point W_2^v (Chelikowsky et al 1973). No published InP band structures include this symmetry point, although it appears that the region around W may represent quite a significant portion of phase space. From the work of Kramer et al (1971) in which the irreducible part of the Brillouin zone is split into two parts, and the density of states in each calculated, this peak is certainly due to band 3 in the volume near the zone edge containing X, W, U and K. Although this calculation considers only p-states, the upper two valence bands are almost entirely p-like, and so the information on this peak is likely to be correct. This peak in the density of states has an energy variously calculated as 2.5eV (Neumann et al), 2.95eV (Chelikowsky and Cohen) and 2.7eV (Kramer et al), all rather lower than our value of 3.1 ± 0.15eV. The two remaining symmetry points, X_5^v and L_3^v, are not well described by the theoretical calculations, particularly when it is recalled that most of these computations are fitted to reflectivity data for three transitions involving these points, $X_3^c - X_5^v$, $X_1^c - X_5^v$ and $L_3^c - L_3^v$. The value of X_5^v (1.75 ± 0.15eV) agrees reasonably well with the figure of about 1.9eV given earlier from an extrapolation of our low-energy UPS results and is in fair agreement with some of the theoretical data, which cover the range 1.6 to 2.3eV. All computed values of L_3^v until the two most recent (Pantelides and Harrison and Chelikowsky and Cohen) lie much too shallow: this is true of all the III-V and II - VI compounds studied by Ley et al (1974). These two recent calculations are explicitly fitted to the XPS data of Ley et al., and give

values for L_3^v the same as found in our measurements.

From these UPS data obtained with $16 \leq h\nu \leq 32$ eV we conclude that all the structure seen corresponds directly to critical point energy levels in the valence bands, although some theoretical calculations of band structure are not in good agreement with our values. As the photon energy is varied, there is almost no change in the position of peaks in the edc's, but the intensity of peaks is severely modulated by matrix element and final state effects. Our determination of some of these energy levels is believed to be much more accurate than XPS values, largely because of the better resolution of our measurements.

The binding energy of the In 4d levels can be determined with high resolution by using photons with energy around 30eV. We find the In $4d_{5/2}$ and $4d_{3/2}$ levels to be situated 16.90 ± 0.05 and 17.65 ± 0.05eV below the valence band maximum . A compilation of other measurements of these energies is given in Table 6.3.

6.3. Surface electronic structure

As with GaP no structure corresponding to emission from filled surface states is observed, since all the features in Figures 6.1 and 6.7 are explicable in terms of bulk band structure. However, some of the peaks are not fitted perfectly from the direct-transition analysis: this was ascribed in Chapter 6.1 to the lack of any sufficiently accurate band structure, but we here reiterate the properties of a surface state to demonstrate conclusively that none of the observed features can be so explained. Surface state emission should occur at a constant initial energy, at all photon energies, and is expected to be removed or modified by adsorbates. None of the features in our edc's fits these criteria. Adsorption of oxygen, to be reported in detail in Chapter 6.5, produced no significant change in the position of the peaks in the energy distribution spectra. Thus we conclude that there is no sharp structure due to filled surface states either within the bulk bandgap or

TABLE 6.3

Binding energies of the In $4d_{5/2}$ and $4d_{3/2}$ levels in InP

Referred to E_v	Referred to E_f	Authority
16.90 17.65		this work
	17.8	Vesely and Kingston (1972)
	17.4 18.1	Gudat et al (1972)
16.8		Ley et al (1974)
17.1 17.88		Shevchik et al (1974)
16.9		Gudat and Eastman (1976)

overlapping the bulk valence bands. Such states may have a large energy spread, or be strongly mixed with valence band states.

Photoemission from filled states extending almost throughout the bulk bandgap has been claimed (Fischer 1966 , 1968). In view of the large noise-to-signal ratio ($\sim$ 20%) and the very small intensity (several orders of magnitude smaller than bulk features) reported for this part of these spectra, it is difficult to attach much importance to this publication. No such effects were seen in experiments by James et al (1970) using a similar photon energy range.

Photoemission partial-yield measurements were performed to look for empty surface states. Some of the spectra obtained are presented in Figure 6.9, together with the absorption coefficient curve from Gudat et al (1972). No significant differences are observable between the bulk absorption and the surface-sensitive absorption monitored by the partial-yield emission. In a preliminary report of these data (McGovern et al 1976 -see Appendix) we tentatively ascribed the features at $h\nu \sim 18.9$ and ~ 19.8 eV to excitation from the spin-orbit split In 4d core level to a vacant surface state above the conduction band minimum. The main evidence for this identification was the weakness of these features in a spectrum taken from a contaminated InP surface, also shown in Figure 6.9. It seems likely that, when the surface is dirty, many excited electrons are scattered to lower final energies than our E^* (6eV) and so all features become less pronounced : it is noticeable that the direct emission from the In $4d_{5/2}$ level at $\sim$ 22.9eV is much less intense than in the spectrum from the clean surface.

It has recently been reported (Gudat and Eastman 1976) that partial-yield measurements indicate a vacant surface state in InP with a peak at 1.0 eV above the valence band maximum, but no spectra are shown

Figure 6.9. Photoemission partial-yield spectra for InP (110). Upper two curves are different clean cleaved surfaces, third curve is from contaminated surface. Lowest curve is absorption coefficient (α) from Gudat et al (1972)

clean

n(E)

$E^* = 6eV$

2×10^5 counts

contaminated

a(cm^{-1})

4.5×10^5

3·5

a

18

20

22

Photon energy (eV)

to enable assessment of the magnitude of this feature. Our data for clean InP consistently show the point at 18.0 eV (1.1eV above the valence band maximum) to be ~ 0.7% above the value expected from a curve fitted smoothly through the other points on the steeply sloping leading edge of the spectra; however, this odd point is also present in the curve for the contaminated surface. Although this effect is very small, it is approximately three times the statistical noise level. We note that the only curve with calibrated axes given by Bauer et al (1977) shows a surface state on ZnSe with peak magnitude above background of only ~ 1.25%. If the small point in our spectra were due to a final surface state, the transition from the In $4d_{3/2}$ level to this state would fall near $h\nu$ = 18.7eV, and could thus not be discriminated from the conduction band peak at that energy.Also, if the surface adsorbates bond to the P atoms, as appears to happen with GaP, an In-derived empty surface state could persist after contamination and this point could be ascribed to a surface state, but I feel that such an assignment for InP cannot be justified from such a small feature. Incidentally, we note that there is no reason to suppose that the In dangling-bond surface state has any different orbital symmetry from the Ga-derived surface state on GaP which was shown to be predominantly p-like. If such a state were exclusively s-or d-like, optical transitions to it from the In 4d levels would be forbidden.

6.4. Band bending

Our experiments were carried out with n-type material supplied by R.R.E., Malvern. This was doped with tin to an excess donor concentration of 3×10^{17} cm^{-3} giving a bulk Fermi level coincident ,within 0.01eV, with the conduction band edge. Thus the bulk value of $E_F - E_v \sim E_g \sim 1.34$eV. The Fermi level of a freshly evaporated film of gold was regularly determined and thus the value of $E_F - E_v$ at the surface is readily found. Emission from the valence band maximum is visible at photon energies from 9.7 to 10.2eV, and data from all other edc's may be included by making suitable

allowance for the difference between the valence band maximum and the highest initial state from which emission is observed. A value of $E_F - E_v = 1.30 \pm 0.1$eV is obtained equal, within experimental error, to the bulk value. No variation with different cleaves was observed. Thus there is no band bending and no surface states within the bulk bandgap.

Measurements of the edc width W give a secondary check on band bending through the relationship $h\nu - W = E_{vac} - E_v$ (Figure 5.14). Again taking account of the lack of emission from the valence band maximum at many photon energies, we find a mean value of $E_{vac} - E_v = 5.7 \pm 0.2$eV. There is reasonable agreement on the magnitude of the photothreshold Φ, which has been variously determined to be 5.69eV (Fischer 1966), 5.6eV (Williams and McGovern 1975) and 5.78eV (Chye et al 1976). Thus we find within experimental error $E_{vac} - E_v = \Phi$ and, bearing in mind the cautionary remarks from Chapter 5.4. about combining surface results from different samples, this lends further slight support to our conclusion on the lack of surface states in the bulk bandgap.

Previous workers have found the Fermi level on InP to be pinned well below the conduction band minimum, within the bulk bandgap. $E_F - E_v$ has been reported to be 1.04 ± 0.1eV (Fischer 1966) and 1.1 ± 0.1 eV (Chye et al 1976). We did not perform any deliberately bad cleaves, all our (110) surfaces exhibiting a smooth mirror-like finish, and no surfaces showed a Fermi level below its bulk value. More careful work may reveal, as recently reported for GaAs (Spicer et al 1976b), that Fermi level pinning is induced by extrinsic states. Huijser et al (1977) have recently suggested, from an empirical model based on results from several III- V compounds, that surface defects might cause the Fermi level on n-type InP to appear ~ 0.2 eV below the conduction band minimum (~ 1.15 eV above the valence band maximum), close to the values of other workers given above.

6.5. Oxidation of InP

Oxygen exposures were made in small steps up to a total of $\sim 10^{10}$ Langmuirs on several clean cleaved InP surfaces. A representative selection of data is given in Figure 6.10 : these spectra are given on the small vertical scale, and are plotted against retarding voltage to illustrate the changes in the leading edge of the edc's. Also included in this figure is an edc from a sample which was cleaved in air before insertion into the vacuum chamber;. this spectrum, taken after the system had been pumped down, baked,and allowed to reach a pressure $\sim 5 \times 10^{-11}$ Torr, exemplifies the general insensitivity to contamination of III- V compounds. The variation of electron affinity with oxygen exposure is given in Figure 6.11, and Figure 6.12 shows the changes in Fermi level position. As with GaP,poor reproducibility of oxygen exposure was observed, although in this case the exposures needed to induce changes varied by less than a factor of ten. This improvement may be merely because, following the experiments on GaP, we were aware of this effect and particular care was taken to ensure similar conditions of total pressure, state of ionization gauge, and so on. No oxygen-sensitive structure is observable in Figure 6.10, the only change being the increase of the lowest-energy feature.

The changes in electron affinity are interesting. Adsorption of oxygen causes χ to decrease and thus the edc's became broader. Although the changes are small, it is noticeable from Figure 6.10 that the edc from the heavily contaminated surface, before cleavage, is about 0.35eV wider than for the clean surface. Simple adsorption of negative oxygen ions onto the surface would provide a negative dipole and thus increase the electron affinity. A possible explanation is based on the concept of electronegativity. If we continue the assumption, discussed in earlier chapters, that the surface states are associated with particular species of surface atom, such that the filled states arise from the dangling bond of the group-V atom

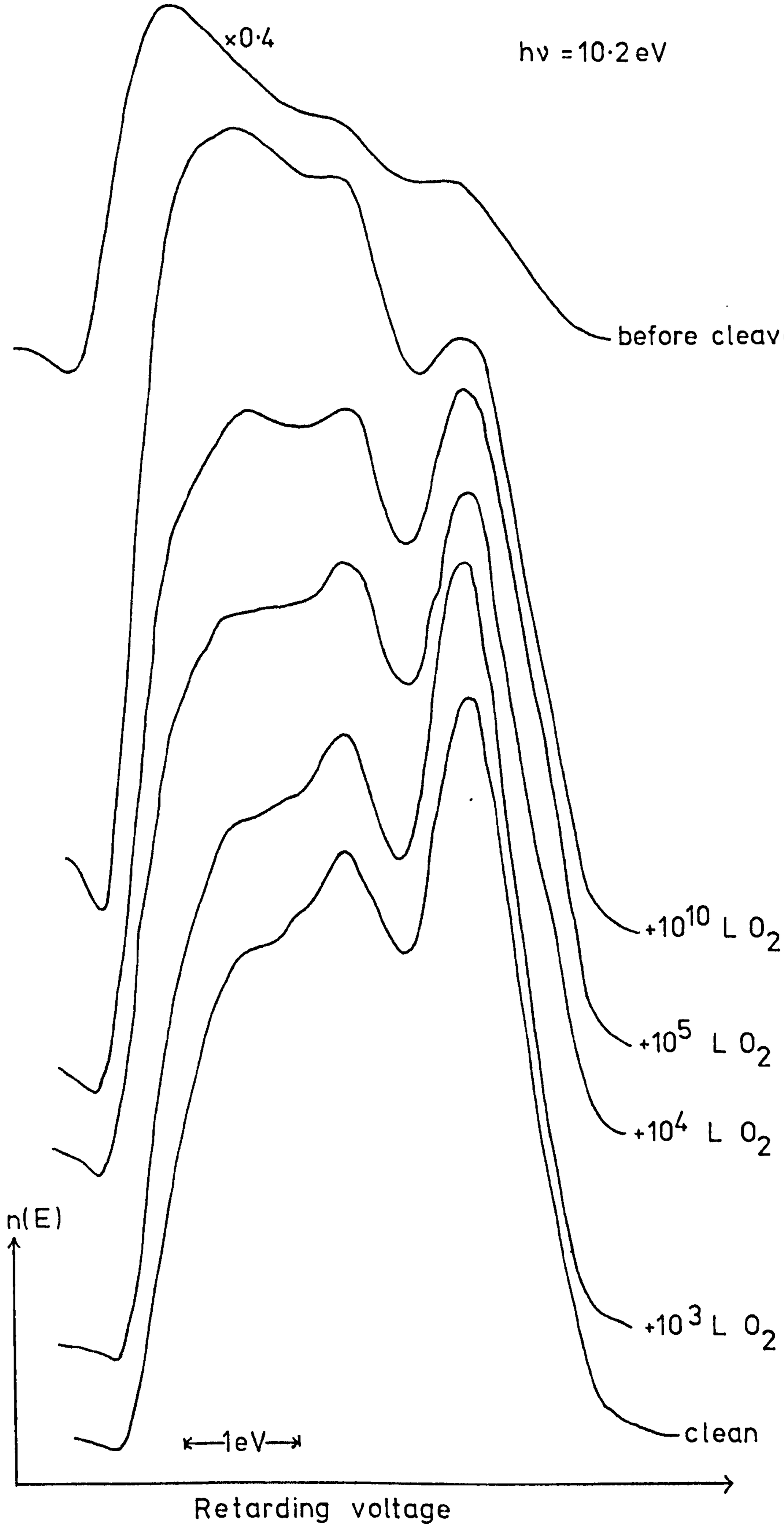

Figure 6.10. Edc's from InP (110) with various exposures of oxygen

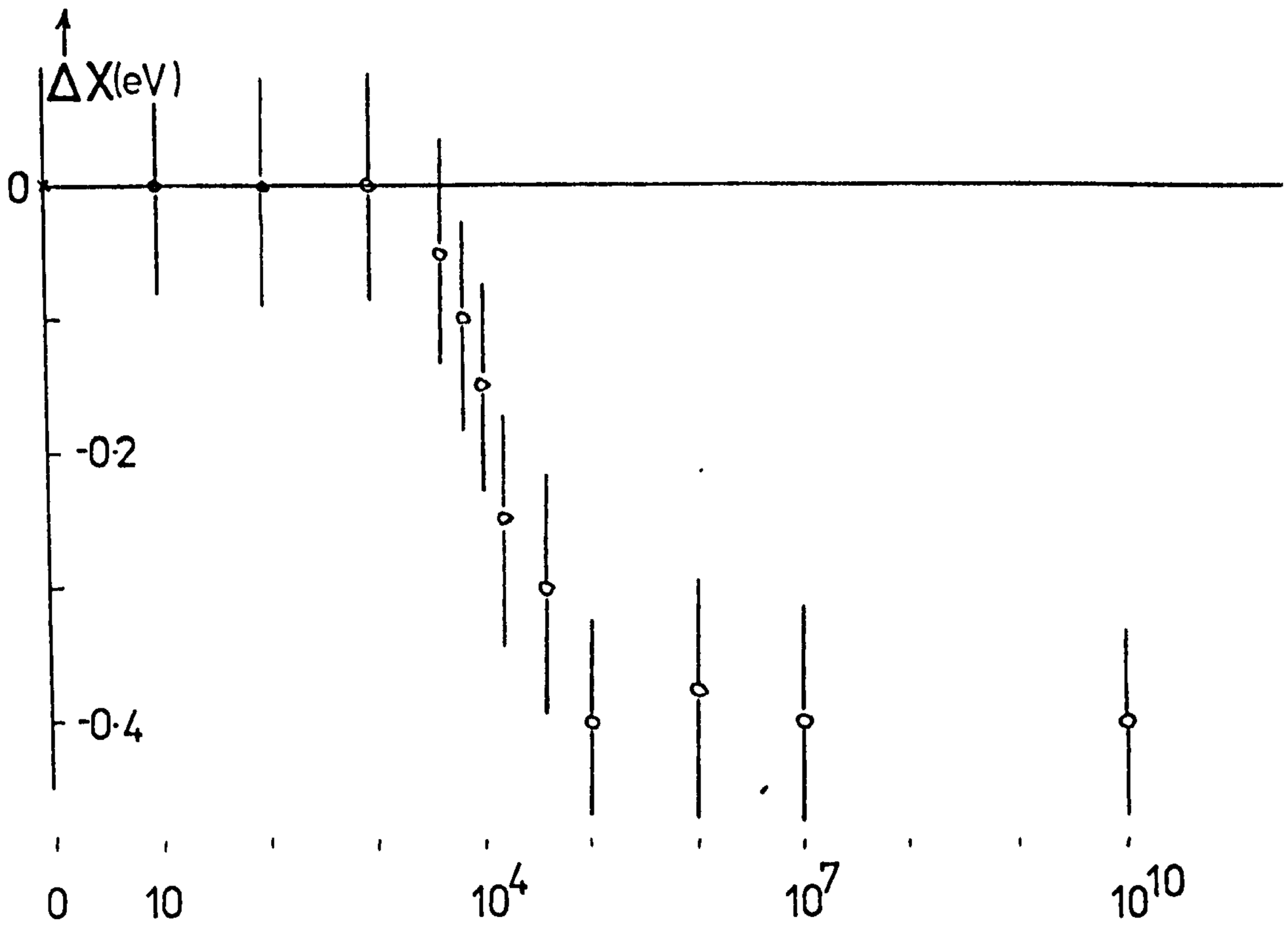

Figure 6.11. Change in electron affinity ($\Delta\chi$) of InP as a function of oxygen exposure

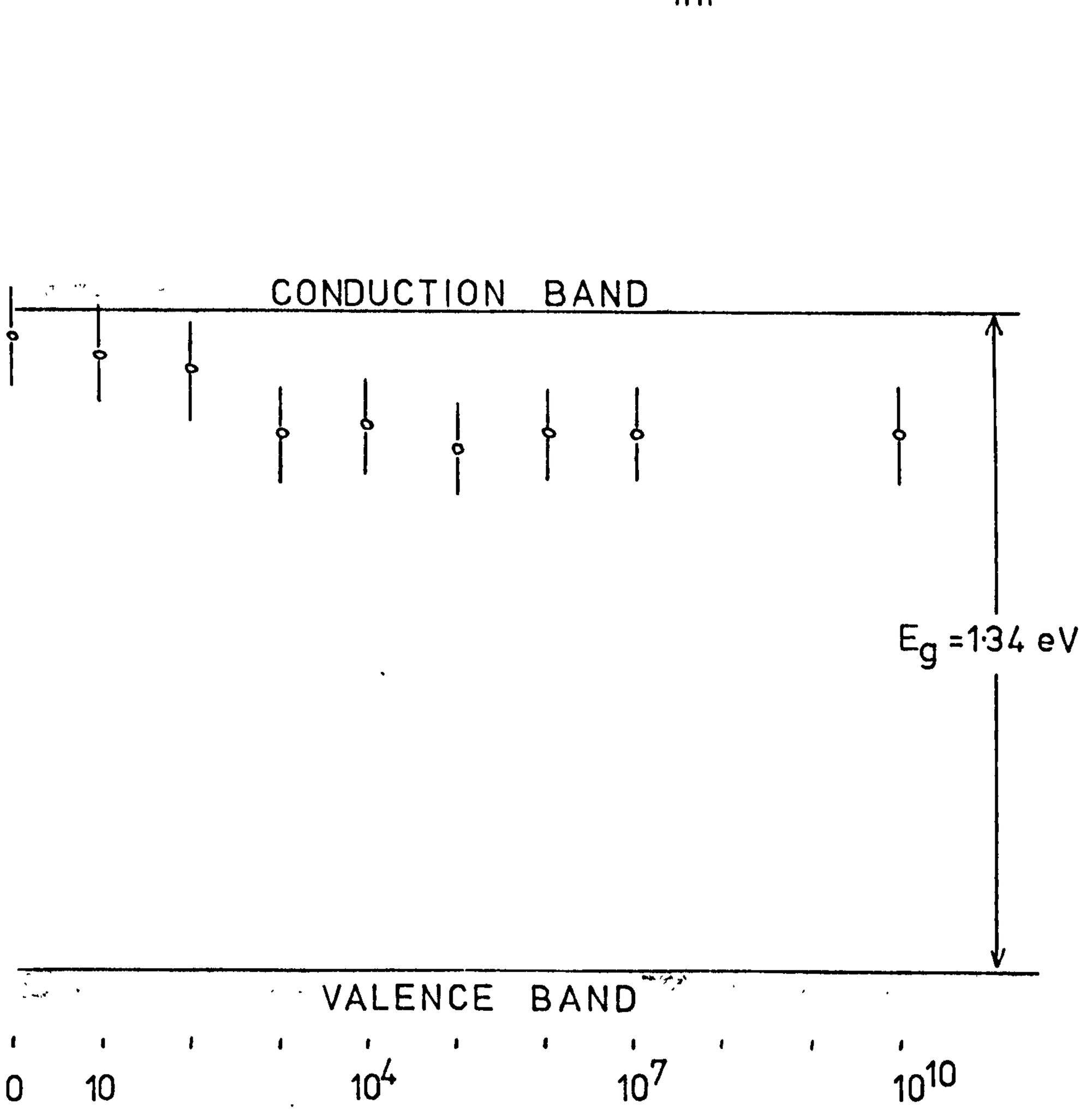

Figure 6.12. Change in Fermi level position on InP as a function of oxygen exposure

(phosphorus) and the empty states from the group-III atom (I n), then the normal chemistry is reversed. In their elemental forms, indium is metallic and phosphorus is electronegative: in InP, the surface phosphorus atoms have the excess electrons and are thus electropositive. If also, as seems possible from the chemical shift experiments on GaAs (Pianetta et al, 1975 and subsequent re-publlcations) and on InP (Spicer et al 1976 b, Lindau et al 1976 c), we assume that oxygen is initially bonded to the group-V atom, then the excess electrons in the P dangling bond will be re-distributed in the P-O bonds. Thus the surface becomes less electropositive and the electron affinity decreases. This appears to be a more realistic explanation than the postulate of oxygen lons going beneath the surface (Chye et al 1977).

Another effect of oxygen adsorption on the width of edc's is that the high-energy edge of the spectra becomes broader. This broadening was not included in the calculations of $\Delta\chi$, which was measured from extrapolations of the two edges of the edc's. What is observed here is that the difference between the highest energy main peak and the apparent valence band maximum increases by up to 0.2 eV as oxygen is adsorbed. Such an effect has not been reported before for oxygen, but was observed with absorption onto InP of caesium (Chye et al 1976). If the above explanation of the adsorption of oxygen is correct, a possible mechanism for the extension of the tail of the valence band emission into the bandgap involves an image potential. It has been suggested (Inkson 1973) that a metal overlayer on a semiconductor surface will give rise to an image potential which attracts electrons in the conduction band and holes in the valence band, causing a rise of the valence band maximum, a fall in the conduction band minimum and a narrowing of the bandgap. Although this was discussed for metallic surface coatings , it seems possible that a similar type of mechanism may hold in this case, particularly since adsorption of oxygen, and consequent partial saturation of dangling bonds, might be expected to change greatly the ionic nature of the surface and its adsorbate layer.

The position of the Fermi level is changed by addition of very small amounts of oxygen, E_F moving downwards into the gap. Exposure to

10^3 L O_2 produces barely detectable changes in the shape of the spectra, but induces a shift of 0.2eV in the Fermi level. From the estimates of sticking coefficient of oxygen on III-V compounds, discussed in Chapter 5, this exposure probably corresponds to less than one-thousandth of a monolayer coverage. Exposures to amounts of oxygen greater than this led to no further change, E_F remaining pinned about 0.25 ± 0.1 eV below the conduction band minimum. This is almost exactly the position found for the clean InP (110) surface by Fischer (1966) and by Chye et al (1976), who reported no change in E_F on oxidation. These results make it appear likely that extrinsic states cause pinning ~ 1.1eV above the valence band maximum, and that this is what has been observed by these other workers. This raises again the possibility that the apparent surface features are determined mainly by the quality of the cleavage and by imperfections in the material. It has recently been reported for GaAs that Fermi level pinning was observed on cleaved surfaces from a crystal 10 x 10 mm in cross-section, but, after reduction of these dimensions to 5 x 5 mm - on the same crystal- no pinning was seen (Spicer et al 1976 b). The cross-sectional dimensions of the InP crystals in the three sets of experiments under discussion are 10 x 10 mm (Chye et al), 8 x 2 mm (Fischer) and 7 x 1.8 mm (our work). It has been found on cleaved GaSb that the surface potential, and hence the band bending, exhibits variations of up to 0.5eV over macroscopic distances across the surface (Fischer and Viljoen 1971) and this is attributed to cleavage-induced strains or defects, which are seen gradually to anneal themselves, or be stabilized by extrinsic states, over a period of days. The electron affinity of these surfaces is said to be well-defined with no spatial or temporal variations. Earlier irreproducible measurements on InP have been ascribed to similar causes (Fischer 1968) .

One further effect was observed during adsorption of oxygen. If the sample was left for a few hours and then re-measured, it appeared that some oxygen had desorbed : the electron affinity increased and the intensity of the edc decreased. It proved difficult to quantify this effect,

partly because of the problems of ensuring stability of the intensity of the light source (which has no external monitor) and of the electronic detection circuitry, and partly because of the difficulty of eliminating changes in the work function of the analyser coating. However, the increase in χ is always $\sim$ 0.1eV, almost irrespective of which stage in the oxidation had been reached - except that the electron affinity never increased above the value for the clean surface, and it appears that the movement of Fermi level is irreversible. Lapses of an hour seldom affected the spectra much, and samples left for about eight hours in a partially-oxidized state always lost some oxygen. It seemed not to matter whether the sample remained illuminated by the u.v. light or was left dark. The desorption is probably related mainly to the partial pressure of oxygen in the vacuum chamber.

6.6. Summary

UPS electron energy distribution curves of InP taken with photon energies between 7 and 12eV have been interpreted in terms of direct optical transitions with the aid of theoretical bulk band structures. None of the published calculations was found to be in agreement with our data. Spectra taken at photon energies in the range 16 to 32 eV enabled the positions of several valence band critical points to be determined with better resolution than is available in XPS. No effects attributable to filled or empty surface states were seen in UPS and the surface Fermi level coincided with its bulk value. No empty surface states were seen with partial-yield spectroscopy. Adsorption of small amounts of oxygen causes the Fermi level to move 0.2 eV below the conduction band edge, and it remains there after heavy oxidation. The electron affinity decreases on oxidation, being 0.35eV lower on a heavily oxidized surface than when freshly cleaved.

CHAPTER 7

GALLIUM ARSENIDE

7.0 Introduction

UPS experiments using photons with energies between 7 and 12 eV were performed on GaAs (110) with the purpose of examining the surface electronic structure. Adsorption of oxygen was used to help to distinguish bulk and surface effects.

The experimental results are summarized at the end of the Chapter, with the main conclusions drawn in Chapter 8 in conjunction with data from GaP and InP.

7.1. UPS of clean GaAs: filled surface states

The electron energy distribution curves obtained in the photon energy range 7.7 to 11.8eV are shown in Figure 7.1. Some raw data are given in Figure 7.2 : the spectra are more noisy than those observed from GaP (Figure 5.3) and InP (Figure 6.2), particularly at high hν, largely because of a poorly transmitting LiF window. This makes the values of yield, plotted in Figure 7.3, rather unreliable towards 11eV. The data of Figure 7.1 are reduced to the structure plot of Figure 7.4.

The yield curve of Figure 7.3 is slightly different from that presented by Eden (1967), which rises rapidly from 10^{-3} at 7eV to 10^{-2} at 8 eV and then remains constant up to the LiF window cut-off. The difference is explicable by band-bending, Eden using heavily-doped p-type material , whereas our results are for lightly-doped n-type GaAs. The bonds are said to bend downwards on their p-type material and so emission of relatively low energy electrons is easier than in n-type GaAs.

The structure plot of Figure 7.4 is so similar to the GaAs results obtained by others and already analysed in detail (Eden 1967, Spicer and Eden, 1968), that it was not felt profitable to attempt a full direct-transition analysis of these low-energy edc's.** Instead, we concentrate on the surface

** We nevertheless note that, despite all the attention given this material over the past fifteeen years, only very recently has the exact form of even the lowest conduction bands been satisfactorily explained (Aspnes 1976).

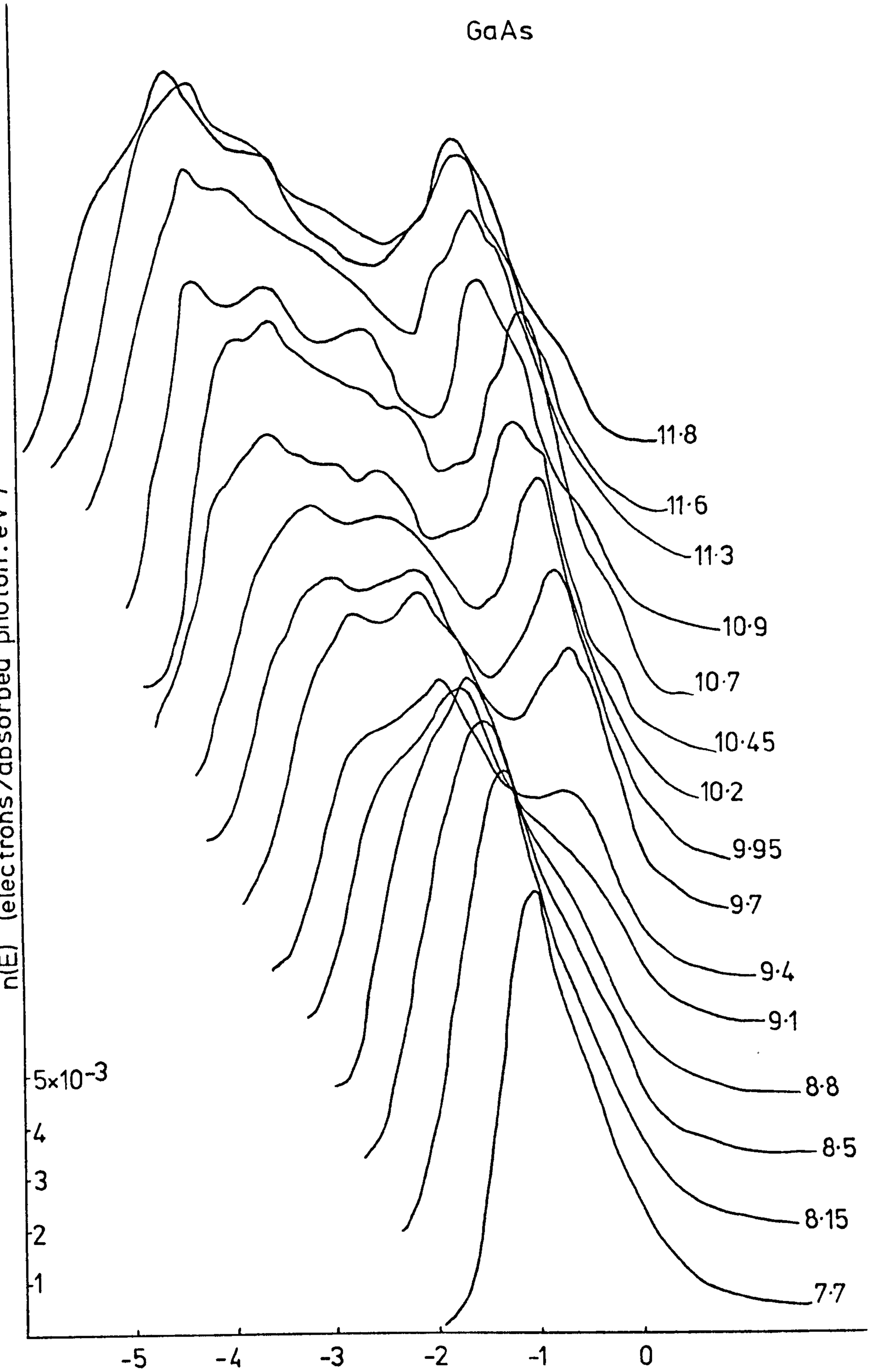

Figure 7.1. UPS electron energy distribution curves from clean GaAs(110) in the photon energy range 7.7 to 11.8 eV.

Figure 7.2. Some raw edc's for GaAs

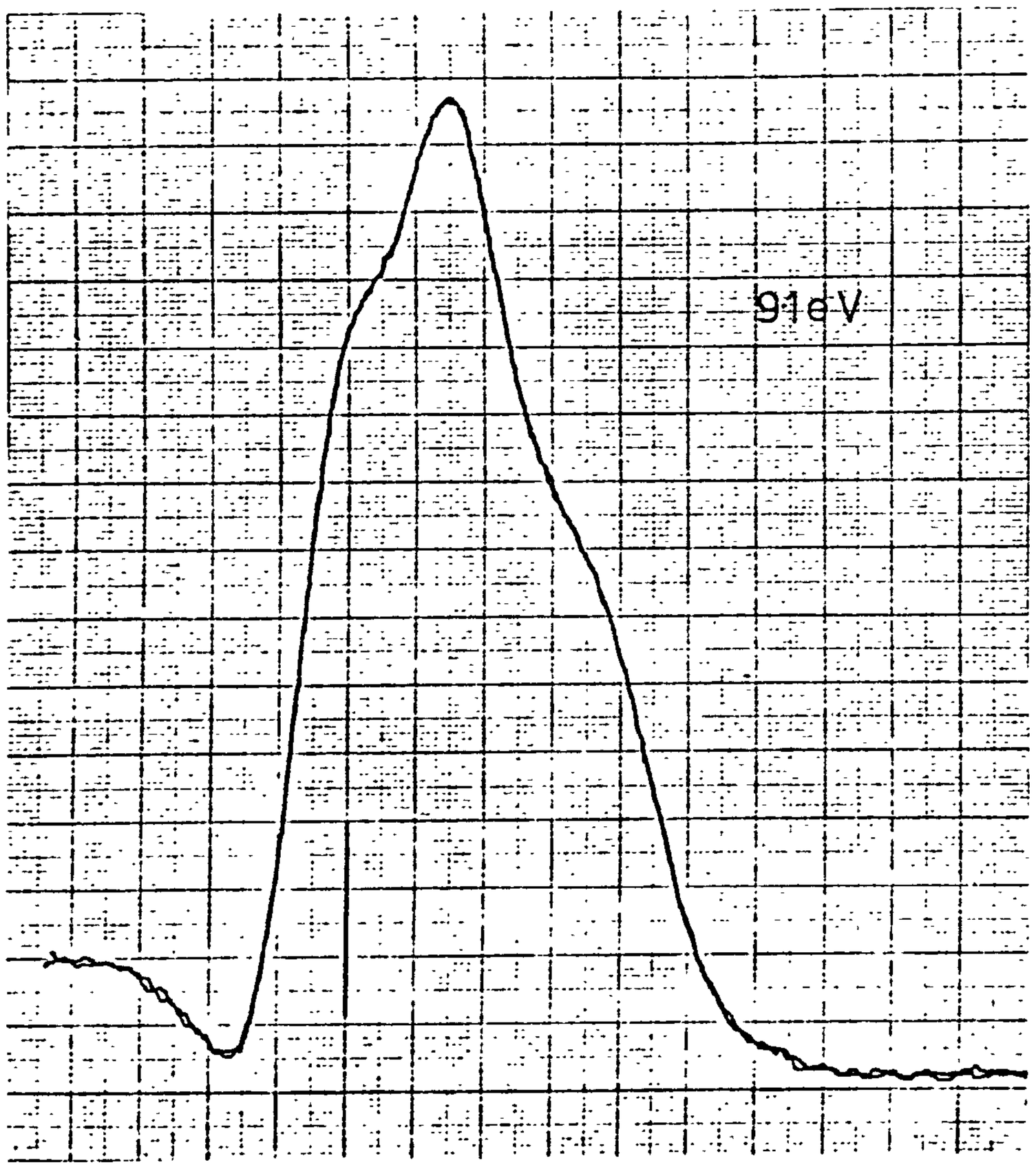

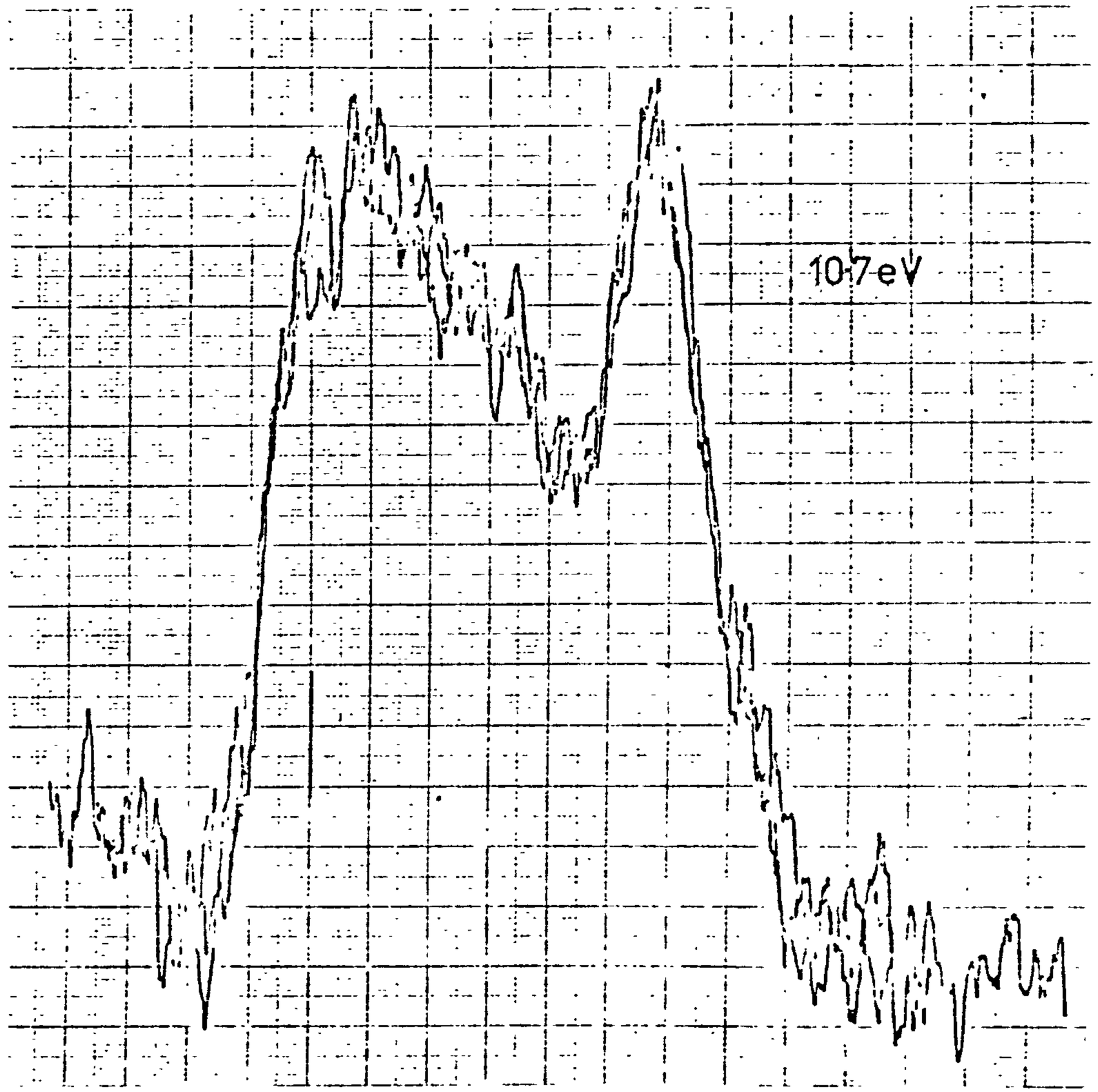

GaAs

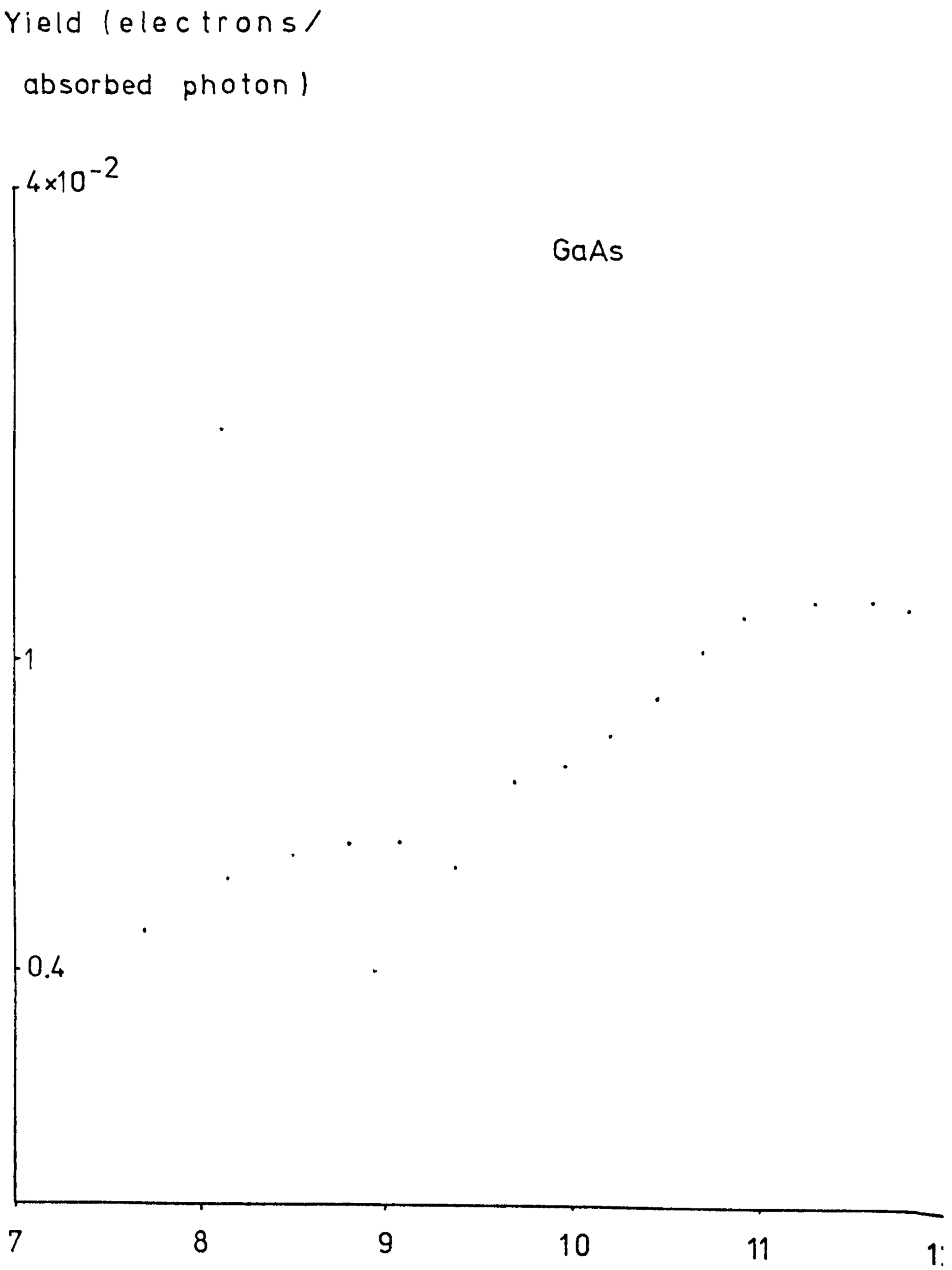

Figure 7.3. Yield versus photon energy for GaAs

GaAs

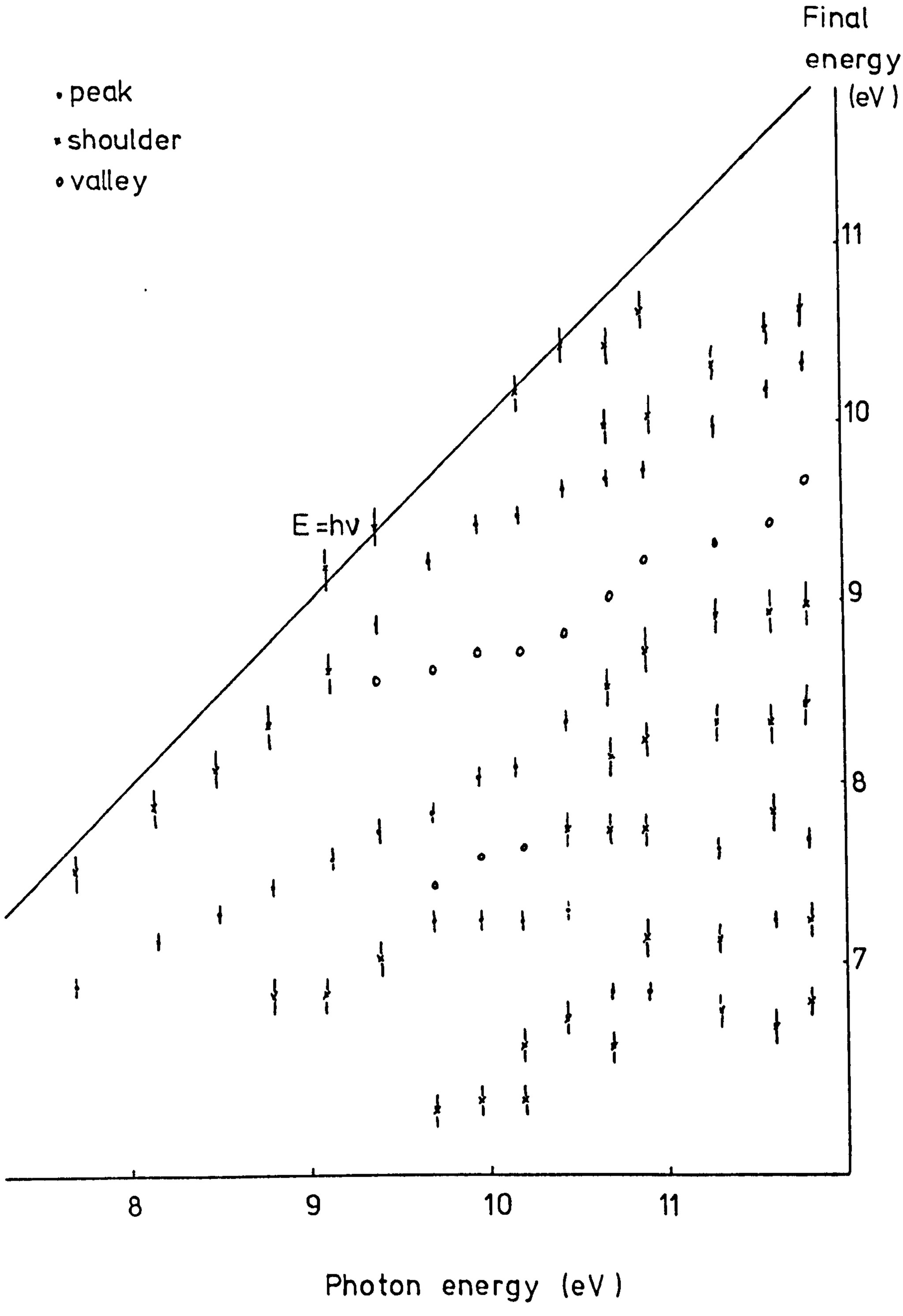

Figure 7.4. Structure plot for GaAs, from Figure 7.1

properties and limit the examination of the edc's to two factors : the energy of conduction band Γ points , so that the Fermi level position may be referred to the valence band maximum, and any structure possibly arising from filled surface states.

Shoulders are seen on the E = hν line at 9.1 - 9.4 and 10.2 -10.45 eV. Results of other experiments and theoretical values for Γ_1^c and Γ_{12}^c are given in Table 7.1, from which it is seen that there is some agreement over the position of these two levels,with the pseudopotential calculations, as appears to be usual, giving values lower than experimentally determined. It is clear that there is a range of photon energies at which emission from the valence band maximum can be seen.

There is no structure which occurs at a fixed initial energy, irrespective of photon energy, as a filled surface state peak is expected to do. The feature within 0.5eV of the E = hν line appears to keep a fairly constant initial energy over the range $8 \leq h\nu \leq 10$eV, but is identified as coming from transitions from bands 3 and 4 to band 9 (going away from Γ_1) over a wide range of k-space (Spicer and Eden 1968). We thus conclude that there is no structure which can be assigned to emission from filled surface states, either within the bulk bandgap or overlapping the bulk valence bands. It is probable, as with GaP and InP, that such states are spread out in energy and may hybridize with bulk bands.

A very interesting result was observed with just one experiment on GaAs, some spectra from which are shown in Figure 7.5. This was the only cleave from all the experiments on GaP, InP and GaAs where a specular (110) face was not revealed and was produced in an attempt to obtain an extra cleave from one crystal by levering the cleaver so that the base of the stainless steel block, rather than the tungsten carbide blade , struck the crystal. The cross-section of the ragged surface is shown in the inset to Figure 7.5,with the positions from which the four edc's were taken also marked. These results differ in several ways from those obtained on normally cleaved surfaces.

TABLE 7.1

Positions of Γ_1^c and Γ_{12}^c in GaAs

Γ_1^c	Γ_{12}^c	method	authority
9.1	10.2	photoemission	this work
9.0	10.2 -10.8	"	Eden (1967)) quoted by) Spicer and
9.1	10.3 - 10.9	"	James (1968)) Eden (1968)
8.33	10.53	electroreflectance	Aspnes et al (1975)
	9.9 - 10.7	photoemission	Gregory and Spicer (1976)
8.1	8.8	empirical pseudopotential	Cohen and Bergstresser (1966), quoted by Eden(1967)
9.0	10.6	empirical OPW	Herman et al (1968); Herman and Spicer (1968)
7.8		empirical pseudopotential	Walter and Cohen (1969)
9.1	10.8	self-consistent OPW	Collins et al (1970)
8.6	8.8	empirical pseudopotential	Saravia and Duomarco (1973)

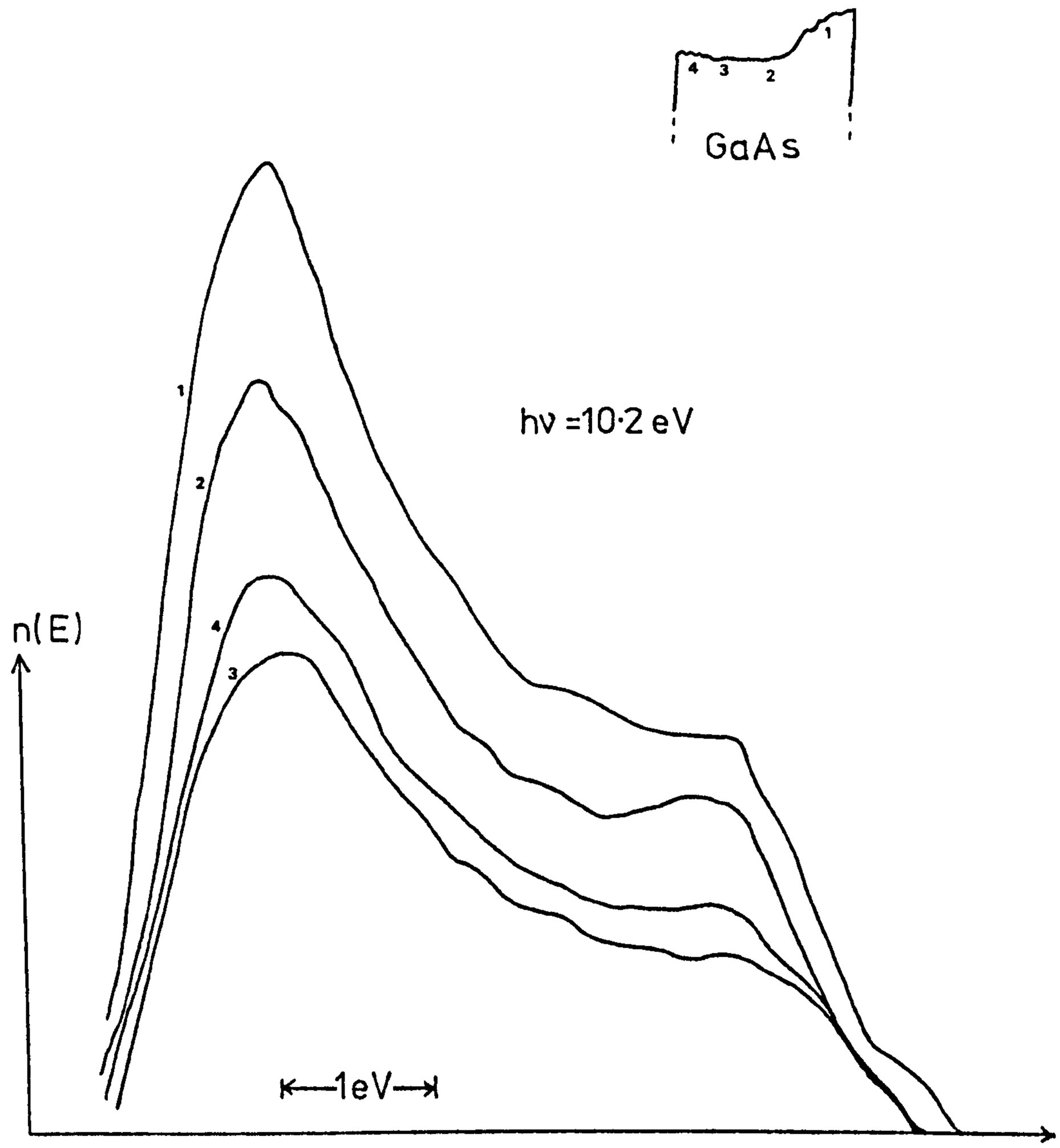

Figure 7.5. Edc's from four different positions across a badly broken GaAs surface. The cross-section of the surface is shown in the inset.

It is seen, by comparison with Figure 7.1, that less fine structure is resoluble in all the spectra, and a large peak of scattered electrons is obtained. Loss of sharpness of edc structure is said to be characteristic of GaAs which exhibits Fermi level pinning (Spicer et al 1976b). The electron energy distribution spectra of Figure 7.5 are particularly interesting in view of results contained in several publications. It is readily seen that the widths of the spectra are different, contrary to the result that the electron affinity is constant, irrespective of imperfections and Fermi level differences (Fischer and Viljoen, 1971). From position 1, emission is seen from above the apparent valence band maximum: this may explain the reported observation of filled surface states on GaAs (Eastman and Grobman 1972), although all other workers have failed to reproduce this result, even with deliberately poor cleaves (Gregory et al 1974). Unfortunately the full significance of the results from this partly-cleaved surface was not appreciated at the time, and oxidation of this surface was not attempted. The third point of note from Figure 7.5 is that the Fermi level is located ~ 0.7 eV above the valence band maximum, as found at positions 2,3 and 4. This will be discussed at greater length in the following section.

7.2. Empty surface states

The GaAs used was grown by the Plessey Co.Ltd., doped with tin to an excess donor concentration around 5×10^{15} cm^{-3}, thus giving a bulk value of $E_c - E_F \sim 0.11$ eV. Since $E_g \sim 1.43$ eV at 300^{o}K, $E_F - E_v \sim 1.32$ eV in the bulk. The surface Fermi level was determined in the usual way from an evaporated film of gold, and emission from E_v is visible for several photon energies, as discussed in Chapter 7.1; hence a value of $E_F - E_v = 1.30 \pm 0.1$ eV is obtained. This is equal, within experimental error, to the bulk value. We therefore find no band bending and no surface states within the bulk bandgap. No variation with different cleaves was observed, with the exception of the badly broken surface, which gave $E_F - E_v = 0.7 \pm 0.1$ eV.

There has been considerable dispute over the position of the Fermi level on the GaAs (110) surface, the results of which are summarized in Table 7.2. From the results contained in this table, it is seen that it now seems to be generally agreed that the Fermi level is at its bulk position on perfectly cleaved surfaces but tends to be pinned near mid-gap on surfaces which are poorly cleaved or otherwise imperfect ; our broken surface exhibited a band bending of $\sim$ 0.6eV.

7.3. Oxidation of GaAs

The effect of increasing oxygen exposure on edc's is shown in Figure 7.6. The electron affinity remained constant, within the experimental error ($\pm$ 0.1 eV). Small doses of oxygen caused the Fermi level to move below its bulk value, and large exposures pinned it near to mid-gap, as shown in Figure 7.7.

No oxygen-sensitive structure is observable in Figure 7.6, the only effect being the increased intensity of the lowest-energy feature. A similar result has recently been reported by Gregory and Spicer (1976 b), who showed from edc's at $h\nu = 11.6$ eV that the adsorbed oxygen gives a peak at an initial energy 4.1 eV below the valence band maximum. The same authors found a small drop in electron affinity after exposures of 10^5 LO_2 on their p-type samples, with χ returning to its original value with heavier coverage, but n-type GaAs showed no change in χ.

The movement of the Fermi level of GaAs with oxygen exposure follows a similar pattern to InP (Figure 6.12), with band-bending induced by oxygen-derived extrinsic states. Gregory and Spicer showed no change with oxygen exposure of E_F on n-type material, with the Fermi level on p-type moving from the valence band edge towards the same mid-gap pinning position reported by them for clean n-type GaAs. However, later work (Spicer et al 1976b) showed that the Fermi level moved from its (unpinned) bulk value on n-type GaAs into the gap with increasing oxygen exposure, in a manner very

Table 7.2

Fermi level position on n-type GaAs

Band-bending	Authority	Remarks
~ 0	this work	~.6 on poor cleave
~ 1.0	Haneman (1959)	broken polycrystalline samples.
0.6	Gobeli and Allen (1965, 1966)	
~ 0	van Laar & Scheer (1967)	
0.8	Dinan et al (1971)	
~ 0.7	Gregory et al (1974) Gregory and Spicer (1976a)	
~ 0	Huijser and van Laar (1975) Huijser et al (1977)	dependent on cleavage quality
~ 0	Gudat et al (1976) Gudat and Eastman (1976)	
~ 0	Spicer et al (1976b)	~ 0.6 on some crystals
~ 0	Guichar et al (1976)	~ 0.7 with some cleaves
~ 0	Lüth et al (1977)	

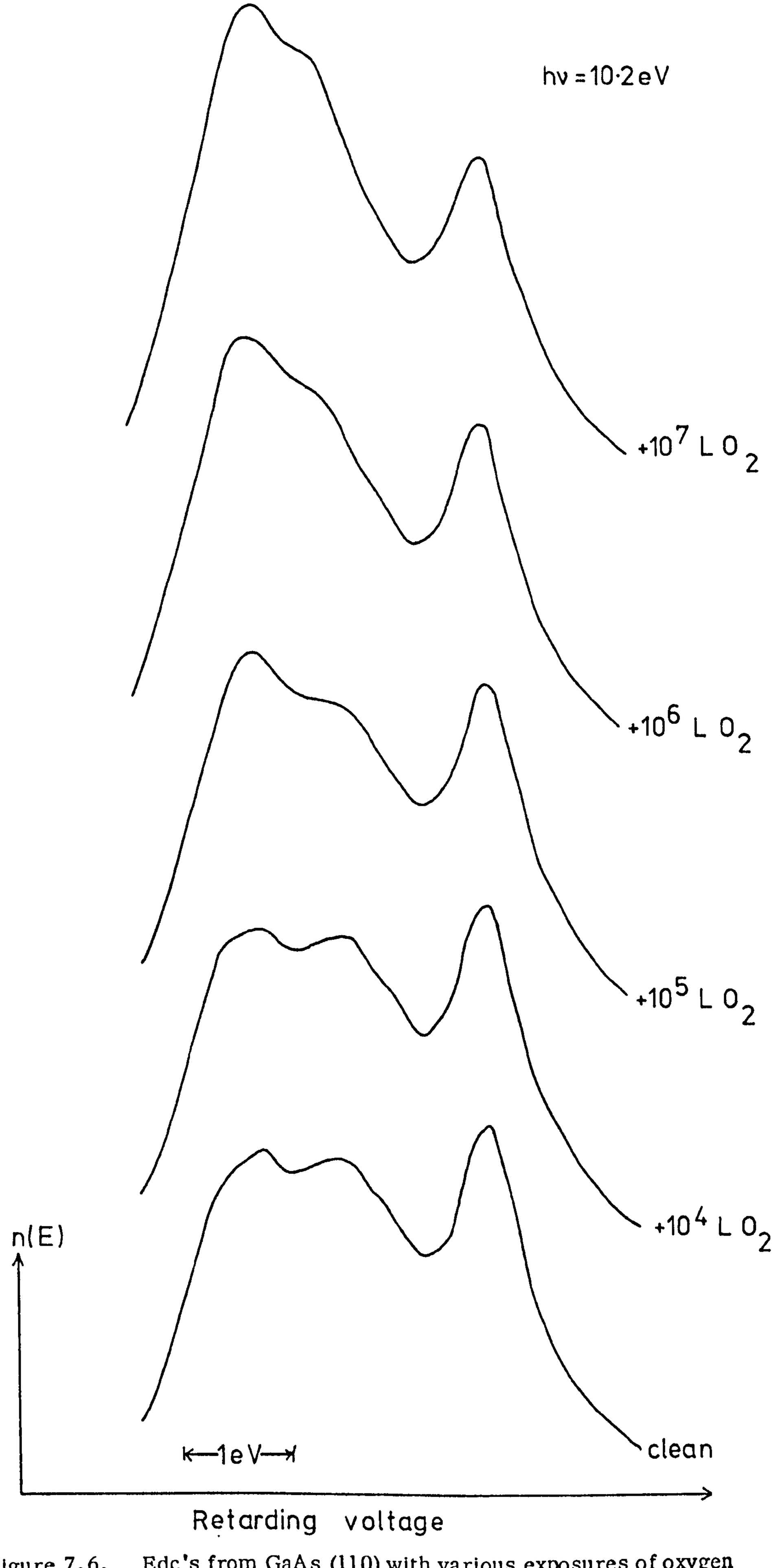

Figure 7.6. Edc's from GaAs (110) with various exposures of oxygen

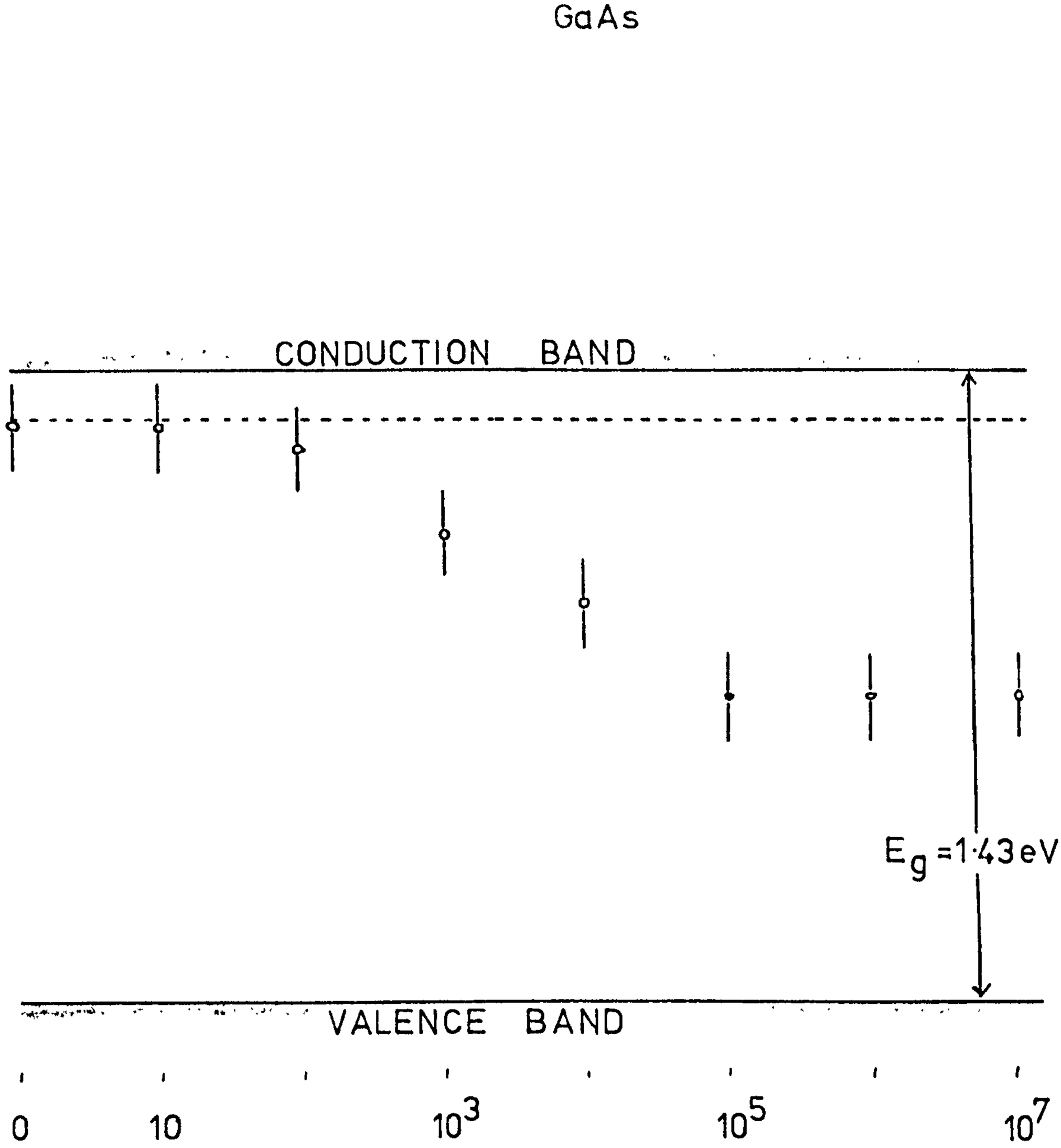

Figure 7.7. Change in Fermi level position on GaAs as a function of oxygen exposure

similar to our Figure 7.7. An almost identical result, based on surface photovoltage and ELS, has very recently been reported (Lüth et al 1977).

7.4. Summary

UPS electron energy distribution curves of GaAs taken with photon energies between 7 and 12 eV are in good agreement with previously published data. No effects attributable to filled or empty surface states were seen on perfectly cleaved surfaces, and the surface Fermi level coincided with its bulk value. A badly broken surface showed evidence of emission from filled surface states and had its Fermi level pinned within the bulk bandgap by empty surface states. Adsorption of oxygen did not remove any structure from the edc's, but small exposures of oxygen caused the Fermi level to move into the bandgap and on heavier oxidation it is pinned ~ 0.6 eV below its bulk level.

CHAPTER 8

CONCLUSIONS

8.0. Conclusions

In this concluding Chapter we combine and summarize the results of our work on the surface electronic properties of GaP, InP and GaAs and discuss them together with other published data. The results which relate to the bulk structure are not dealt with here since they have been summarized in Chapters 5 and 6 and the surface properties form the central subject of this Thesis.

The most important point to arise from our work is the absence of filled surface states within the bulk bandgap on the cleavage faces of GaP, InP and GaAs and the similar absence from the bandgap of all but the tail of the empty surface state distribution on InP(110) and GaAs(110). Empty surface states have been found on GaP(110) pinning the Fermi level 1.50 eV above the valence band maximum. Surface state data from u.h.v. - cleaved surfaces are now available for six III-V compounds : GaP, GaAs, GaSb, InP , InAs and InSb. It now seems likely that surface states are absent from the bulk bandgap in all of these semiconductors except for the empty states on GaP. It is interesting to consider why GaP appears to be different, although we remark here that there is no inherent reason to expect the precise details of all these compounds to be the same. We must discuss the possibility that the Fermi level pinning is not in fact caused by a GaP intrinsic state, but is induced by extrinsic factors, such as contamination, cleavage quality or material perfection. The main argument against the first two factors is the reproducibility of the results. We have not been able to observe any significant differences in the UPS edc's or the Ferml level pinning position on several cleaves from different samples (although all were cut from the same single crystal). It has been suggested (Spicer et al 1976b) that the material perfection in some way affects the surface properties. While we were not able to test this hypothesis by using samples

obtained from different sources, our results are almost identical to those reported on GaP supplied by Philips Research Laboratories (Netherlands) (Huijser et al 1977). Although we must remain aware of the possibility that this result on GaP is in fact due to an extrinsic effect -- inspection of Table 7.2 shows that until recently the majority of results wrongly indicated states within the bulk bandgap of GaAs-- there is theoretical backing for the existence of surface states on GaP and not on the other III-V semiconductors. The bandgap of GaP (2.24eV) is almost 1eV greater than that of GaAs and InP, while the remaining compounds of the six considered here have bandgaps < 0.7 eV. The model of Levine and Freeman (1970), discussed in Chapter 2.4, shows that the empty surface state moves away from the conduction band minimum, farther into the bandgap, as the bandgap is increased. Some of the details of this model may not be correct -- in particular their conclusion that the cations are rotated out of the surface, which was based on the inadequate experimental results then available -- but all the trends found have been confirmed by later calculations. We thus have some confidence that our data for GaP are truly representative of the intrinsic states of the clean (110) surface.

The lack of bandgap surface states on InP and GaAs (and also, apparently, on GaSb, InSb and InAs) raises interesting questions on the mechanism of Schottky barrier formation since the existence of intrinsic surface states pinning the Fermi level in mid-gap has traditionally been invoked to explain these phenomena (Bardeen 1947). Consideration of these effects has been outside the scope of this Thesis, but it can be asserted that intrinsic surface states in the bandgap are not necessary for formation of a Schottky barrier. Much effort is currently being expended in examining the modification of surface properties by a metal overlayer, both experimentally (Rowe et al 1975, Gudat et al 1976) and theoretically (Louis et al 1976 , Louie et al 1977). Studies of metal-semiconductor junctions carefully formed under controlled conditions on atomically clean surfaces should help to

elucidate the nature of intrinsic surface states as well as the metal-induced extrinsic states.

The derivation of the filled surface states from the anion and the empty surface states from the cation was discussed in Chapter 2 from the theoretical viewpoint. This association has been confirmed by several experimental investigations. Two particular results, both from surfaces which were not included in our experiments, seem conclusive. First, photoemission partial-yield spectra taken on GaSb(110) showed transitions to an empty surface state with excitation from the Ga 3d core level but no transition was seen from the Sb 4d level (Eastman and Freeouf 1975). Secondly, UPS and ELS on the polar faces of GaP revealed filled surface states on the phosphorus-rich GaP ($\bar{1}\bar{1}\bar{1}$) surface and empty states on the gallium-rich (111) surface (Jacobi 1975).

Our measurements lend support to these results. Partial-yield spectra from GaP revealed an empty surface state, with predominantly p-symmetry, by excitation from the Ga 3d level. In view of the recent suggestion (Bauer et al 1977) that anion s-like empty orbitals exist for covalent surfaces (including GaAs) and mixed s-like anion and cation wavefunctions make up the unoccupied surface states on more ionic semiconductors, it is of great interest to extend the measurements reported here to include excitation from other core levels.

The question of the bonding site of oxygen on III-V semiconductor surfaces is still the subject of considerable dispute. The core level shift measurements of Spicer and colleagues on InP (110) and GaAs(110) are said to indicate initial bonding exclusively to the anion, although we recall that it seems that the great difference between the shifts recorded on oxidation of elemental Ga and As has been ignored by these workers. ELS of GaAs(110), on the other hand, shows that transitions to the empty, Ga-derived, surface state are partly suppressed by even the smallest exposures of oxygen,

and this is interpreted to mean that the Ga, as well as the As, atoms are involved in the initial stages of bonding (Ludeke 1977). The model suggested to explain this has oxygen atoms bridging nearest-neighbour and second-nearest-neighbour Ga and As surface atoms (Figure 8.1)

Our AES data on the oxidation of GaP (110) apparently indicate great perturbation of the surface P atoms, with P-O cross-transitions induced, and no visible effect of oxygen on the Ga peaks even when the replacement of the ELS surface plasmon by a semiconductor-oxide interface plasmon showed that considerable numbers of oxygen atoms must have stuck to the surface. However, the fact that very large exposures of oxygen, including heating in oxygen and examining a surface before u.h.v. cleaning (which should have consisted mainly of the usual chemical oxides, Ga_2O_3 and $GaPO_4$), showed no significant effects (chemical shift, cross-transitions, etc.) on the main Ga peaks makes it probable that this technique is not sensitive to Ga-O bonding. The reasons for this are not clear, particularly since very heavy chemical oxidation of GaP (Oda and Sugano 1974) and oxidized gallium (Schön 1973) do show large changes in the Ga-derived Auger peaks, both Ga-O interatomic transitions and chemical shifts of up to 5eV being seen.

The UPS study of oxygen adsorption on GaP (110) reported here showed no change in the Fermi level pinning position, except possibly on the surface accidentally exposed to air. This may indicate that the Ga atoms, from which the empty surface state is derived, are not involved in the initial stages of oxidation. Although it might appear strange that a dangling bond surface state persists unperturbed even after adsorption of considerable quantities of contaminants, such a result has been reported elsewhere for several systems (GaAs+Pd (Eastman and Freeouf 1975), InSb+Sb and +O (Gudat et al 1976)), and has theoretically been made plausible : the calculations of Chelikowsky and Cohen (1976) show that, when the surface relaxation is included, the Ga dangling bond surface state on GaAs (110) is mainly localized along the bonding direction (Figure 2.13), and no longer protrudes from the crystal surface.

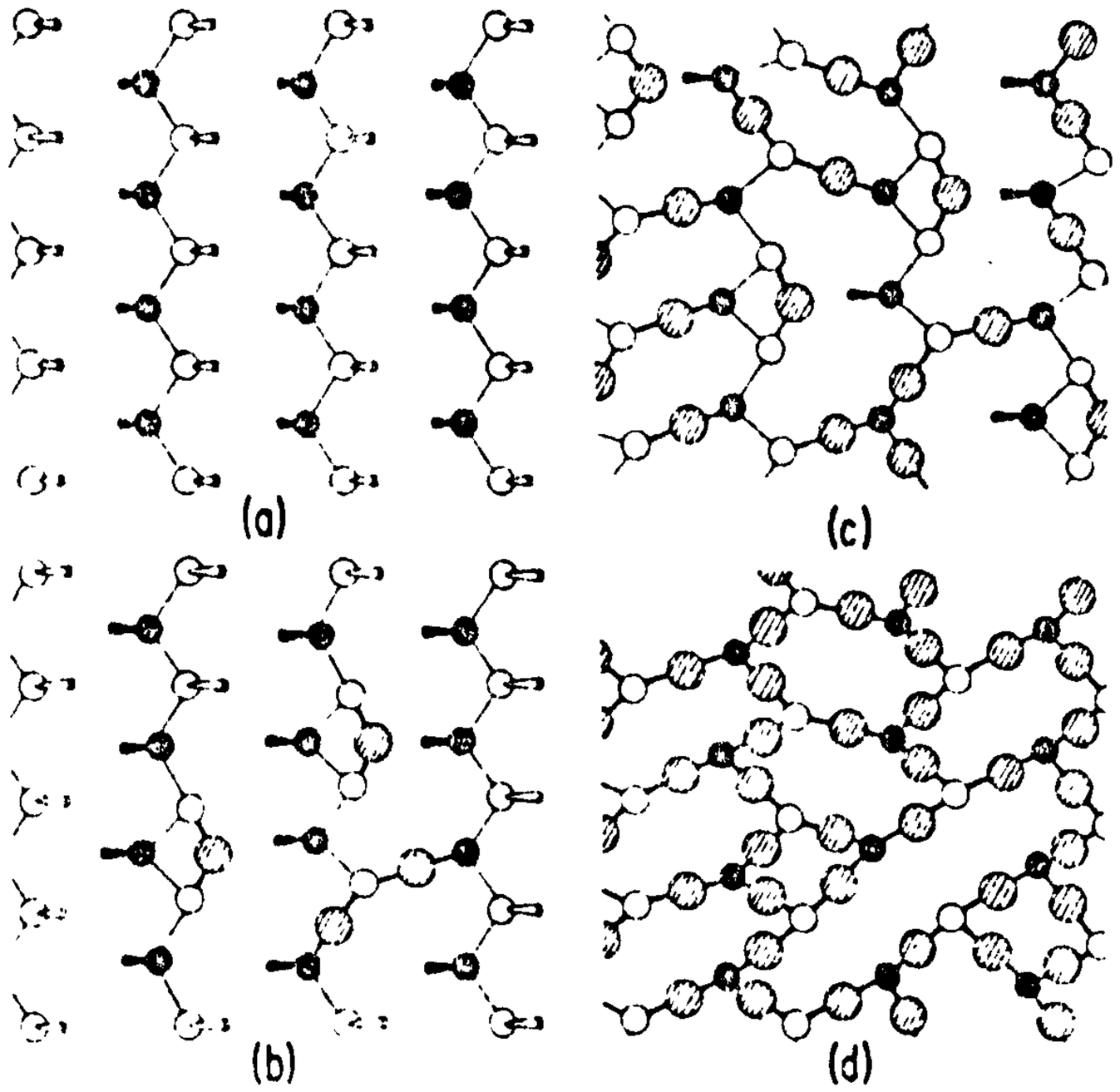

Figure 8.1. Possible model for adsorption of oxygen on GaAs(110). (a) clean surface; (b) initial stages of oxygen adsorption; (c) near half-monolayer coverage; (d) fully oxidized surface layer. The oxygen atoms are raised above the surface plane. The open and solid cones represent empty and filled dangling bonds. From Ludeke (1977).

The change in the Fermi level pinning position on n-type InP(110) and GaAs(110) with very small oxygen exposures cannot be accommodated in such a scheme, however. We must conclude in this case that extrinsic states are induced within the bulk bandgap which pin the Fermi level at approximately the same positions as have recently been reported to be characteristic of clean surfaces (Gregory and Spicer 1976a, Chye et al 1976). In these cases no shift of E_F on oxygen exposure was seen. It is not clear why there is no change in the Fermi level position on GaP whereas InP and GaAs are sensitive to very small coverages of oxygen ($\ll 10^{-3}$ monolayer). It is possible that, by chance, oxygen-induced extrinsic states on GaP fall at an energy which serves to pin the Fermi level in the same position as the edge of the intrinsic surface state band; perhaps the details of the surface relaxation differ slightly, making the GaP cleavage face more stable.

Finally, we consider some experiments which would help to elucidate the nature of the electronic structure of III -V semiconductor surfaces. Angularly-resolved photoemission is an obvious suggestion: the pronounced three-fold symmetry of the filled dangling bond surface state on silicon has been strikingly demonstrated by this means (Rowe et al 1974) and the existence of occupied surface states degenerate in energy (but not wavevector) with the bulk valence band has been shown in this way (Knapp and Lapeyre 1976). The dispersion of the states may be a better indication of their surface nature than sensitivity to adsorbates. It should also be possible to obtain a similar effect by keeping the angle constant and varying $h\nu$ (M^{c}Govern et al 1976) and the use of synchrotron radiation at photon energies $\geq$ 20eV should also assist in reducing the electron-electron scattering length and thus make UPS more surface-sensitive. The strong polarization of synchrotron radiation, a property which has yet to be exploited fully in solid-state physics, could help to reveal the symmetry of surface states. Experiments demonstrating the power of polarization-dependent angle-integrated edc- and CIS- measurements have recently been reported (Margaritondo et al 1977).

In view of the importance of knowing exactly the relaxed surface structure of III-V semiconductors, it is obviously imperative that the one set of LEED intensity-voltage data yet published be augmented by results for other compounds, and, despite the immense computational complexity, more thorough examination of all possible surface structures (including, for instance, changes in bond lengths) should be worthwhile. Angularly-resolved Auger emission or photoemission from core levels may help to determine the surface structure, although the analysis is likely to be complex, particularly in view of the pronounced asymmetry of the initial state expected for the dangling bond. The extension of EXAFS to study surface atomic species (Lee 1976) could be useful here and it has very recently been suggested (P.J.Feibelman, E.J.McGuire and K.C.Pandey, personal communication) that the different Auger lineshapes expected from the two constituent surface atoms should also help to distinguish between different models for the surface relaxation. Ion scattering spectroscopy could prove a more useful technique as it is sensitive only to the outermost atoms on the surface; ion neutralization spectroscopy may similarly be used to look at the electronic structure of the surface states.

It is impossible to over-emphasize the importance of having as many surface-sensitive probes as possible in the same system, so that all may be used to examine the same surface under the same conditions. Perhaps the ideal apparatus in which to continue the research reported in this Thesis would be a u.h.v. chamber equipped with LEED/AES/ELS, attached to a stable, high-intensity synchrotron radiation source ($20 \leq h\nu \leq 200$eV) in such a way that the polarization vector could be readily changed, with analysers suitable for recording angularly-resolved edc's and CIS spectra and partial-yield distributions.

REFERENCES

Abbati, I. and L.Braicovich, 1974, Riv. del Nuovo Cim. 4 , 205.

Adawi, I., 1964 , Phys. Rev. 134 , A788.

Alward, J.F. and C.Y.Fong , 1975, J.Phys. C 8 , 882.

Apker, L., E.Taft and J.Dickey, 1948, Phys. Rev. 74 , 1462.

Appelbaum, J.A. and D.R.Hamann, 1974 , Phys. Rev.Lett. 32 , 225.

Appelbaum, J.A. and D.R.Hamann, 1976, Rev.Mod. Phys. 48 , 479.

Arthur, J.R., 1967, J.Appl. Phys. 38 , 4023.

Ashcroft, N.W. and W.L.Schaich, 1969, Proc.Symp. on Density of States, publ. N.B.S., Washington, p.129.

Ashcroft, N.W., 1974, Proc. IVth Conf. on VUV Physics, Hamburg, p.533.

Aspnes, D.E., C.G.Olson and D.W.Lynch, 1975, Phys.Rev. B12 , 2527.

Aspnes, D.E., 1976, Phys. Rev. B14, 5331.

Auger, P., 1925, J.Phys. Radium 6 , 205.

Ball, G. and D.J.Morgan, 1972a, Phys. Stat. Sol.(b) 50 , 199.

Ball, G. and D.J.Morgan, 1972b, Phys. Stat. Sol. (b) 52 , K131.

Bardeen, J.,1947, Phys. Rev. 71 , 717.

Bassani, F. and M.Yoshimine, 1963, Phys. Rev. 130 , 20.

Bauer, R.S., R.Z.Bachrach, S.A.Flodstrom and J.C.McMenamin, 1977, J.Vac. Sci. Tech. 14 , 378.

Bayliss, C.R. and D.L.Kirk, 1975, Thin Solid Films 29 , L35.

Bayliss, C.R. and D.L.Kirk, 1976, J.Phys. D 9 , 233.

Bearden, J.A. and A.F.Burr, 1967, Rev. Mod. Phys. 39 , 125.

Benazeth, C., L.Viel and N.Colombie, 1972, Surf. Sci. 32 , 618.

Berglund, C.N. and W.E.Spicer, 1964, Phys. Rev. 136 , A1030.

Bishop, H.E., J.P.Coad and J.C.Rivière, 1972, J.Electron Spectrosc. 1 , 389.

Bloch, F., 1928, Z. Physik 52 , 555.

Brodén , G., S.B.M. Hagström and C.Norris, 1973, Phys. Kondens.Materie 15 ,327

Brundle, C.R., 1974, J.Vac.Sci.Tech. 11 , 212.

Brundle, C.R., M.W.Roberts, D.Latham and K.Yates, 1974, J.Electron Spectrosc. 1 , 241.

Calandra, C. and G.Santoro, 1975, J.Phys. C 8 , L86

Calandra, C. and G. Santoro, 1976, J.Phys. C 9 , L51.

Cardona, M., W.Gudat, B.Sonntag and P.Y.Yu, 1970, Proc.Xth Intern.Conf. on Physics of Semiconductors, p. 209.

Caroli, C., D.Lederer-Rozenblatt, B.Roulet and D.Saint-James, 1973, Phys. Rev. B8 , 4552 .

Chadi, D.J. and M.L.Cohen, 1975a, Phys. Rev. B11 , 732.

Chadi, D.J. and M.L.Cohen, 1975b, Phys. Stat. Sol. (b) 68 , 405.

Chang, C.C., 1971, Surf. Sci. 25 , 53.

Chelikowsky, J.R., D.J.Chadi and M.L.Cohen, 1973, Phys.Rev. B8 , 2786.

Chelikowsky, J.R. and M.L.Cohen, 1974, Phys. Rev. Lett. 32 , 674.

Chelikowsky, J.R. and M.L.Cohen, 1976a, Phys. Rev. B13 , 826.

Chelikowsky, J.R. and M.L.Cohen, 1976b, Phys. Rev. B14 , 556.

Chelikowsky, J.R., S.G.Louie and M.L.Cohen, 1976, Phys. Rev. B14, 4724

Chung, M.F. and L.H.Jenkins, 1970, Surf.Sci. 22 , 479.

Chye, P.W., I.A.Babalola, T.Sukegawa and W.E.Spicer, 1976, Phys. Rev. B13, 4439

Chye, P.W., T.Sukegawa, I.A.Babalola, H.Sunami, P.E.Gregory and W.E.Spicer, 1977, Phys. Rev. B15 , 2118.

Çiraci, S. and B.Bell, 1974, Solid State Commun. 15 , 575.

Citrin, P.H., J.E.Rowe and S.B.Christman, 1976, Phys.Rev. B14 , 2642

Coad, J.P., H.E.Bishop and J.C.Rivière, 1970, Surf.Sci. 21 , 253.

Codling, K., 1973, Rep. Prog.Phys. 36 , 541.

Cohen, M.L. and T.K.Bergstresser, 1966, Phys. Rev. 141 , 789.

Cohen, M.L. and V.Heine, 1970, Solid State Physics 24 , 37.

Collins, T.C., D.J.Stukel and R.N.Euwema, 1970, Phys.Rev.B1, 724

Davison, S.G. and J.D.Levine, 1970, Solid State Physics 25 , 1.

Davisson, C.J. and L.H.Germer, 1927, Phys. Rev. 30 , 705.

Dinan, J.H. , L.K.Galbraith and T.E.Fischer, 1971, Surf. Sci. 26 , 587.

Doniach, S., 1970, Phys. Rev. B2 , 3898.

Dorn, R., H.Lüth and G.J.Russell, 1974, Phys. Rev. B10 , 5049.

Duke, C.B., 1973, "Electron Emission Spectroscopy", ed. W.Dekeyser, publ. D.Reidel, Dordrecht, Holland, pp 1 - 149.

Duke, C.B., A.R.Lubinsky, B.W.Lee and P.Mark, 1976, J.Vac.Sci.Tech. 13, 761

Eastman, D.E. and J.J.Donelon, 1970, Rev. Sci. Instrum. 41 , 1648.

Eastman, D.E., 1972, Chapter 6 in "Techniques of Metals Research, " Vol.6 , Part I, ed.E.Passaglia, publ. Wiley-Interscience, New York.

Eastman, D.E. and W.D.Grobman, 1972, Phys. Rev.Lett. 28 , 1327.

Eastman, D.E. and W.D.Grobman, 1972, Phys. Rev. Lett. 28 , 1378.

Eastman, D.E., J.L.Freeouf and M.Erbudak, 1973, J. de Phys. C6 , 37 .

Eastman, D.E., 1974, Proc. IVth Conf. on VUV Physics, Hamburg, p.417.

Eastman, D.E. and J.L.Freeouf, 1974, Phys. Rev. Lett. 33 , 1601.

Eastman, D.E., W.D.Grobman, J.L.Freeouf and M.Erbudak, 1974, Phys. Rev. B9, 3473.

Eastman, D.E. and J.L.Freeouf, 1975, Phys. Rev.Lett. 34 , 1624.

Eden, R.C., 1967, Ph.D. Thesis, Stanford University.

Eden, R.C., 1970, Rev.Sci. Instrum. 41 , 252.

Einstein, A., 1906, Ann. der Physik 20 , 199

Fan, H.Y., 1945, Phys. Rev. 68 , 43.

Feibelman, P.J. and D.E.Eastman, 1974, Phys. Rev. B10, 4932.

Feibelman, P.J., 1975, Phys. Rev. B12, 1319.

Feuerbacher, B. and B.Fitton, 1972, Phys. Rev.Lett. 29 , 786.

Feuerbacher, B. and R.F.Willis, 1976, J.Phys. C 9 , 169.

Fischer, T.E., 1966, Phys. Rev. 142 , 519.

Fischer, T.E., 1966, Phys. Rev. 147 , 603.

Fischer, T.E., 1968, Helv. Phys. Acta 41, 827

Fischer, T.E. and P.E.Viljoen, 1971, Phys.Rev.Lett. 26 , 1475.

Floquet, G., 1883, Ann. Sci.Ecole Norm.Sup. Paris 12 , 47.

Flores, F., E.Louis and J.Rubio, 1972, J.Phys. C 5 , 3469.

Fowler, R.M., 1931, Phys. Rev. 38 , 45.

Freeouf, J.L., M.Erbudak and D.E.Eastman, 1973, Solid State Commun. 13 , 771

Freeouf, J.L. and D.E.Eastman, 1975, CRC Crit.Rev.Solid State Sci. 5 , 245.

Freeouf, J.L., 1976, Phys. Rev. Lett. 36 , 1095.

Froitzheim, H. and H.Ibach, 1975, Surf. Sci. 47 , 713.

Gadzuk, J.W., 1976, in "Electronic Structure and Reactivity of Metal Surfaces, " ed. E.G.Derouane and A.A.Lucas, publ. Plenum Press.

Galbraith, L.K. and T.E.Fischer, 1972, Surf. Sci. 30 , 185.

Gallon, T.E. and J.A.D.Matthew, 1972, Rev. Phys. Technol. 3 , 31.

García, N., 1975, Solid State Commun. 17 , 397.

García-Moliner, F. and J.Rubio, 1969, J.Phys. C 2 , 1789.

García-Moliner , F. and F.Flores, 1976 , J.Phys. C 9 , 1609.

Gaspar, R., 1954, Acta Phys. Acad. Sci. Hung. 3 , 263.

Gobeli, G.W. and F.G.Allen, 1965, Phys. Rev. 137 , A245.

Gobeli, G.W. and F.G.Allen, 1966, Chapter 11 of "Semiconductors and Semimetals, " Vol.2, ed. R.K.Willardson and A.C.Beer, publ. Academic Press, New York.

Gregory, P.E., W.E.Spicer, S.Çiraci and W.A.Harrison, 1974, Appl. Phys. Lett. 25 , 511.

Gregory, P.E. and W.E.Spicer, 1975, Phys. Rev. B12 , 2370.

Gregory, P.E. and W.E.Spicer, 1976a, Phys. Rev. B13 , 725.

Gregory, P.E. and W.E.Spicer, 1976b, Surf. Sci. 54 , 229.

Grobman, W.D. and D.E.Eastman, 1974, Phys .Rev.Lett. 33 , 1034.

Grobman, W.D., D.E.Eastman, J.L.Freeouf and J.Shaw, 1974, Proc.XIIth Intern. Conf. on Physics of Semiconductors, p.1275.

Grobman, W.D., 1975, Comments Solid State Physics 7 , 27.

Grobman, W.D., D.E.Eastman and J.L.Freeouf, 1975, Phys.Rev.B12 , 4405.

Grove, A.S., 1967, "Physics and Technology of Semiconductor Devices, " publ. John Wiley, New York.

Gudat, W. and C.Kunz, 1972, Phys. Rev.Lett. 29 , 169.

Gudat, W., E.E.Koch, P.Y.Yu, M.Cardona and C.M.Penchina, 1972, Phys. Stat. Sol. (b) 52 , 505.

Gudat, W., D.E.Eastman and J.L.Freeouf, 1976, J.Vac. Sci. Tech. 13 , 250.

Gudat, W., and D.E.Eastman, 1976, J.Vac. Sci. Tech. 13 , 831.

Gulchar, G.M., C.A.Sebenne and G.A.Garry, 1976, Phys. Rev.Lett. 37 , 1158.

Hall, R.N. and J.H.Racette, 1964, J.Appl. Phys. 35 , 379.

Haneman, D., 1959, J.Phys. Chem. Solids, 11 , 205.

Harrison, W.A., 1973, Phys. Rev. B8 , 4487.

Hayes, W., 1972, Contemp. Phys. 13 , 441.

Heine, V., 1964, Surf. Sci. 2 , 1.

Herman, F., 1964, Proc.VIIth Intern. Conf. on Physics of Semiconductors, p.3.

Herman, F., R.L.Kortum, C.D.Kuglin and R.A.Short, 1966,
J.Phys. Soc. Japan 21 Suppl., 7.

Herman, F., R.L.Kortum, C.D.Kuglin, J.P.Van Dyke and S.Skillman, 1968,
"Methods in Computational Physics, " Vol.8, publ.Academic Press,New York
p. 193.

Herman, F. and W.E.Spicer, 1968, Phys. Rev. 174 , 906.

Herman, F., R.L.Kortum, I.B.Ortenburger and J.P.Van Dyke. 1969,
Aerospace Research Labs. Report ARL 69-0080.

Hermeking, H., 1973, J.Phys. C 6 , 2898.

Herring, C., 1940, Phys. Rev. 57 , 1169.

Hertz, H., 1887, Ann. der Physik u. Chemie 31 , 983.

Howells, M., C.Norris and G.P.Williams, 1977, J.Phys. E 10, 259.

Huijser, A. and J.Van Laar, 1975, Surf. Sci. 52 , 202.

Huijser, A., J.Van Laar and T.L.Van Rooy, 1977, Surf. Sci. 62 , 472.

Ibach, H. and J.E.Rowe, 1974a, Phys. Rev. B9 , 1951 .

Ibach, H. and J.E.Rowe, 1974b, Surf. Sci. 43 , 481.

Inkson, J.C., 1973, J.Phys. C 6 , 1350.

Jacobi, K., 1975, Surf. Sci., 51 , 29.

Jacobi, K. and W.Ranke, 1976, J.Electron Spectros. 8 , 225.

James, L.W., 1968, Ph.D. Thesis, Stanford University.

James , L.W. and J.L.Moll, 1969, Phys. Rev. 183 , 740.

James, L.W., J.P.Van Dyke, F.Herman and D.M.Chang, 1970, Phys.Rev.B1,3998 .

Janak, J.F., D.E.Eastman and A.R.Williams, 1970, Solid State Commun. 8 , 271.

Janak. J.F., A.R.Williams and V.L.Moruzzi, 1975, Phys. Rev.B11, 1522 .

Janssen, A.P., R.Schoonmaker, J.A.D.Matthew and A.Chambers, 1974,
Solid State Commun. 14 , 1263.

Joannopoulos, J.D. and M.L.Cohen, 1974a, Phys. Lett. 49A, 391 .

Joannopoulos, J.D. and M.L.Cohen, 1974b, Phys. Rev. B10 , 5075.

Johannessen, J.S., W.E.Spicer and Y.E.Strausser, 1976, J.Appl.Phys. 47 ,3028.

Jones, R.O., 1969, "Structure and Chemistry of Solid Surfaces, "
publ. John Wiley, New York, p.14 - 1.

Jones, R.O., 1972, J.Phys. C 5 , 1615.

Jones, R.O., 1976, Chapter 2 of "Surface Physics of Semiconductors and Phosphors, " ed. C.G.Scott and C.E.Reed, publ.Academic Press, London.

Kane, E.O., 1962, Phys. Rev. 127 , 131.

Kennedy, D.J. and S.T.Manson, 1972, Phys. Rev. A5 , 227.

Kirby, R.E. and D.Lichtman, 1974, Surf. Sci. 41 , 447.

Knapp, J.A. and G.J.Lapeyre, 1976, J.Vac. Sci. Tech. 13 , 757.

Kohn, W. and L.Sham, 1965, Phys. Rev. 140 , A1133.

Kramer, B., K.Maschke and P.Thomas, 1971, Phys. Stat.Sol.(b) 48 , 635.

Krollkowski, W.F. and W.E.Spicer, 1970, Phys. Rev. B1 ,478.

Kronig, R. de L. and W.G.Penney, 1931, Proc. Roy. Soc., A130, 499.

Lander, J.J., 1953, Phys.Rev. 91 , 1382.

Lane, T., C.J.Vesely and D.W.Langer, 1972, Phys. Rev. B6, 3770.

Langer, D.W., 1973, Festkörperprobleme 13, 193.

Langreth, D.C., 1973, Nobel Symposium 24 , "Collective Properties of Physical Systems," ed.B.I.Lundquist and S.Lundquist, publ. Academic Press, New York, p.210.

Lapeyre, G.J., J.Anderson, P.L.Gobby and J.A.Knapp, 1974, Phys. Rev. Lett. 33 , 1290.

Lapeyre, G.J. and J.Anderson, 1975, Phys. Rev.Lett. 35 , 117 .

Lee, P.A., 1976, Phys. Rev. B13, 5261.

Leonhardt, G., A.Berndtsson, J.Hedman, M.Klasson, R.Nilsson and C.Nordling, 1973, Phys.Stat.Sol. (b) 60 , 241.

Leonhardt, G., 1975, Soviet Phys. - Solid State 17 , 1.

Levine, J.D. and P.Mark, 1966, Phys. Rev. 144 , 751.

Levine, J.D., 1968, Phys. Rev. 171 , 701.

Levine, J.D. and S.G.Davison, 1968, Phys. Rev. 174, 911 .

Levine, J.D. and S.Freeman, 1970, Phys.Rev.B2 , 3255

Ley, L., R.A.Pollak, F.R.McFeely, S.P.Kowalczyk and D.A.Shirley, 1974, Phys. Rev. B9, 600 .

Lindau, I. and S.B.M.Hagström, 1971, J.Phys. E 4, 936 .

Lindau, I. and W.E.Spicer, 1974, J.Electron Spectrosc. 3 , 409.

Lindau, I., P.Pianetta, K.Y.Yu and W.E.Spicer, 1976a, Phys.Rev.B13, 492.

Lindau, I., P.Pianetta, K.Y.Yu and W.E.Spicer, 1976b, J.Vac. Sci. Tech. 13 , 269.

Lindau, I., P.Pianetta and W.E.Spicer, 1976c, Proc.XIIIth Intern.Conf. on Physics of Semiconductors, p.122.

Lindau, I., P.Pianetta, C.M.Garner, P.W.Chye, P.E.Gregory and W.E.Spicer, 1977, Surf. Sci. 63 , 45.

Louie, S.G., J.R.Chelikowsky and M.L.Cohen, 1977, Phys.Rev. B15, 2154 .

Louis, E., F.Yndurain and F.Flores, 1976, Phys.Rev. B13 , 4408.

Lubinsky, A.R., C.B.Duke, B.W.Lee and P.Mark, 1976, Phys.Rev.Lett.36 ,1058.

Ludeke, R. and A.Koma, 1975a, CRC Crit. Rev.Solid State Sci. 5 , 259.

Ludeke, R. and A.Koma, 1975b, Phys. Rev. Lett. 34 , 817.

Ludeke, R. and A.Koma, 1976, J.Vac. Sci. Tech. 13 , 241.

Ludeke, R., 1977, Solid State Commun. 21 , 1815.

Lukeš, F., 1975, Surf. Sci. 49 , 344.

Lüth, H. and G.J.Russell, 1974, Surf. Sci. 45 , 329.

Lüth, H., M.Büchel, R.Dorn, M.Liehr and R.Matz, 1977, Phys.Rev.B15 , 865.

McDonnell, L., B.D.Powell and D.P.Woodruff, 1973, Surf.Sci. 40 ,669.

McGovern, I.T., R.H.Williams and D.Norman, 1976, "Photoelectron Emission" : Proc.Daresbury Laboratory Study Weekend, p.26.

McGovern, I.T., A.Parke and R.H.Williams, 1976, J.Phys. C 9 , L511.

MacRae, A.U. and G.W.Gobeli, 1964, J. Appl.Phys. 35 , 1629.

MacRae, A.U. and G.W.Gobeli, 1965, Chapter 6 of "Semiconductors and Semimetals, " Vol.2, ed.R.K.Willardson and A.C.Beer, publ. Academic Press, New York.

Mahan, G.D., 1970, Phys. Rev. B2 , 4334.

Many, A., Y.Goldstein and N.B.Grover, 1965, "Semiconductor Surfaces, " publ. North-Holland, Amsterdam.

Margaritondo, G. and J.E.Rowe , 1977, Phys.Lett.59A, 464.

Margaritondo, G., J.E.Rowe and S.B.Christman, 1977, Phys.Rev. B15, 3844.

Margoninski, Y., 1976, J.Appl. Phys. 47 , 3868.

Martin, L., A.Couget and F.Pradal, 1973, Comptes Rendues B 276, 51 .

Mayer, H. and H.Thomas, 1957, Z.Physik 147, 419.

Mayer, J.W., L.Eriksson and J.A.Davies, 1970, "Ion Implantation in Semiconductors, " publ.Academic Press, New York.

Mitchell, K.A.R., 1973, Contemp. Phys. 14 , 251.

Mityagin, A.Yu, V.P.Orlov and N.Ya.Cherevatskii, 1972, Soviet Phys. - Solid State 13 , 1815.

Mityagain, A.Yu, V.P. Orlov and N.Ya.Cherevatskii, 1973a, Soviet Phys.- Crystallography 18 , 268.

Mityagin, A.Yu., V.P.Orlov, K.A.Khronopulo and N.Ya.Cherevatskii, 1973b, Soviet Phys. - JETP 36 , 906.

Morgan, A.E. and W.J.M. Van Velzen, 1973, Surf. Sci. 40 , 360.

Morgan, A.E., 1974, Surf. Sci. 43 , 150.

Nefedov, V.I., Ya.V. Salyn, E.P.Domashevskaya, Ya.A.Ugai and V.A.Terekhov, 1975, J.Electron Spectrosc. 6 , 231.

Neumann, H., E.Hess and I.Topol, 1975, Czech. J.Phys. B25, 174 .

Nilsson, P.-O. and D.E.Eastman, 1973, Phys. Scripta 8 , 113.

Norman, D. and G.P.Williams, 1976, "Photoelectron Emission " : Proc. Daresbury Laboratory Study Weekend, p.23.

Norman, D. and D.K.Skinner, 1977, J.Phys. D10 , L151.

Norman, D., I.T.McGovern and C.Norris, 1977, Phys. Lett. A.

Oda, T. and T.Sugano, 1974, Ann. Rep.Eng.Res.Inst. Fac.Eng.Univ.Tokyo, 33 , 153.

Ortenburger, I.B. and W.E.Rudge, 1972, IBM Research RJ-1041.

Palmberg, P.W., 1971, Proc.Conf. on Electron Spectroscopy, ed.D.A.Shirley, publ. North-Holland, Amsterdam, p.835.

Pandey, K.L. and J.C.Phillips, 1974, Phys. Rev. Lett. 32 , 1433.

Pantelides, S.T. and W.A.Harrison, 1975, Phys.Rev. B11, 3006.

Park, R.L. and J.E.Houston, 1973, J.Vac. Sci.Tech. 10 , 176.

Pendry, J.B., 1974, "Low Energy Electron Diffraction," publ. Academic Press, London.

Pendry, J.B., 1976, Surf.Sci. 57 ,679.

Pianetta, P., I.Lindau, C.M.Garner and W.E.Spicer, 1975, Phys.Rev.Lett. 35 , 1356.

Pianetta, P., I.Lindau, C.M.Garner and W.E.Spicer, 1976, Phys. Rev.Lett. 37 , 1166.

Pierce, D.T., 1975, Acta Electronica 18 , 69.

Pollak, F.H., C.W.Higginbotham and M.Cardona, 1966, J.Phys.Soc. Japan, 21 Suppl., 20.

Prutton, M., 1971, Metals and Materials 5 , 57.

Ranke, W. and K.Jacobi, 1975, Surf.Sci. 47 , 525.

Ranke, W. and K.Jacobi, 1977, Surf. Sci. 63 , 33.

Redhead, P., J.P.Hobson and E.V.Kornelson, 1968, "The Physical Basis of Ultra-High Vacuum," publ.Chapman and Hall.

Risley, J.S., 1972, Rev. Sci. Instrum. 43 , 95.

Ritchie, R.H., 1957, Phys. Rev. 106 , 874.

Rivière, J.C., 1973, Contemp. Phys. 14, 513.

Rosebury, F., 1965,"Handbook of Electron Tube and Vacuum Techniques, " publ. Addison-Wesley.

Rowe, J.E. and H.Ibach, 1974, Phys. Rev. Lett. 32 , 421.

Rowe, J.E. and N.V.Smith, 1974, Phys. Rev. B10 , 3207.

Rowe, J.E., M.M.Traum and N.V.Smith, 1974, Phys.Rev.Lett. 33 , 1333.

Rowe, J.E., S.B.Christman and G.Margaritondo, 1975, Phys.Rev.Lett.35 ,1471.

Rubenstein, M., 1966, J.Electrochem. Soc. 113 , 540.

Samson, J.A.R., 1967, "Vacuum Ultraviolet Radiation Physics," publ. John Wiley, New York.

Saravia, L.R. and J.L.Duomarco, 1973, J.Phys.Chem.Solids 34 , 1661.

Sar-El, H.Z., 1967, Rev.Sci.Instrum. 38 , 1210.

Schaich, W.L. and N.W.Ashcroft, 1970, Solid State Commun. 8 , 1959.

Schaich, W.L. and N.W.Ashcroft, 1971, Phys.Rev. B3, 2452.

Schön, G., 1973, J.Electron Spectrosc. 2 , 75.

Seraphin, B.O. and H.E.Bennett, 1966, Chapter 13 of "Semiconductors and Semimetals," Vol.3, ed.R.K.Willardson and A.C.Beer, publ. Academic Press, New York.

Sevier, K.D., 1972, "Low Energy Electron Spectrometry," publ. Wiley-Interscience, New York.

Shevchik, N.J., J.Tejeda and M.Cardona, 1974, Phys.Rev. B9, 2627.

Shirley, D.A., 1975, J.Vac.Sci.Tech. 12 , 280.

Shockley, W., 1939, Phys. Rev. 56 , 317.

Siegbahn, K., C.Nordling, A.Fahlman, R.Nordberg, K.Hamrin, J.Hedman, G.Johansson, T.Bergmark, S.-E.Karlsson, I.Lindgren and B.Lindberg, 1967, "ESCA-Atomic ,Molecular and Solid State Structure studied by means of Electron Spectroscopy," publ. Almquist and Wiksells, Uppsala.

Slater, J.C., 1951, Phys. Rev. 81 , 385.

Smith, N.V.,1971, CRC Crit. Rev.Solid State Sci. 2 , 145.

Spicer, W.E., 1966, in "Optical Properties and Electronic Structure of Metals and Alloys," ed.F.Abelès, publ.North-Holland, Amsterdam, p.296.

Spicer, W.E., 1967, Phys. Rev. 154 , 385.

Spicer, W.E. and R.C.Eden, 1968, Proc.IXth Intern. Conf. on Physics of Semiconductors, p.65.

Spicer, W.E., 1974, Proc. IVth Conf. on VUV Physics, p.545.

Spicer, W.E. and P.E.Gregory, 1975, CRC Crit. Rev.Solid State Sci. 5 ,231.

Spicer, W.E., P.W.Chye, P.E.Gregory, T.Sukegawa and I.A.Babalola,1976a, J.Vac.Sci.Tech. 13 , 233.

Spicer, W.E., I.Lindau, P.E.Gregory, C.M.Garner. P.Pianetta and P.W.Chye, 1976b, J.Vac. Sci. Tech. 13 , 780.

Spicer, W.E., I.Lindau, P.Pianetta, C.M.Garner and K.Y.Yu, 1976c, Proc.Intern.Symp.on Photoemission, publ. E.S.A.,Noordwijk,p.97.

Stein, E.A. and R.A.Ferrell, 1960, Phys. Rev. 120 , 130.

Stokowski, S.E. and D.D.Sell, 1972, Phys.Rev. B5, 1636.

Tamm, I., 1932, Z.Physik 76 , 849.

Tamm, I., 1933, Physik Z. Sowjet. 1 , 733.

Taylor, N.J., 1969, Rev. Sci. Instrum. 40 , 792.

Thiry, P., Y.Petroff, R.Pinchaux, J.R.Chelikowsky and M.L.Cohen, 1976, Solid State Commun. 20 , 1107.

Van Laar, J. and J.J.Scheer, 1967, Surf. Sci. 8 , 342.

Van Velzen, W.J.M. and A.E.Morgan, 1973, Surf.Sci. 39 , 255.

Varea de Alvarez, C., J.P.Walter, M.L.Cohen, J.Stokes and Y.R.Shen, Phys. Rev. B6, 1412.

Vesely, C.J. and D.L.Kingston, 1973, Phys. Rev. B8 , 2685.

Vyatkin, A.P., N.K.Maksimova, A.S.Poplavnoi, V.E.Stepanov and V.A.Chaldyshev, 1970, Soviet Phys.-Semiconductors 4 , 775.

Wagner, C.D. and P.Biloen, 1973, Surf. Sci. 35, 82.

Wagner, L.F. and W.E.Spicer, 1972, Phys. Rev.Lett. 28 , 1381.

Walter, J.P. and M.L.Cohen, 1969, Phys. Rev. 183 , 763.

Williams, R.H. and I.T.McGovern, 1975, Surf. Sci. 51 , 14.

Williams, R.H., 1976, "Photoelectron Emission" : Proc.Daresbury Laboratory Study Weekend, p.11.

Zashkvara, V.V., M.I.Korsunskii and O.S.Kosmachev, 1966, Soviet Phys.- Tech. Phys. 11 , 96.

Zucca, R.R.L., J.P.Walter, Y.R.Shen and M.L.Cohen, 1970, Solid State Commun. 8 , 627.

Appendix -- Publications

Preliminary reports of some of the UPS work from Chapters 5 and 6 have been published as follows :

"Photoemission from cleaved (110) surfaces of Gallium Phosphide, " by D.Norman and G.P.Williams, pp. 23-25 in "Photoelectron Emission " : Proceedings of Daresbury Laboratory Study Weekend, March 1976.

"Photoemission studies of Indium Phosphide, " by I.T.McGovern, R.H.Williams and D.Norman, pp. 26 - 28 in above reference.

The discussion of electron beam enhanced oxidation from Chapter 5 has been published as:

" Electron beam effects during oxygen adsorption, " by D.Norman and D.K.Skinner, J.Phys. D-- Applied Physics, 10 , L151-4 , (1977).

A report of the results on surface states on GaP, from Chapter 5, has been accepted for publication under the title :

" Surface states on Gallium Phosphide, " by D.Norman, I.T.McGovern and C.Norris , Phys. Lett. A - to be published.

Other parts of this Thesis may be submitted for publication in due course.